Universidade do Porto
Faculdade de Engenharia
FEUP

Carlos Adolfo Grande

Propane/Propylene Separation by Adsorption Processes

Porto, 2004

Propane / Propylene Separation by Adsorption Processes

A Dissertation Presented to the

UNIVERSIDADE DO PORTO

For the degree of Doctor in Chemical Engineering

by

Carlos Adolfo Grande

Supervisor: Prof. Alírio E. Rodrigues

LSRE - Laboratory of Separation and Reaction Engineering

Department of Chemical Engineering

Faculty of Engineering

University of Porto

November 3, 2004.

UNIVERSIDADE DO PORTO
Faculdade de Engenharia
BIBLIOTECA
N.º 78375
CDU
Data 18 / 1 / 2005

Abstract

In this thesis the separation of propane-propylene streams is studied. Vacuum Pressure Swing Adsorption, VSA-PSA, is considered as an alternative to distillation practiced in industry where large amounts of energy are required. When using adsorption technology the key in the process design is a selective adsorbent. In this work, some commercial adsorbents were considered: narrow silica gel (Grace Davison), wide silica gel (Grace Davison), zeolite 5A (Grace Davison), dealuminated H-mordenite (Süd Chemie), Carbon Molecular Sieve CMS4A (Takeda) and zeolite 4A (CECA). Adsorption equilibrium and kinetics of pure propane and propylene were measured in those adsorbents. At partial pressures of 100kPa, none of the adsorbents have equilibrium selectivity higher than 3, but in both 4A molecular sieves, differences of at least one order of magnitude between the diffusivity of propane and propylene were observed.

To enhance the equilibrium selectivity towards propylene new adsorbents were tested: exchanged mordenite and clinoptilolite and SBA-15 impregnated with different amounts of Ag^{+}. From these materials, the Ag/SBA-15 with relation Ag/SiO_2=0.5 was the best one having equilibrium selectivity higher than 10 at 100kPa.

A new manometric chromatographic unit was built to measure binary adsorption equilibrium on CMS4A and zeolite 4A and also to extend capabilities for pure component adsorption equilibrium to pressures up to 500kPa. Binary fixed-bed experiments at different propane-propylene molar fractions were performed in a laboratory unit already existing in our laboratory.

Adsorption equilibrium and kinetics of pure gases were measured in a square honeycomb monolith containing zeolite 4A. A mathematical model for pure component adsorption from a mixture adsorbate – inert gas in a square channel monolith was developed. Its simplification applied only for dilute systems was solved in gPROMS and further simplifications were solved for more concentrated mixtures.

Finally, VSA-PSA experiments and simulations were performed in CMS 4A and zeolite 4A. A cycle comprising 5 steps was used: pressurization, feed, rinse, depressurization and blowdown at 10kPa where purified propylene is obtained. This cycle was also used to perform the simulations of Ag/SBA-15=0.5.

For Ag/SBA-15 = 0.5 and starting with equimolar mixture high purity propylene (>99%) can only be obtained with low recovery (63%). For the case of CMS 4A, starting with a 52/48 propylene to propane mixture, low purity propylene (80- 85%) was produced with high recovery (around 90%). VSA-PSA experiments were also performed with zeolite 4A (CECA) with two mixtures with different propylene to propane ratio: 54/46 and 85/15. The effect of some operating variables used were studied: step times, temperature, inert content and feed pressure (parameter studied only by simulations). Increasing the temperature, purity decreases and recovery and productivity increase. The low value of propane diffusivity in zeolite 4A allows a strong minimization on the rinse step without significant purity decrease. The crystal size of the sample was also varied; VSA-PSA study performed only by simulations based on pure component adsorption equilibrium and kinetics measured in four different samples of zeolite 4A prepared in laboratory with sizes ranging from 0.3 – 22 μm. With 4A zeolite crystals having a diameter of 5μm polymer grade propylene can be obtained (99.61%) with recovery of 83.1% and productivity of 2.25 mol/h.kg.

Resumo

Nesta tese a separação da mistura propano/propileno é estudada. A adsorção por modulação de pressão com vácuo, VSA-PSA, é considerada como uma alternativa à destilação praticada na indústria mas que requer grandes quantidades de energia. Em adsorção, o ponto chave do processo é encontrar um adsorvente selectivo. Neste trabalho foram considerados alguns adsorventes comerciais: sílica gel de poros estreitos (Grace Davison), sílica gel de poros largos (Grace Davison), zeólito 5A (Grace Davison), H-mordenite (Sud Chemie), peneiro molecular de carbono CMS4A (Takeda) e zeólito 4A (CECA). O equilíbrio e a cinética de adsorção de propano e propileno puros foram medidos. A pressões parciais de 100kPa, nenhum dos adsorventes tem selectividade de equilíbrio maior do que 3, com a excepção dos peneiros moleculares 4A em que se observaram diferenças de pelo menos uma ordem de magnitude entre a difusividade do propano e propileno.

Para aumentar a selectividade de equilíbrio relativamente ao propileno novos adsorventes foram testados: mordenite modificada, clinoptilolite e SBA-15 impregnado com diferentes quantidades de Ag^{+}. Destes materiais, o Ag/SBA-15 com uma razão de Ag/SiO2=0.5 foi o melhor, com uma selectividade de equilíbrio maior que 10 à 100kPa.

Uma nova unidade de cromatografia manométrica foi construída para medir o equilíbrio de adsorção binária em CMS4A, zeólito 4A e também para aumentar a capacidade de determinação do equilíbrio de adsorção de componentes puros a pressões até 500kPa. Experiências binárias em leito fixo, a diferentes fracções molares de propano e propileno, foram executadas numa unidade laboratorial já existente.

O equilíbrio e cinética de adsorção de gases puros foram medidos num monolíto quadrado contendo zeólito 4A. Foi desenvolvido um modelo matemático para adsorção de componente puro de uma mistura adsorbato/gás inerte num canal quadrado do monolíto. Esta simplificação foi aplicada apenas para sistemas diluídos e resolvida no gPROMS, enquanto que outras simplificações foram aplicadas para misturas mais concentradas.

Finalmente, experiências e simulações de VSA-PSA foram executadas em CMS 4A e zeólito 4A. Um ciclo composto por 5 passos foi usado para a obtenção de propileno purificado: pressurização, alimentação, lavagem, despressurização e regeneração a 10kPa. Este ciclo foi o usado para executar as simulações de Ag/SBA-15=0.5.

Para Ag/SBA-15 = 0.5 iniciando com uma mistura equimolar, alta pureza de propileno (>99%) apenas pode ser obtida com baixa recuperação (63%). Para o caso da CMS 4A, e iniciando com uma mistura 52/48 de propileno/propano, foi produzido propileno de baixa pureza (80-85%) mas com alta recuperação (~90%). Experiências de VSA-PSA foram também realizadas em zeólito 4A (CECA), utilizando duas misturas de diferentes razões propileno/propano: 54/46 e 85/15. O efeito de algumas variáveis de operação foi estudado: tempo dos passos, temperatura, conteúdo de inertes e pressão de alimentação (parâmetro estudado apenas por simulação). Aumentando a temperatura a pureza decresce mas a recuperação e produtividade aumentam. O baixo valor da difusividade do propano em zeólito 4A permite um grande decréscimo no passo de lavagem sem diminuição significativa da pureza. O tamanho do cristal da amostra foi também variado; simulou-se a performance do VSA-PSA, baseados no equilíbrio e cinética de adsorção dos componentes puros, medidos em quatro amostras diferentes de zeólito 4A, preparadas em laboratório com tamanhos entre 0.3-22 μm. Para cristais da zeólito 4A de diâmetro 5 μm, propileno de qualidade polimérica pode ser obtido (99.61%) com recuperação de 83.1% e produtividade de 2.25 mol/h.kg.

Résumé

Dans cette thèse la séparation des courants de propane-propylène a été étudiée. Le procédé de séparation par adsorption avec des modulations de pression VSA-PSA (Vacuum Pressure Swing Adsorption) est considéré comme une réelle alternative à la distillation industrielle jugée coûteuse en raison de sa grande consommation d'énergie. L'idée d'utiliser la technologie d'adsorption repose en fait sur la sélectivité de l'adsorbant. Dans cette étude, quelques adsorbants commerciaux ont été utilisés : gel de silice au pore étroit et au pore large (Grace Davison), zéolithe 5A (Grace Davison), H-mordenite déaluminisée (Süd Chemie), tamis moléculaire de carbone CMS4 (Takeda), zéolithe 4A (CECA). Les cinétiques et les équilibres d'adsorption du propane et du propylène pur ont été mesurés avec ces adsorbants. A une pression partielle de 100 kPa, aucun de ces adsorbants n'a une sélectivité d'équilibre au dessus de 3, tandis que dans les tamis moléculaires 4A, des différences d'au moins un ordre de magnitude entre la diffusivité du propane et du propylène ont été observées.

Pour améliorer la sélectivité de l'équilibre vers le propylène, de nouveaux adsorbants ont été testés: mordénite, clinoptilolithe et du SBA-15 imprégnés avec différentes quantités de Ag^{+}. A partir de ces matériaux, le Ag/SBA-15 en relation avec Ag/SiO_2=0.5 se révéla le meilleur adsorbant, en ayant une sélectivité d'équilibre supérieure à 10 pour une pression de 100 kPa.

Une nouvelle unité manométrique chromatographique, a été mise au point pour mesurer des équilibres d'adsorption binaires en CMS4 et zéolithe 4A, et aussi pour étendre les possibilités de mesure des équilibres d'adsorption pour des composés purs à des pressions supérieures à 500 kPa. Des expériences binaires de lit fixe à différentes fractions molaires furent réalisées dans une unité déjà existante dans notre laboratoire.

Les cinétiques et les équilibres d'adsorption de gaz purs ont été mesurés dans un carré de monolithe en nid d'abeille contenant de la zéolithe 4A. Un modèle mathématique pour l'adsorption de composés purs par un mélange d'adsorbat – un gaz inerte dans un canal carré d'un monolithe - fut développé. Sa simplification appliquée seulement pour des systèmes dilués a été résolue en gPROMS, et les autres simplifications furent résolues pour des mélanges plus concentrés.

Finalement, les expériences et les simulations VSA-PSA furent réalisées dans du CMS 4A et de la zéolithe 4A. Un cycle comprenant 5 étapes a été utilisé : pressurisation, alimentation, rinçage, dépressurisation, et régénération à 10 kPa où le propylène purifié est obtenu. Ce cycle fut aussi utilisé pour réaliser des simulations de Ag/SBA-15 = 0.5.

Pour Ag/SBA-15=0.5 en commençant avec un mélange équimolaire, seul du propylène de haute pureté (>99 %) pu être obtenu avec de faibles récupérations (63 %). Pour le cas du CMS 4A, en débutant avec un mélange propane-propylène 52/48, du propylène de faible pureté (80-85%) a été produit avec un taux de récupération élevé (autour de 90%). Les expériences VSA-PSA furent réalisées avec la zéolithe 4A (CECA) avec deux mélanges différents en taux de propane-propylène: 54/46 et 85/15. Les effets des variables utilisées ont été étudiés: le spas de temps, la température, et la pression d'alimentation (paramètre étudié seulement par simulation). En augmentant la température, la pureté diminue et le taux de récupération ainsi que la productivité augmente. La faible valeur de la diffusivité du propane dans la zéolithe 4A permet une forte diminution de l'étape de rinçage sans une baisse de pureté significative. La taille du cristal de l'échantillon fut également étudiée; l'étude VSA-PSA réalisée uniquement par simulation est basée sur des cinétiques et des équilibres d'adsorption mesurés dans 4 échantillons différents de zéolithe 4A préparés en laboratoire avec une gamme de taille comprise entre 0.3 μm - 22 μm. Avec des cristaux de zéolithe 4A ayant un diamètre de 5 μm , le propylène peut être obtenu avec un taux de récupération de 83.1% et une productivité de 2.25 mol/h.kg.

Resumen

En esta tesis se estudia la separación de corrientes de propano y propileno. El proceso de separación por adsorción con modulación de vacío y presión, VSA-PSA es evaluado como una alternativa a la destilación, practicada en la industria y donde se requieren grandes cantidades de energía. Cuando se utiliza una tecnología basada en la adsorción, la llave en el diseño de procesos es un adsorbente selectivo. En este trabajo consideramos algunos adsorbentes comerciales: silica gel (Grace Davison) de poro estrecho y poro ancho, zeolita 5A (Grace Davison), H-mordenita dealuminizada (Süd-Chemie), tamiz molecular de carbono CMS4A (Takeda) y zeolita 4A (CECA). Se han medido equilibrios y cinéticas de absorción de propano y propileno puros en estos adsorbentes. A una presión parcial de 100 kPa, ninguno de los adsorbentes tiene una selectividad de equilibrio mayor a 3, mientras que en los tamices moleculares 4A, se observan diferencias de por lo menos un orden de magnitud entre la difusividad de propano y propileno.

Para mejorar la selectividad de equilibrio hacia propileno, hemos probado nuevos materiales: mordenita y clinoptilolita intercambiadas y SBA-15 impregnada con diferentes cantidades de Ag^+. De estos materiales, la muestra Ag/SBA-15 con relación $Ag/SiO_2 = 0.5$ fue la mejor con una selectividad de equilibrio mayor a 10 a 100 kPa.

Una nueva unidad manométrica – cromatográfica fue construida para medir equilibrios de adsorción binarios en CMS4A y zeolita 4A y también para extender las posibilidades de medición de equilibrio de absorción hasta presiones de 500 kPa. Experiencias binarias de lecho fijo con diferentes fracciones molares de propano y propileno fueron realizadas en una unidad de laboratorio ya existente.

Equilibrio y cinética de absorción de gases puros se han medido en un monolito cuadrado que contiene zeolita 4A. Un modelo matemático para la adsorción de un componente para una mezcla adsorbato – inerte en un canal cuadrado de un monolito fue desarrollado. Su simplificación, aplicable solo para sistemas diluidos fue resuelta en gPROMS y otras simplificaciones fueron utilizadas para mezclas más concentradas.

Finalmente, experimentos y simulaciones de VSA-PSA fueron realizados en CMS4A y zeolita 4A. Un ciclo compuesto por 5 etapas fue utilizado: presurización, alimentación, lavado, despresurización y regeneración a 10 kPa donde es obtenido el propileno purificado. Este ciclo también fue utilizado para realizar simulaciones en Ag/SBA-15 = 0.5.

Para la Ag/SBA-15 = 0.5 comenzando con una mezcla equimolar, solo se ha obtenido propileno con alta pureza (>99%) con bajas recuperaciones (63%). Para el caso del CMS4A, comenzando con una mezcla 52/48 (propileno/propano), se ha producido propileno con baja pureza (80-85%) y con alta recuperación (alrededor de 90%). Experimentos de VSA-PSA fueron realizados con la zeolita 4A (CECA) con dos mezclas de diferentes relaciones de propano y propileno: 54/46 y 85/15. Se estudió el efecto de algunas variables de operación: tiempos de paso, temperatura, contenido de inerte y presión de alimentación. Aumentando la temperatura disminuye la pureza y aumentan la recuperación y productividad. El bajo valor de difusividad de propano en zeolita 4A permitió una fuerte disminución en el tiempo de lavado sin una disminución significante de la pureza. El tamaño de cristal de la muestra de zeolita 4A también fue variado; se ha hecho un estudio de VSA-PSA solo con simulaciones, basado en datos de equilibrio y cinética de adsorción de componentes puros medidos en cuatro muestras de zeolita 4A preparadas en laboratorio con tamaños desde 0.3 – 22 μm. Con cristales de zeolita 4A con un diámetro de 5μm, se podría obtener propileno grado polímero (99.61%) con recuperación de 83.1% y productividad de 2.25 mol/h.kg.

Acknowledgments

In this section I prefer to acknowledge the people that makes my work a nice thing to carry on, in the language I use to communicate with them.

Gostava de agradecer ao Prof. Alírio Rodrigues, não só pela orientação deste trabalho, mas pela sua amizade e pelo exemplo diário e ensino de como chegar ao fim do dia tendo dado 110%. También quería agradecer al Prof. Carlos Gigola que siempre será una referencia importante, no solo como investigador, sino como una excelente persona.

Aos professores do LSRE, em particular a Dra. Eugénia Macedo e ao Dr. José Loureiro, e aos funcionarios do DEQ, pelo seu apoio durante este tempo em Portugal.

También quería agradecer a los profesores, investigadores y funcionarios que trabajan en FUNDASUR y PLAPIQUI (Bahía Blanca, Argentina) por la ajuda prestada al comienzo de este trabajo. También quería agradecer a los profesores universitarios, secundarios y de la escuela primaria.

Agradeço a Fundação para a Ciência e Tecnologia e ao Fundo Social Europeu, pelo suporte financeiro através da bolsa SFRH/BD/11398/2002. Ao Governo Português e ao FEDER, pelo projecto POCTI/1999/EQU/32654. Também agradeço a bolsa ALFA NSPnet ALR/B7-3011.94.04-6.0018.9 com a que deu começo este trabalho.

A la gente que participó en el proyecto CYTED V.8, Catalizadores y Adsorbentes para el Medio Ambiente y Calidad de Vida, por las interesantes discusiones sobre materiales para la separación de propano y propileno, pero sobretodo por los muy buenos momentos compartidos.

To all the people that give me adsorbent samples: Santiago Tort (Grace Davison, Barcelona), Randall Victory (PQ, Kansas), Prof. Dr. Ing. H.-G Fritz (Sttutgart), Miguél Autié (CNIC, Cuba), Elena I. Basaldella y Norberto Firpo (CINCECA, La Plata) and Süd Chemie, CECA and Takeda Corporation. Da mesma forma queria agradecer a Dra. Daniela Silva (CEMUP, Porto) e ao Dr. Rui Fernandes (IBMC, Porto) pelo excelente trabalho na caracterização dos adsorventes.

Aos colegas que me ajudaram neste trabalho: José Antonio Silva, Avelino Da Silva, Rodrigo Davesac, Rui Soares, José Luciano Soares, Daniel Araújo, Ganesh Kumar, Marta Otero, Diana Azevedo, Vera Mata, Viviana Silva, Eduardo Oliveira, etc.

A todos mis amigos de Argentina por darme todo el apoyo necesario para esta travesía transoceánica.

Aos meus amigos do Porto por tratarem-me como se estivesse "na minha casa" ou melhor ainda: Mafalda, Isabel, Paulo, Manuela, Eduardo, Peter, Luciano, Jorge, Marta, Christopher, Ricardo, Susana, etc. Também queria agradecer a gente que foi a minha familia nestes anos fora do meu país: Diana, Epitacio, Gabi, Cecilia e Beatrice, Joyce e Alneu, Vera, Lino e Maria, Celina, Viviana, Daniel e Ganesh.

A minha esposa, Simone Cavenati, que me apoia dia a dia e com quem, com amor, comparte comigo os bons e os maus momentos. Ela também me deu o melhor dos presentes imagináveis: a nossa princesa Eugenia Giovanna. Ela é o centro da minha vida (soy yo, después de mi), e também é a maior fonte de inspiração que conheço.

Tengo que agradecer especialmente a quién fue el ejemplo de todo una vida de como dar lo mejor de lo mejor durante 24 horas por día. Simplemente, gracias MAMA.

A Dios, que por milagro o por acaso del destino, me ha colocado en esta posición privilegiada de poder agradecer a todas las personas que me ayudaron a lo largo de toda mi vida.

Contents

Abstract i

Resumo ii

Résumé iii

Resumen iv

Acknowledgments v

Chapter 1. Introduction 1

1.1 Relevance and Motivation 1

1.2 Objectives and Outline 4

Chapter 2. Adsorption equilibrium of propane and propylene on commercial adsorbents 13

2.1 Theoretical 13

2.2 Experimental Methodology 19

2.3 Silica Gel 24

2.4 Zeolite 5A 32

2.5 Dealuminated H-mordenite 40

2.6 Carbon Molecular Sieve 4A 43

2.7 Zeolite 4A 49

2.8 Conclusions 58

Chapter 3. Binary Propane-Propylene Adsorption Equilibrium on Commercial Adsorbents **67**

3.1 Introduction 67

3.2 Theoretical 68

3.3 Experimental 74

3.3.1 Data handling 77

3.3.2 Manometric Isotherm Equipment (MIE) description and measurement protocols 78

3.3.3 HeliumCalibration 82

3.3.4 Thermodynamic Consistency Test (TCT) 84

3.4 Binary adsorption equilibrium on zeolite 4A 87

3.5 Binary adsorption equilibrium on carbon molecular sieve 4A 92

3.6 Conclusions 97

Chapter 4. Adsorption kinetics of propane and propylene on commercial adsorbents **105**

4.1 Theoretical 105

4.1.1 Adsorption uptake 106

4.1.2 Zero Length Column, ZLC 113

4.1.3 Dilute breakthrough curves 116

4.1.4 Procedure for parameter fitting to experimental data 118

4.2 Experimental 119

4.3 Adsorbents 122

4.3.1 Silica Gel 122

4.3.2 Zeolite 5A pellets and crystals 132

4.3.3 Carbon Molecular Sieve 139

4.3.4 Zeolite 4A 153

4.4 Conclusions 165

Chapter 5. Adsorption equilibrium and kinetics on laboratory-made adsorbents 173

5.1 Zeolite 4A crystals 173

5.1.1 Background 173

5.1.2 Zeolite 4A synthesis and characterization 175

5.1.3 Adsorption equilibrium 176

5.1.4 Adsorption Kinetics 179

5.2 Exchanged natural zeolites 185

5.3 SBA-15 and silver exchanged SBA-15 189

5.3.1 SBA-15 synthesis and characterization 191

5.3.2 Adsorption equilibrium of pure gases 196

5.3.3 Adsorption kinetics of pure gases 203

5.4 Conclusions 209

Chapter 6. Adsorption of Propane and Propylene in Zeolite 4A Honeycomb Monolith 215

6.1 Introduction 215

6.2 Experimental 217

6.3 Adsorbent characterization 221

6.4 Theoretical analysis of adsorption equilibrium and kinetics 225

6.5 Adsorption equilibrium and kinetics of propane and propylene 240

6.6 Fixed bed adsorption experiments 247

6.7 Conclusions 254

Chapter 7. Separation of Propane and Propylene by Pressure Swing Adsorption, PSA **263**

7.1 PSA propane-propylene separation: state of the art 263

7.2 Adsorbent selection 266

7.3 Experimental 269

7.4 Theoretical 271

7.5 π-complexation adsorbents: Ag/SBA-15 = 0.5 284

7.6 Carbon Molecular Sieve 4A Takeda 290

7.7 Zeolite 4A CECA 301

7.7.1 Fixed bed experiments 303

7.7.2 Definition of operating variables 305

7.7.3 Temperature selection 306

7.7.4 VSA-PSA experiments with zeolite 4A: initial runs 307

7.7.5 Cyclic Steady State (CSS) and multiplicity of steady states 310

7.7.6 Improving the step times (process variables) 312

7.7.7 Effect of crystal size 318

7.7.8 Decrease in the nitrogen content 325

7.7.9 Effects of temperature 328

7.7.10 Effect of step pressures 332

7.7.11 Mixtures with ratio 85% propylene – 15 % propane 335

7.7.12 Degassing of the zeolite by heat treatment 338

7.8 Conclusions 341

Chapter 8. Conclusions and Recommendation for Future Work **353**

8.1 Conclusions of Ph.D. work 353

8.2 Recommendations for future work 359

1. Introduction

1.1 Relevance and Motivation

Propylene is one of the oldest petrochemical feedstock with high demand in the last years (Parkinson, 2004). Most of the propylene is used in polypropylene production (Bedell, 2003), which applies in multiple fields like trays, toys, packaging materials, etc. Other important applications are in the production of acrylonitrile (for synthetic fiber confection), oxo-chemicals (cumene, cresols and acrolein), propylene oxide (sterilization reactive) and ethylene-propylene rubber (EPR), which is used mainly as a replacement of the metal parts in automobiles and is one of the most rate-growing commodities of petrochemical industry.

The main source of propylene is the steam cracking of gas oil, where the main products are gasoline and fuel oil and propylene is obtained as a by-product. In 1992, 80% of the worldwide production was obtained by steam cracking (Ullman's Encyclopedia, 2003). The other source of propylene is the Fluidized Catalytic Cracking (FCC), which is the largest source of propylene in the United States, but has limited opportunities to increase its production because the ratio propylene – ethylene is close to the theoretical maximum. An emerging technology for propylene production is propane dehydrogenation. Although propylene supply is in much less amount than from steam cracking and FCC, the four licensed technologies (CATOFIN from ABB Lummus, OLEFLEX from UOP, FBD from Snamprogetti and STAR from Phillips Petroleum) are increasing the number of plants over the world, particularly in the Middle East. In the Iberian Peninsula (Tarragona, Spain), the first plant of propane dehydrogenation is a joint venture of BASF (51%, Germany) and Sonatrach (49% Algeria) with OLEFLEX technology, and made its start-up in 2003. This plant has a

production capacity of 350,000 tons/year of propylene from liquefied petroleum gas (LPG) from Algeria (supplied by Sonatrach).

Table 1.1. Propylene composition requirements for polymer and chemical grade [*].

Composition	Chemical grade	Polymer grade
Propylene, %	92-95	99.5-99.8
Propane, ppm	Remainder	Remainder
Acetylene, ppm	< 10	< 2
Ethylene, ppm	< 20	< 20
Ethane, ppm	< 2000	< 100
Propyne, ppm	< 20	< 5
Propadiene, ppm	< 20	< 5
C_{4+}, ppm	< 1000	< 10
Hydrogen, ppm	< 10	< 10
Nitrogen, ppm	< 50	< 50
Oxygen, ppm	< 5	< 5
Carbon monoxide, ppm	< 5	< 5
Carbon dioxide, ppm	< 5	< 5
Sulfur, ppm	< 5	< 1
Water, ppm	< 25	< 10

*** Determined by gas chromatography. Source: Ullman´s Encyclopedia, 2003.**

The production of propylene-based polymers requires high purity propylene. The product specification of polymer-grade propylene is detailed in Table 1.1. The amount of other unsaturated olefins and particularly acetylene and dienes has to be very

small to avoid undesired polymer cross-linking or even rubber production. For the production of the other chemicals, chemical grade propylene is used. Chemical-grade propylene specification is also listed in Table 1.1.

In the olefin separation train of a petrochemical plant, propylene is separated from propane in the C_3-splitter tower as the overhead product. The C_3 splitter is commonly the fourth distillation column in the separation train (after de-methanizer, de-ethanizer and de-propanizer columns). A large number of theoretical plates and large refluxes are required to obtain polymer grade propylene because relative volatility of both compounds is very similar (1.06 to 1.1 depending on operative conditions). The simplified flowsheet of the C_3 splitter is shown in Figure 1.1. The condenser and compressor are not smaller as draw in the figure because they have to account for a recycle to product ratio around 12. The large energy requirements are due to this high reflux ratio; i.e., the large power consumed by the compressor unit.

The operating conditions of a C_3-splitter depend strongly on the heat network integration in the refinery. Conditions for a column with a feed of 100 tons/h (60% propylene, 38% propane, 2% butane) to produce polymer grade propylene requires 232 plates, a reflux ratio of 12.6 and operates at 40-60ºC at 25 bars (Gokhale et al., 1995). The C_3 splitter with such number of plates result in a very tall column that can be divided into two smaller units in windy regions. If the industry is not inserted in a petrochemical complex and buys refinery propylene (60 – 70% propylene balanced with propane + 4% of other paraffins) for further propylene utilization, lower temperatures, ranging from –15ºC to 10ºC are preferred.

Due to the high costs of the separation by distillation, many alternatives were explored over the years (Eldridge, 1993). One of the first alternative processes tested was the liquid separation using Ag^+ and Cu^+ ions (Dunlop et al., 1968; Marcinkowsky et

al., 1979). Chloride and nitric salts were tested. The propylene is retained in the salt by π-complexation bonds with the cation and then separated by flushing the saturated liquid. This process is not used in industry basically due to the very high cost of the silver salts and the relatively complex pre-purification of the propane-propylene stream before contact with the silver salt; hydrogen sulfide and acetylene react irreversibly with silver ions producing hazardous compounds (Marcinkowsky et al., 1979). The hazardous nature combined with the global economics of this process was high enough to prefer distillation.

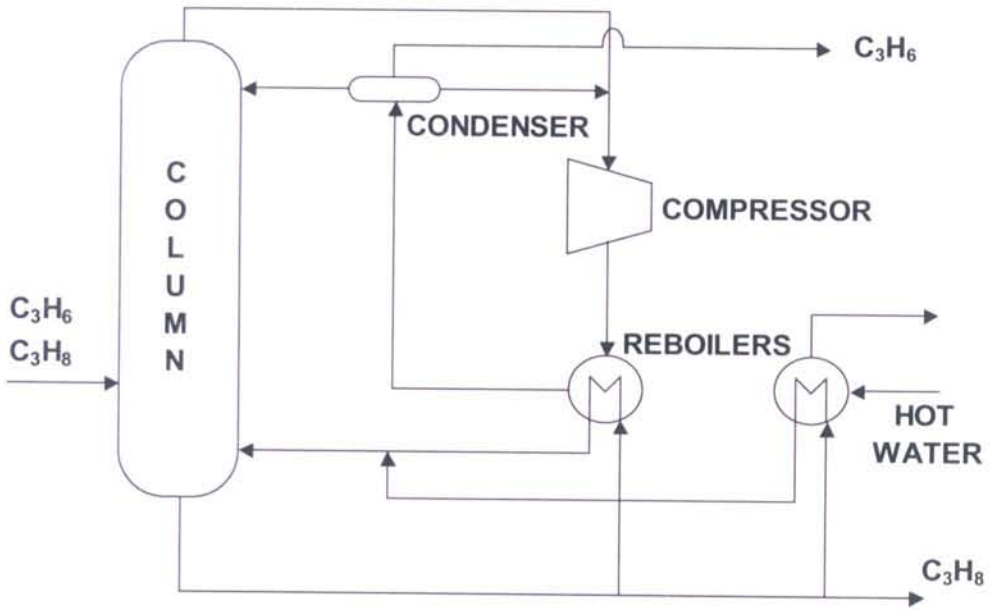

Figure 1.1. Simplified schematic flowsheet of the C_3 splitter with integrated heat scheme.

1.2 Objectives and Outline

Most of the research done in propylene separation over the last thirty years was to improve the distillation process. Many works in the 90´s dealt with adsorption as an alternative process. In this process, the aid of a material with a high surface area, the

adsorbent, is used to retain propylene mainly by interactions of the double bond with some surface groups. As propane is also retained in different amounts by physical forces too, a certain selectivity of the adsorbent towards propylene exists. Due to lack of exact information of the adsorbent, it is very difficult to simulate the pure gas adsorption in a solid, particularly those with non-uniform structures. For this reason, the investigation of each adsorbent requires a minimum set of laboratory measurements of equilibrium and kinetics of adsorption of pure gases. This kind of research (propane and propylene pure gas adsorption) was not new and in fact one of the first works in adsorption dealt with the adsorption of both hydrocarbons on silica gel (Lewis et al., 1950a, b). A discussion of the different adsorbents tested for this separation will be described in the following chapters.

The objective of this work was to achieve polymer grade propylene using an alternative process to distillation: Pressure Swing Adsorption (PSA). The difficulty to overcome in this process is to separate molecules with very similar properties where the main difference is in the polarizability, higher in propylene due to the double bond (Da Silva, 1999).

The PSA separation process involves a fixed bed column filled with an appropriate adsorbent that adsorbs preferentially propylene and also produces purified propane. When the adsorbent is saturated with propylene, by changing the pressure of the system, the olefin is desorbed from the column partially regenerating the bed to start a new cycle. This process is known in industry and is actually used in air separation to produce nitrogen and oxygen, n-iso paraffin separation, hydrogen purification and air drying as some examples (Yang, 1987; Schröter, 1993; Ruthven et al., 1994; Silva, 1998). Specifically about PSA process for propane-propylene separation, many works from different groups have been patented. The first one dealt with zeolite 4A and is at

the origin of the CATOFIN® process (Ramachandran et al., 1994). With this process, propylene purity higher than 99% was obtained with recovery higher than 85% starting with a stream containing 12% of propane. In a subsequent patent, the PSA was placed after the cracker thus receiving hydrogen and C_1-C_3 for ethylene and/or propylene enrichment (Ramachandran et al., 1998). Although only one example was given, in this case purity and recovery were not as good as in the previous case. A similar case was later presented for ethane-ethylene separation using partially exchanged zeolite 4A (Bülow et al., 2001). Three different works have been published using ALPO-14 in PSA-VSA propylene enrichment reporting high purity propylene (>99%) with recovery in excess of 90% starting from a mixture 70-30% propylene-propane, although no PSA-VSA experiment was reported in these works to validate the simulations (Cheng and Wilson, 2001a-b; Cheng et al., 2002). The area of π-complexation adsorbents, although vast can be roughly summarized in three works that condense much of the work done up to now on this topic. The patent by Yang and coworkers involves the preparation by various techniques of different supports containing ionic transition metals (mainly Ag^+) as complexing agent; the best performance has been obtained using silver nitrate dispersed in silica with high purity propylene and recovery around 45 % (Yang et al., 2002). Other adsorbents using Ag^+ were obtained dispersing silver nitrate in bentonite compounds with some promoters by proprietary process (Cho et al., 2001). With one of these adsorbents, purity of ethylene higher than 99% was obtained although no indication of recovery was given (Cho et al., 2002).

This work is not the starting point at the Laboratory of Separation and Reaction Engineering (LSRE) using this process for propane-propylene separation. In fact an extensive work, including the installation and operation of a PSA laboratorial unit, was performed by Dr. F. A. da Silva using zeolite 4A and zeolite 13X as adsorbents (Da

Silva, 1999). Also for this reason, an extensive review on the history of this separation was omitted and his work remains as a complete reference for this task. In this work a set of commercial and laboratory made adsorbents were tested for this separation. In some adsorbents, the PSA cycle previously proposed was modified to enhance the overall PSA performance.

At the very early stages of this work it was noticed that the adsorbent selectivity was the key factor to improve. Following that, one of the aims of this work was to extend the existing database of potential adsorbents for propane-propylene separation. For that purpose, adsorption characteristics (adsorption equilibrium and kinetics) of pure propane and propylene were measured in several available commercial adsorbents: wide pore (low surface area) silica gel (WSG), narrow pore (large surface area) silica gel (NSG), zeolite 5A, dealuminated H-mordenite, carbon molecular sieve 4A and zeolite 4A. As the separation with zeolite 4A is kinetically limited, additional experiments involving crystals with different sizes were performed to evaluate the best crystal size for this particular separation. Also, a monolithic honeycomb containing zeolite 4A as adsorbent was tested to assess the effect of pressure drop in a column and to see the real effect in the crystal size of this zeolite in the performance of a PSA. Additionally, some other materials were tested: natural clinoptilolites and mesoporous ordered silica SBA-15. The π-complexation bond of the olefin molecule with silver ion (Yang, 2003) was evaluated in the SBA-15 mesoporous ordered silica (Zhao et al., 1998) with two different silver loadings.

This work is divided into eight chapters. Chapter 1 is a brief introduction, pointing out the relevance and motivation and the objectives of the work. Chapter 2 deals with adsorption equilibrium (measurements and analysis) of pure gases on the commercial adsorbents cited above. Chapter 3 contains the results of adsorption

equilibrium measurements of the binary mixture of propane and propylene in carbon molecular sieve (Takeda) and zeolite 4A (CECA) extrudates by a manometric-chromatographic unit developed for this purpose during the course of this work. Chapter 4 summarizes the experimental results of adsorption kinetics at infinite dilution of pure propane and propylene in various commercial adsorbents. Most of the measurements were performed by the ZLC (Zero Length Column) technique (Eic and Ruthven, 1988). Also other methods like dilute breakthrough curves and adsorption uptake were used for kinetic measurements, particularly in the case of very slow diffusing species. Chapter 5 deals with the adsorption equilibrium and kinetics of pure gases in the laboratory-made adsorbents mentioned above: natural clinoptilolites cation exchanged in laboratory, SBA-15 and the two samples of SBA-15 loaded with different contents of silver and four different samples of zeolite 4A crystals with different crystal sizes. Chapter 6 is focused on the characterization of a ceramic honeycomb monolith prepared by extrusion of zeolite 4A crystals and the ceramic material. The monolith was characterized by measuring adsorption equilibrium and kinetics of pure propane and propylene and further measuring adsorption dynamics in breakthrough experiments at several hydrocarbon concentrations. Chapter 7 shows experimental and modeling results in the PSA unit available at the LSRE. Simulation results are presented for the best sample of Ag^{+}-impregnated SBA-15 due to the small amount of material prepared. Experimental data in the laboratory PSA unit were measured using zeolite 4A and carbon molecular sieve (CMS) 4A. In the CMS sample several binary breakthrough experiments were performed showing a very difficult separation at high propylene concentration, confirmed by PSA experiments with a 52/48 propylene to propane ratio.

Separation runs using zeolite 4A were performed with two mixtures with different propylene to propane ratio: 54/46 and 85/15, with much better results. In this

case the effect of several operating variables (step times, temperature, inert content and feed pressure) in the unit performance were studied. Finally, Chapter 8 has the conclusions of this work and some suggestions for future work.

References

Bedell, M. W.; Ruziska, P. A.; Steffens, T. R. *On-Purpose Propylene From Olefinic Streams*. Tulane Engineering Forum, ExxonMobil Chemical Company, **2003**.

Bülow, M.; Guo, C. J.; Shen, D.; Fitch, F. R.; Shirley, A. I.; Malik, V. A. *Separation of Alkenes and Alkanes*. U.S. Patent 6,200,366, **2001**.

Cheng, L. S.; Wilson, S. T. *Process for Separating Propylene from Propane*. U.S. Patent 6,293,999, **2001a**.

Cheng, L. S.; Wilson, S. T. *Vacuum Swing Adsorption Process for Separating Propylene from Propane*. U.S. Patent 6,296,688, **2001b**.

Cheng, L. S.; Padin, J.; Rege, S. U.; Wilson, S. T.; Yang, R. T. *Process for Purifying Propylene*. U.S. Patent 6,406,521, **2002**.

Cho, S. H.; Han, S. S.; Kim, J. N.; Choudary, N. V.; Kumar, P.; Bhat, S. G. T. *Adsorbents, Method for the Preparation and Method for the Separation of Unsaturated Hydrocarbons for Gas Mixtures*. U.S. Patent, 6,315,816, **2001**.

Cho, S. H.; Han, S. S.; Kim, J. N.; Chue, K-T; Choudary, N. V.; Kumar, P. *Adsorbents and Methods for the Separation of Ethylene and Propylene and/or Unsaturated Hydrocarbons from Mixed Gases*. U.S. Patent 6,468,329, **2002**.

Da Silva, F. A. *Cyclic Adsorption Processes: Application to Propane / Propylene Separation*. Ph.D. Dissertation, University of Porto, Portugal, **1999**.

Dunlop, A. K.; Blytas, G. C.; Bell, E. R. *Separation of Hydrocarbons by cuprous salts*. U.S. Patent 3,401,112, **1968**.

Eic, M.; Ruthven, D. M. A New Experimental Technique For Measurement of Intracrystalline Diffusivity. *Zeolites*, **1988**, 8, 40-45.

Eldridge, R. B. Olefin/Paraffin Separation Technology: a Review. *Ind. Eng. Chem. Res.*, **1993**, 32, 2208-2212.

Gokhale, V.; Hurowitz, S.; Riggs, J. B. A Comparison of Advanced Distillation Control Techniques for a Propylene/Propane Splitter. *Ind. Eng. Chem. Res.*, **1995**, 34, 4413-4419.

Lewis, W. K.; Gilliland, E.; Chertow, B.; Cadogan, W. Pure Gas Isotherms. *Ind. Eng. Chem.*, **1950a**, 42, 1326-1332.

Lewis, W. K.; Gilliland, E.; Chertow, B.; Cadogan, W. Hydrocarbon Gas Mixtures. *Ind. Eng. Chem.*, **1950b**, 42, 1319-1326.

Marcinkowsky, A. E.; Keller, G. E. II; Verma, S. K. *Olefin Separation Process*. U.S. Patent 4,174,353, **1979**.

Parkinson, G. Mastering Propylene Production. *Chem. Eng. Process*, **2004**, 8-11.

Ramachandran, R.; Dao, L. H.; Brooks, B. *Method of Producing Unsaturated Hydrocarbons and Separating the Same from Saturated Hydrocarbons*. U.S. Patent 5,365,011, **1994**.

Ramachandran, R.; Dao, L. H. *Process for Recovering Alkenes from Cracked Hydrocarbon Streams*. U.S. Patent 5,744,687, **1998**.

Ruthven, D. M.; Farooq, S., Knaebel, K. S. *Pressure Swing Adsorption*, VCH Publishers, New York, **1994**.

Schröter, H.-J. Carbon molecular sieves for gas separation processes. *Gas Sep. and Pur.*, **1993**, 7, 247-251.

Silva, J. A. C. *Separation of n/iso – Paraffins by Adsorption Process*. Ph.D. Dissertation, University of Porto, Portugal, **1998**.

Ullmann's Encyclopedia of Industrial Chemistry; 7ª Edition, Wiley-VCH, Verlag GmbH & Co..KGaA, **2003**.

Yang, R. T. *Gas Separation by Adsorption Processes.* Butterworths, Boston, **1987**.

Yang R. T. *Adsorbents. Fundamentals and Applications,* New Jersey: J. Wiley, **2003**.

Yang, R. T.; Padin, J.; Rege, S. U. *Selective Adsorption of Alkenes Using Supported Metal Compounds*. U.S. Patent 6,423,881, **2001**.

Zhao, D.; Feng, J.; Huo, Q.; Melosh, N.; Fredrickson, G. H.; Chmelka, B. F.; Stucky, G. D. Triblock Copolymer Syntheses of Mesoporous Silica with Periodic 50 to 300 Angstrom Pores. *Science*, **1998**, 279, 548.

2. Adsorption Equilibrium of Propane and Propylene on Commercial Adsorbents

In an adsorption separation process, the adsorption equilibrium behavior of the pure components to be separated is the fundamental information needed for the modeling and equipment design.

In this chapter, we will present experimental data of propane and propylene on several commercial adsorbents. The adsorbents studied were two samples of silica gel (with wide and narrow pores), zeolite 5A extrudates, highly dealuminated H-mordenite, carbon molecular sieve 4A, and zeolite 4A. Results for crystals of zeolite 5A are also presented. Experimental data were fitted with different models for learning purposes and also with the intention of having the possibility of a good description of equilibrium at low pressures, extrapolation of equilibrium at non-measured temperatures or pressures together with the minimum of fitting parameters.

2.1 Theoretical

When a certain species, here called adsorbate, is allowed to be in contact with a clean porous solid, named adsorbent, some of the molecules of the fluid phase get "stacked", or adsorbed, in the surface of the solid. As this is a spontaneous phenomenon some heat is released. Although this is a dynamic process, after some time, a steady state is achieved: the adsorption equilibrium state. The adsorption equilibrium expresses the degree of interaction of the adsorbate with the surface of the adsorbent by specific physical or chemical forces. For a separation process where adsorption and desorption are involved, the interest is mainly focused on physical interactions or weak chemical

interactions, where the energetic barrier can be easily reversed by a change of operating conditions, i. e., temperature or pressure variations or a combination of both.

Adsorption equilibrium is typically studied at a fixed temperature by varying the concentration, or pressure in the case of gas adsorption (isotherm measurements). Another strategy less applied is the measurement of the amount adsorbed at a fixed pressure by varying the temperature (isosteres).

For the interpretation of adsorption isotherms many models are available in literature. In this work we will focus only in some models that can be applied to isotherms of Type I in the IUPAC classification, i.e., isotherms having a single saturation limit corresponding to monolayer formation and without capillary condensation and/or multilayer adsorption.

The models considered below were divided in two categories: the exponential family of models where adsorption is considered as a volumetric process of pore filling and the Langmuir reducible models where adsorption is viewed as a layer formation until the saturation capacity is achieved.

The exponential family of isotherms is grouped in the theory of volume filling of micropores (TVFM), initially developed by Polanyi (Polanyi, 1932; Jaroniec, 1997). The fundamental parameter of the theory is the adsorption potential $A = R_g T \ln(P^o/P)$ where P^o is the saturated vapor pressure. The physical meaning of the adsorption potential is the work required to remove a molecule from its location in the adsorbed phase to the gas phase (considered as ideal). The TVFM is based on the invariance of the adsorption potential with temperature. This was experimentally confirmed for microporous adsorbents but not completely satisfactory for large pore and non-porous adsorbents. The Polanyi's characteristic curve qV_s versus $f(A/V_s)$ is the locus of all the isotherms for a particular adsorbate – adsorbent system, where q is the adsorbed phase

concentration (expressed in mmol/g) and V_s is the volume of the adsorbate considered as a saturated liquid.

Dubinin related the adsorption potential with the differential molar work of adsorption, $-\Delta G$. The fundamental assumption is that the degree of filling $\theta = q/q_{max}$ is a function of the adsorption potential A, such that $\theta = f(A/E_o)$. The generalized Dubinin equation assumes that the pore size distribution is described by a Gamma function and can be expressed as (Hutson and Yang, 1997)

$$q = q_{max} \exp\left[-\left(\frac{R_g T \ln \frac{P^o}{P}}{E_o}\right)^d\right] \qquad [2.1]$$

where q_{max} is the maximum loading, E_o is the characteristic energy of adsorption and d is the third fitting constant of the equation. The constant d was initially supposed to be an integer. Its physical meaning has been attributed to the number of degrees of freedom that the adsorbed molecules lost, being one or nearly one for hydrocarbons adsorbed on silica gel and nearly 3 for zeolites (Suzuki, 1990).

The Dubinin – Radushkevich equation assumes that the pore size distribution is Gaussian ($d = 2$).

It has to be pointed out that the generalized Dubinin model is not thermodynamically correct, predicting an incorrect Henry limit. This problem is common to all the exponential isotherms (Jaroniec, 1984), but the prediction of multicomponent adsorption is good enough if the isotherm fits well the experimental data (Richter et al., 1989).

The other way to describe adsorption is based on a layer-by-layer mechanism. Most of the different published models that can be grouped in this category can be derived thermodynamically from the Gibbs isotherm:

$$A_s\left(\frac{\partial \pi}{\partial P}\right)_T = \frac{R_g T}{P} q' \qquad [2.2]$$

where A_s is the adsorbent surface area, q' is the number of adsorbed molecules by area of adsorbent and π is the spreading pressure which corresponds to the difference in surface tension between a clean surface and a surface covered with adsorbate (Myers and Prausnitz, 1965). The spreading pressure cannot be measured experimentally and to give a practical application to the Gibbs isotherm, an equation of state to describe the adsorbed phase behavior has to be introduced and then integrated. The Langmuir model, together with many others can be derived in this way (Yang, 1987; Do, 1998).

Langmuir gave the first interpretation of adsorption equilibrium in 1918 as a dynamic equilibrium with equal rates of adsorption and desorption (Langmuir, 1918). The model assumes that the adsorbent is composed of identical localized sites and each site can accommodate only one molecule. Also, the energy of adsorption is constant in all the sites and there is no interaction between adsorbed molecules. This model is expressed by

$$\frac{q}{q_{max}} = \frac{K_{eq} P}{1 + K_{eq} P} \qquad [2.3]$$

where K_{eq} is the adsorption constant, P is the pressure of the system, q is the amount adsorbed, q_{max} is the maximum adsorption capacity of the adsorbent (only considering monolayer adsorption). The constant K_{eq} is expressed as the Van't Hoff equation (Eq. 2.4) where K_{eq}^{o} is the adsorption constant at infinite temperature and $(-\Delta H)$ is the heat of adsorption on the homogeneous surface. As adsorption processes are always exothermic, K_{eq} decreases with temperature. The value of K_{eq}^{o} should be as small as possible, implying that at infinite temperature, the adsorption is almost zero.

$$K_{eq} = K_{eq}^{o} e^{(-\Delta H)/R_g T} \qquad [2.4]$$

When the amount adsorbed is far small compared with the adsorption capacity of the adsorbent or when the pressure of the gas is very small, the model reduces to the Henry type equation

$$q = q_{\max} K_{eq} P = HP \qquad [2.5]$$

The Henry relation is the linear model that describes adsorption equilibrium of any gas in the low-pressure range. A good Henry constant measurement or prediction is the key for a correct multicomponent equilibrium prediction (Talu, 1998).

As expressed above, the equilibrium description of the Langmuir model is completely idealized. The model does not account for any interaction between the adsorbate, mobile adsorption, different adsorption energies or any kind of heterogeneity in the solid, etc. Many models were published to account for these effects. Fowler and Guggenheim add the interaction effect between adsorbing molecules (Fowler and Guggenheim, 1939). When the adsorbed molecules are free to move on the adsorbent surface (mobile adsorption), the Langmuir equation is modified to a model known as Volmer isotherm (Volmer, 1947). The temperature independent parameter q_{max} was also modified to account for thermal expansion at higher temperatures (Yang and Doong, 1985). With the aim of accounting for adsorbent heterogeneity and optimize the computational time of multicomponent prediction, the FastIAS (Fast Ideal Adsorbed Solution) was developed (O´Bryen and Myers, 1985). The purpose of this work is not to review different adsorption equilibrium models and many good references with a large extent of possibilities to describe adsorption equilibria can be found in literature (Ruthven, 1984; Yang, 1987; Malek and Farooq, 1996; Do, 1998; Silva, 1998).

One of the most used models to describe adsorption equilibrium behavior is the one proposed by Toth (Toth, 1971). The equation relating the pressure and the amount adsorbed is:

$$q = \frac{q_{max} K_{eq} P}{\left[1 + (K_{eq} P)^n\right]^{1/n}} \qquad [2.6]$$

The parameter n ranges between 0 and 1 and is a measurement of the heterogeneity of the solid while q_{max} and K_{eq} have the same meaning as in the Langmuir model. The model is Langmuir reducible for $n = 1$ when the solid is homogeneous. The adsorption constant varies with temperature with a Van't Hoff dependence as expressed by eq. [2.4]. This isotherm was used for many different systems showing great ability for fitting experimental data (Valenzuela and Myers, 1989) and has also been successfully applied for propane and propylene on zeolites 13X and 4A (Da Silva and Rodrigues, 1999).

Another model that deserves a special attention is the multisite Langmuir model for homogeneous adsorbents derived by Nitta and coworkers using statistical thermodynamic arguments and initially used for treatment of hydrocarbon equilibrium data on microporous adsorbents (Nitta et al., 1984). This model has also been capable to fit correctly adsorption equilibrium data of $C_1 - C_{10}$ paraffins in zeolite 5A (Silva and Rodrigues, 1999).

If we neglect adsorbate – adsorbate interactions, the model can be expressed as

$$\theta = K_{eq} P (1 - \theta)^a \qquad [2.7]$$

where $\theta = q/q_{max}$ is the fractional amount of adsorbate in the adsorbed phase, q_{max} is the saturation capacity and a is the number of neighboring sites occupied by each adsorbate molecule. The Van't Hoff law describes the temperature dependence of the equilibrium constant K_{eq}. When the number of neighboring sites is unity ($a = 1$), the Nitta model reduces to the Langmuir equation. The main drawback of the Nitta equation is its implicit form, which will imply high computational time for parameter optimization. However, once the parameters are optimized the equation can be written as $P = f(\theta)$ for

any other future use, i.e., breakthrough curve modeling. Also, the theoretical basis of the derivation together with its flexibility for experimental data fitting makes it a suitable model to use in equilibrium interpretation. Also, it has a direct extension to multicomponent systems that will be described later.

A more general theory based on the mass-action law, where the Nitta model is a special case, has been recently proposed (Bhatia and Ding, 2001). This model was in fact a new derivation of the Vacancy Solution Theory developed in the 80's using the Flory-Huggins activity coefficients (Cochran and Danner, 1985).

The isosteric heat, Q_{ST}, corresponds to the energy of adsorption released in the adsorption process. It is a function of temperature and coverage and is described by the Clapeyron equation:

$$Q_{ST} = -R_g T^2 \left[\frac{\partial \ln P}{\partial T} \right]_q \qquad [2.8]$$

Note that the derivative has to be evaluated at constant amount adsorbed. In order to obtain a confident value of the isosteric heat of adsorption, isotherms at least at three temperatures have to be measured.

2.2 Experimental Methodology

Adsorption equilibrium was measured by two methods: gravimetric and manometric. The gravimetric equipment, already available at the laboratory, allows experimental data to be collected up to atmospheric pressure (or 100 kPa). With the manometric equipment, the pressure range can be increased up to 500 kPa. Of course the gravimetric device has better accuracy in the measurement of the amount adsorbed since it is not influenced by an error in the pressure transducer. On the other hand, the manometric equipment has many advantages: basically, it is a very cheap unit to be

built, the quantity of adsorbent in each measurement is higher diminishing the risk of heterogeneity of the sample and it allows to measure equilibrium in the whole pressure range that will be used in the PSA (Pressure Swing Adsorption) unit. Also, in a manometric equipment the dead volumes can be minimized and the thermal effects can be measured locally (a thermocouple can be inserted in the sample) thus providing all the conditions for complete measurement of the diffusion kinetics in the same experiment. The advantages and disadvantages of both methods has been extensively discussed elsewhere (Do, 1998; Rouquerol, et al., 1999)

The gravimetric device used was a CI – Robal microbalance (Willshire, UK) operated in closed system. A complete description of the system is done in Figure 2.1. The microbalance has an accuracy of $\pm 10^{-5}$ grams while the pressure transducer (Lucas-Schaevitz) is $\pm$ 0.04 kPa. Temperature is controlled within $\pm$ 1K and the limit of the oven is 1273 K, although the limit of the whole equipment should be round 800 K due to heat losses. The pressure range of the equipment is from vacuum to atmospheric pressure limited by the microbalance unit. A vacuum of 10^{-5} kPa was used in this work, imposed by the vacuum pump. The system is different from the one reported before and the simpler array was obtained for the specific case of working in close system where pulses of pressure are being injected periodically to the unit, instead of a continuous flow of an inert stream carrying the adsorbate (Silva, 1998).

Before any equilibrium measurements, the adsorbent has to be activated. By activation we understand the protocol used for water and air desorption prior to the hydrocarbon adsorption measurements. As water is very strongly adsorbed in most of the adsorbents, this procedure was always performed under vacuum ($< 10^{-5}$ kPa) at high temperature. The high temperature activation and entire protocol depends on the adsorbent structure and on the gases that will be adsorbed.

At least three adsorption equilibrium experiments were performed for each adsorbent. When atmospheric pressure was reached, desorption run begins. After desorption, a new activation procedure was performed to ensure the same thermal treatment of the adsorbent in all the experiments.

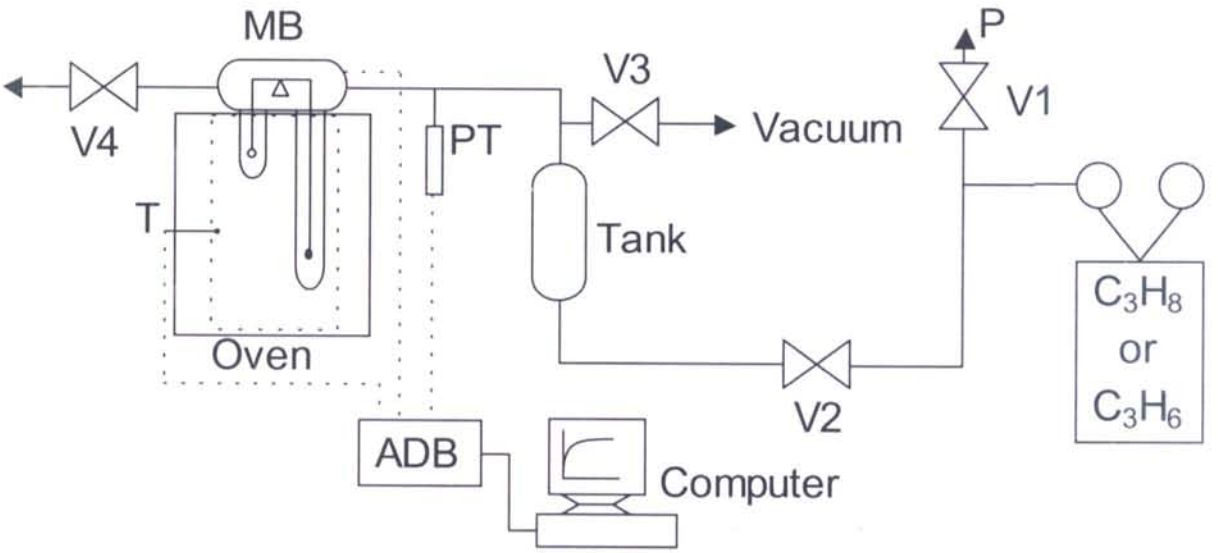

Figure 2.1. CI-Robal scheme for adsorption equilibrium measurements. V1-V4 are on-off valves, ADB is the Acquisition Data Board, PT is the Pressure Transducer, T is a thermocouple for controlling the oven temperature and MB is the microbalance.

The manometric unit was built for binary equilibrium measurements and will be designed as MIE (Manometric Isotherm Equipment). Pure gas adsorption equilibrium is also easily measurable in this unit. Its original design was modified to allow reliable kinetic measurements at high temperatures. A description of the final design that was used for all the experiments is shown in Figure 2.2. The temperature was measured within ± 1K. The accuracy of the pressure transducer (Lucas-Schaevitz) was ± 0.05 kPa while its range was from 0 to 500 kPa. A four-head diaphragm vacuum pump (ILMVAC, Germany) allows a vacuum of at least 10^{-5} kPa. The K-thermocouple (Omega, USA) was inserted in the middle of the adsorbent column. Pressure and temperature signals were recorded in a computer by means of an Advantech acquisition

data board (Advantech, USA). A complete description of the equipment and the procedure used for pure and binary adsorption equilibrium and pure gas kinetic measurements will be made in following chapters. Activation was also performed in vacuum at high temperatures.

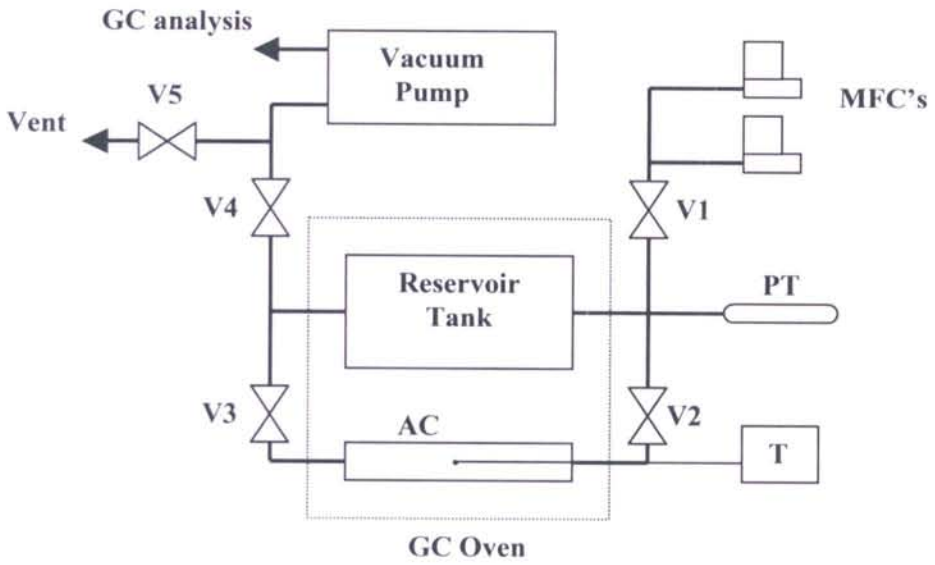

Figure 2.2 – MIE scheme. AC: adsorption chamber, PT: pressure transducer, MFC: mass flow controller, Vi: valves.

All gases used in this report were provided by Air Liquide: propane N35, and propylene N24 (purity greater than 99.95 and 99.4%, respectively).

The models described in the theoretical section were employed for fitting experimental data. For this purpose, a non-linear set of equations (one equation per equilibrium point) has to be solved simultaneously. In all the cases, for each equilibrium point, the mathematical function for the parameter optimization was the Square of Residuals (SOR) defined by (Malek and Farooq, 1996):

$$SOR(\%) = 100 \sum \left(q_{experimental} - q_{calculated} \right)^2 \qquad [2.9]$$

From the mathematical dependence of the equilibrium constant with temperature that is described by the Van't Hoff equation very small values of the parameter K_{eq}^{o} are

expected. This was a serious limitation for some software that could not make any optimization until this parameter was fixed (most of them was because accuracy of 10^{-8} was near the K_{eq}^{o} value). The solution to this problem was to solve this multi-parametric nonlinear fitting in MATLAB (Matrix Laboratory, The MathWorks. Inc.), which provides by default an accuracy of 10^{-16} for all the variables involved. Also, the optimization was made by a robust routine called *fmins*, which employs the Nelder Mead Simplex Method of direct search (Morgan, 1997).

Adsorption equilibrium data of pure propane and propylene was measured in the following adsorbents:

- Narrow Silica Gel, NSG (Silica gel 127, lot 9800608601, Grace Davison, Spain) at 303, 323 and 343 K.
- Wide Silica Gel, WSG, (Silica gel W127, lot 98026312.01, Grace Davison, Spain) at 303, 323 and 343 K.
- Zeolite 5A pellets, Z5A, (Sylobead 522, lot 9900268401, Grace Davison, Spain) at 323, 343, 373 and 423 K.
- Zeolite 5A crystals, Z5Ac, (5A Activated Powder, lot 602961079901, PQ Corp, USA) at 323, 343, 373 and 423 K.
- H-Mordenite with Si/Al = 30, H-MOR, (free sample (30g), Süd Chemie, Germany) at 323 and 343 K.
- Carbon Molecular Sieve 4A, CMS4A, (MSC 4A, lot M965, Takeda Corp, Japan) at 343, 373 and 423 K.
- Zeolite 4A, Z4A, (Zeolite 4A Extrudates, lot 2097, CECA, France) at 373, 423 and 473 K.

2.3 Silica Gel

Silica gel has the nominal chemical formula $SiO_2 \cdot x\,H_2O$ and is a solid, amorphous form of hydrous silicon dioxide. The structure of silica gel is an interconnected random array of polymerized silicate particles (micelles), which define its final properties. Micelles are spheroidal with 10 – 2 nm in diameter resulting in high surface areas of ca. 300 – 1000 m^2/g SiO_2, respectively. Control of the surface area, porosity, and surface chemistry of silica gel has led to numerous and diverse uses (Ullmann's Encyclopedia, 2003).

Pure silica gel has a hydroxylated surface covered with silanol groups. These hydroxyl groups are neither very acidic nor basic, with $pK_a \approx 6$ and an isoelectric point at ca. pH 2. The hydroxylated surface is hydrophilic and adsorbs moisture that can be desorbed thermally at 373 – 473 K. Higher temperature results in irreversible lost of (-OH) bonds of the structure damaging the gel.

Silica gel was tested as adsorbent for the propane – propylene separation by Lewis et al.,1950a. The equilibrium data reported suggested a separation factor around 4 in the range of pressure and temperature studied (270-370 K and 0-1 atm). All pure component isotherms have Type I behavior and could be correlated by the Polanyi's theory of pore filling. Recent reports with silica gel with surface area over 600 m^2/g show excellent agreement with the data of Lewis (Ghosh et al., 1993; Järvelin and Fair, 1993).

In this work equilibrium data of propane and propylene over two samples of Grace Davison silica gel are reported; one with a high superficial area and narrow pore diameter, named as NSG, and the other with low superficial area and wider pores, named WSG. The samples were analyzed by mercury intrusion (Instituto Pedro Nunes, Coimbra) to determine the macropore size distribution.

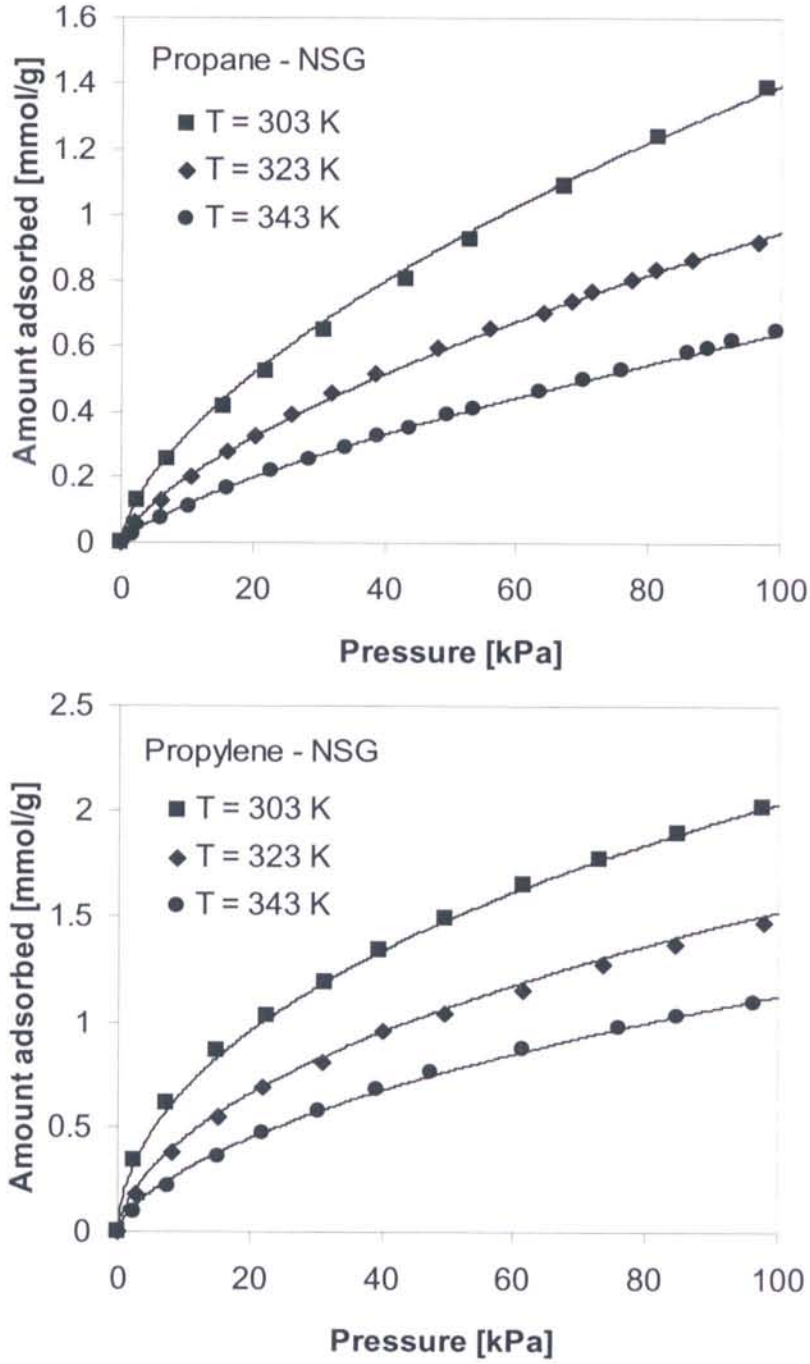

Figure 2.3. Adsorption equilibrium of propane and propylene on NSG at 303, 323 and 343 K. Solid lines are the generalized Dubinin model fitting.

For the WSG the average value was recorded at 120 Å. For the NSG sample, the average diameter value cannot be detected because the minimum value of detection is 60Å. In this case, we used the value of 44Å given by the customer. Other significant

physical properties of both materials were provided by the customer and are reported in Table 2.1. The pellet density was measured in our laboratory by mercury picnometry at ambient pressure and temperature (Suzuki, 1990) and compared with the mercury intrusion value at 1.0 atm. The results are in very good agreement and in the other adsorbents tested this technique will be applied.

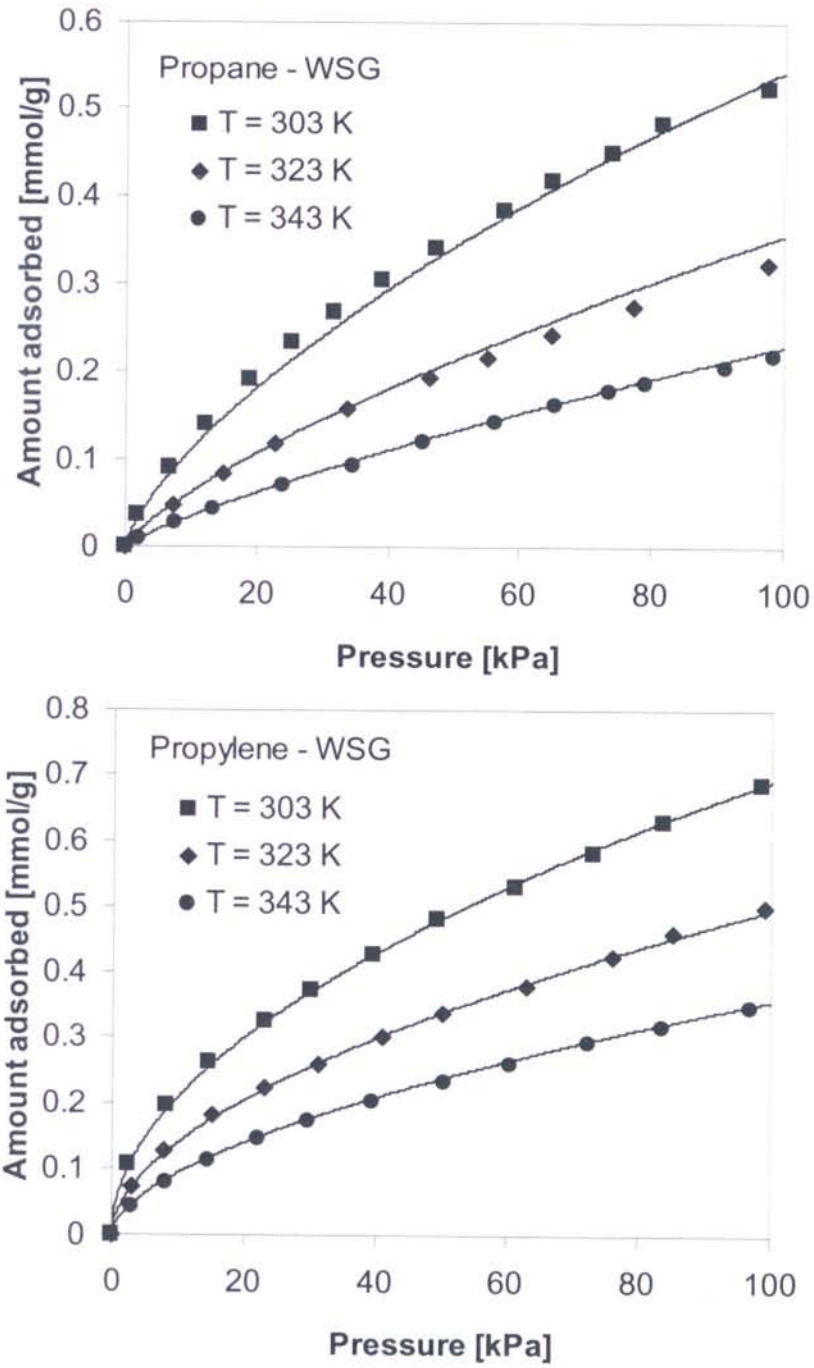

Figure 2.4. Adsorption equilibrium of propane and propylene on WSG at 303, 323 and 343 K. Solid lines are the generalized Dubinin model fitting.

Figure 2.3 shows equilibrium data obtained for propane (a) and for propylene (b) on NSG at 303, 323 and 343 K, while Figure 2.4 shows corresponding data on WSG. In the case of NSG the equilibrium was measured in the CI-Robal gravimetric unit and also in the manometric equipment.

Numerical values were reported elsewhere (Grande and Rodrigues, 2001). A comparison between the data obtained in the MIE equipment and the gravimetric data is shown in Figure 2.5 for the case of propane equilibrium on NSG. Note that the lower temperature reported with the MIE was 308 K, which was the minimum temperature that can be controlled by the oven of the equipment. All data collected show an excellent agreement between the gravimetric and the manometric techniques.

Table 2.1. Physical properties of Grace Davison NSG and WSG pellets.

Adsorbent	Narrow silica gel	Wide silica gel
Surface Area (m^2/g)	780	340
Average Pore Diameter (Å)	44	120
Average pellet porosity	0.4	0.58
Bulk Density (g/cm^3)	0.72	0.40
Particle Density (g/cm^3)	1.26	0.92
Solid Density (g/cm^3)	2.10	2.18
Water adsorption (%wt, 50%RH)	30	13

When new experimental data of a previously investigated system are obtained, the first thing to do is to compare them with other published data. The Polanyi potential

is a very useful tool for this purpose; for the same adsorbate – adsorbent all the experimental data should fall in the same characteristic curve. The procedure used for representing the experimental points was described previously (Moon and Tien, 1993). Fugacities were approximated with partial pressures because data at low pressure (gravimetric data) were represented. Polanyi plots are presented in Figure 2.6a for narrow silica gel and Figure 2.6b for wide silica gel. Excellent agreement was observed when NSG was compared with previous data (Lewis et al., 1950b; Malek and Farooq, 1995). In Figure 2.7 the adsorbed phase concentration was also expressed as q' in $mmol/m^2$ to normalize the data of both adsorbents (NSG and WSG). Minor differences were observed between both materials indicating the same kind of physical interaction for propane and propylene with the silica gel surface. Comparison of WSG with other published data was not possible because no previous works with C_3 hydrocarbon adsorption on a low superficial area silica gel were found.

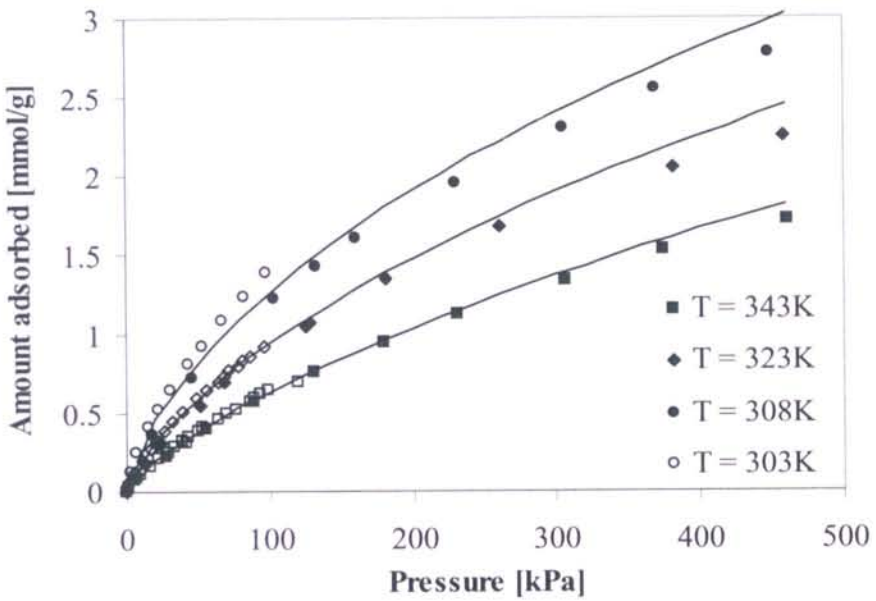

Figure 2.5. Adsorption equilibrium of propane on NSG at 303, 323 and 343 K determined by gravimetric and manometric techniques. Solid lines are the generalized Dubinin model fitting with the parameters obtained from the low-pressure data fitting.

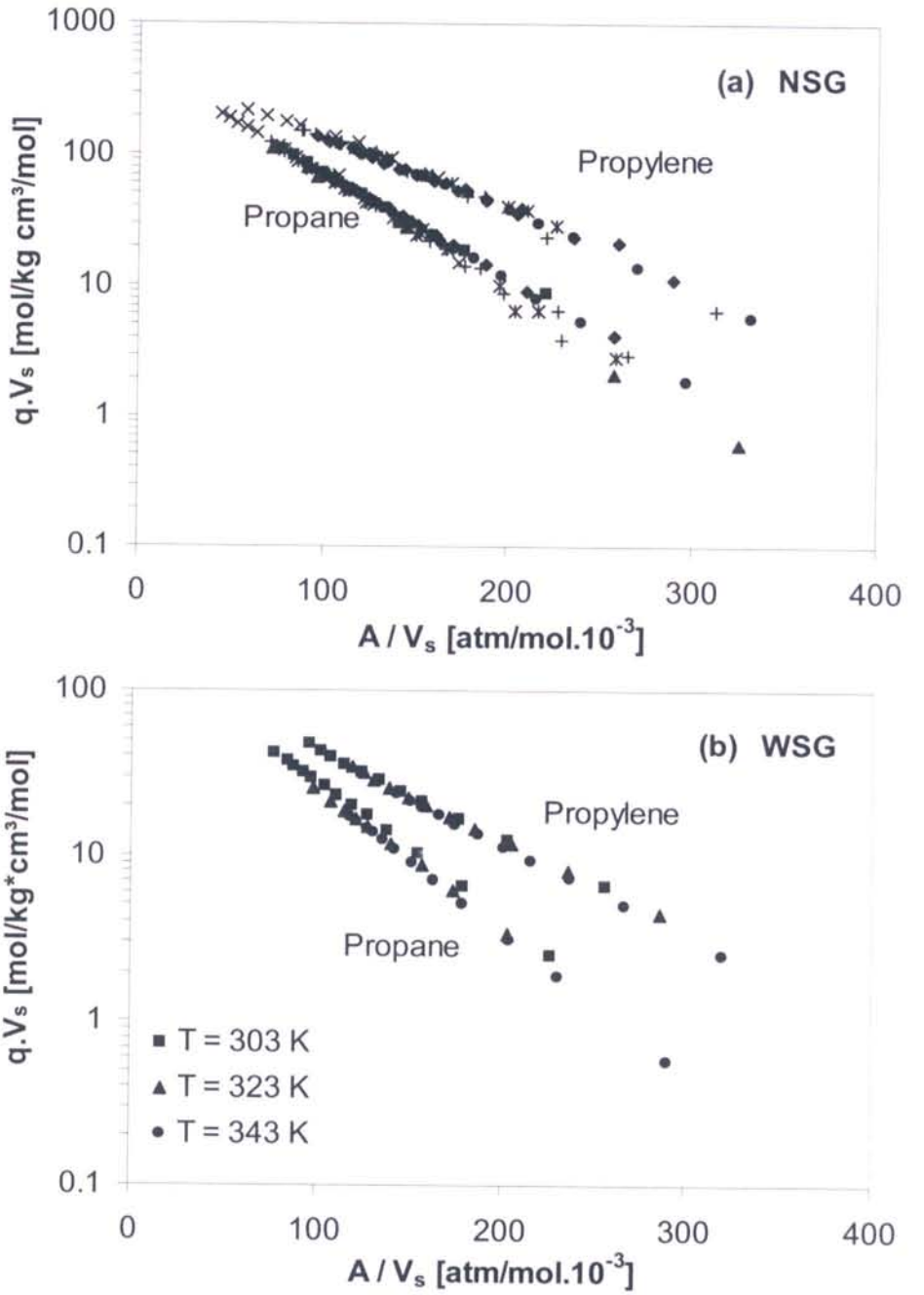

Figure 2.6. Polanyi's characteristic curves, $q.V_s$ versus A/V_s, of propane and propylene: (a) C_3H_6 and C_3H_8 on Narrow Silica Gel (NSG), (b) C_3H_6 and C_3H_8 on Wide Silica Gel (WSG). (a): This work, ■ 303 K; ▲323 K; ● 343 K; x Lewis et al (1950), 278 K; + Lewis et al (1950), 293 K ; * Lewis et al (1950), 343 K; ▲ Malek and Farooq (1995); (b) All points correspond to this work.

The values fitted with the generalized Dubinin model are represented as solid lines in Figures 2.3 and 2.4. As shown in the figures, the fitting is very good in the

temperature and pressure range studied. One can expect, however, higher deviations at very low pressures, where the Dubinin model is thermodynamically inconsistent. In the case of NSG, the fitting of the MIE data was done using the initial parameters estimated with the gravimetric data in the 0-100 kPa pressure range. We can see that the predictive nature of the Dubinin isotherm is excellent and that the Polanyi's theory of the characteristic curve can be used with great confidence. We proved that for any silica gel material, at least for both C_3, the only data required is the superficial area that may vary for different materials.

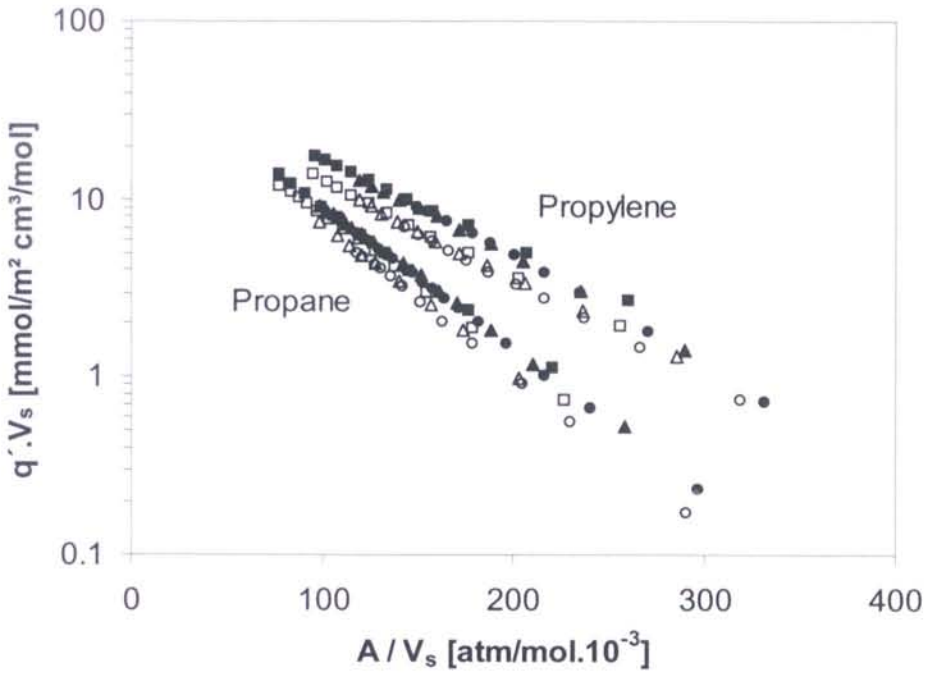

Figure 2.7. Normalized Polanyi's characteristic curves, q'.V_s versus A/V_s, of C_3H_6 and C_3H_8 on NSG and WSG (q' represented in mmol/m²). Solid points are NSG and empty points are WSG.

Table 2.2 shows the parameters of the Dubinin equation for propane and propylene on NSG and WSG estimated using the low-pressure gravimetric data. The value of the constant *d* is near one showing that the adsorbate (propane and propylene) looses only one degree of freedom when adsorbed in silica gel as expected for hydrocarbons with molecular sizes at least five times smaller than the pore size (Suzuki,

1990). For NSG the characteristic energy of adsorption of propylene is 7.09 kJ/mol, 2 kJ/mol higher than that for propane (5.05 kJ/mol). For WSG this parameter is nearly the same for both gases (4.66 and 4.78 kJ/mol for propane and propylene, respectively). It can be seen from the experimental isotherms that the interactions of both gases are not the same. It can be concluded that in the WSG-hydrocarbon systems, the parameters of the Dubinin model have no physical meaning, even when the fitting of experimental results is very accurate. This can be due to problems of the model when dealing with mesoporous adsorbents (Hutson and Yang, 1997).

Table 2.2. Fitting parameters of the Generalized Dubinin model applied to experimental data at 303, 323 and 343 K

System	q_{max} [mmol/g]	E_o [J/mol]	d	(SOR%)
C_3H_8 – NSG	4.680	5047	1.153	0.284
C_3H_6 – NSG	4.925	7089	1.262	0.713
C_3H_8– WSG	2.045	4667	1.158	0.187
C_3H_6– WSG	2.646	4781	0.993	0.036

The heats of adsorption for all systems were estimated with the Clausius-Clapeyron relation and are presented in Figure 2.8. The isosteric heat of adsorption decreases with the degree of coverage, with a logarithmic decay. Predictions of the isosteric heats with the Dubinin equation lead always to a logarithmic decay expression. The decay in the isosteric heat can be explained by the heterogeneity of the adsorbent (at low coverage, the molecules adsorb in the more active sites blocking them and leaving the less active sites for higher coverages (Thomas and Thomas, 1967). In NSG, for coverages higher than 0.4 mmol/g the difference in the heats of adsorption of

propylene and propane corresponds to the difference in the energies of adsorption (E_o). The isosteric heat of adsorption was also calculated from other data (Lewis et al., 1950b). The same behavior was observed with differences of ± 3kJ/mol when compared with the NSG adsorbent. Decrease in the isosteric heat of adsorption was also reported for higher alkanes adsorbed on silica gel (Gordon and Glandt, 1998). The heats of adsorption at 100 kPa were approximately twice the value of the heat of vaporization.

With the data presented on both materials, we can conclude that they adsorb propane and propylene according to their area, and so for PSA applications it will be better to use the narrow pore material, NSG that has the higher surface area.

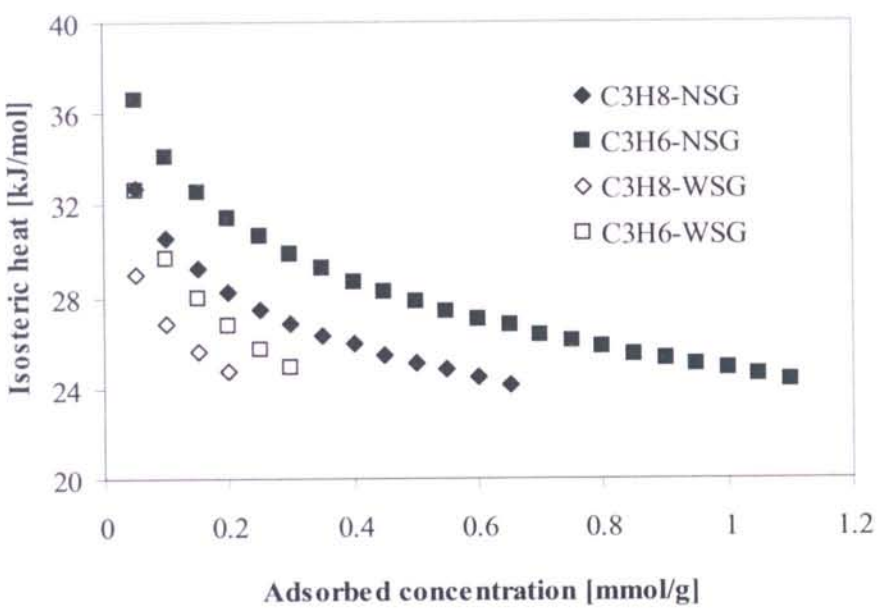

Figure 2.8. Isosteric heat of adsorption calculated by the Clausius – Clapeyron equation at 303 K as a function of the adsorbed phase concentration.

2.4 Zeolite 5A

Zeolite 5A is commonly used for the separation of iso-normal paraffins (Silva, 1998) by size exclusion. The zeolite cage of the calcium zeolite 5A has an internal volume of 776 $Å^3$ formed by a cubic lattice of sodalites. The free aperture of the pore is

4.2 Å allowing the passage of molecules with a kinetic diameter less than 4.9 Å (Ullman's Encyclopedia, 2003). Zeolite 5A was also tested for the propane / propylene separation, but not in a large extent (Järvelin and Fair, 1993). Adsorption of $C_1 - C_4$ was reported (Loughlin et al., 1990) but propylene adsorption data are scarce (Järvelin and Fair, 1993; Ruthven and Derrah, 1972); it has been reported that coke can be formed in the adsorption process under certain conditions (Boucheffa et al., 1997).

In this work, we report adsorption equilibrium of propane and propylene on zeolite 5A pellets and also in zeolite 5A crystals. The 5A pellets were kindly provided by Grace Davison (Barcelona, Spain) and will be called Z5A while PQ Corporation (Kansas, USA) provided the pure crystals that will be named Z5Ac.

The activation of the samples was carried out in vacuum ($<10^{-5}$ kPa) at 593 K for 10 hours. The heating rate to reach this temperature was 1 K/min. This activation temperature is the one recommended for zeolites in general (Breck, 1974).

The samples were analyzed by mercury intrusion (Instituto Pedro Nunes, Coimbra) to determine the macropore size distribution. A single peak at 500 Å was found indicating that this is the average macropore diameter. The other physical properties are listed in Table 2.3. Crystal density of 1.57 g/cm^3 was assumed from other reports (Ruthven and Derrah, 1972). The structure of the zeolite crystals in both samples was studied by Scanning Electron Microscopy (SEM) and the results are presented in Figure 2.9 together with the X-ray diffraction patterns to show the chemical composition of both samples. Both zeolites are calcium zeolites and the only difference between them is the magnesium and Si/Al ratio, but that is only because of the inert clay binder used in the preparation of the pellets. The crystal radius in both materials is near the same being 1.1 and 1.0 μm for the Z5A and Z5Ac samples, respectively.

The experimental adsorption equilibrium data were obtained in the CI-Robal unit at four different temperatures (343, 373, 423 and 473 K) for propane and propylene over zeolite 5A pellets and crystals; they are presented in Figures 2.10 and 2.11, respectively (Grande et al., 2002). In both samples, the most adsorbed gas is propylene and all isotherms are Type I with complete reversibility. The selectivity for propylene is better at higher temperatures.

The loading in the zeolite pellets is in agreement with previous data (Ruthven and Derrah, 1972). In other works previously reported, the adsorption capacity of propane and propylene were lower but no indication of the amount of zeolite in the

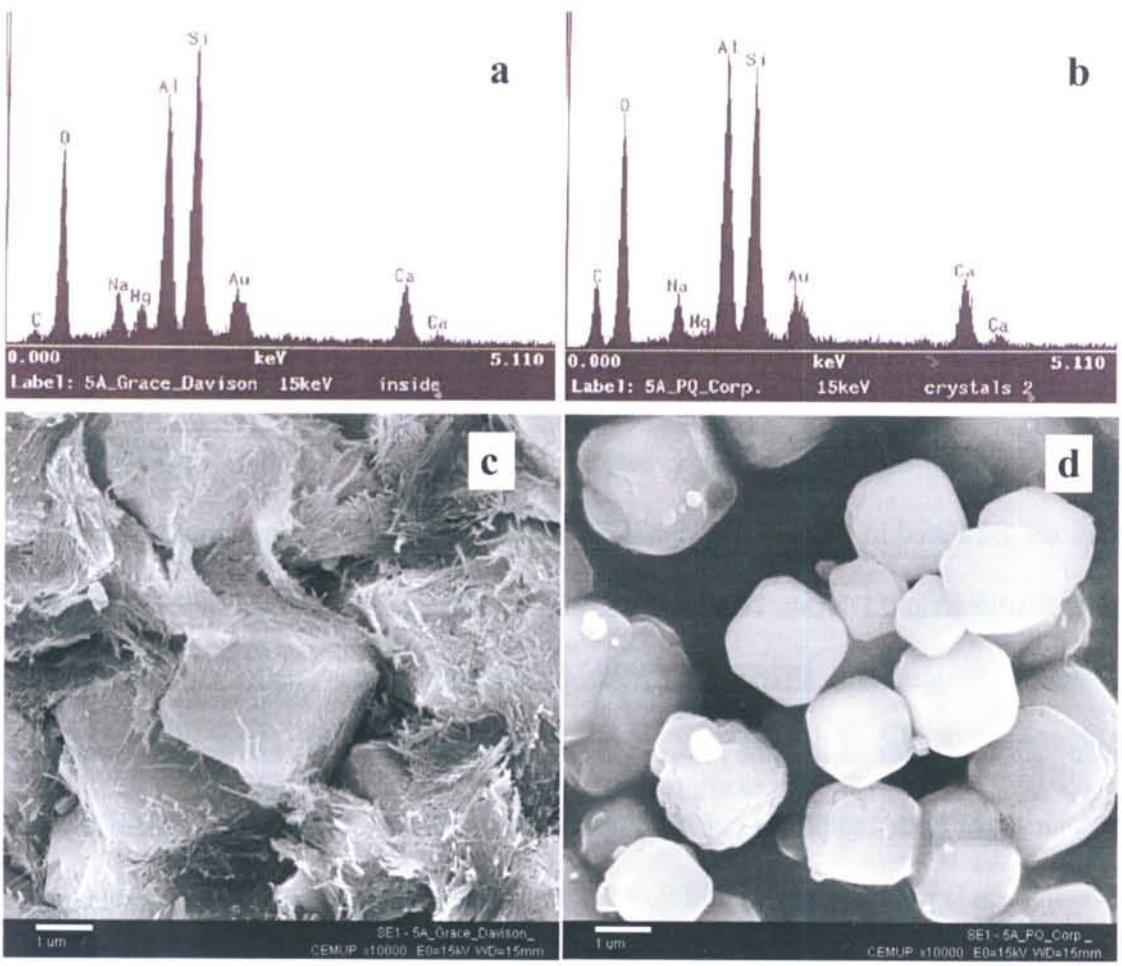

Figure 2.9. Zeolite 5A morphology and composition. *a* and *b*, Grace Davison 5A pellets and PQ Corp. crystal X-ray diffraction patterns, *c* and *d*, pellets and crystal morphology.

pellets was given (Youngquist et al., 1971; Järvelin and Fair, 1993). The activation procedure can also influence the loading capacity reported in those papers.

Table 2.3. Physical properties of zeolite 5A samples

Adsorbent properties	Value
Pellet solid density [g/cm^3]	1.74
Pellet density [g/cm^3]	1.13
Pellet porosity	0.35
Mean pore radius [Å]	500
Crystal radius (pellets) [μm]	1.1
Crystal radius (crystals) [μm]	1.0
Crystal density [g/cm^3]	1.57 [a]

[a] Assumed value (Ruthven and Derrah, 1972).

In Figures 2.10 and 2.11, the dashed lines represent the Toth isotherm while the solid lines correspond to the generalized Dubinin model. The fitting parameters of both models are given in Table 2.4. The Dubinin equation fits the data very well, considering that it has only three parameters. The characteristic energy, E_o for propane and propylene in both samples is nearly the same, showing interactions of the same kind. The parameter *d* has values higher than two in all the cases indicating that the molecules loose at least two degrees of freedom (Suzuki, 1990). Small differences in the parameter *d* can be due to fitting errors.

The fitting with the Toth model has also a good quality. For this model four constants were necessary and the computation time was higher than for the Dubinin isotherm. The extra computing time is due to the fact that the convergence of the Simplex Method is more difficult because of the exponential description (with two

parameters) of the adsorption constant. The same problem was observed in all Langmuir reducible models. The parameter n shows a strong heterogeneity of the adsorbent and the maximum loadings were slightly higher than those predicted by the Dubinin model.

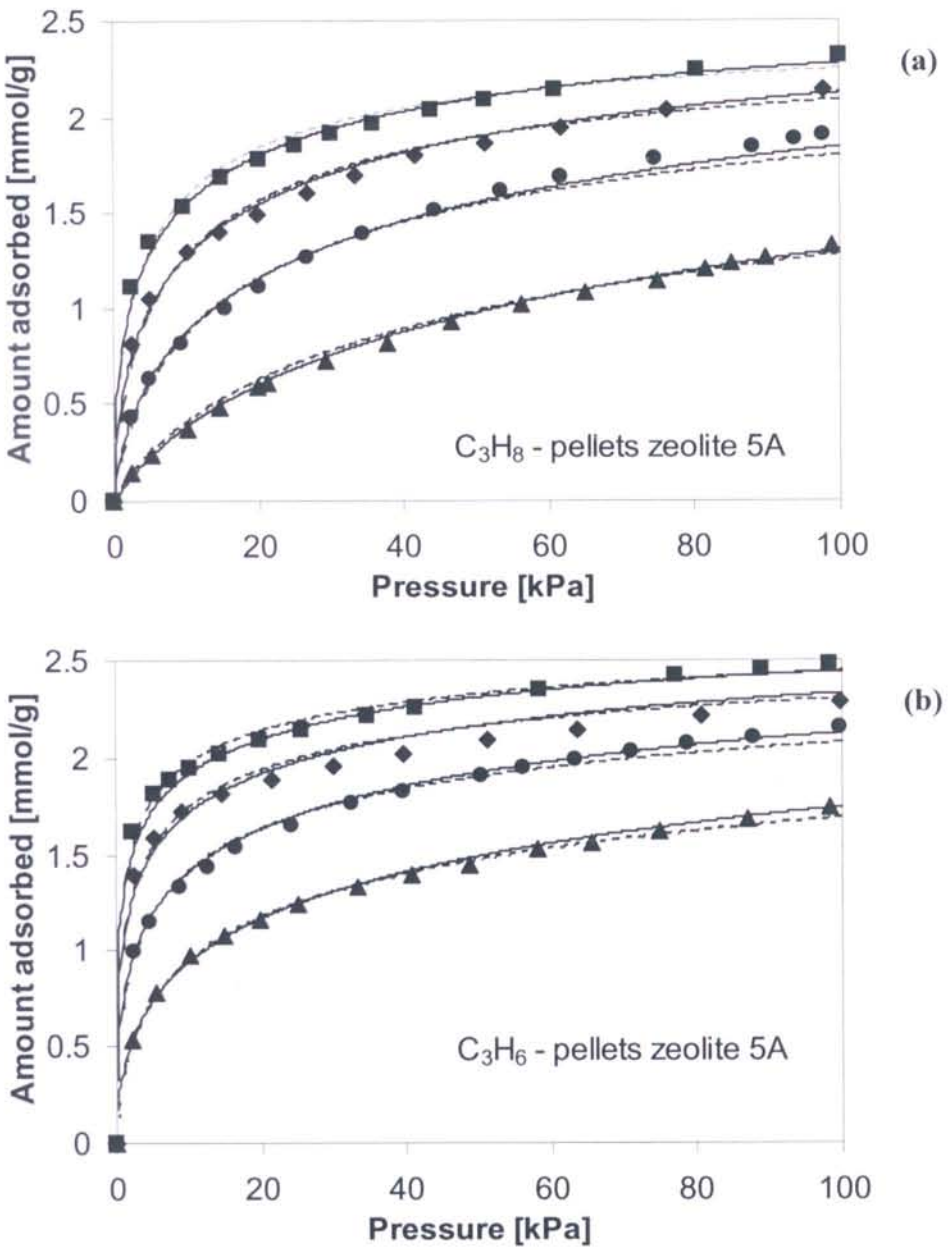

Figure 2.10: Adsorption equilibrium isotherms in 5A zeolite pellets (Grace Davison) of: (a) propane, (b) propylene. Symbols: ■ T = 323 K, ◆ T = 343 K, ● T = 373 K, ▲ T = 423 K. Solid lines – Dubinin model and dashed lines – Toth model.

Assuming that in both zeolites crystals (within the pellets from Grace Davison and crystals from PQ Corp) the adsorption loading is the same for propane and for propylene, we calculate the amount of clay binder of the pellets. The ratio of amount adsorbed in pellets and crystals of propane and propylene as a function of pressure is shown in Figure 2.12. The amount adsorbed on the pellets is 71% of the crystals indicating that the amount of inert is 29%.

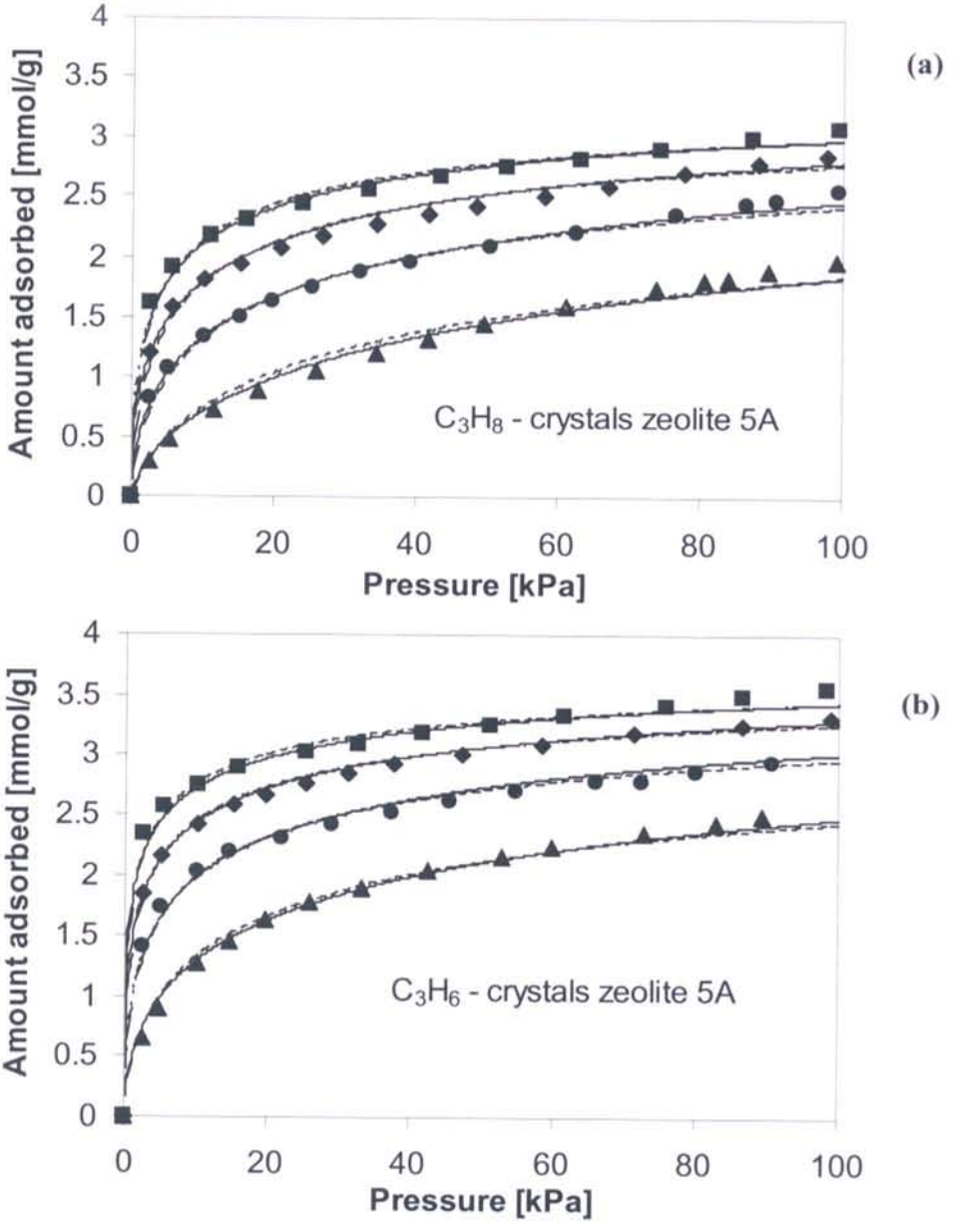

Figure 2.11: Adsorption equilibrium isotherms in 5A zeolite crystals (PQ Corp.) of: (a) propane, (b) propylene. Symbols: ■ T = 323 K, ◆ T = 343 K, ● T = 373 K, ▲ T = 423 K. Solid lines – Dubinin model and dashed lines – Toth model.

Isosteric heat of adsorption was estimated using the Clausius – Clapeyron equation with the experimental data described by the Dubinin isotherm. The isosteric heat plotted as a function of the amount adsorbed is similar for pellets and crystals in both gases; see Figure 2.13.

Table 2.4 – Generalized Dubinin and Toth parameters for propane and propylene

Generalized Dubinin model parameters			
System	q_{max} [mmol/g]	E_o [kJ/mol]	d
C_3H_8 – crystals	3.37	19.4	2.24
C_3H_6 – crystals	3.75	23.4	2.28
C_3H_8 – pellets	2.56	18.2	2.47
C_3H_6 – pellets	2.71	23.4	2.13

Toth model parameters				
System	q_{max} [mmol/g]	K_{eq}^{o} [kPa]$^{-n}$	$(-\Delta H)$ [kJ/mol]	n
C_3H_8 – crystals	3.64	4.30×10^{-3}	15.2	0.46
C_3H_6 – crystals	4.02	1.33×10^{-2}	14.0	0.40
C_3H_8 – pellets	2.61	4.94×10^{-4}	19.9	0.58
C_3H_6 – pellets	2.93	2.02×10^{-3}	13.4	0.36

A complete set of at least eight isotherm experiments was repeated with the same sample. No significant changes were observed. No coke formation at higher temperatures was noticed; otherwise, in the second set of experiments the adsorption capacity would has been lower and the kinetic experiments would be different (Silva et al., 2000). Also, the isotherm measurements should not be completely reversible.

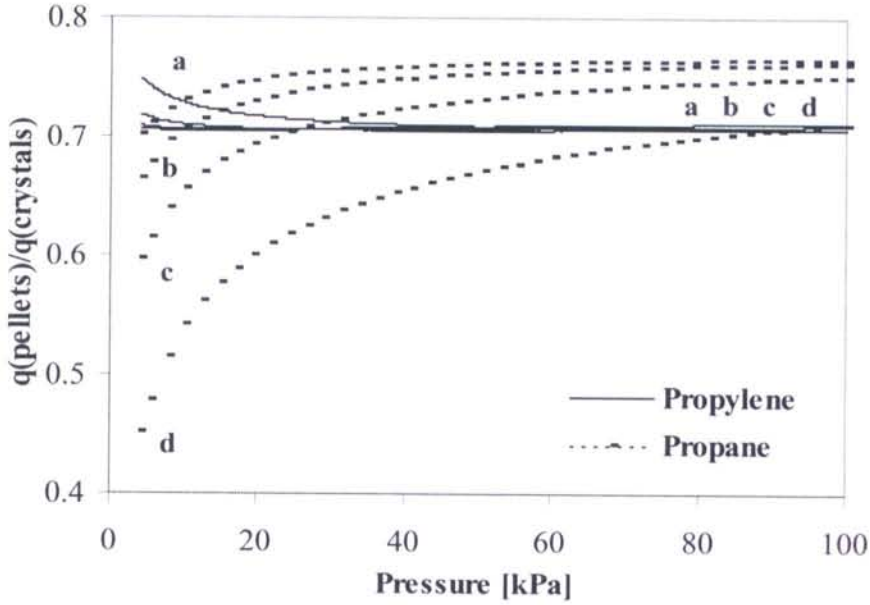

Figure 2.12 – Inert binder determination from equilibrium data: pellet / crystal loading ratio as a function of pressure. (a) 323 K; (b) 343 K; (c) 373 K and (d) 423 K. Full lines – propylene; dashed lines – propane.

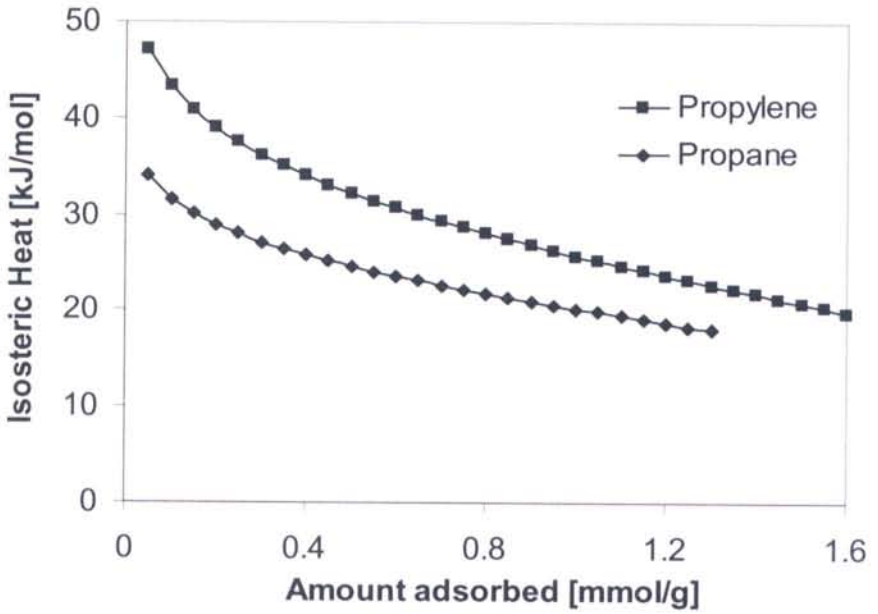

Figure 2.13 – Isosteric heat of propane and propylene on zeolite 5A pellets as a function of amount adsorbed.

2.5 Dealuminated H-mordenite

Mordenite is one of the members of the zeolite group of minerals. Its crystal structure is orthorhombic. There are two types of channels with different geometry and sizes; continuous and elliptical channels with dimensions of 6.7 x 7.0 Å while the secondary channels, commonly named as pockets, are 2.9 x 5.7 Å separated by 2.8 Å restrictions. These dimensions were for natural Na-Mordenite (Breck, 1974). The structure of H-Mordenite is presented in Figure 2.14. For H-MOR, the pores are larger allowing adsorption of other molecules. For dealuminated mordenites, the dealumination process is supposed to enlarge the main and side – pockets. This effect is more pronounced for the side – pockets than for the main channels (Moreno and Poncelet, 1997). Mordenite uses reported in literature are mainly in the catalysis area and include the NOx reduction (Chung, 1999; Marcus and Cormier, 1999) and exhaust gas treatment. Only scarse literature is published in the use of mordenite in an adsorption process (Izumi, 2002).

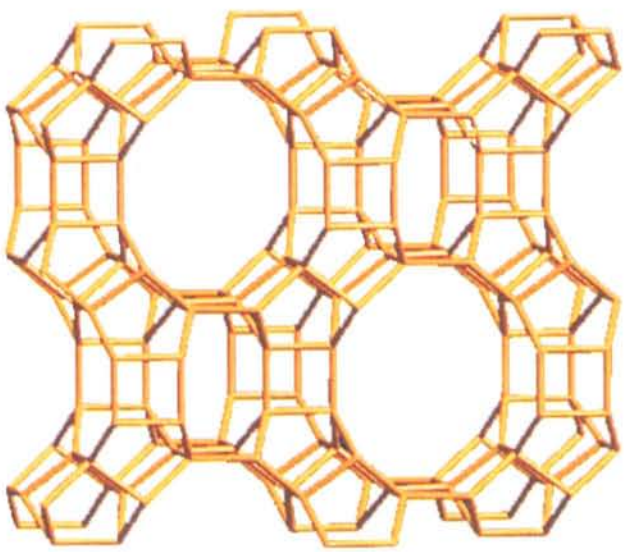

Figure 2.14. Crystal structure of H-mordenite.

The same procedure as with the other materials was applied for isothermal measurements in the MIE equipment. An activation temperature of 593 K for 12 hours in vacuum (< 10^{-5} kPa) was used, as with the other zeolites. The measurements of propylene at 343 K are shown in Figure 2.15. After the initial retention of propylene, the measurements are not completely reversible. According to some publications where there is come degree of irreversibility, the sample was activated and a new measurement was done (second). The behavior was observed again and also for in a third experiment the amount retained was decreasing. No more experiments were performed. Note that the term "adsorption equilibrium" or "isotherm" is not being employed because a large material retention is happening and consequently a reaction is taking place. The same trend were measured at 323 K and 373 K.

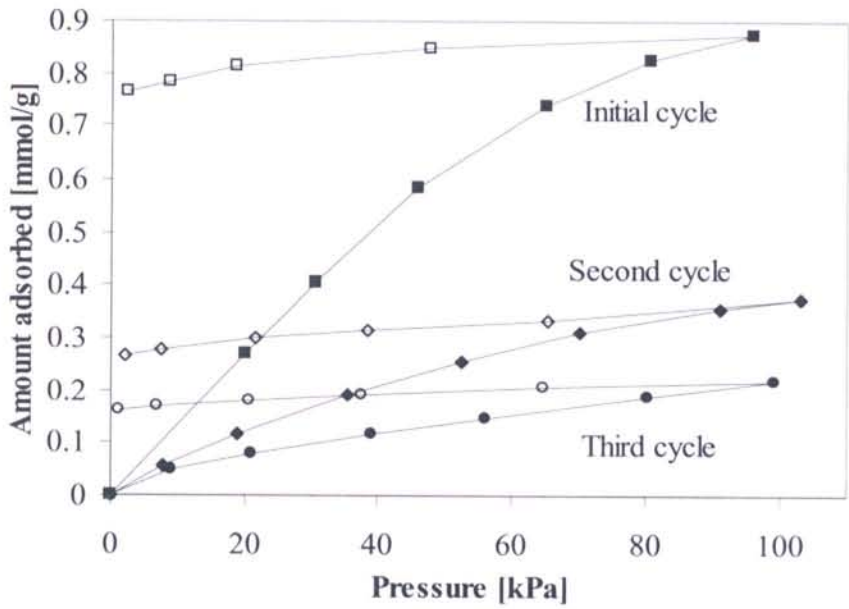

Figure 2.15. Adsorption measurements of propylene on dealuminated H-mordenite at 343 K. After the initial cycle, sample was activated and after measure the second cycle, a new activation was performed. (Solid lines are to guide the trendline of the curves)

The adsorption and reaction (polymerization) of propylene on H-mordenite and dealuminated H-mordenite as already discussed by Chiappetta et al, 1999. Possible

mechanisms of allylic carbocations are produced by loss of H_2 forming $C_nH_{2n-1}^+$ at room temperature and $C_nH_{2n-3}^+$ and $C_nH_{2n-5}^+$ at higher temperatures. The reaction is carried out by formation of a π-complex between the propylene and the Brönsted acid site(s). An H-mordenite with Si/Al = 27 (Norton, USA) was used to support this mechanism, although we verify the same results. In practice that means that at lower temperatures, the propylene molecule "breaks" when adsorbed in the stronger Brönsted acid sites and when the sample is heated for activation, the coking reaction between all the dissociated parts chemically adsorbed occurs. A demonstration of coking is shown by the initial and final visual state of the pellets used for the measurements at 343 K (Figure 2.16). The initial sample is white while the sample after three measurements is completely brown showing a massive formation of coke, and thus eliminating the possibility of using this material for the propane / propylene separation by adsorption in a cyclic process.

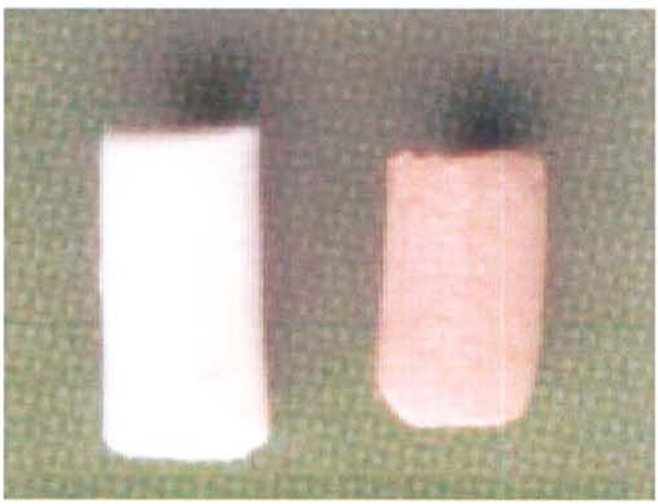

Figure 2.16. Pellets of dealuminated H-mordenite before and after three measurements of propylene adsorption.

2.6 Carbon Molecular Sieve 4A

The use of activated carbons for the propane / propylene separation has shown a small selectivity of the materials towards propylene (Lewis et al., 1950; Järvelin and Fair, 1993). With the appearance of new technologies for material preparation, a new carbon material with a micropore radius below 5 Å and a relatively narrow pore size distribution was used for air separation. At present, all carbon materials produced with narrow pore size distribution are called Carbon Molecular Sieve, or CMS.

Carbon molecular sieves are adsorbents that can be produced from many different organic sources: bituminous coal, bones, coconut shell, etc. The final micropore size depends on the pyrolysis and activation steps in the manufacturing process (Jüntgen, 1981; Kyotani, 2000). The micropore size is generally assumed as uniform (very narrow pore size distribution). The main use of CMS adsorbent has been the nitrogen extraction from air (Schröter and Jüntgen, 1988; Ruthven et al., 1986; Reid and Thomas, 1999) by means of a kinetic separation where both components are nearly equally adsorbed but diffusion of oxygen is around 30 times faster. A new alternative use was the kinetic separation of methane from CO_2 / CH_4 streams (Prasetyo and Do, 1999; Casa-Lillo et al., 1998; Jayaraman, et al., 2003) and even the difficult separation CH_4 / N_2 (Quinglin, et al., 2003).

Propane and propylene adsorption equilibrium is particularly well documented for CMS 5A (Yang, 1987; Chihara et al., 1978; Nakahara et al., 1981; Nakahara et al., 1982) and for other home-prepared sieves (Vyas et al., 1994; Horikawa et al., 2002), although data for CMS 4A is very scarce. Recent investigations in CMS 4A (Bergbau – Forschung with pore size ranging from 3 to 5Å) showed that both molecules were totally excluded (Rege et al., 1998).

An extensive characterization of a carbon molecular sieve 4A kindly provided by Takeda Corp. (Japan) will be provided here. Also, propane and propylene equilibrium isotherms were measured at 343, 373 and 423 K with the MIE equipment. The activation or regeneration procedure was at 523 K in vacuum (< 10^{-5} kPa) for a period of at least 16 hours. The weight loss during the activation was not higher than 9% indicating that the sample adsorbs only minor amounts of air and moisture.

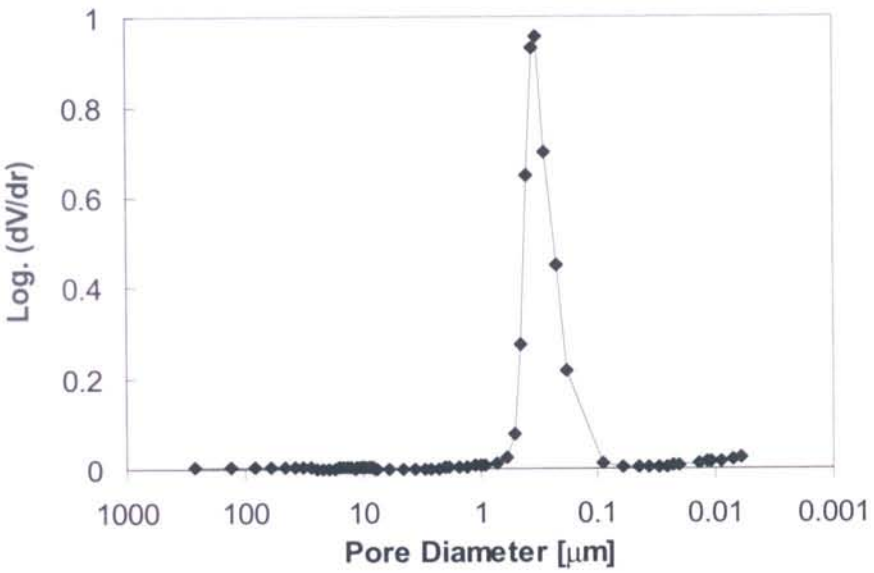

Figure 2.17. Macropore size determination by mercury intrusion

The macroporosity of the sample was measured by mercury intrusion (Instituto Pedro Nunes, Coimbra). This analysis was performed in a Poresizer 9320 (Micromeritics) in a range of pressures between 0.5 and 30,000 psia for a pore determination between 360 μm and 60 Å. The results shown in Figure 2.17 indicate that the average macroporosity size is 0.3 μm. This value is typical for carbon molecular sieves, although when compared with other CMS samples it looks relatively narrow (Jüntgen, 1981).

In this adsorbent, the microporosity measured by carbon dioxide adsorption at ambient temperature (Cazorla-Amorós et al., 1998) may be more reliable than with

nitrogen adsorption at 77K due to possible partial exclusion (or very slow diffusion rate) of the nitrogen molecule. Carbon dioxide adsorption equilibrium at 297 K was measured in a RUBOTHERM microbalance (Bochum, Germany). Details of the equipment will be given in Chapter 5. Each point of equilibrium was measured only after one hour; i.e., the time needed to ensure constant weight (equilibrium). The isotherm presented here has been measured twice with reproducible results and was completely reversible. Activation of the sample was performed at 523 K for 4 hours and in vacuum (< 10^{-5} kPa). The isotherm obtained at 297 K up to pressures of 3,000 kPa is presented in Figure 2.18.

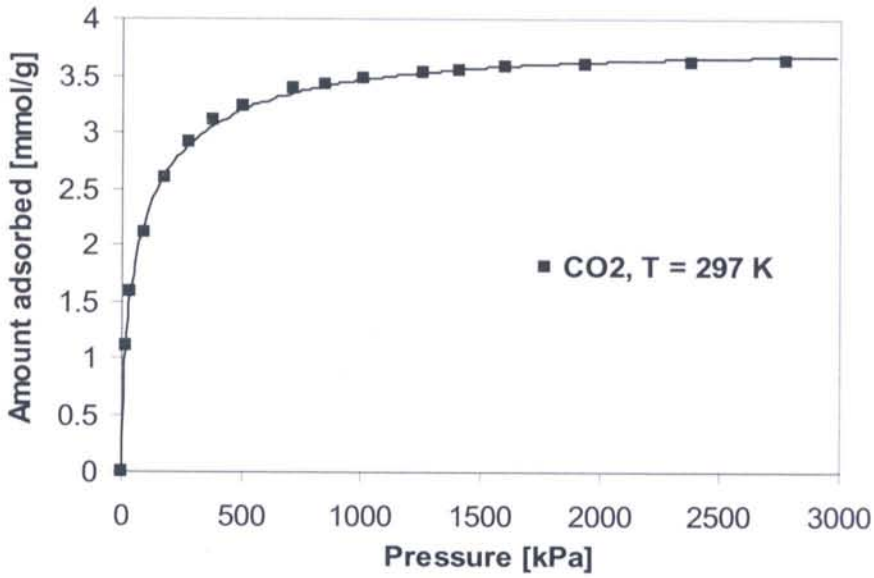

Figure 2.18. Carbon dioxide adsorption on CMS 4A Takeda at 297 K. Solid line represents the Generalized Dubinin model.

For pressures up to 1,000 kPa the typical plateau was almost reached in a value around 3.5 mmol/g. Data are in agreement with other works published using a CMS Takeda 4A adsorbent (Dubinin and Stoeckli, 1980). The isotherm was fitted (solid line in Figure 2.18) with the generalized Dubinin equation using: q_{max} = 3.6976 mmol/g, E_o = 13,599 J/mol and n = 2.46. The parameters are also in reasonable agreement with

published parameters for carbon dioxide in CMS 5A (Suzuki, 1990). As suggested in other works, when the value of n cannot be fitted correctly to a value of 2 or 3 this corresponds to a mixture of very fine micropores (in this case around 4 Å) and some other larger micropores (Dubinin and Stoeckli, 1980). The value of 6 Å as average pore size has been attributed to this sample with measurements of adsorption calorimetry and probing molecules by other independent researchers involved in the propane/propylene CYTED project (Sepúlveda-Escribano and Rodriguez-Reinoso, 2001).

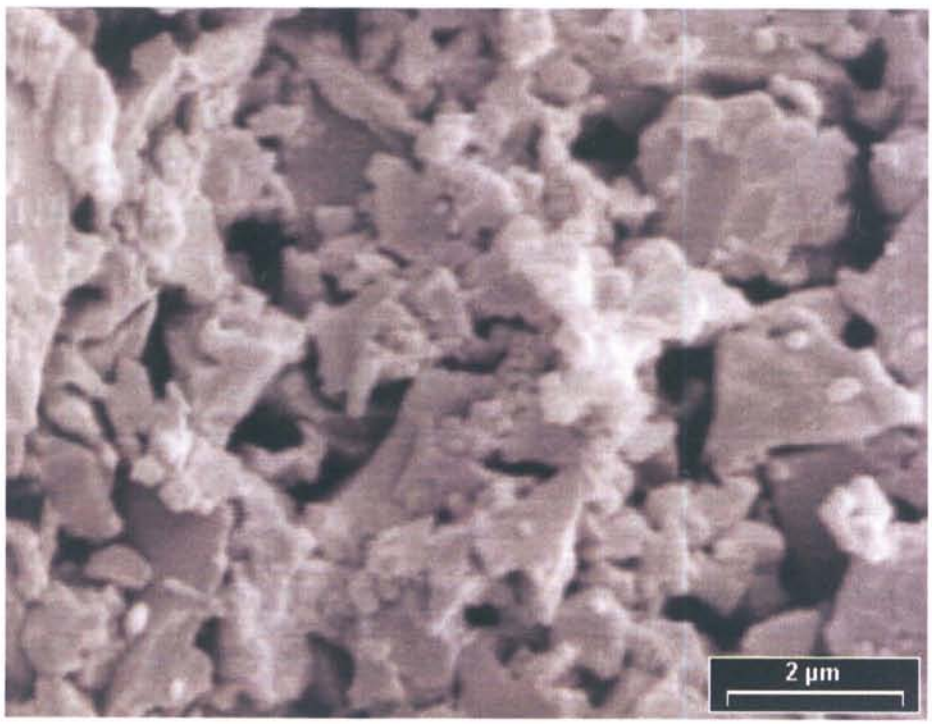

Figure 2.19. Scanning Electron Microscopy of the adsorbent CMS4A

To complete the physicochemical characterization, Scanning Electron Microscopy (SEM) has been used to determine the micropore structure. We will call "crystal", in analogy with zeolites, all the agglomeration of crystalline structures of the sample where the main amount of micropores is located. Morphology of the sample can be seen in Figure 2.19; it is clear that an average "crystal" size is very hard to be defined

for the case where micropore controls the diffusion process, so the parameter D_c/r_c^2 will be reported. Also the shape is not very well defined, reason why we will consider the slip-shape geometry of the micropores in case of micropore controlled diffusion for kinetic calculations (MacElroy et al., 1999).

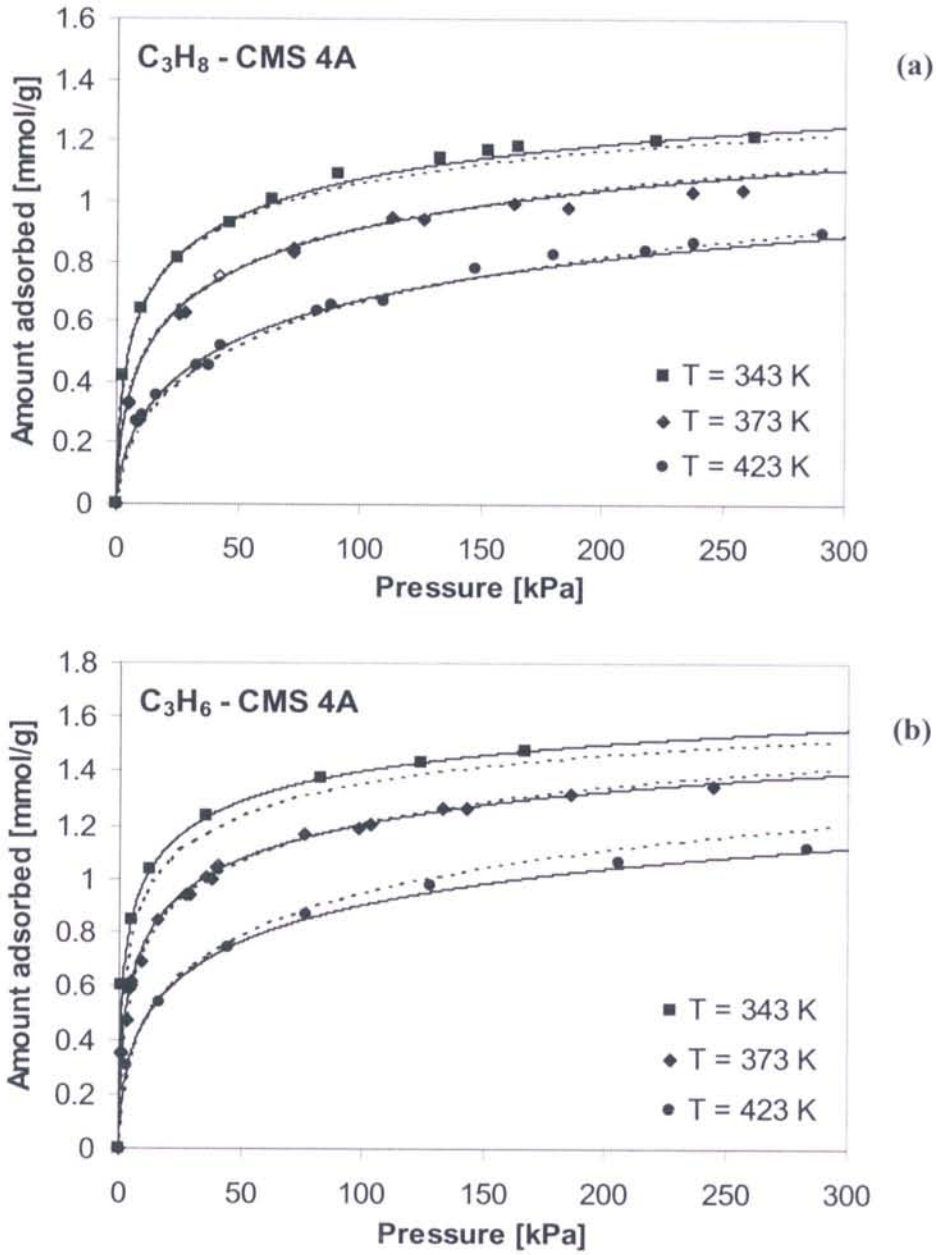

Figure 2.20. Adsorption equilibrium of propane (a) and propylene (b) at 343, 373 and 423 K on CMS 4A Takeda. Solid lines are the Toth model and dotted lines the Dubinin – Radushkevich model.

Adsorption equilibrium isotherms of propane and propylene at 343, 373 and 423 in the 0 – 300 kPa pressure range are shown in Figures 2.20. Solid lines in figures correspond to the Toth model fitting while dotted lines are the Dubinin- Radushkevich model (Grande et al., 2003a). At the lower temperature measured, the saturation plateau is reached at 200-250 kPa for both gases. Clearly, the selectivity of the material towards propylene is not high: in the low-pressure range the ratio of Henry constants (H_{C3H6}/H_{C3H8}) is 2.3 at 343 K and 1.7 at 423 K. The fitting parameters of both models are shown in Table 2.5. Propylene data at 343 K are comparable with those in previous reports at 323 K on CMS 5A (Nakahara, et al., 1982).

Table 2.5 – Propane and propylene adsorption on CMS 4A equilibrium parameters

Dubinin – Radushkevich				
Sorbate	q_{max} [mmol/g]	E_o [kJ/mol]		d [-]
C_3H_8	1.367	18.23		2
C_3H_6	1.669	21.23		2
Toth				
Sorbate	q_{max} [mmol/g]	K_{eq}^{o} [kPa]$^{-n}$	(-ΔH) [kJ/mol]	n [-]
C_3H_8	1.757	$1.81.10^{-2}$	11.46	0.356
C_3H_6	1.927	$1.32.10^{-2}$	14.35	0.325

Note that for the fitting of both adsorption isotherms, the Dubinin – Radushkevich model has been used instead of the Dubinin – Astakhov model. The Dubinin – Astakhov model does not fit the data correctly always giving steepest isotherms. This is another indication of a wide micropore size distribution, like in activated carbons. The Toth model describes the data with higher accuracy, particularly

in the low-pressure range, which is important for binary adsorption equilibrium predictions (Talu, 1998).

Using the Dubinin – Raduschkevich fitting of the equilibrium data, the isosteric heat of adsorption for both hydrocarbons was calculated with the Clausius–Clapeyron equation obtaining a heat of adsorption that depends on the amount adsorbed. This dependence is a decreasing function, which ranges from almost 40 to 10 kJ/mol in the case of propylene and from 35 to 10 kJ/mol for propane. The higher values obtained at the initial loading of the adsorbent (35 kJ/mol) are comparable with the reported values on CMS 5A (Chihara, et al., 1978).

2.7 Zeolite 4A

Zeolites 4A have, like all A type zeolites, a truncated octahedron structure composed by sodalite cages. The difference between zeolite 4A and 5A is on the type of cations that counterbalances the negative charge (-1) of the AlO_2 groups. In the case of zeolite 4A is sodium while for 5A is calcium, opening the channels (Yang, 2003).

The main use of zeolite 4A is as detergent builder. In middle 70' it was determined that the level of phosphates causes ecological problems in superficial waters (rivers and lakes mainly) and after some years of research, it was found that zeolite 4A with crystal size around 3.5 μm and narrow particle size distribution can be used as water-insoluble detergent builder. This application accounts for the increase of zeolite production representing around 90% of the total amount of zeolites (Ullmann's Encyclopedia, 2003). The second application for zeolite 4A is adsorption of carbon dioxide in natural gas streams and natural gas drying in relatively dry streams where this adsorbent can be used instead of zeolite 3A that is more expensive.

Zeolite 4A can be prepared from pure chemicals and hence the impurities are negligible or, the most employed way in commercial adsorbents, is to prepare it by the hydrothermal reaction of dehydroxylated kaolin with aqueous sodium hydroxide (Breck, 1974). In this process, purification of kaolin is needed to separate the ancillary mineral impurities particularly iron and titanium, (Chandrasekhar et al., 1997).

Adsorption equilibrium of propane and propylene on zeolite 4A has been previously reported in literature (Järvelin and Fair, 1993; Rege et al., 1998; Da Silva and Rodrigues, 1999). The loading capacity of both gases in these works is similar and in all of them propane is adsorbed only in minor quantities. Zeolite 4A has already been tested as a possible adsorbent to separate propane/propylene by Pressure – Vacuum Swing Adsorption, PSA – VSA obtaining propylene purity of 96% (Da Silva, 1999). Zeolite 4A is already used in an industrial patent in the BOC PETROFIN ™ process (Ramachandran et al., 1994).

Equilibrium data of propane and propylene at 373, 423 and 473 K will be reported here. Adsorption equilibrium measurements were performed in the MIE (manometric) equipment. The activation of the sample in all the cases was carried out at 593 K for a period of 24 hours under vacuum ($< 10^{-5}$ kPa) with a heating rate of 1 K/min. This period was much higher than the 10 hours used with the zeolite 5A because the propane has a very low diffusivity and to ensure that it was desorbed from previous experiments, a longer period was employed.

Zeolite 4A was kindly provided by CECA (France). Two samples were received. The first one has some problems for propylene adsorption and will be termed CECA1 while the second sample that presented good results will be called Z4A.

In the CECA1 sample, after activation at 593 K the sample does not adsorb propylene. This sample has a strange color (more red) than ordinary zeolites. After this

"standard" activation temperature for zeolites, a higher temperature of 673 K was used. After this activation, some propylene was adsorbed. The adsorption of propylene was very low when compared with previous works (Da Silva and Rodrigues, 1999). In order to compare the differences between the CECA1 and Z4A samples, the adsorption equilibrium of propylene at 373 and 473 K is plotted in Figure 2.21. Clearly, the amount of propylene adsorbed by the CECA1 sample is smaller, particularly at higher pressures. However, adsorption kinetics of propylene in both materials is similar in the whole pressure range studied. With these results, we cannot explain this difference by a pore blocking of the structure and more analysis should be made.

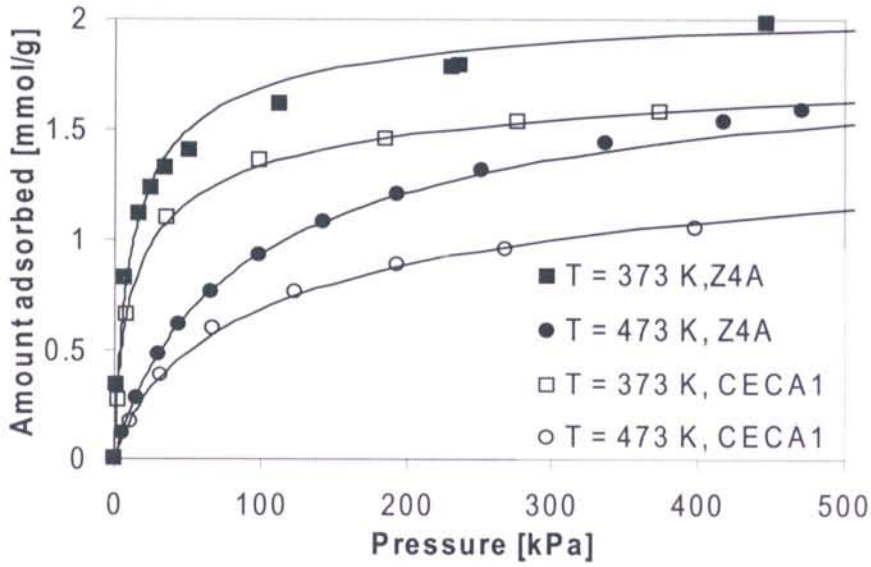

Figure 2.21. Adsorption Equilibrium of zeolite 4A samples CECA1 and Z4A at 373 and 473 K.

The problems in the CECA1 sample are related with its chemical nature. This was detected by SEM analyses and from the X-ray diffraction pattern of the equipment that was coupled with the SEM. In Figure 2.22 the SEM and X-ray diffraction pattern of both samples is shown. Some small amounts of iron can be seen in the X-ray pattern of the CECA1 sample and not in the Z4A. If we analyze the SEM image of the CECA1 sample with higher resolution, we can distinguish the crystals and an amorphous

structure that was not seen in the Z4A sample. In Figure 2.23 a closer SEM image together with selected X-ray patterns measured on the amorphous part (P1 spectrum) and on the crystal surface (P2 spectrum) are shown. Clearly, the iron and a small amount of titanium are deposited in these non-desired structures present in the CECA1 sample and revealing some problems in the pelletization process or in the purification of the materials used for the zeolite production.

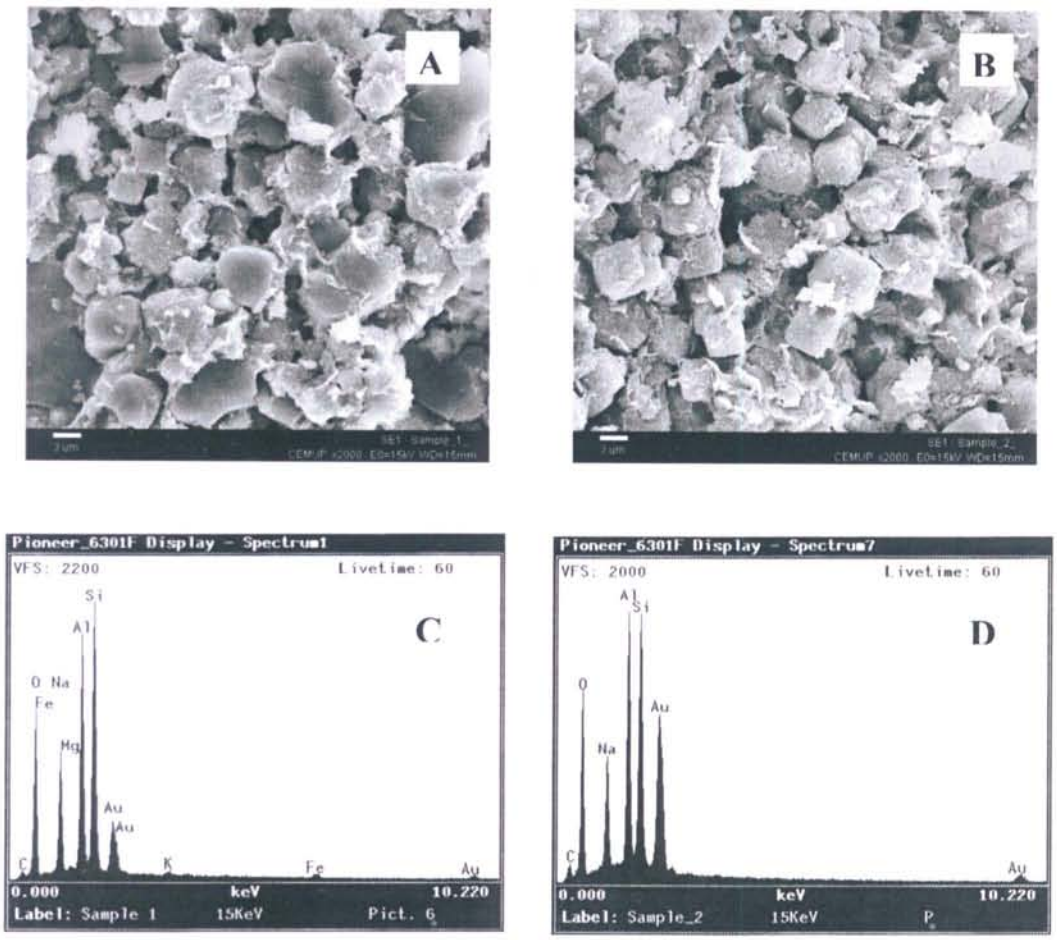

Figure 2.22 – SEM images of CECA1 (A) and Z4A (B). The chemical composition of both samples is also given: CECA1 (C) and Z4A (D).

In the following citations of zeolite 4A we will consider the results obtained with the Z4A sample. Physical properties of the Z4A sample are listed in Table 2.6.

In Figure 2.24 new data of adsorption equilibrium of propane at 423 and 473 K are presented with higher concentrations of propane on the adsorbed phase indicating

some hydrocarbon adsorption on the zeolite structure and not only on the binder. No desorption data was measured. Equilibrium measurements were extremely slow taking three days per equilibrium point for the lower temperature (423 K) measurements and two days for each measurement at 473 K (Grande et al., 2003b). For this reason, no equilibrium measurements were performed at 373 K. The amount adsorbed was more than 1 mol/kg at 423 K and 100 kPa.

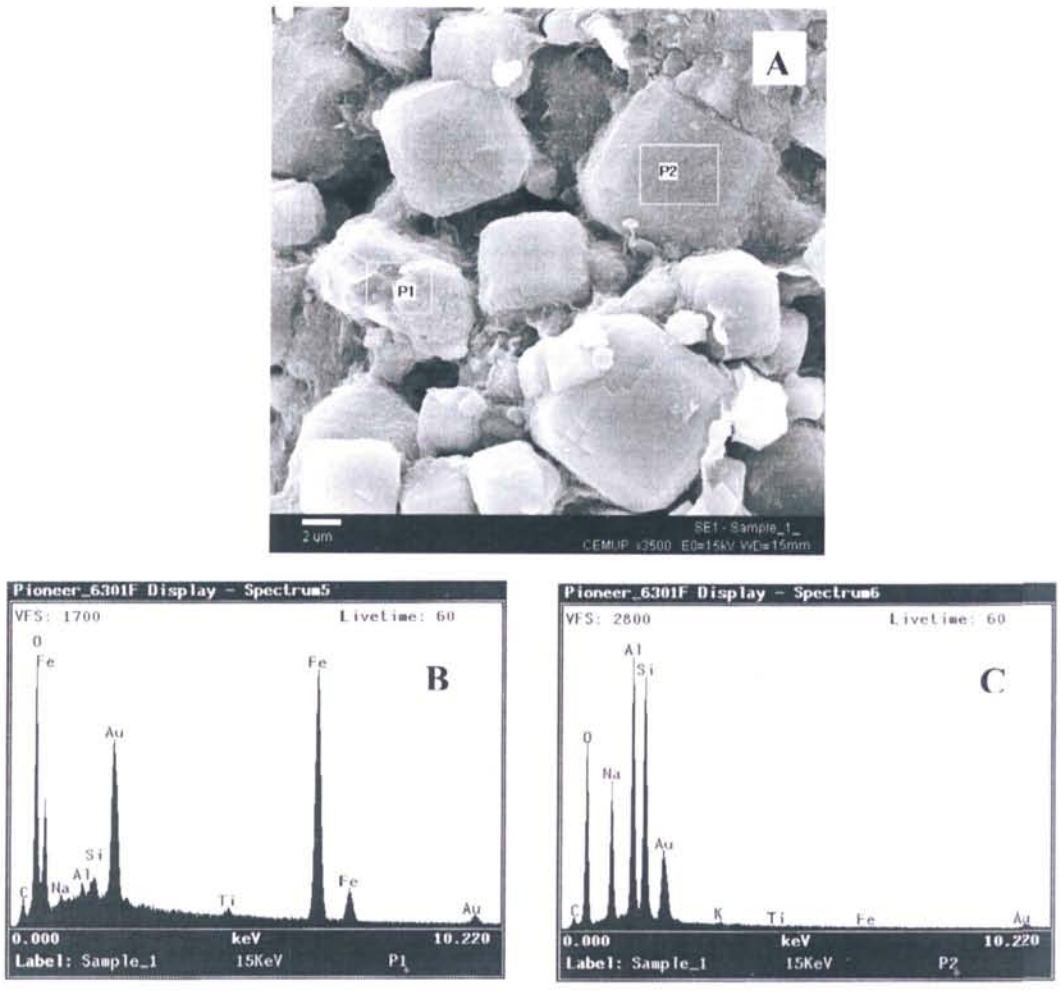

Figure 2.23 – Detailed SEM images of CECA1 (A). The chemical composition of both indications (P1 and P2, respectively) are shown in (B) and (C).

The measurements after three hours contact are also shown in Figure 2.24 (points not in equilibrium). The difference with the amount adsorbed in equilibrium is

large and this set of data is in agreement with other published works (Järvelin and Fair, 1993; Da Silva and Rodrigues, 1999). Note that the dependence with temperature is weak, something that can be explained by a combination of equilibrium and kinetic effects (i.e., at high temperatures, the amount adsorbed is smaller, but the diffusivity is higher).

Table 2.6 Zeolite 4A physical properties

Adsorbent density [g/cm³]	1.21
Adsorbent porosity [-]	0.315
Zeolite average crystal radius [cm]	1.9×10^{-4}
Average extrudate diameter [cm]	0.055

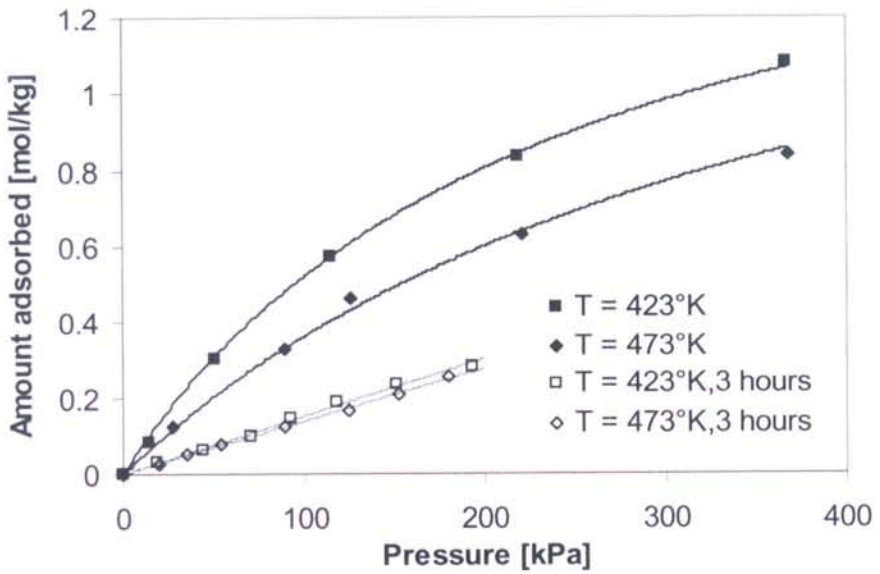

Figure 2.24. Adsorption equilibrium of propane on zeolite 4A CECA. Symbols: ■ T = 423 K, ◆ T = 473 K and solid lines – Langmuir model. Empty symbols are the loading measured after 3 hours.

When we consider the size and shape of the propane molecule and the opening of the zeolite structure, we are assuming that the molecules as well as the zeolite channels are rigid (Xiao and Wei, 1992). With the equilibrium results shown in Figure 2.24 it is clear that propane passes through the zeolite channels, but we still do not known the mechanism of diffusion. Also, this mechanism cannot be predicted

successfully via molecular simulations using rigid molecules and zeolite 4A channels (Zhang et al., 2003).

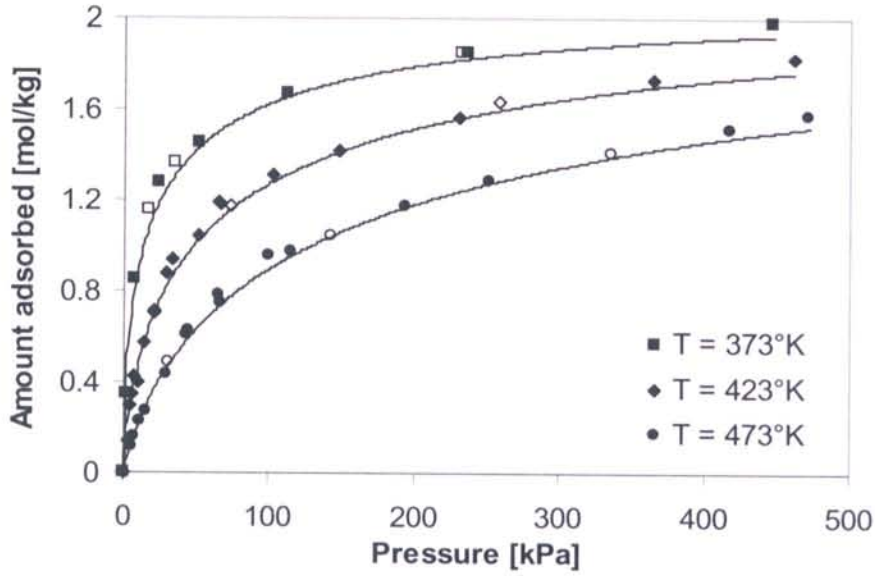

Figure 2.25. Adsorption equilibrium of propylene on zeolite 4A CECA. Symbols: ■ T = 373 K, ♦T = 423 K, ● T = 473 K and solid lines – Dubinin model. Empty symbols are desorption points.

Data were fitted very well with the Langmuir model. The fitting parameters are listed in Table 2.7. The description of these data by the generalized Dubinin model was not possible due to the difficulties of an exponential equation to reproduce the initial linear behavior of propane equilibrium.

Propylene adsorption is shown in Figure 2.25. Here equilibrium was also measured at 373 K. In the lower pressure range (0 – 100 kPa), these data are in agreement with other published data (Järvelin and Fair, 1993; Da Silva and Rodrigues, 1999). These isotherms were fitted with the generalized Dubinin equation with a good quality in all the pressure range. Equilibrium parameters for propylene are also detailed in Table 2.7. Langmuir and Toth models give poor fits in the high-pressure range.

Table 2.7. Fitting parameters of the Dubinin model for propylene adsorption equilibrium and for Langmuir model for propane adsorption equilibrium on zeolite 4A.

C_3H_6 – zeolite 4A	q_{max} [mol/kg]	E_o [J/mol]	d
	2.0779	21,277	2.753
Propane equilibrium parameters: Langmuir model			
C_3H_8 – zeolite 4A	q_{max} [mol/kg]	$K_{eq}^{\ o}$ [kPa]$^{-1}$	$(-\Delta H)$ [J/mol]
	1.7525	$4.22\ 10^{-5}$	16,214.6

Because none of the theories used before (generalized Dubinin and Toth) could be applied to both components with good accuracy, an alternative and more realistic analysis was performed using the Nitta model. The multisite model is a thermodynamically consistent model and fits well the data of propane and propylene. Propylene fitting was good in all the pressure range studied. The fitting of propane is the same as with the Langmuir model because the Nitta model is Langmuir reducible. The saturation capacity of propane is imposed by the thermodynamic constraint $a_i q_{mi} = \text{constant}$ (Sircar, 1995). Relating the temperature dependence of the equilibrium constants by the Van't Hoff equation, the isosteric heat of both gases can be obtained. The values for propane and propylene are 15.5 and 28.2 kJ/mol. The values are constant with loading because we assume that the adsorbent is homogeneous by fitting the data with this model. The value for propylene is a little smaller than 30 kJ/mol reported elsewhere (Da Silva and Rodrigues, 1999). The parameters are detailed in Table 2.8.

We analyze the low-pressure range fitting of propylene in the Virial domain (Talu, 1998). This was made by plotting the isothermal data in the form $ln(P/q)$ versus q. This kind of plots is known as "Virial domain" representation and is shown in Figure 2.26. We can see that in the low-pressure range the fitting of the Nitta model at lower

temperatures is not very good. The solid line represents the Dubinin model and the dotted line the multisite model. In Figure 2.26, the Virial model, which enhances the fitting in the low-pressure range, is also shown. The Virial model is given by:

$$H = \frac{q}{P}\exp\left(2A_1 q + \frac{3}{2}A_2 q^2 + \frac{4}{3}A_3 q^3 + \ldots\right) \qquad [2.10]$$

The parameters of this fitting are shown in Table 2.9 and the propylene results are also shown in Figure 2.26. The Henry constant, H, has an exponential temperature dependence while a linear dependence was observed for the virial coefficients A_i.

The multisite model shows a good fitting at 473 K, a small deviation at 423 K and a larger deviation at 373 K. These deviations will lead us to poor predictions on multicomponent adsorption equilibrium as will be shown later.

Table 2.8. Fitting parameters of the multisite Langmuir model of Nitta for propane and propylene adsorption equilibrium at 373, 423 and 473 K.

Gas	q_{max} [mmol/g]	a [-]	K_{eq}(373 K) [kPa^{-1}]	K_{eq}(423 K) [kPa^{-1}]	K_{eq}(473 K) [kPa^{-1}]
C_3H_6	2.600	2.612	0.0714	0.0288	0.0103
C_3H_8	3.103	2.189	-	0.0024	0.0015

The zeolite sample was the same for all the experiments reported. Near 3 grams of adsorbent were used. After three months of continuous exposure of propylene at high temperatures and pressures, the initial pure propylene experiment was completely reproducible indicating that no coke was formed.

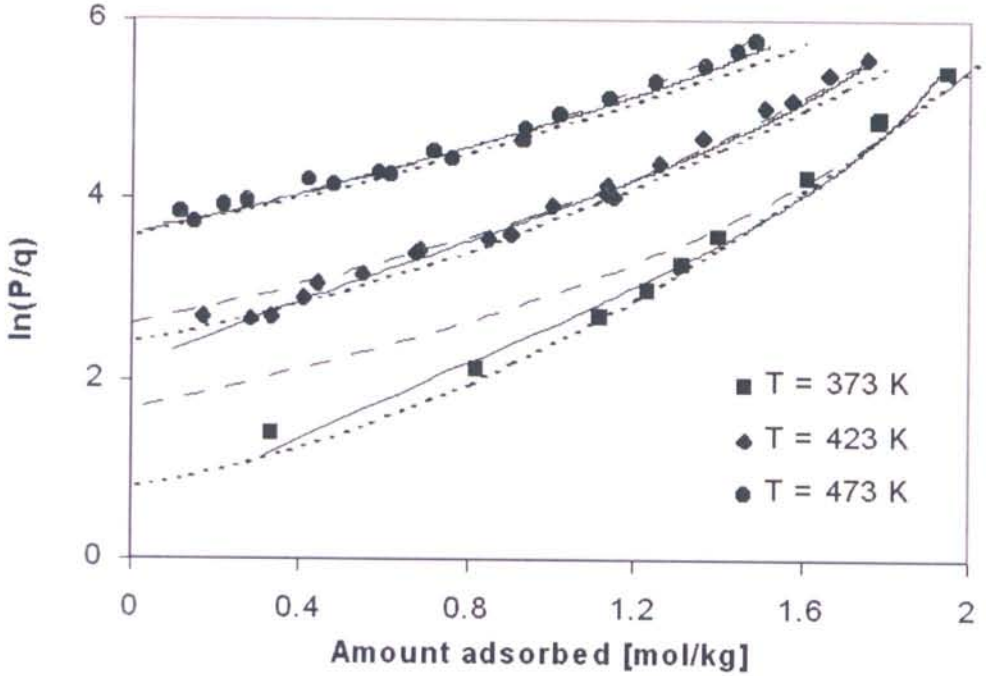

Figure 2.26. Virial domain plot of propylene adsorption equilibrium. Symbols: ■ T = 373 K, ♦T = 423 K, ● T = 473 K, solid lines – Dubinin model, dashed lines – Nitta model and dotted lines – Virial model.

Table 2.9. Fitting parameters of the Virial model for propylene adsorption equilibrium at 373, 423 and 473 K.

Temperature [K]	H [mmol/g.kPa]	A_1 [g/mmol]	A_2 [g/mmol]^2
373	0.453	0.428	0.498
423	0.089	0.450	0.300
473	0.027	0.475	0.160

2.8 Conclusions

In this Chapter, propane and propylene adsorption equilibrium on seven adsorbents was measured. Also, a new manometric equipment, MIE (manometric isotherm equipment), was built and data were measured in the pressure range between 0-500 kPa and extending the laboratory capabilities for measurement adsorption equilibrium to pressures up to 700 kPa.

All the adsorbents were selective to propylene and present isotherms of Type I. The molecular sieves 4A (zeolite and carbon molecular sieve) presented the best adsorption equilibrium selectivity with values of 2.5 for zeolite 4A at 100 kPa and 423 K and 1.7 for CMS4A at 100 kPa and 373 K. Selectivity values for the other commercial adsorbents at the same pressure were smaller: 1.3 for NSG at 323 K and 1.1 for zeolite 5A (343 K).

Nomenclature

a_i	number of neighboring sites occupied by component *i* (Nitta model)
A	adsorption potential, kJ/mol
A_i	virial coefficients (Virial model), $(mol/kg)^{-i}$
A_s	superficial area of the adsorbent, m^2
d	parameter of the generalized Dubinin model
E_o	characteristic adsorption energy, kJ/mol
H	Henry constant, mol/(kg kPa)
K_{eq}	equilibrium constant, kPa^{-1}
$K_{eq}^{\ o}$	equilibrium constant at the limit $T \rightarrow \infty$, kPa^{-1}
n	Heterogeneity parameter of the Toth model
P	pressure, kPa
P^o	pressure of the saturated gas, kPa
q	adsorbed phase concentration, mol/kg
q'	adsorbed phase concentration, mol/m^2
q_{max}	maximum adsorbed phase concentration, mol/kg
Q_{ST}	isosteric heat of adsorption, kJ/mol
R_g	ideal gas constant, 8.314 kJ/mol.K

T	temperature, K

Greek Letters

θ_i	fractional coverage of component *i* on the adsorbed phase
$(-\Delta H)$	heat of adsorption, kJ/mol

References

Bhatia, S. K.; Ding, L. P. Vacancy Solution Theory of Adsorption Revisited. *AIChE J.*, **2001**, 47, 2136-2138.

Boucheffa, Y.; Thomazeau, C.; Cartraud, P.; Magnoux, P.; Guisnet, M.; Jullian, S. Formation of carbonaceous compounds from propene and isobutene over a 5A zeolite. Influence of temperature on their compositions and locations. *Ind. Eng. Chem. Res.*, **1997**, 36, 3198-3204.

Breck, D. W. *Zeolite Molecular Sieves: Structure, Chemistry and Use*. Wiley, New York, 1974.

Casa-Lillo, M. A.; Alcañiz-Monge, J.; Raymundo-Piñero, E.; Cazorla-Amorós, D.; Linares-Solano, A. Molecular Sieve Properties of General-Purpose Carbon Fibres. *Carbon*, **1998**, 36, 1353-1360.

Cazorla-Amorós, D.; Alcañiz-Monge, J.; Casa-Lillo, M. A.; Linares-Solano, A. CO_2 as an Adsorptive to Characterize Carbon Molecular Sieves and Activated Carbons. *Langmuir*, **1998**, 14, 4589-4596.

Chandrasekhar, S.; Raghavan, P.; Sebastian, G.; Damodaran, A. D. Brightness improvement studies on 'kaolin based' zeolite 4A. *Applied Clay Science*, **1997**, 12, 221-231.

Chiappetta, R.; Bodoardo, S.; Geobaldo, F.; Fajula, F.; Garrone, E. Propene adsorption and Reaction on Zeolites and Pillared Clays., *Res. Chem. Int.*, **1999**, 25(1), 111-129.

Chihara, K.; Suziki, M.; Kawazoe, K. Adsorption Rate on Molecular Sieving Carbon by Chromatography. *AIChE J.*, **1978**, 24, 237-246.

Cochran, T. W.; Kabel, R. L.; Danner, R. P. Vacancy solution theory of adsorption using Flory-Huggins activity coefficient equations. *AIChE J.*, **1985**, 31(2), 268-277.

Chung, S. Y.; Oh, S-H; Kim, M. H.; Nam, L-S; Kim, Y.G. Hydrothermal Stability of Dealuminated Mordenite Type Zeolite Catalysts for the Reduction of NO by C3H6 Under Lean-Burn Condition, *Catalysis Today*, **1999**, 54, 521-529.

Da Silva, F. A. *Cyclic Adsorption Processes: Application to Propane / Propylene Separation*. Ph.D. Dissertation, University of Porto, Portugal, **1999**.

Da Silva, F. A.; Rodrigues A. E. Adsorption equilibria and kinetics for propylene and propane over 13X and 4A zeolite pellets. *Ind. Eng. Chem. Res.*, **1999**, 38, 2434-2438.

Do, D. D. *Adsorption Analysis: Equilibria and Kinetics*. Imperial College Press, London, **1998**.

Dubinin, M. M.; Stoeckli, H. F.; Homogeneous and Heterogeneous Micropore Structures in Carbonaceous Adsorbents, *J. Col. Interface Sci.* **1980**, 75(1), 34-42.

Ghosh, T. K.; Lin, H.; Hines, A. L. Hybrid Adsorption – Distillation Process for Separating Propane and Propylene. *Ind. Eng. Chem. Res.*, **1993**, 32, 2390-2399.

Gordon, P. A.; Glandt, E. D. *Alkane Adsorption on Microporous Silica Gel.* FOA6, Elsevier, 105-110, **1998**.

Grande, C. A.; Rodrigues, A. E. Adsorption Equilibria and Kinetics of Propane and Propylene in Silica Gel. *Ind. Eng. Chem. Res.*, **2001**, 40, 1686-1693.

Grande, C. A.; Gigola, C. E.; Rodrigues, A. E. Adsorption of Propane and Propylene in Pellets and Crystals of Zeolite 5A, *Ind. Eng. Chem. Res.*, **2002**, 41, 85-92.

Grande, C. A.; Silva, V.M.T.M.; Gigola, C.; Rodrigues, A. E. Adsorption of Propane and Propylene Onto Carbon Molecular Sieve. *Carbon*, **2003a**, 41, 2533-2545.

Grande, C. A.; Gigola, C.; Rodrigues, A. E. Propane-Propylene Binary Adsorption on Zeolite 4A. *Adsorption*, **2003b**, 9, 321-329.

Horikawa, T.; Hayashi, J.; Muroyama, K. Preparation of Molecular Sieving Carbon from Waste Resin by Chemical Vapor Deposition. *Carbon*, **2002**, 40, 709-714.

Hutson, N. D.; Yang, R. T. Theoretical Basis for The Dubinin – Radushkevich (D – R) Adsorption Isotherm Equation. *Adsorption*, **1997**, 3, 189-195.

Izumi, J.; Yasutake, A.; Tomonaga, N.; Tsutaya, H.; Oka, N. Development of High performance Gas Separation Process Using Gas Adsorption. *Mitsubishi Heavy Ind. Tech. Review.*, **2002**, 39(1), 6-10.

Jaroniec, M. *Physical Adsorption on Heterogeneous Surfaces*. in Fundamentals of adsorption, A. L. Myers (ed.), Engineering Foundation, New York, 239-248, **1984**.

Jaroniec, M. Fifty Years of the Theory of the Volume Filling of Micropores. *Adsorption*, **1997**, 3, 187-188.

Järvelin, H.; Fair, J. R. Adsorptive Separation of Propane – Propylene Mixtures. *Ind. Eng. Chem. Res.*, **1993**, 32, 2201-2207.

Jayaraman, A.; Chiao, A. S.; Padin, J.; Yang, R. T.; Munson, C. L. Kinetic Seaparation of Methane/Carbon Dioxide by Molecular Sieve Carbons. *Sep. Sci. and Tech.*, **2002**, 37(11), 2505-2528.

Jüntgen, H.; Knoblauch, K.; Harder, K. Carbon Molecular Sieves: Production from Coal and Applications in Gas Separation. *Fuel*, **1981**, 60, 817-822.

Kyotani, T. Control of Pore Structure in Carbon. *Carbon*, **2000**, 38, 269-286

Langmuir, I. The Adsorption of Gases on Plane Surfaces of Glass, Mica and Platinum. *J. Am. Chem. Soc.*, **1918**, 40, 1361-1403.

Lewis, W. K.; Gilliland, E.; Chertow, B.; Cadogan, W. Pure Gas Isotherms. *Ind. Eng. Chem.*, **1950a**, 42, 1326-1332.

Lewis, W. K.; Gilliland, E. R.; Chertow, B.; Hoffman, W. H.; Bareis, D. Vapor - Adsorbate Equilibrium I (and III). *J. Am. Chem. Soc.*, **1950b**, 72, 1153-1163.

Loughlin, K. F.; Hasanain, M. A.; Abdul – Rehman, H. B. Quaternary, Ternary. Binary, and Pure Component Sorption on Zeolites 2. Light Alkanes 5A and 13X Zeolites at Moderate to High Pressures. *Ind. Eng. Chem. Res.*, **1990**, 29, 1535-1546.

MacElroy, J. M. D.; Friedman, S. P.; Seaton, N. A. On the Origin of Transport Resistances Within Carbon Molecular Sieves. *Chem. Eng. J.*, **1999**, 72, 1015-1027.

Malek, A.; Farooq, S. Determination of Equilibrium Isotherms Using Dynamic Column Breakthrough and Constant Flow Equilibrium Desorption. *J. Chem. Eng. Data*, **1995**, 40, 25-32.

Malek, A.; Farooq, S. Comparison of isotherm models for hydrocarbon adsorption on activated carbon. *AIChE J.*, **1996**, 42, 3191-3201.

Marcus, B. K.; Cormier, W. E. Going Green with Zeolites. *Chem. Eng. Prog.*, **1999**, 95, 47-53.

Moon, H.; Tien, C. Further Work on the Prediction of Gas-Mixture Adsorption Equilibrium Using the Potential Theory. *Sep. Technol.*, **1993**, 3, 161-167.

Moreno, S.; Poncelet, G. Dealumination of Small- and Large-Port Mordenites: A Comparative Study. *Microporous Mater.*, **1997**, 12, 197-222.

Morgan, S. S. A comparison of Simplex Method Algorithms, Ms Thesis, Univ. of Florida, 1997 (www.cise.ufl.edu/~davis/Morgan/index.htm).

Myers, A. L.; Prausnitz, J. M.; Thermodynamics of mixed-gas adsorption, *AIChE J.*, **1965**, 11(1), 121-127.

Nakahara, T.; Hirata, M.; Komatsu, S. Adsorption of a Gaseous Mixture of Ethane and Propane on a Carbon Molecular Sieve. *J. Chem. Eng. Data*, **1981**, 26, 161-163.

Nakahara, T.; Hirata, M.; Mori, H. Adsorption of a Gaseous Mixture of Ethylene and Propylene on a Carbon Molecular Sieve. *J. Chem. Eng. Data*, **1982**, 27, 317-320.

Nitta, T.; Shigetomi, T.; Kuro-Oka, M.; Katayama, T. An adsorption isotherm of multi-site occupancy model for homogeneous surface. *J. Chem. Eng. Japan*, **1984**, 17, 39-45.

O'Brien, J. A.; Myers, A. L.; Physical adsorption of gases on heterogeneous surfaces, *J. Chem. Soc. Faraday Trans.*, **1984**, 80(1), 1467-1477.

Polanyi, M. Theories of Adsorption of Gases. General Survey and Some Additional Remarks. *Trans. Farad. Soc.*, **1932**, 28, 316-333.

Prasetyo, I.; Do, D. D. Pore Structure Alteration of Porous Carbon by Catalytic Coke Deposition. *Carbon,* **1999**, 37, 1909-1918.

Qinglin, H.; Sundaram, S. M.; Farooq, S. Revisiting Transport of Gases in the Micropores of Carbon Molecular Sieves, *Langmuir*, **2003**, 19, 393-405.

Ramachandran, R.; Dao, L. H.; Brooks, B. *Method of Producing Unsaturated Hydrocarbons and Separating the Same from Saturated Hydrocarbons*, U.S. Patent 5,365,011, 1994.

Rege, S. U.; Padin, J.; Yang, R. T. Olefin/Paraffin Separations by Adsorption - Pi-Complexation vs. Kinetic Separation. *AIChE J.,* **1998**, 44, 799-809.

Richter, E.; Schultz, W.; Myers, A. L. Effect of Adsorption Equation on Prediction of Multicomponent Adsorption Equilibria by the Ideal Adsorbed Solution Theory. *Chem. Engng. Sci.,* **1989**, 44, 1609-1616.

Reid, C. R.; Thomas, K. M. Adsorption of Gases on a Carbon Molecular Sieve Used for Air Separation: Linear Adsorptives as Probes for Kinetic Selectivity. *Langmuir,* **1999**, 15, 3206-3218.

Rouquerol, F.; Rouquerol, J; Song, K. *Adsorption by Powders and Porous Solids.* Academic Press, London, **1999**.

Ruthven, D. M.; Derrah, R. I. Sorption in Davison 5A Molecular Sieves. *Can. J. Chem. Eng.*, **1972**, 50, 743-747.

Ruthven, D. M. *Priciples of adsorption and adsorption processes*, Wiley, New York, **1984**.

Ruthven, D. M.; Raghavan, N. S.; Hassan, M. M. Adsorption and Diffusion of Nitrogen and Oxygen in a Carbon Molecular Sieve. *Chem. Eng. Sci.*, **1986**, 41, 1325-1332.

Schröter H. J.; Jüntgen H. Gas Separation by Pressure Swing Adsorption Using Carbon Molecular Sieves. In: Adsorption: Science and Technology, NATO ASI Series (Rodrigues, LeVan and Tondeur editors), Netherlands: Kluwer Academic Publishers; **1988**.

Sepúlveda-Escribano, A.; Rodrígues-Reinoso, F. *Separación de Propano/Propileno-Desulfuración de Naftas.* CYTED V.8 meeting, Porto, Portugal (*in Spanish*), 27-29 August, **2001**.

Silva, J. A. C. *Separation of n/iso – Paraffins by Adsorption Process.* Ph.D. Dissertation, University of Porto, Portugal, **1998**.

Silva, J. A. C.; Rodrigues, A. E. Multisite Langmuir model applied to the interpretation of sorption of n-paraffins in 5A zeolite. *Ind. Eng. Chem. Res.*, **1999**, 38, 2432-2438.

Silva, J. A.; Mata, V. G.; Dias, M. M.; Lopes, J.C.; Rodrigues, A. E. Effect of Coke in the Equilibrium and Kinetics of Sorption on 5A Molecular Sieve Zeolites, *Ind. Eng. Chem. Res.*, **2000**, 39, 1030-1034.

Sircar, S.; Influence of Adsorbate Size and Adsorbent Heterogeneity on IAST, *AIChE J.*, **1995**, 41, 1135-1145.

Suzuki, M. *Adsorption Engineering.* Elsevier, Tokio, **1990**.

Talu, O. Needs, Status, Techniques and Problems with Binary Gas Adsorption Experiments, *Adv. Col. Interf. Sci.*, **1998**, 76-77, 227-269.

Thomas, J. M.; Thomas, W. J. *Introduction to the principles of heterogeneous catalysis.* Academic Press, London, **1967**.

Toth, J. State equations of the solid – gas interface layers. *Acta Chim. Acad. Sci. Hung.*, **1971**, 69, 311-328.

Ullmann's Encyclopedia of Industrial Chemistry; 7ª Edition, Wiley-VCH, Verlag GmbH & Co..KGaA, **2003**.

Valenzuela, D. P.; Myers, A. L. *Adsorption equilibrium data handbook.* Prentice Hall, New Jersey, **1989**.

Vyas, S. N.; Patwardhan, S. R.; Vijayalakshmi, S.; Sri Ganesh, K. Adsorption of Gases on Carbon Molecular Sieves, *J. Col. Interf. Sci.*, **1994**, 168, 275-280.

Xiao, J.; Wei, J. Diffusion Mechanism of Hydrocarbons in Zoelites-I. Theory. *Chem. Eng. Sci.*, **1992**, 47, 1123-1141.

Yang, R. T. *Gas Separation by Adsorption Processes.* Butterworths, Boston, **1987**.

Yang R. T. *Adsorbents. Fundamentals and Applications.* New Jersey, J. Wiley, **2003**.

Yang, R T.; Doong, S. J.; Gas separation by pressure swing adsorption: A pore-diffusion model for bulk separation. *AIChE J.*, **1985**, 31(11), 1829-1843.

Youngquist, G. R.; Allen, J. L.; Eisenberg, J. Adsorption of Hydrocarbons by Synthetic Zeolites, *Ind. Eng. Chem. Prod. Res. Develop.*, **1971**, 10, 308-314.

Zhang, Y.; Furukawa, S-I.; Nitta, T. Molecular Simulation Studies on Adsorption of Propane/Propylene in NaA Zeolite by Using Monte Carlo Technique., *J. Chem. Eng. Japan*, **2003**, 36(9), 1085-1094.

3. Binary Propane - Propylene Adsorption Equilibrium on Commercial Adsorbents

It is the purpose of this chapter to extend the characterization of two selected adsorbents by measuring binary propane-propylene adsorption equilibrium and predicting its behavior purely based in single-component adsorption equilibrium information. For this objective, a manometric–chromatographic unit was built and operated. Binary adsorption data were measured in two commercial adsorbents used for the pure component determinations: zeolite 4A (CECA) and carbon molecular sieve 4A (Takeda Corp). The methodology used for the prediction of binary adsorption equilibrium is also discussed.

3.1 Introduction

An adsorption process involves a mixture of gases entering simultaneously to a column filled with an adsorbent. Although we can predict multicomponent adsorption equilibrium by knowing the pure component behavior, this prediction may have large errors. Success in the prediction of multicomponent adsorption equilibrium is the key for a confident modeling and design of an adsorber. It was reported in literature that many systems have non-ideal behavior. The non-idealities can be such that one component can be the most adsorbed for a certain molar fraction and the less adsorbed in another molar fraction (at constant T and P). By analogy with gas – liquid equilibrium we will call the point where the molar fraction in the gas and in the adsorbed phases are the same as an azeotropic point. Many systems having an azeotrope have been reported (Talu and Zwiebel, 1986; Markmann and Mersmann, 1998). This effect is observed particularly when one of the components is polar and the other one is

non-polar, although many other considerations (like when the isotherms of the pure components cross each other) have to be taken into account (Do and Do, 1999). For a mixture of low chain hydrocarbons, azeotropes have not been reported, but deviations up to 50% from the ideal behavior have been observed (Ghosh et al., 1993; Costa et al., 1981). Particularly for the case of propane-propylene mixture, binary adsorption equilibrium has been reported for activated carbon (Lewis et al., 1950), zeolite 13X (Liapis et al., 1993) and silica gel (Lewis et al., 1950), showing deviations from ideality under certain conditions (Ghosh et al., 1993).

3.2 Theoretical

There are many models to describe adsorption equilibrium of multicomponent mixtures. Roughly they can be divided as descriptive models, where some multicomponent data are required, and predictive ones based on pure component adsorption to fit multicomponent data (Siperstein and Myers, 2001). Here we will only focus on some predictive models. Reviews with many of the predictive models published are available in literature (Ruthven, 1984; Yang, 1987; Do, 1998). A comparison using many of them to fit a given set of adsorption equilibrium data was also performed (Ahmadpour et al., 1998). In the case of the propane - propylene mixture, a comparison of several models can also be found (Da Silva, 1999).

The first model proposed to describe multicomponent adsorption equilibrium was the extension of the Langmuir equation. The same assumptions as for the pure component equation (the adsorbent is composed of identical localized sites and each site can accommodate only one molecule; the energy of adsorption is constant in all the sites and there is no interaction between adsorbed molecules) are applied to obtain (Yang, 1987):

$$q_i = \frac{q_{\max,i} K_{eq,i} P_i}{1 + \sum K_{eq,i} P_i} \qquad [3.1]$$

where $q_{max,i}$ and $K_{eq,i}$ are the maximum adsorption capacity and adsorption constant of component i, respectively. Although this equation is the most used for adsorber description, many systems do not obey the pure component Langmuir description and thus the binary prediction will also fail.

A more appropriate model with direct extension to multicomponent systems is the multisite Langmuir of Nitta. This model considers the solid as homogeneous but allows a single molecule to adsorb in more than one adsorption site. If we neglect adsorbate – adsorbate interactions, the multicomponent model can be expressed as (Nitta et al., 1984)

$$\theta_i = K_{\mathrm{eq},i} y_i P \left(1 - \sum \theta_i\right)^{a_i} \qquad [3.2]$$

where $\theta_i = q_i/q_{max,i}$ is the fractional amount of component i in the adsorbed phase, $q_{max,i}$ is the saturation capacity of component i, y_i is the molar fraction of component i in the gas phase, P is the equilibrium pressure and a_i is the number of neighboring sites occupied by component i. The equilibrium constant $K_{eq,i}$ is described by an Arrhenius law as explained in Chapter 2 for single component adsorption equilibrium. The saturation capacity of each gas is imposed by the thermodynamic constraint $a_i q_{\max,i} = \text{constant}$ (Sircar, 1995) to satisfy a material balance of sites in the adsorbent.

The Ideal Adsorbed Solution Theory (IAST) was the first complete model that describes multicomponent adsorption equilibrium with a theoretical thermodynamic background (Myers and Prausnitz, 1965). It is a widely used model to describe multicomponent equilibria because it requires only single-component adsorption parameters being purely predictive. This theory is obtained by equating the chemical potential of a species in the gas and in the adsorbed phases and stating that the adsorbed

phase is constituted by N-components and is ideal. This adsorbed phase is created by mixing pure adsorbed gases at constant surface potential. The mathematical framework of this theory is

$$-\frac{\phi_i}{R_g T}=\int_0^{P_i^0}\frac{q_i}{P}dP \qquad [3.3]$$

$$\phi_i{}^0\left(P_i{}^0,T\right)=\phi(P,T,y_i)=\text{constant} \qquad [3.4]$$

$$x_i=\frac{P}{P_i{}^0}y_i \qquad [3.5]$$

$$\left(\frac{1}{q_t}\right)=\sum_i\frac{x_i}{q_i\left(P_i^0\right)} \qquad [3.6]$$

where ϕ_i is the surface potential (or spreading pressure multiplied by the total area of the adsorbent), q_i is the amount adsorbed of component i, q_t is the total amount adsorbed, P is the total pressure of the system, y_i and x_i are the gas and adsorbed molar fractions of component i, and P_i^0 is the pressure equilibrium of the pure component at the surface potential of the mixture.

Other advantage of this model is that it puts no restrictions on the description of pure component equilibrium and so, different models can describe pure component adsorption equilibrium of the different gases. This is important because a good description of pure component adsorption equilibrium (particularly at low pressures) is very important to predict well the multicomponent behavior (Richter et al., 1989; Talu, 1998). When the multisite Langmuir model is used for the fitting of pure component data and introduced in the IAST model to predict binary mixtures, an analytical result is available (Sircar, 1995):

$$\theta_1=\frac{a_1K_{eq,1}Py_1\theta_1{}^0\left(\theta_2{}^0\right)^2\left(1-\theta_1{}^0\right)^{a1}}{a_1K_{eq,1}Py_1\theta_1{}^0\left(\theta_2{}^0\right)^2\left(1-\theta_1{}^0\right)^{a1}+a_2K_{eq,2}Py_2\theta_2{}^0\left(\theta_1{}^0\right)^2\left(1-\theta_2{}^0\right)^{a2}} \qquad [3.7]$$

$$\theta_2 = \frac{a_2 K_{eq,2} P y_2 \theta_2^{\,0} \left(\theta_1^{\,0}\right)^2 \left(1-\theta_2^{\,0}\right)^{a2}}{a_1 K_{eq,1} P y_1 \theta_1^{\,0} \left(\theta_2^{\,0}\right)^2 \left(1-\theta_1^{\,0}\right)^{a1} + a_2 K_{eq,2} P y_2 \theta_2^{\,0} \left(\theta_1^{\,0}\right)^2 \left(1-\theta_2^{\,0}\right)^{a2}} \qquad [3.8]$$

$$a_2(a_1-1)\theta_1^{\,0} + a_1 a_2 \ln\left(1-\theta_1^{\,0}\right) = a_1(a_2-1)\theta_2^{\,0} + a_1 a_2 \ln\left(1-\theta_2^{\,0}\right) \qquad [3.9]$$

$$K_{eq,1} y_1 \frac{\left(1-\theta_1^{\,0}\right)^{a1}}{\theta_1^{\,0}} + K_{eq,2} y_2 \frac{\left(1-\theta_2^{\,0}\right)^{a2}}{\theta_2^{\,0}} = \frac{1}{P} \qquad [3.10]$$

$$x_1 = \frac{a_2 \theta_1}{a_2 \theta_1 + a_1 \theta_2} \qquad [3.11]$$

where θ_1 and θ_2 are the fractional amounts of components 1 and 2 in the adsorbed phase, respectively and a_1 and a_2 are the number of sites occupied by adsorbed molecules of components 1 and 2, respectively.

We must mention that the introduction of the IAS theory in a PSA simulation for bulk gas separation requires many iterations to solve eqns [3-6] increasing severely the computational time and thus analytical expressions are always preferred.

In the IAS theory the adsorbed phase is considered as ideal, situation that cannot be applied to all systems. Many factors can make the adsorbed phase to follow non-ideal behavior (very different size and polarity of the components, adsorbate-adsorbate interactions as well as strong heterogeneity of the adsorbent are the most common).

The Vacancy Solution Theory, VST, was originally developed in the early 80' (Suwanayuen and Danner, 1980a,b). The adsorbed phase was considered as a non-ideal mixture of adsorbed molecules and unoccupied sites termed vacancies. The original theory made use of Wilson equations to calculate the activity coefficients. Later, the Flory – Huggins was used to calculate the activity coefficients (Cochran et al., 1985). The VST has an inconsistency in binary selectivity predictions in the Henry law limit (Talu and Myers, 1988). Recently, the Flory – Huggins form of the VST, termed VST –

FH, has been revisited and corrected (Bhatia and Ding, 2001). The new form of the VST – FH was reduced to the multisite Langmuir model (Nitta et al., 1984).

The corrected VST – FH has multiple advantages to describe adsorption equilibrium for the propane – propylene system: it is thermodynamically consistent at high and low pressures, has analytical extension to binary mixtures, describes non-ideal adsorption even predicting azeotropes and fundamentally, the prediction of multicomponent equilibrium based on pure component data is very good.

The corrected form of the VST – FH model is (Bhatia and Ding, 2001):

$$\frac{\theta_i}{\left(1-\sum_{j=1}^{N}\theta_j\right)^{\nu_i}} = \frac{\nu_i K_{eq,i}}{q_v^{\infty} R_g T} y_i P \qquad [3.12]$$

$$\theta_i = \frac{q_i \nu_i}{q_v^{\infty}} \qquad [3.13]$$

$$K_{eq,i} = \frac{R_g T q_v^{\infty} \exp(\alpha_{iv}) \exp(-\Delta G^0 / R_g T)}{(1+\alpha_{iv})} \qquad [3.14]$$

$$\nu_i = (1+\alpha_{iv}) \qquad [3.15]$$

$$\ln(\gamma_i^{a}) = 1 - \ln\left(\sum_{j=1}^{N+\nu} \frac{X_j}{(1+\alpha_{ij})}\right) - \left(\sum_{j=1}^{N+\nu} \frac{X_j}{(1+\alpha_{ij})}\right)^{-1} \qquad [3.16]$$

$$X_i = \frac{\theta_i}{\nu_i\left(1-\sum_{j=1}^{N}\theta_j(\nu_j-1)/\nu_j\right)} \qquad [3.17]$$

$$X_v = \frac{\left(1-\sum_{j=1}^{N}\theta_j\right)}{\left(1-\sum_{j=1}^{N}\theta_j(\nu_j-1)/\nu_j\right)} \qquad [3.18]$$

where q_i is the amount adsorbed of component i, $(-\Delta G^0)$ is a standard excess free energy, θ_i is the surface coverage (including the vacancies), X_i is the molar fraction

(vacancies are included) q_v^{∞} is the maximum vacancies concentration per weight of adsorbent, $(1+\alpha_{iv})$ are the Flory Huggins parameter that represents the ratio of molecular to vacancy area, v_i is the number of vacancies consumed per molecule adsorbed and R_g is the ideal gas constant.

Equations [3.12-3.14] can describe the pure component data that are then used in equations [3.16-3.18] to predict multicomponent behavior while equation [3.15] is written for thermodynamic consistency. The Flory – Huggins parameters are subjected to the following constraints:

$$\alpha_{jj} = 0 \qquad [3.19]$$

$$\alpha_{jk} + 1 = (\alpha_{ji} + 1)(\alpha_{ik} + 1) \qquad [3.20]$$

$$\alpha_{kj} + 1 = (\alpha_{jk} + 1)^{-1} \qquad [3.21]$$

for i,j,k = 1,2,...N, v. The parameter $q_v^{\infty} = q_v + \sum v_j q_j$ where q_v is the total amount of vacancies should not necessarily be the same for all gases. Note that in this model the vacancies are treated as a component of the mixture.

Another analytical equation that can be used in PSA units for propane-propylene separation is the multicomponent extension of the Toth model (see Chapter 2). This extension is given by (Da Silva, 1999):

$$q_i = q_{\max,i} \frac{K_{eq,i} P y_i}{\left[1 + \left(\sum_{i=1}^{N} K_{eq,i} P y_i\right)^{n_{mix}}\right]^{1/n_{mix}}} \qquad [3.22]$$

$$n_{mix} = \sum_{i=1}^{N} y_i n_i \qquad [3.23]$$

The use of the mixed heterogeneity parameter described in equation [3.23] is an empirical rule to overcome possible difficulties when the values of n_i of the components are very different.

3.3 Experimental

Adsorption equilibrium of binary mixtures is much more complicated to measure than pure component adsorption equilibrium. This is because there are three degrees of freedom instead of two as in vapor-liquid equilibria for example. The additional degree of freedom is given by the adsorbent. Also, the amount of each gas cannot be directly measured and has to be calculated from mass balances after measurements performed in the non-adsorbed phase (Talu, 1998). Usually, gas composition, temperature and total pressure are fixed to define the state of the system.

The most used devices to measure multicomponent adsorption equilibrium are gravimetric and manometric devices coupled with an appropriate analysis unit to monitor the non-adsorbed phase. In gas adsorption, the most used device for concentration measurement is a gas chromatograph, although many other techniques like Fourier Transform InfraRed (FTIR) spectroscopy (Rege and Yang, 2001) and frequency response (Polinski and Naphtali, 1963; Yasuda and Yamamoto, 1985; Sward and LeVan, 2003) can be applied. Another way to measure multicomponent adsorption is dynamic methods, like breakthrough curve measurements (Malek and Farooq, 1995). When considering the manometric and gravimetric methods, although the error in the total amount adsorbed is much less in the gravimetric device, the error in the molar fractions (determined by GC) is the same for both units. Detailed discussion about the benefits/disadvantages and the errors of these techniques has been published elsewhere (Talu, 1998).

At the beginning of this work at the LSRE, a gravimetric device with the limiting pressure of 100 kPa was available and it was located far away from the existent GC available to analyze propane – propylene mixtures. For this reason, a "mobile" manometric unit was designed and built. The main advantages of the unit were the low price investment together with the opportunity to extend the pressure range in the measurement of pure and multicomponent adsorption equilibrium.

Manometric Isotherm Equipment, MIE, was the name given to the manometric device able to measure adsorption equilibrium of pure components and binary mixtures and also kinetics of adsorption of pure components. The fundamentals of the equipment can be more easily explained by the scheme in Figure 3.1: a valve connects two individual chambers of known empty volume (Sircar, 1999). All the system is at the same temperature. Initially all the system is without adsorbate (vacuum) and the valve is closed. In the reservoir tank V_r a known amount of a gas mixture is inserted by the feed line. When pressure and temperature in the reservoir tank are stabilized, the valve is opened. The instantaneous decrease of pressure corresponds to the expansion of the gas into a larger volume and further decrease of the pressure with time is due to adsorption. After some time the equilibrium state is reached. When a mixture of gases is used, the equilibration time is not only dependent on the diffusion rate of the gas into the solid but also in their own molecular diffusivities to move through the pipelines in or out the adsorbent chamber. As the empty volume of the adsorption chamber V_o is known by helium calibration, a molar balance between the initial and final states gives the amount adsorbed. After equilibrium is reached, the valve is closed and the gas phase composition in the reservoir tank is analyzed by chromatography (in this case by Flame Ionization Detector, FID). A molar balance in both components will, by difference, give the composition of the adsorbed phase. Also, two different outlets were implemented in

the unit: when the pressure after reaching equilibrium is less than atmospheric, a vacuum pump is required to send the gases to the GC. Also, after analysis, to proceed to another binary measurement, the adsorbates have to be completely removed from the system by means of a vacuum pump. The other line is exactly to take care of the opposite situation: the vacuum pump cannot tolerate high pressure and part of the gas has to be purged (to exhaust) until near atmospheric pressure is reached. It should be stressed that an exhaust line is inserted in the equipment to protect the vacuum pump when the pressure in the reservoir tank is high.

This technique is traditionally called volumetric but as we are in fact measuring the pressure to calculate the adsorbed phase concentration it was called manometric (Rouquerol et al., 1999).

In any manometric unit, the errors in the total amount adsorbed are due to variations in the system temperature and the error of pressure measurements. Errors in chamber volume determination will produce an entire displacement of the set of data and are not incremented by successive measurements.

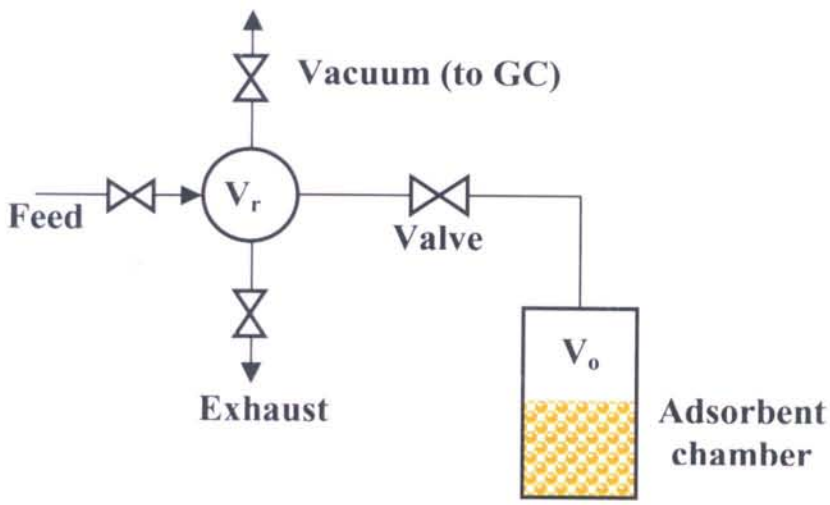

Figure 3. 1. Schematic diagram of the manometric-chromatographic unit, MIE

The main advantage when compared to gravimetric is that this equipment is much cheaper and it allows acquiring middle-pressure data without the need of a specialized device.

3.3.1 Data handling

Initially, we will explain the pure component data handling, although the same analysis will be used later for multicomponent mixtures. A pure gas is expanded from a reservoir volume of known volume V_r into a sample chamber containing a known amount of adsorbent w_s. The void volume of the sample chamber (total empty volume – volume of solid adsorbent) is V_o. The whole system is at the same temperature. When the adsorbent is clean, a transient molar balance is (Sircar, 2001)

$$V_r C^o{}_{r,i} = (V_r + V_o) C_i + \omega_s \langle \overline{q_i} \rangle \qquad [3.24]$$

where $C^o{}_{r,i}$ is the initial gas concentration of component i in the reservoir, C_i is the transient gas concentration of component i in the entire system and $\langle \overline{q_i} \rangle$ is the particle averaged amount adsorbed for component i. As we are interested in the adsorption equilibrium, this value is the same value as the local amount adsorbed, q_i, in the entire pellet and will be used in the rest of this chapter.

Equation [3.24] is a mass balance stating that the initial number of moles inserted in the tank reservoir is then distributed in the void volume and adsorbed by the adsorbent. The situation when the adsorbent is clean is described by this equation, although for pure component measurements, a sequential series of measurements were carried out. A more general equation that includes the possibility of a not clean adsorbent is presented here for step *(j+1)* with a prior completed equilibrium measurement performed in step *j*:

$$q_i\Big|^{j+1} = q_i\Big|^{j} + \frac{V_r}{\omega_s}\left[C^{o}{}_{r,i}\Big|^{j+1} - C_i\Big|^{j+1}\right] + \frac{V_o}{\omega_s}\left[C_i\Big|^{j+1} - C_i\Big|^{j}\right] \qquad [3.25]$$

Note that for $j = 0$, equation [3.25] reduces to equation [3.24] with the conditions of clean adsorbent: $q_i\Big|^{0} = C_i\Big|^{0} = 0$. In order to translate the concentration to the measured variable (pressure) the ideal gas law was always used.

As expressed before, the MIE is able to measure pure gas adsorption kinetics by monitoring the pressure decay with time (adsorbent uptake curve). The mathematical framework used to describe the kinetic measurements (diffusivity determinations) will be addressed in Chapter 4.

The procedure for binary adsorption equilibrium measurements is the same as the one for pure gases. The only difference is that in the case of multicomponent mixtures, the manometric unit by itself can only measure the total amount adsorbed and not the partial amount adsorbed of each gas. After measurements of the total adsorbed phase concentration, V2 and V3 are closed and GC analyzes the gas stored in the reservoir tank, as explained in section 3.2.2. Knowing the molar fraction of each component in the gas phase, equation [3.24] can be applied for each of the components to determine the adsorbed phase molar fractions.

3.3.2 Manometric Isotherm Equipment (MIE) description and measurement protocols

The scheme of the constructed equipment was shown in Figure 2.2. Temperature limitations are 305 – 673 K (minimum and maximum temperatures controllable of the GC oven) in the 0 – 500 kPa pressure range. The pressure transducer gives the pressure limit of the equipment and changing this device the upper pressure limit can be moved up to around 2,000 kPa where some of the mechanical connections (particularly the

thermocouple) may leak. However, if a high-pressure transducer is used the error in the low-pressure measurements may be quite large. The temperature in the reservoir and adsorbent chambers are controlled by a CG oven (Gira 1600, France) within ± 1K and the pressure transducer (Lucas Schaevitz, Type P9073-0102, Serial 218171, England) measures the pressure with an error of ± 0.04 kPa. The four-head membrane vacuum pump (ILMVAC, Germany) reaches high vacuum (less than 10^{-5} kPa) without contamination of the outlet gas going to analysis. The maximum pressure going to the head of the vacuum pump must not exceed 130 kPa. Higher pressures will broke at least one of the heads of the pump, which are very hard to replace. The outlet of the vacuum pump is directly connected to the GC, which has an additional vacuum pump at the end of the line allowing the multi-port valve to be filled with the sample. The gas exiting the MIE is at near atmospheric pressure and without this additional vacuum pump; the pressure decay produced by the 1/16" loops will be large enough to produce loss of the sample to the exhaust system. The K-thermocouple (Omega, USA) was inserted very slowly in the middle of the adsorbent column to prevent crushing of the pellets. The view of the complete unit is shown in Figure 3. 2.

Pressure and temperature sensors are connected to a computer using a PLC-818HG board (Advantech, USA). The software used (executable file) was fully developed in Visual Basic 5.0 CCE and allows the user to monitor and record pressure and temperature signals in a single file with a fixed pre-defined interval of time (one second by default).

At the outlet of the vacuum pump the equipment is connected to a GC (Chrompack) with a Flame Ionization Detector (FID), where a multivalve system (Vici, Valco) of 12 loops is installed. The GC configuration and use was detailed elsewhere (Da Silva, 1999). All the connecting lines and the loops are previously in vacuum ($<10^{-5}$

kPa). To check the purity in all the loops, a blank analysis is previously performed. The carrier gas used is nitrogen N50, a non-detectable gas by FID. After V2 and V3 are closed, the pressure (when working over atmospheric pressure) is regulated by V5 to 110 kPa to protect the vacuum pump (the entrance of the vacuum pump must be lower than 130 kPa). After the pressure equilibration, the sample goes to analysis. As the process is very fast, the switching of the loops should be made fast to fill 8 of the 11 loops available. Always the last loop filled should not be taken into account because the analysis has the gas in the loop and the gas that passes in all the GC tubes that produces saturation in the signal of the FID. The error in the molar fractions of the gas phase collected in the eight loops was always less than ± 0.2%.

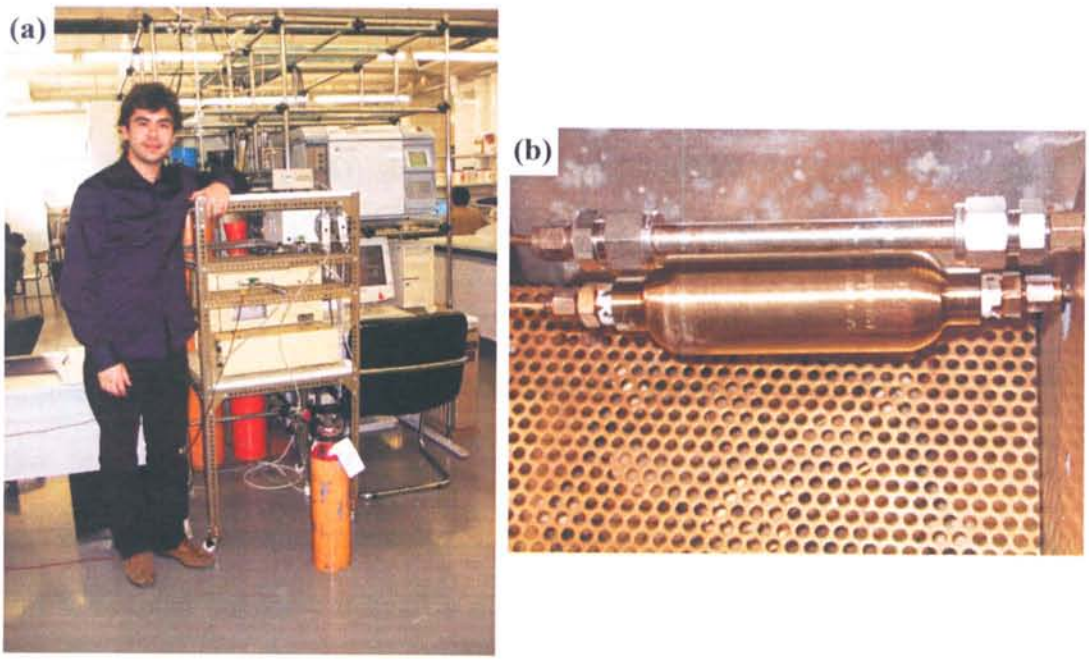

Figure 3. 2. View of the manometric-chromatographic unit, MIE (a) and detailed view of the reference tank and adsorbent chamber (b).

The MIE equipment can also be used to measure adsorption equilibrium measurements of pure components. The routine for pure component measurements is

similar to the one used in the gravimetric device. Initially all the system is in vacuum and all the valves are closed. The desired gas to be measured is inserted by opening V1. When the desired pressure is achieved, after one or two minutes for stabilization (gas enters at ambient temperature), V2 and V3 are simultaneously opened for adsorption of the gas. After equilibrium was reached (determined by a constant value of pressure and temperature), V2 and V3 are closed and a new amount of gas is allowed to enter to the system. The desorption run can be measured in a similar way. In the case of adsorption equilibrium with a final pressure higher than 130 kPa, before desorption run is performed, the pressure in the reference volume has to be lowered up to 120 kPa by opening V5. The vacuum pump is turned on with V2 and V3 closed, and V4 is opened for gas evacuation. In this work, total evacuation was used. When the reference volume is evacuated, V4 is closed and after stabilization V2 and V3 are simultaneously opened.

The routine for multicomponent measurements is the same as the one for pure components, except that only one point was measured and after the adsorbent was again activated. After lowering the pressure in the case of adsorption at pressures higher than 130 kPa, the vacuum pump is turned on and V4 is opened to allow the gas in the reference volume to be pushed by the vacuum pump to fill the loops in the multivalve system. Another technique also applied successfully was to close V2 and V3 and after fill the reservoir tank with helium to a pressure higher than 400 kPa and then open V4 to send the gas directly to the GC without the aid of the vacuum pump.

Note that in the experimental set-up there is no re-circulating pump. In the case of pure component measurements, the existence of this mixing is not important, although in the case of binary mixtures, problems with the molecular diffusivity in the tubing (smaller diameter connections) may arise. To determine the time required for a complete mixing of the gases, experiments without any adsorbent in the chamber at

three different molar relations and three different times (8, 16 and 24 hours) were performed. In all the cases, equilibration was completely ensured only after 16 hours. For security all binary equilibrium points reported here were measured at least after two days of contact adsorbate-gases.

3.3.3 Helium calibration

The volume of the reservoir tank together with all the tubing between V1 – V2 and V3 – V4 is 51.26 cm^3 and the volume of the adsorption chamber and tubing between V2 – V3 is 4.79 cm^3 (measured geometrically). With these values also very good agreement was shown in measuring the adsorption equilibrium isotherms of propane and propylene on NSG as shown in Chapter 2.

Before any equilibrium measurements, the adsorbent has to be stored in the adsorption chamber and the leak test has to be performed. As an example of the whole procedure we will detail the employed for the measurements with zeolite 4A (CECA) extrudates.

A sample of 3.0040 g (wet weight) of zeolite 4A (CECA, France) was stored in the adsorbent chamber. The activation of the sample was made at 593 K for a minimum period of 24 hours. After the initial activation, the system was tested to detect eventual leaks in vacuum ($< 10^{-5}$ kPa) at ambient temperature for 5 days and no changes (within the error of the pressure transducer) were observed.

The second step is to account for the volume of the solid part of the adsorbent in the cell (for calculation of V_o). For this, a so-called "calibration with helium" was performed. The helium calibration is the measurement of the free volume in the adsorbent chamber by expansion in it of a known amount of gas previously stored in the reservoir tank. By free volumes we understand the column voidage, tubing between V3

and V2 and the pore network where the helium molecules can penetrate. The main assumption of this helium calibration is that helium is not adsorbed on the sample. This is acceptable at low pressure and high temperatures. The values we are interested in are the initial pressure of helium in the reference tank, $P^{o}_{r,i}$, and the final pressure (reference tank plus free space in the adsorbent chamber), $P^{f}_{r,i}$. As can be seen in Figure 2.2, the system has V2, V3 and the pressure sensor outside the oven and in some part of the tubing a temperature gradient may be high. Thus the helium calibration was performed at several temperatures. As an example of the measurements, one of the measurements performed at 291 K is shown in Figure 3.3. The equilibration of the pressure is almost instantaneous and does not vary in at least 250 seconds (time when run was stopped). No variations in temperature were recorded in all the calibration procedure performed at ambient temperature (291 K), 373, 423 and 473 K.

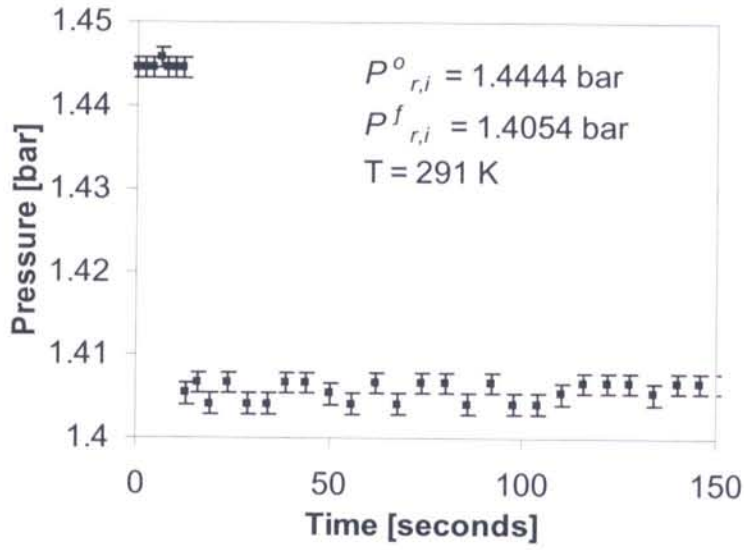

Figure 3.3 – Example of "helium calibration curve". The higher pressure corresponds to the helium initial pressure in the reservoir tank and the lower pressure is after opening the valves and expanded the gas in V_o

No significant variations within the error of the measurements were detected when comparing the measurements at different temperatures, indicating that the effect

of the temperature gradient in the tubing causes no detectable errors. A possible explanation of this can be due to the symmetry of the construction. The portion of tubing outside the oven that belongs to the reference tank is almost equal to the portion of tubing from the adsorption chamber. When counting the total amount of moles, the underestimation in one cell will compensate with the overestimation in the other. Of course the temperature gradient affects less than 1% of the total volume of the equipment. In the calibration procedure it was observed that oven instability (between 2-3K) might cause 5% error in the $P^{o}_{r,i} / P^{f}_{r,i}$ estimation.

The calibration curves are also useful to calculate the solid density of the adsorbent. In fact, the calibration curves are normally called as helium picnometry measurements (Suzuki, 1990). We are assuming that no helium is adsorbed and ideal gas behavior. The solid density, ρ_s, can be obtained by

$$\rho_s = \frac{\omega_s}{V_r\left(1-\frac{P_{r,i}}{P_{r,i}}\right)+V_o} \qquad [3.26]$$

The adsorbent weight (w_s) reported before was affected by a factor of 0.8 due to adsorption of air and water. This factor was determined in previous gravimetric analysis where the adsorbent lost 20% weight in the activation procedure.

Applying the data obtained in the calibration, the average value of the solid density of the zeolite 4A (CECA) is 1.82 g/cm³. This solid density together with the particle density of 1.21 g/cm³ (determined by mercury picnometry) results in a particle porosity of $\varepsilon_p = 0.34$.

3.3.4 Thermodynamic Consistency Test (TCT)

The measurement of multicomponent adsorption equilibrium data is much more time consuming than measuring pure component adsorption equilibrium. That is the

reason why much less literature is found dealing with this topic. Also, the multicomponent data is only calculated and not directly measured and thus influence of errors are enhanced (Talu, 1998). It is desirable thus to have good multicomponent data to calibrate theories for adsorber design. One way to establish the "good quality" of the data is to perform a thermodynamic consistency test to probe its validity (Myers and Sircar, 1972; Valenzuela and Myers, 1989).

In this work we will limit the analysis of the thermodynamic consistency test (TCT) to a binary mixture. This TCT relies in the use of the non-isothermal Gibbs adsorption equation expressed in terms of the Gibbsian Surface Excess (GSE) variables (Sircar, 1996):

$$d\phi = -S^m dT - \sum_i q_i{}^m d\mu_i \qquad [3.27]$$

where ϕ is the surface potential of the Gibbsian adsorbed phase, S^m is the excess entropy and μ_i is the equilibrium chemical potential of component i in the gas phase at constant P, T and y_i. Superscript m refers to the values calculated in the adsorbed mixture. This equation may be integrated and differentiated offering two possibilities to check the consistency of binary data.

Integrating equation [3.27] (Rao and Sircar, 1999) the Integral test is obtained:

$$\frac{\phi_1^*(P) - \phi_2^*(P)}{R_g T} = \int_0^1 \frac{\left(q_1{}^m y_2 - q_2{}^m y_1\right)}{y_1 y_2} dy_1 \Bigg|_{T,P} \qquad [3.28]$$

where q_i^m is the excess adsorbed phase concentration of component i in the multicomponent system and y_i is the gas phase molar fraction of component i (satisfying the constraint $y_1 + y_2 = 1$) and ϕ_i^* is the surface potential of adsorption of pure gas i that can be determined from pure gas adsorption isotherms as:

$$\frac{\phi_i^*(P)}{R_g T} = -\int_0^P \frac{q_i^*}{P} dP \Bigg|_T \qquad [3.29]$$

where q_i^* is the excess adsorbed phase concentration of component i calculated from pure component gas adsorption isotherms.

The integral test allows the calculation of the left hand side of equation [3.28] from pure component adsorption data while the right hand side has to be calculated from data at constant P and T varying y_1 (and consequently y_2).

The differential test is much more rigorous than the integral test and if satisfied, the integral test would also be obeyed. The differential test for a binary mixture is expressed by (Rao and Sircar, 1999):

$$q_1^*(P,T) = q^m(P,T,y_1) - P\frac{d}{dP}\left[\int_{y_1}^{1}\left\{\frac{q_1^m y_2 - q_2^m y_1}{y_1 y_2}\right\}_{P,T} dy_1\right]_{T,y_1} \qquad [3.30]$$

$$q_2^*(P,T) = q^m(P,T,y_1) + P\frac{d}{dP}\left[\int_{y_1}^{1}\left\{\frac{q_1^m y_2 - q_2^m y_1}{y_1 y_2}\right\}_{P,T} dy_1\right]_{T,y_1} \qquad [3.31]$$

subjected to the constraint

$$q^m = \sum_i q_i^m \qquad [3.32]$$

The left hand side of equations [3.30] and [3.31] can be evaluated from pure component data. The right hand side requires data at constant T and P with different y_i and also data at constant T, y_1 at different P which is much more difficult to obtain experimentally.

Even though, the integral and differential tests presented here are not only for experimental data but can be used as tools for determining if a new model obeys basic rules when extended to multicomponent mixtures. As an example when the integral test is performed to the multisite Langmuir model we obtain (Rao and Sircar, 1999):

$$\frac{\phi_1^*(P)-\phi_2^*(P)}{R_g T} = q_{\max,1}(1-a_1)\frac{q_1^*}{q_{\max,1}} - q_{\max,2}(1-a_2)\frac{q_2^*}{q_{\max,2}} - a_1 q_{\max,1}.\ln\left[\frac{1-\frac{q_1^*}{q_{\max,1}}}{1-\frac{q_2^*}{q_{\max,2}}}\right] \quad [3.33]$$

Because the multisite Langmuir model obeys equation [3.33] we can say that this equation is thermodynamically consistent. The same integral test for the Toth equation requires that $q_{max,i}$ should be the same for both components as well as n_i (heterogeneity parameter).

The influence of the Henry constant determination of pure components has a crucial effect in the surface potential calculations of pure component calculations as shown by Talu (Talu, 1998).

When the data collected are not-isobaric and/or not at the same temperature and also the experimental points are scarce to perform the integral in an accurate way there is another rule that can be applied to the data, although less rigorous than the test presented above. The thermodynamic consistency of the data can be roughly checked by the intersection rule: at constant T and P any pair of thermodynamically consistent x-y curves cross at least once in the region $0 < x_1 < 1$ (Valenzuela and Myers, 1989).

3.4 Binary adsorption equilibrium on zeolite 4A

After the loading of the adsorbent, follows the calibration with helium shown in last section and then pure component measurements, as reported in Chapter 2. The final stage of equilibrium measurements is the binary propane-propylene adsorption equilibrium that will be reported here. First, we have to mention that in all the binary experiments, propylene was initially adsorbed alone and only after equilibrium was reached, propane was injected to the system. Even when the equilibration time of the system is between 16 and 24 hours, as propane takes around three days to reach

equilibrium, the binary mixture was allowed to stay in contact with the adsorbent for 72 hours per point. Also, as propane adsorption equilibrium was only measured at 423 and 473 K, these temperatures were chosen to measure binary data. As the goal of these measurements is only to know if the behavior of the mixture is ideal or not, only one pressure was triggered, 100 kPa. As pointed out before, the final pressure in a manometric unit cannot be controlled and so most of the points were not really at 100 kPa but around this value.

The binary data was analyzed by two strategies:

STRATEGY 1: The generalized Dubinin model describes pure gas adsorption equilibrium of propylene while propane adsorption equilibrium obeys the Langmuir isotherm. Parameters of the fitting with these models are reported in Chapter 2. These equations were introduced in the mathematical framework of the IAST (equations [3.3-3.6]) to predict binary adsorption equilibrium.

STRATEGY 2: the Nitta model describes pure component adsorption equilibrium of both gases (parameters reported in Chapter 2) and prediction of binary data is performed by equations [3.7-3.11].

In Figure 3.4 we plot the *x-y* (adsorbed vs. gas phase molar fractions of the most adsorbed compound, propylene) diagram for propane – propylene at 423 K. The total pressure used for simulations was 100 kPa, although at the temperatures studied, total pressure has only a slight influence in the *x-y* diagram (solid lines). The experimental points are also plotted in this diagram and confirm the predictions. Complete information of the binary results is detailed in Table 3.1 for data storage (Grande et al., 2003). Note that the total pressure of the points is scatter and in all the cases the IAST (when used with the Dubinin model for propylene and Langmuir model for propane) predicts very well the data. This indicates that the binary mixture in the conditions

studied behaves like an ideal mixture. The corresponding data and predictions for 473 K are plotted in Figure 3.5 (experimental information is listed also in Table 3.1). The prediction of the theory is very good and the mixture is also ideal in these P-T conditions.

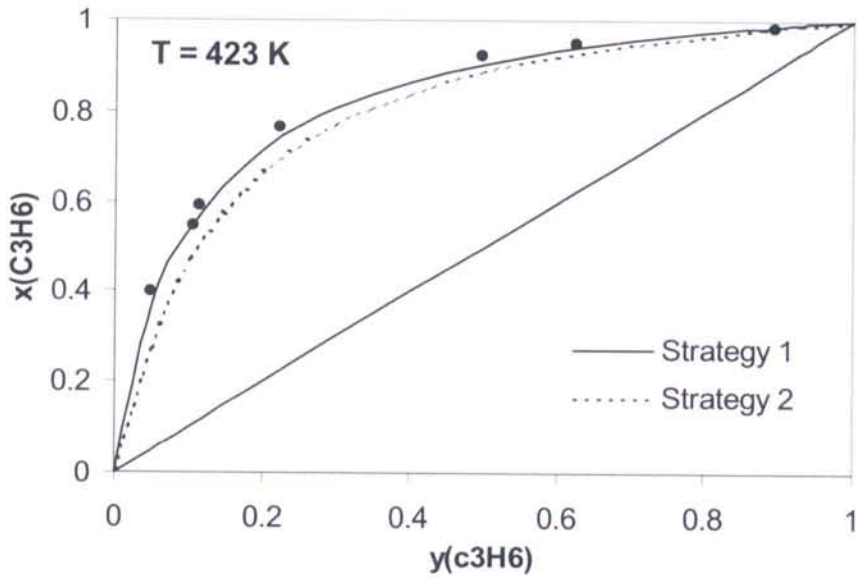

Figure 3.4: x-y diagrams at 423 K of propane – propylene equilibrium on zeolite 4A extrudates (CECA). Solid line – IAST with Dubinin (propylene) and Langmuir (propane) models and dashed line – IAST with multisite Langmuir model for both gases.

As the total pressure in all the points is different, a plot of the adsorbed phase concentrations vs. the molar fractions is not possible to build, but the total adsorbed phase concentration predicted with the IAST is plotted against the experimental values in Figure 3.6. Also, because of the non-isobaric nature of the data and the small number of points, the integral consistency test (Myers and Sircar, 1972) could not be performed. Although, the interception rule is obeyed at large propylene molar fractions (Valenzuela and Myers, 1989).

Table 3.1: Propane – propylene binary adsorption equilibrium at 423 and 473 K on zeolite 4A extrudates (CECA).

P [kPa]	y	x	q_t [mol/kg]	q_{sim} [mol/kg]
T = 423 K				
84.61	0.050	0.399	0.5731	0.5910
37.97	0.106	0.545	0.4503	0.4278
104.15	0.114	0.590	0.8192	0.7829
145.42	0.224	0.766	1.0924	1.0477
107.45	0.496	0.923	1.1420	1.1385
99.51	0.624	0.946	1.1657	1.1771
98.41	0.895	0.971	1.2716	1.2633
T = 473 K				
102.93	0.062	0.284	0.4595	0.4358
90.84	0.117	0.403	0.4983	0.4455
94.26	0.282	0.661	0.5989	0.5780
99.39	0.414	0.789	0.6769	0.6747
106.35	0.589	0.906	0.8098	0.7864
118.99	0.957	0.993	0.9515	0.9691

A second analysis was performed using the Nitta model to fit pure component adsorption and use in the IAST model. The multisite model is thermodynamically consistent model and fits well the data of propane and propylene (see Chapter 2). The fitting of propane is the same as with the Langmuir model because the Nitta model is Langmuir reducible, although its saturation capacity is imposed by the thermodynamic constraint $a_i q_{\max,i} = \text{constant}$ (Sircar, 1995). Binary adsorption equilibrium data at 473

K was well fitted with the multisite Langmuir model. The x-y plot at 423 K shows some deviations from experimental data. This deviation observed at 423 K may be due to some difference between the experimental data of pure component and the fitting of the multisite Langmuir model at low pressures (Henry constant) as observed in Figure 2.26.

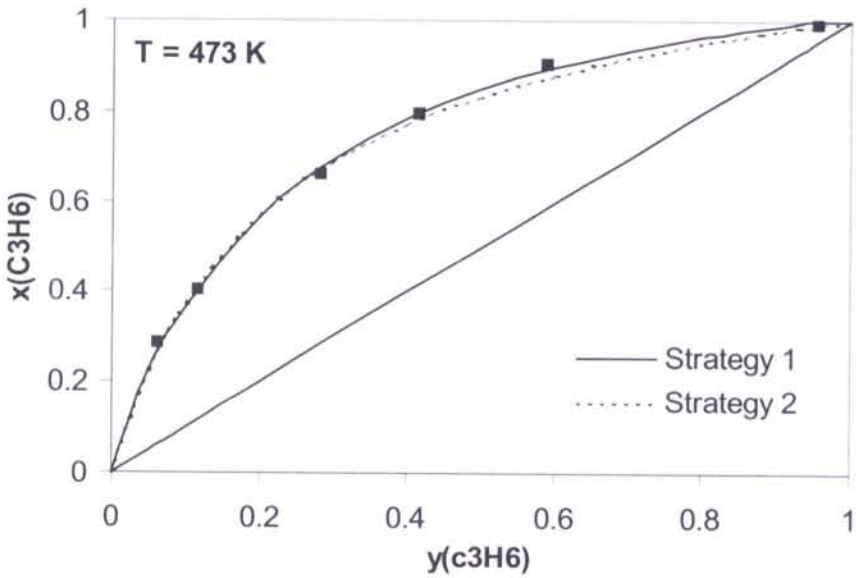

Figure 3.5: x-y diagrams at 473 K of propane – propylene equilibrium on zeolite 4A extrudates (CECA). Solid line – IAST with Dubinin (propylene) and Langmuir (propane) models and dashed line – IAST with multisite Langmuir model for both gases.

The model described by eqns [3.7-3.11] is the theoretical solution of the IAS theory using the multisite Langmuir model for description of pure gas adsorption. Even though the multisite Langmuir model has a direct expansion to multicomponent mixtures (equation 3.2). The fitting of the binary data presented here by equation [3.2] with the parameters extracted from pure gases is equivalent to the fitting of eqns [3.7-3.11] shown here. The multicomponent extension of this model (equation 3.2) is very suitable for PSA modeling.

The zeolite sample was the same for all the experiments reported in this chapter and in Chapter 2. Near 3 grams of adsorbent were used. After three months of

continuous exposure of propylene at high temperatures and pressures, the initial pure propylene experiment was completely reproducible indicating that no coke was formed.

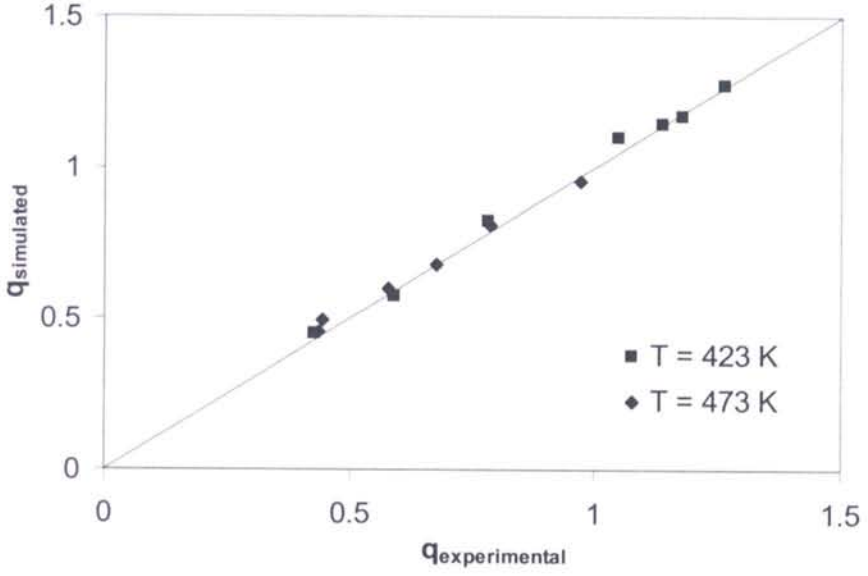

Figure 3.6: Comparison of the experimental total amount adsorbed with the predicted by IAST with Dubinin (propylene) and Langmuir (propane) models.

3.5 Binary adsorption equilibrium on carbon molecular sieve 4A

Besides zeolite 4A, another interesting adsorbent that was studied was the carbon molecular sieve 4A from Takeda Corp. Some experience was acquired with the measurement on zeolite 4A binary equilibrium. The main inconvenient of the data presented in section 3.4 is the final pressure that is different in almost all the samples. Even when this is one of the main disadvantages of the manometric-chromatographic technique (Sircar, 1999), under certain conditions, this problem can be circumvented. Assuming that the mixture is ideal, we proceed as explained before: first introducing propylene and when equilibrium was reached, propane is inserted. By assuming ideal behavior, we predict the moles adsorbed of each component and accounting the moles that have to remain in the gas phase, the moles that have to be inserted of each gas can be calculated. If the targeted pressure is not achieved we have the first indication that

the mixture is non-ideal, although this has to be confirmed by measuring the molar fractions of the gas phase.

For this adsorbent, only the middle temperature used in pure gas measurements was measured, 373 K. The total pressure targeted for the measurements were 47 and 255 kPa. The *x-y* (adsorbed vs. gas phase molar fractions of the most adsorbed compound, propylene) diagram at 47 kPa is shown in Figure 3.7. In this case only the multisite Langmuir model (solid line) was used for the prediction of binary behavior based on pure component data and its prediction compared with experimental binary data. In Figure 3.8 the total amount adsorbed versus y_{C3H6} is also shown together with prediction of multisite Langmuir model (solid line) at 47 kPa. Similar plots for a different total pressure of 255 kPa are shown in Figures 3.9 and 3.10. The prediction with the multisite Langmuir model (solid line in figures) is also very good. Experimental data plotted in these figures are tabulated in Table 3.3 for data storage and further application and/or model testing.

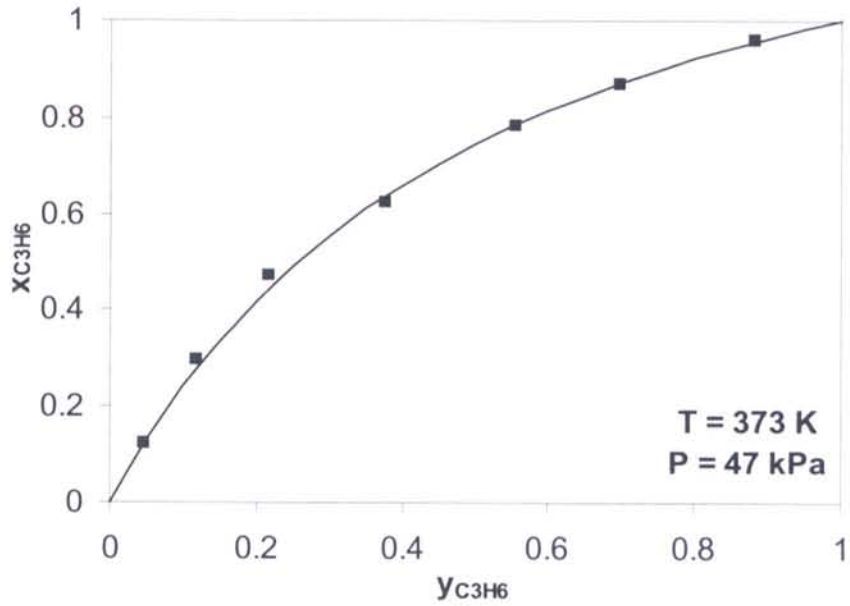

Figure 3.7: x-y diagrams at 373 K of C_3H_6-C_3H_8 on CMS 4A at pressures near 47 kPa. Solid line - multisite Langmuir prediction at 47 kPa.

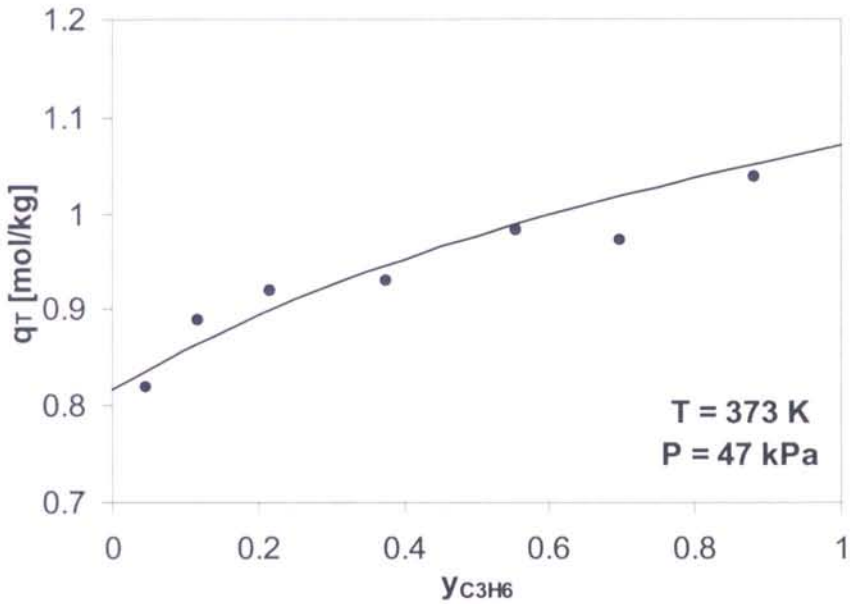

Figure 3.8: Total adsorbed phase concentration at 373 K for C_3H_6-C_3H_8 on CMS 4A at pressure around 47 kPa. Solid line - multisite Langmuir prediction at 47 kPa.

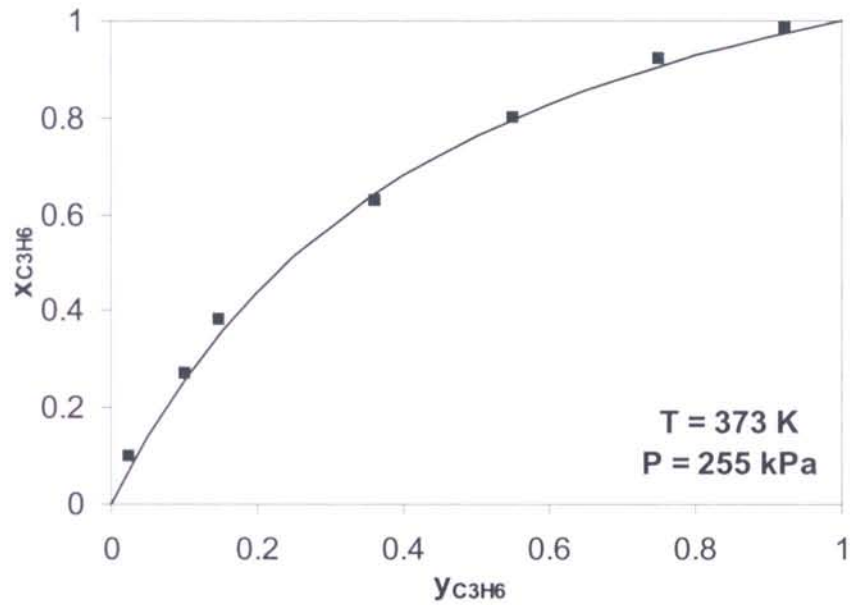

Figure 3.9: x-y diagrams at 373 K of C_3H_6-C_3H_8 on CMS 4A at pressures near 255 kPa. Solid line - multisite Langmuir prediction at 255 kPa.

In Figures 3.8 and 3.10 the point around $x_{C3H6} = 0.7$ is apparently outside the prediction of the model. Note from Table 3.3 that the total pressure of these two points is smaller than 47 and 255 kPa, respectively. Both points were measured without any calculation in case of ideal behavior, presenting as in the case of zeolite 4A the non-

isobaric characteristic. If the subject is to determine whether the behavior of the mixture is ideal or not, a constant value of the pressure is not very important. Even though in this case we were interested in testing the new equipment used for binary data measurements so the data had to be collected in such a way to allow us to perform the thermodynamic consistency test (TCT) of the data.

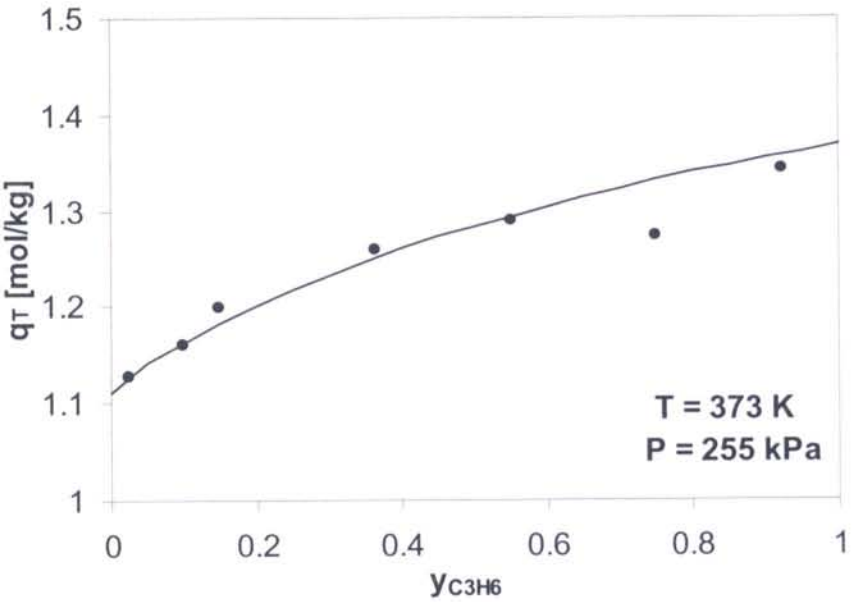

Figure 3.10: Total adsorbed phase concentration at 373 K for C_3H_6-C_3H_8 on CMS 4A at pressure around 255 kPa. Solid line - multisite Langmuir prediction at 255 kPa.

Table 3.2. Integral thermodynamic consistency test (TCT) for binary adsorption equilibrium of propane- propylene mixtures on CMS 4A (Takeda Corp.).

Pressure [kPa]	$\frac{\phi_1^*(P)-\phi_2^*(P)}{R_g T}$ [mmol/g]	$\int_0^1 \frac{\left(q_1^m y_2 - q_2^m y_1\right)}{y_1 y_2} dy_1 \Big\|_{T,P}$ [mmol/g]	|Difference|
47	1.091	1.010	0.081
255	1.678	1.580	0.098

Table 3.3: Propane – propylene binary adsorption equilibrium at 373 K at 47 and 255 kPa total pressure on carbon molecular sieve 4A extrudates (Takeda Corp).

P [kPa]	y_{C3H6}	x_{C3H6}	q_t [mmol/g]
T = 373 K			
47.25	0.882	0.960	1.037
46.92	0.117	0.291	0.858
47.37	0.047	0.124	0.840
46.89	0.217	0.455	0.920
47.14	0.377	0.624	0.929
46.92	0.555	0.782	0.982
42.00	0.698	0.869	0.972
249.43	0.550	0.800	1.288
249.86	0.362	0.627	1.258
251.02	0.148	0.373	1.195
249.68	0.025	0.100	1.127
249.27	0.922	0.982	1.341
249.66	0.100	0.271	1.160
244.30	0.750	0.921	1.273

The TCT was performed following equation [3.28]. On the left hand side the surface potential of pure gases was calculated using equation [3.29]. Then the right hand side of equation [3.28] was calculated only with binary data (see Table 3.2). Both terms have to be equal, but due to some experimental errors, there is a difference between them. The numerical values of these terms are shown in Table 3.3 for the pressures of

47 and 255 kPa. The difference between both terms is acceptable and is comparable with previous TCT results (Rao and Sircar, 1999).

3.6 Conclusions

In this chapter we have reported adsorption equilibrium of binary propylene – propane mixtures; two new sets of data not previously reported in literature were presented. For measurements a new manometric-chromatographic unit, MIE (Manometric Isotherm Equipment) was designed and built and its operation was described here.

Adsorption equilibrium of propane-propylene mixtures on zeolite 4A was presented. The experimental results were correlated with two different models: the IAS theory using two different isotherms for pure gases (Dubinin model for propylene and Langmuir model for propane). With this description of pure data the prediction of binary equilibrium is very good. A second analysis was performed using the multisite Langmuir model with also a good prediction of binary behavior. For the simplicity of this model it will be used in further applications (multicomponent breakthrough and PSA modeling).

Binary adsorption equilibrium was also measured on carbon molecular sieve 4A (Takeda Corp.) at two different pressures, 47 and 255 kPa. Prediction of the binary behavior was done with the multisite Langmuir model showing good agreement with experimental data. In this case data were measured at near constant pressures of 47 kPa and also 255 kPa. All points measured were used to perform the integral thermodynamic consistency test of the data showing that the data presented in this work are thermodynamically consistent and can be used for model calibration.

Nomenclature

a_i	number of neighboring sites occupied by component *i* (Nitta model)
C_i	bulk molar concentration of component *i* in the gas phase, mol/m^3
$C^o_{r,i}$	initial bulk molar concentration of component *i* in the reservoir of the MIE equipment, mol/m^3
K_{eq}	equilibrium constant, kPa^{-1}
$K_{eq}{}^o$	equilibrium constant at the limit T → ∞, kPa^{-1}
n_i	Heterogeneity parameter of the Toth model for component *i*
n_{mix}	Heterogeneity parameter of the Toth model for the mixture
N	number of components of the mixture (including vacancies in the VST model)
P	pressure, kPa
P_i	partial pressure of component *i* in the mixture, kPa
P_i^o	equilibrium pressure of component *i* at the surface tension of the mixture, kPa
$P^o{}_{r,i}$	initial pressure of component *i* in the reservoir of the MIE equipment, kPa
$P^f{}_{r,i}$	final pressure of component *i* in the reservoir of the MIE equipment, kPa
q_i	adsorbed phase concentration of component *i*, mol/kg
q_i^*	adsorbed phase concentration of pure gas *i* in single component adsorption experiments, mol/kg
q_i^m	excess adsorbed phase concentration of component *i* in the multicomponent system, mol/kg
$q_i\|^{j+1}$	adsorbed phase concentration of component *i* in step (j+1), mol/kg

$\langle \overline{q_i} \rangle$ adsorbed phase concentration of component *i* in step (j+1), mol/kg

q_v maximum amount of vacancies, mol/kg

q_v^{∞} maximum vacancy concentration per mass weight, mol/kg

q_t total adsorbed phase concentration, mol/kg

$q_{max,i}$ maximum adsorbed phase concentration of component *i*, mol/kg

R_g Ideal gas constant, 8.314 J/mol.K

S^m excess entropy of the mixture, J/mol.K

T temperature, K

V_o void space volume in the MIE experiments, m^3

V_r reference (initial) volume in the MIE experiments, m^3

ω_s adsorbent weight, kg

x_i molar fraction of component *i* in the adsorbed phase

X_i molar fraction of component *i* in the adsorbed phase including vacancies (valid only for VST model)

y_i molar fraction of component *i* in the gas phase

Greek Letters

$(1+\alpha_{iv})$ ratio of molecular to vacancy area in the VST model (Flory Huggins parameter)

ρ_p adsorbent density, kg/m^3

ρ_s density of the solid material that constitutes the adsorbent, kg/m^3

θ_i fractional coverage of component *i* on the adsorbed phase

θ_i^o fractional coverage of pure component *i* on the adsorbed phase corresponding to the pressure P_i^o

$(-\Delta G)$ standard excess free energy, J/mol

γ_i^a activity coefficients of component *i* in the adsorbed phase

v_i number of vacancies consumed per molecule adsorbed

ϕ surface tension of the mixture, J/kg

ϕ_i surface tension of component *i* in the mixture, J/kg

ϕ_i^* surface tension of adsorption of pure gas *i* in single component adsorption experiments, J/kg

ϕ_i^o surface tension of component *i* in pure component adsorption at pressure P_i^o, J/kg

Λ concentration variation parameter

μ_i equilibrium chemical potential of component *i* in the gas phase at constant *P*, *T* and y_i

References

Ahmadpour, A.; Wang, K.; Do, D. D. Comparison of Models on the Prediction of Binary Equilibrium Data of Activated Carbons. *AIChE J.*, **1998**, 44(3), 740-752.

Bhatia, S. K.; Ding, L. P. Vacancy Solution Theory of Adsorption Revisited. *AIChE J.*, **2001**, 47, 2136-2138.

Cochran, T. W.; Kabel, R. L.; Danner, R. P. Vacancy Solution Theory of Adsorption Using Flory – Huggins Activity Coefficient Equations. *AIChE J.*, **1985**, 31, 268-277.

Costa, E.; Sotelo, J. L.; Calleja, G.; Marrón, C. Adsorption of Binary and Ternary Hydrocarbon Gas Mixtures on Activated Carbon: Experimental Determination and Theoretical Prediction of the Ternary Equilibrium Data. *AIChE J.*, **1981**, 27(1), 5-12.

Da Silva, F. A. *Cyclic Adsorption Processes: Application to Propane / Propylene Separation*. Ph.D. Dissertation, University of Porto, Portugal, **1999**.

Da Silva, F. A.; Rodrigues A. E. Adsorption equilibria and kinetics for propylene and propane over 13X and 4A zeolite pellets. *Ind. Eng. Chem. Res.*, **1999**, 38, 2434-2438.

Do, D. D. *Adsorption Analysis: Equilibria and Kinetics*. Imperial College Press, London, **1998**.

Do, D. D.; Do, H. D. On the Azeotropic Behaviour of Adsorption Systems. *Adsorption*, **1999**, 5, 319-329.

Ghosh, T. K.; Lin, H.; Hines, A. L. Hybrid Adsorption – Distillation Process for Separating Propane and Propylene. *Ind. Eng. Chem. Res.*, **1993**, 32, 2390-2399.

Grande, C. A.; Gigola, C.; Rodrigues, A. E. Propane-Propylene Binary Adsorption on Zeolite 4A, *Adsorption*, **2003**, 9, 321-329.

Khodakov, A. Y.; Rees, L. V. C. Effect of Propane on the Kinetics of Carbon Dioxide Adsorption in NaA Zeolites, *Gas Sep. Purif.*, **1995**, 9(4), 253-257.

Lewis, W. K.; Gilliland, E.; Chertow, B.; Cadogan, W. Hydrocarbon Gas Mixtures. *Ind. Eng. Chem.*, **1950**, 42, 1319-1326.

Liapis, A.; Findley, M.; Johnson, J.; Jetz, S.; Finebrock, Q. Rates and equilibria of adsorption and desorption of propane and propylene on 13X molecular sieves determined experimentally using a differential sorption bed system, *Sep Technol.*, **1992**, 2, 141-154.

Malek, A.; Farooq, S. Determination of Equilibrium Isotherms Using Dynamic Column Breakthrough and Constant Flow Equilibrium Desorption. *J. Chem. Eng. Data*, **1995**, 40, 25-32.

Markmann, B.; Mersmann A. Prediction and Correlation of Multicomponent Adsorption Equilibria of Different Sized, Polar and Polarizable Gases on Energetically Heterogeneous Adsorbents at High Pressures. FOA-6, **1998,** 93-98.

BIBLIOTECA F.E. PORTO

Myers, A. L.; Prausnitz, J. M. Thermodynamics of Mixed-Gas Adsorption, *AIChE J.*, **1965**, 11, 121-127.

Nitta, T.; Shigetomi, T.; Kuro-Oka, M.; Katayama, T. An adsorption isotherm of multi-site occupancy model for homogeneous surface. *J. Chem. Eng. Japan*, **1984**, 17, 39-45.

Polinski, L. M.; Naphtali, L. M. A Novel Technique for Characterization of Adsorption Rates on Homogeneous Surfaces. *J. Phys. Chem.*, **1963**, 67, 369-375.

Rege, S. U.; Yang, R. T. A Novel FTIR Method for Studying Mixed Gas Adsorption at Low Concentrations: H2O and CO2 on NaX Zeolite and γ-Alumina. *Chem. Eng. Sci.*, **2001**, 56, 3781-3796.

Richter, E.; Schultz, W.; Myers, A. L. Effect of Adsorption Equation on Prediction of Multicomponent Adsorption Equilibria by the Ideal Adsorbed Solution Theory, *Chem. Eng. Sci.*, **1989**, 44, 1609-1616.

Rouquerol, F.; Rouquerol, J.; Song, K. *Adsorption by Powders and Porous Solids.* Academic Press, London, **1999**.

Ruthven, D. M. *Principles of adsorption and adsorption processes*. Wiley, New York, **1984**.

Siperstein, F.; Myers, A. L. Mixed Gas Adsorption. *AIChE J.*, **2001**, 47, 1141-1159.

Sircar, S. Influence of Adsorbate Size and Adsorbent Heterogeneity on IAST, *AIChE J.*, **1995**, 41, 1135-1145.

Sircar, S. Data Representation for Binary and Multicomponent Gas Adsorption Equilibria. *Adsorption*, **1996**, 2, 327-330.

Sircar, S. Gibbsian Surface Excess for Gas Adsorption – Revisited, *Ind. Eng. Chem. Res.*, **1999**, 38, 3670-3682.

Sircar, S. Measurement of Gibbsian Surface Excess, *AIChE J.*, **2001**, 47, 1169-1176.

Suwanayuen S.; Danner, R. P. A Gas Adsorption Isotherm Equation Based on Vacancy Solution Theory. *AIChE J.*, **1980a**, 26, 68-76.

Suwanayuen S.; Danner, R. P. Vacancy Solution Theory of Adsorption from Gas Mixtures. *AIChE J.*, **1980b**, 26, 76-84.

Suzuki, M. *Adsorption Engineering.* Elsevier, Tokio, **1990**.

Sward, B.K.; LeVan, D. Frequency Response Method for Measuring Mass Transfer Rates in Adsorbents via Pressure Perturbation, *Adsorption*, **2003**, 9(1), 37-54.

Talu, O. Needs, Status, Techniques and Problems with Binary Gas Adsorption Experiments, *Adv. Col. Interf. Sci.*, **1998**, 76-77, 227-269.

Talu, O.; Myers, A. L. Letter to the Editor. *AIChE J.*, **1998**, 34, 1931-1932.

Talu, O.; Zwiebel, I. Multicomponent Adsorption Equilibria of Nonideal Mixtures. *AIChE J.*, **1986**, 32(8), 1263-1276.

Valco Home page, http://www.valco.com/support/app/st_japp.htm

Valenzuela, D. P.; Myers, A. L. *Adsorption equilibrium data handbook.* Prentice Hall, New Jersey, **1989**.

Yang, R. T. *Gas Separation by Adsorption Processes.* Butterworths, Boston, **1987**.

Yasuda, Y.; Yamamoto, A. Zeolitic Diffusivities of Hydrocarbons by the Frequency Response Method. *J. Catal.*, **1985**, 93, 176-181.

4. Adsorption Kinetics of Propane and Propylene on Commercial Adsorbents

The purpose of this chapter is to quantify the kinetics of adsorption of pure propane and propylene on the commercial adsorbents used in Chapter 2 for adsorption equilibrium, namely: wide and narrow-pore silica gel, zeolite 5A pellets and crystals, carbon molecular sieve 4A and zeolite 4A. Measurements were carried out by three different techniques: Zero Length Column (ZLC), dilute breakthrough curves and adsorption uptakes in the manometric unit, MIE that will be analyzed and compared.

4.1 Theoretical

The adsorption equilibrium is a dynamic state established between the molecules in the gas phase and the ones in the adsorbed phase for a particular gas concentration and temperature. When one of these conditions is changed, the molecules experience a net driving force to move to another equilibrium state. This change takes time. The molecules in the gas phase have to move from the bulk phase into the inner part of the pellets passing through a possible resistance outside of the particle (film mass transfer resistance). Once inside it has to diffuse into the larger pores (macropore diffusion) finding an ideal location where to adsorb. Particularly in the case of adsorption in a bidisperse adsorbent, most of the molecules are adsorbed in the zeolite crystals or microporous network in the case of a carbon molecular sieve. They might find another resistance in the pore mouth of the micropores (barrier resistance at the mouth of the micropores). Finally it has to diffuse into the micropores (micropore diffusion) to the adsorption site(s) where adsorption takes place. An additional possibility is that the molecule has some difficulties to adsorb in the adsorption sites again delaying the

equilibrium state. This last resistance is not usual in adsorption processes and will not be considered in this thesis. As can be understand in this preface, when we termed "kinetics of adsorption" we are referring to the "kinetics of diffusion" of a certain molecule from the bulk gas phase to the sites where it will be adsorbed.

This diffusion process can be very slow particularly when the micropores have a size close to the molecular kinetic diameter or very fast when the molecule is very small when compared to the pores of the adsorbent. The rate of diffusion is also very important in the design of an adsorption process. In fact, separation of nitrogen/oxygen using carbon molecular sieves is based on the difference in the rates of diffusion of both molecules (Schröter, 1993). Also it is very important to know which technique will be used for such measurements. Some techniques are very good to detect very fast diffusion kinetics while others are more appropriate for slow kinetics as will be shown later.

Intuitively, when measuring adsorption equilibrium we can figure out the time constant of diffusion. As examples, when one pressure was changed to another value in the case of wide pore silica gel, the new equilibrium state was reached within 15 minutes, while for the system propane-zeolite 4A the same process took three days. Even though, this "idea" is not enough to design an adsorption process and more appropriated techniques have to be applied.

4.1.1 Adsorption uptake

All the diffusional processes are different and for this reason adequate techniques for measuring them might be different.

Independently of the accuracy, the most employed technique for measuring adsorption kinetics is the adsorption uptake. This measurement can be done in a

gravimetric or in a manometric unit when collecting the adsorption equilibrium data only with the extra effort of collecting enough points from one equilibrium state to another. This technique can be performed in two ways: starting from an evacuated (clean) adsorbent and increasing the concentration only in the range where the adsorption equilibrium isotherms are linear, or rising the concentration to a higher value. The first case is known as differential uptake and the second as integral uptake (Ruthven, 1984). In the case of a differential uptake the analysis is much simpler because as the concentration is still small, the entire process is isothermal and also the isotherm is linear. In the case of an integral uptake, the system may not have isothermal behavior and non-linear equilibrium adsorption models might be required. Also, in both differential and integral uptakes, the fact of having a finite amount of gas to be adsorbed has to be taken into account: the pressure in the initial and final state will be different. Additionally, the diffusivity coefficients may be not independent of concentration leading to different values when comparing both protocols. In the MIE equipment, both cases can happen: in the case of a slightly adsorbed species, the linear range of the isotherm will extend to higher pressures and adsorption kinetics measured under differential uptake assumptions considering concentration variations during the experiments. In the case of strongly adsorbed species, the pressure in the reference tank has to be relatively high because otherwise it will drop to very small values after adsorption; therefore, the accuracy will be lower. In this case, the concentration variation together with the non-linearity of the adsorption equilibrium has to be considered. Also in this case if adsorption is fast, the heat of adsorption cannot be rapidly released and thermal effects have to be taken into account.

We will discuss the general case of the integral uptake in a bidisperse adsorbent and then present the particular solution of a differential uptake with linear isotherm and isothermal behavior.

In a traditional batch experiment the clean adsorbent is placed in a well-stirred tank immersed in a very large medium (considered as infinite) or in a semi-infinite medium of the gas which diffusion will be measured. In the analysis of the batch technique used in this work we have no stirring device so, as a first approximation, we will consider that the fluid is stagnant. As the measurements were performed with bidisperse extrudates, macropore and micropore resistances were considered and also as the fluid is static, a mass transfer external resistance was included in the model.

In any batch experiment, when the adsorbent is clean, the molar balance between times 0 and t is (Sircar, 2001)

$$P = \left[\frac{V_r P_o - R_g T w_s \langle \bar{q} \rangle}{V_r + V_o} \right] \qquad [4.1]$$

where P_o and $P(t)$ are the initial and bulk gas pressure at time t, V_r and V_o are the reference and void column volumes (Sircar, 2001), R_g is the ideal gas constant and w_s is the adsorbent mass used. The micropore-averaged amount adsorbed $\bar{q}$ and the extrudate-averaged amount adsorbed $\langle \bar{q} \rangle$ are defined by

$$\bar{q} = \frac{3}{r_c^3} \int_0^{r_c} q r^2 \, dr \qquad \langle \bar{q} \rangle = \frac{2}{R_p^2} \int_0^{R_p} \bar{q} R \, dR \qquad [4.2]$$

where R_p and r_c are the radius of the extrudate and the crystal, respectively. When writing these equations we are assuming that the extrudates can be considered as infinite cylinders and the crystal as perfect spheres. Equation [4.1] is a mass balance saying that the number of moles initially present in the tank reservoir is finally distributed in the void volume and adsorbed by the adsorbent. We have assumed ideal gas behavior and

also that the calibration procedure with helium (to determine the V_o value) was performed in such conditions that no helium was adsorbed by the adsorbent.

The Fickian description of diffusion in a spherical zeolite crystal or microporous network in a CMS (where micropores are located) is

$$\frac{\partial q}{\partial t} = \frac{1}{r^2}\frac{\partial}{\partial r}\left[D_c r^2 \frac{\partial q}{\partial r}\right] \qquad [4.3]$$

where D_c is the micropore or crystal diffusivity. This equation has to be solved with the following initial and boundary conditions

$$q_{(r,0)} = 0 \qquad [4.4]$$

$$\left.\frac{\partial q}{\partial r}\right|_{(0,t)} = 0 \qquad [4.5]$$

$$q_{(r_c,t)} = q_s = f(C_p) \qquad [4.6]$$

The micropore diffusivity has an exponential dependence with temperature described by:

$$D_c = D_c^{\circ} \exp(-E_a/R_g T) \qquad [4.7]$$

where D_c^o is the limiting diffusivity at infinite temperature and E_a is the activation energy.

Equation [4.6] is the condition of adsorption equilibrium at the crystal surface. In this work, the isotherm used was the multisite Langmuir model (Nitta et al., 1984):

$$\left(\frac{q_s}{q_{max}}\right) = K_{eq} P_p \left[1 - \left(\frac{q_s}{q_{max}}\right)\right]^a \qquad [4.8]$$

where q_{max} is the maximum amount adsorbed, a is number of neighboring sites occupied per molecule and K_{eq} is the adsorption constant which has an Arrhenius exponential temperature dependence as:

$$K_{eq} = K_{eq}^{\,0} \exp(-\Delta H / R_g T) \qquad [4.9]$$

where $K_{eq}^{\ 0}$ is the adsorption constant at the limit of $T \to \infty$ and $(-\Delta H)$ is the isosteric heat of adsorption at zero coverage (Sircar, 1995).

The mass balance in a volume element of the extrudate is represented by:

$$\varepsilon_p \frac{\partial C_p}{\partial t} + \rho_p \frac{\partial \bar{q}}{\partial t} = \frac{1}{R} \frac{\partial}{\partial R} \left[\varepsilon_p D_p R \frac{\partial C_p}{\partial R} \right] \qquad [4.10]$$

with initial condition:

$$C_{p(R,0)} = 0 \qquad [4.11]$$

and boundary conditions:

$$\varepsilon_p D_p \left. \frac{\partial C_p}{\partial R} \right|_{(R_p,t)} = k_f \left(C - C_p \right)_{(R_p,t)} \qquad [4.12]$$

$$\left. \frac{\partial C_p}{\partial R} \right|_{(0,t)} = 0 \qquad [4.13]$$

where D_p is the pore diffusion coefficient, ε_p is the pellet porosity, C_p is the gas concentration in the macropores, R_p is the pellet radius and k_f is the film mass transfer resistance in the external surface of the extrudate.

The linking between the pressure and the concentration (in the bulk and macropores) is the ideal gas equation, which is assumed to be valid in the entire range of pressure and temperatures used in this work.

$$P = CR_gT \qquad P_p = C_pR_gT \qquad [4.14]$$

where C is the hydrocarbon concentration in the bulk phase and P_p is the pressure of hydrocarbon in the macropores.

The pore diffusivity is a function of the molecular and Knudsen diffusion and the temperature dependence is described by the Bosanquet equation. In this case of pure gas measurements, instead of the molecular diffusivity, the self-diffusivity was employed (Bird, Stewart and Lighfoot, 2002):

$$\frac{1}{D_p} = \frac{\tau_p}{D_{AA}} + \frac{\tau_p}{D_K} \qquad [4.15]$$

with

$$D_{AA} = \frac{4.186.10^{-6}}{M_w^{1/2}} \frac{P_c^{2/3}}{T_c^{1/6}} \frac{1}{C} \qquad [4.16]$$

$$D_K = 9700 r_p \sqrt{\frac{T}{M_w}} \qquad [4.17]$$

where τ_p is the tortuosity of the pellet, M_w is the molecular weight of the gas (mol/g), r_p is the pore radius (cm) and P_c (atm) and T_c (K) are the critical pressure and temperature, respectively. In equation [4.15] the first term of the r.h.s. corresponds to the self-diffusivity D_{AA} (cm²/s) while the other term is the Knudsen diffusion, D_K (cm²/s). In equation [4.16], the bulk gas concentration, C has to be expressed in mol/cm³.

For fast-adsorbed species, the heat released in the initial moments of adsorption is not easily dispersed and so the energy balance has to be coupled to the mass balance because the process cannot be assumed as isothermal. The energy balance in the gas phase is expressed by:

$$\frac{\varepsilon_c P C_{vg}}{R_g T} \frac{\partial T}{\partial t} + (1-\varepsilon_c) \frac{2}{R_p} h_f (T - T_s) + \frac{2}{R_w} h_w (T - T_w) = 0 \qquad [4.18]$$

where ε_c is the bed porosity, C_{vg} is the constant volume specific heat capacity of the gas mixture, T, T_s and T_w are the gas, solid and wall temperatures and h_w and h_f are the film heat transfer between the gas and the wall and between the gas and the solid particles, respectively. Eq. [4.18] is similar to a packed balance without the velocity terms (Da Silva, 1999). The energy balance for the solid phase is:

$$\rho_p C_{ps} \frac{\partial T_s}{\partial t} = \frac{2}{R_p} h_f (T - T_s) + \rho_p (-\Delta H) \frac{\partial \langle q \rangle}{\partial t} \qquad [4.19]$$

where C_{ps} is the constant pressure specific heat capacity of the solid. The initial condition for both energy balances is:

$$T_{(0)} = T_{s(0)} = T_w \qquad [4.20]$$

The film mass and heat transfer parameters were estimated assuming that the fluid is stagnant by:

$$Sh = \frac{R_p k_f}{D_{AA}} = 1 \qquad [4.21]$$

$$Nu = \frac{R_p h_f}{k_g} = 1 \qquad [4.22]$$

where k_g is the thermal conductivity of the gas. For the convective heat transfer coefficient between the gas and the wall column, the Wasch and Froment correlation as stagnant fluid was used (Da Silva, 1999):

$$\frac{h_w R_w}{k_g} = 10\gamma \qquad [4.23]$$

where γ is a relation of conductivities and has been assigned a value of $\gamma = 7$.

A simplification that can be done when the temperature increments are not large is to assume that gas thermal conductivity and C_{vg} and C_{ps} have constant values and that they do not change with temperature and pressure.

Note that in this analysis we have not included the possibility of a surface barrier resistance in the pore of the micropores like happens with some kind of carbon molecular sieves (Qinglin et al., 2003). In this case, equation [4.6] has to be replaced with

$$\frac{3}{r_c} D_c \left.\frac{\partial q}{\partial r}\right|_{r=r_c} = k_b (q_s - q)_{r=r_c} \qquad [4.24]$$

where k_b is the barrier mass transfer coefficient at the mouth of the micropore.

This set of partial differential equations has not analytical solution and has to be solved numerically. There is a special case of analytical solution when the only the micropore resistance is important (spherical crystals) and when the process is isothermal and also the entire experiment is performed under conditions of linear adsorption equilibrium. The adsorption uptake is given by (Ruthven, 1984; Kärger and Ruthven, 1992):

$$\frac{q}{q_s} = 1 - 6\sum_{n=1}^{\infty} \frac{\exp(-D_c \alpha_n^{\,2} t / r_c^{\,2})}{9\Lambda/(1-\Lambda) + (1-\Lambda)\alpha_n^{\,2}} \qquad [4.25]$$

where D_c is the micropore diffusivity, r_c is the crystal radius and $\Lambda = (C_o - C_{eq})/C_o$ with C_o being the initial concentration and C_{eq} the concentration of the gas phase when equilibrium is reached. Roots α_n are calculated by $\tan(\alpha_n) = 3\alpha_n / [3 + (1/\Lambda - 1)\alpha_n^{\,2}]$.

4.1.2 Zero Length Column

The Zero Length Column (ZLC) is a powerful technique for measurements of diffusivities of pure gases in porous solids (Eic and Ruthven, 1988). The procedure is to saturate a small amount of adsorbent with a dilute mixture of adsorbate until equilibrium in the adsorbed phase is reached. Then the inlet is switched to an inert stream to clean the adsorbent. From this desorption curve the diffusivity and equilibrium parameters are extracted. This technique has been extensively used for diffusivity measurements in zeolites (Ruthven and Xu, 1993; Hufton and Ruthven, 1993; Cavalcante et al., 2000).

In the case of a bidisperse adsorbent, macropore, micropore or both resistances can be important in the diffusion process. There are three ways to assess their relative importance:

1) To perform similar experiments with two inert gases: if the micropore resistance is the controlling diffusion mechanism, the curves should be independent of the inert gas (Da Silva and Rodrigues, 1999).
2) To perform the experiments in the desired temperature range and then carry out one experiment at a much higher temperature. At high temperatures macropore resistance should control the diffusion (Schneider and Smith, 1968).
3) Experiments with different pellet size: in the case of spherical pellets the curves will depend on R_p^2 if macropore resistance is controlling and will be independent of the pellet size if micropore diffusion resistance controls. In the transition regime the dependence of the curves with pellet size will vary between these extremes.

The second alternative is the easiest way to treat bidisperse adsorbents; however, polymerization can occur in the case of olefins or desorption can be much faster at high temperatures. Alternatives 1 and 3 require the same number of experiments but when the dilute mixture is previously prepared in a bottle, option 3 is much faster than option 1.

In the following analysis we will consider that the homogeneous equation and the Fick's law of diffusion can be applied to the kinetic measurements of a sorbate in an extrudate by ZLC. The mass transfer control is limited by macropore or micropore diffusion and sorbate concentrations used are low enough to describe adsorption equilibrium by the Henry law (linear isotherm).

With these assumptions, solutions for infinite slabs, infinite cylinders and spheres were obtained (Brandani and Ruthven, 1996; Silva, 1998):

$$\frac{C}{C_o} = 2L\sum_{n=1}^{\infty} \frac{\exp\left(-D_{ap}\beta_j^{\,2} t/\ell^2\right)}{\beta_j^{\,2} + L(L+1-n)} \qquad [4.26]$$

where n = 0, 1 and 2 for slabs, cylinders and spheres respectively, C and C_o are the instantaneous and initial gas phase concentration respectively, $D_{ap} = \varepsilon_p D_p/[\varepsilon_p+(1-\varepsilon_p)K_{eq}]$ is the apparent diffusivity and K_{eq} is the equilibrium constant, ℓ is the representative spatial dimension of the pellet (radius for infinite cylinder and sphere and half length for infinite slab) and L is the ZLC parameter.

$$L = \frac{Q_P \ell^2}{(n+1)K^* V_s D_{ap}} \qquad [4.27]$$

where Q_p is the purge flowrate, $K^* = \varepsilon_p+(1-\varepsilon_p)K_{eq}$ and V_s is the volume of adsorbent in the cell. The roots β_j for the different geometries are given by

Slabs	Cylinder	Spheres
$\beta_j \tan(\beta_j) - L = 0$	$\beta_n J_1(\beta_n) - L J_0(\beta_n) = 0$	$\beta_k \cot(\beta_k) + L - 1 = 0$

[4.28]

where J_0 and J_1 are Bessel functions of first kind of order zero and one respectively.

For the case of micropore control, the apparent diffusivity has to be replaced by the crystal diffusivity and the spatial coordinate is with respect to the crystal.

The long time response (LTR) for spherical pellets assuming linear equilibrium model is:

$$\ln\left(\frac{C}{C_o}\right) \cong \ln\left(\frac{2L}{\beta_1^2 + L(L+1-n)}\right) - \frac{\beta_1^2 D_{ap} t}{R_p^2} \qquad [4.29]$$

For large values of the parameter L, the approximation $\beta_1 = \pi$ is valid although the ratio C/C_o is still a function of L, which includes the purge flowrate. Equation [4.29] indicates that for sufficiently high flow rates, under kinetic control, the effective diffusivity is independent of the purge flow rate. Plotting eq. [4.29] as $\ln(C/C_o)$ *versus* time and fitting it to the long times desorption data, the slope is $-\beta_1^2 D_{ap}/R_p^2$.

4.1.3 Dilute breakthrough curves

When the amount adsorbed is very small or when adsorption kinetics are extremely fast, ZLC has a sudden drop very near to the baseline of the experimental set-up and cannot be accurately measured. In this case, another technique that can be employed to measure adsorption equilibrium (with less limitations about the mass of adsorbent) are breakthrough curves. Even though, kinetic measurements for fast diffusing species will have the complication of other resistances that can be ignored in ZLC experiments under certain conditions. In the breakthrough technique, a step gradient in the concentration is imposed into a packed column. Measuring the concentration at the outlet of the column, the adsorption kinetics as well as the adsorption equilibrium can be computed.

In this chapter we will only concentrate in dilute breakthrough curves. In all the experiments we have used a clean adsorbent and imposed a step concentration of 1% of the desired hydrocarbon dilute with an inert gas. The advantage of these experiments is that we are almost ensuring that the whole run is under linear adsorption equilibrium conditions, and as the amount of gas adsorbed is very small when compared to the total amount of gas fed, the velocity in the entire column can be considered constant. In accordance to the "trace system" assumption, the process is also assumed to be isothermal.

For the analysis of the dilute breakthrough curves we will consider the case of a bed filled with a bidisperse adsorbent where the flow can be considered as axial dispersed flow. Additionally to the macropore – micropore resistances we have included the possibility of a film resistance in the external surface of the pellets. The mass balance in a differential element of the column can be described as (Ruthven, 1984):

$$\frac{\partial C}{\partial t}+\left(\frac{1-\varepsilon_c}{\varepsilon_c}\right)\varepsilon_p\frac{\partial\langle C\rangle}{\partial t}+\left(\frac{1-\varepsilon_c}{\varepsilon_c}\right)\rho_p\frac{\partial\langle\bar{q}\rangle}{\partial t}=D_{ax}\frac{\partial^2 C}{\partial z^2}-u_i\frac{\partial C}{\partial z} \qquad [4.30]$$

with initial condition:

$$C_{(0,z)}=0 \qquad [4.31]$$

and Danckwerts boundary conditions:

$$D_{ax}\left.\frac{\partial C}{\partial z}\right|_{(t,0)}=u_i(C-C_o) \qquad [4.32]$$

$$\left.\frac{\partial C}{\partial z}\right|_{(t,L)}=0 \qquad [4.33]$$

where D_{ax} is the axial dispersion coefficient, ε_c is the porosity of the column, $\langle C\rangle$ is the particle-averaged concentration in the macropores of the pellet and u_i is the interstitial gas velocity. The pellet-averaged concentration in the macropores is defined as:

$$\langle C\rangle=\frac{2}{R_p^{\,2}}\int_0^{Rp}CR\,dR \qquad [4.34]$$

The micropore – macropore resistances are described using equations [4.3-4.13]. In equation [4.15] the self-diffusivity is replaced by the molecular diffusivity.

Once the equilibrium has been verified and calculated from dynamic experiments, the kinetic parameters determined by ZLC will be confronted with the one needed to fit the breakthrough curves. In order to use the bidisperse model above, we need to calculate the axial dispersion coefficient and the film mass transfer resistance. The axial diffusion coefficient has been calculated by (Ruthven, 1984):

$$D_{ax}=(0.45+0.55\varepsilon_c)D_m+\gamma_2 2R_p u_i \qquad [4.35]$$

where γ_2 is constant with value of 0.5 and D_m is the molecular diffusion coefficient.

To calculate the film mass transfer coefficient, the correlation proposed by Wakao and Funazkri has been used (Ruthven, 1984):

$$Sh = 2.0 + 1.1 Sc^{1/3} \mathrm{Re}^{0.6} \qquad [4.36]$$

with the dimensionless numbers defined by:

$$\mathrm{Re} = \frac{\rho_g u_i d_p}{\mu_g} \qquad Sc = \frac{\mu_g}{\rho_g D_m} \qquad Sh = \frac{2\mathrm{R}_p k_f}{D_m} \qquad [4.37]$$

4.1.4 Procedure for parameter fitting to experimental data

Once experimental data are obtained, some model has to be used for data treatment and interpretation. This model is implemented in a computer program and fitted to the data giving as final result the parameter or parameters of the model that better describes the data for a given acceptable error. All the simulations were made in MATLAB. The minimization routine used finds the minimum of the objective function using the Nelder – Mead Simplex Method of direct search (Morgan, 1997).

For this purpose, an error function must be defined. In Chapter 2 we have used the Square of Residuals (SOR) for fitting the adsorption equilibrium data.

In the case of ZLC curves, the range of the ordinate (C/C_o) is very wide and the SOR will mainly account for the larger concentrations ignoring the tail of the curve corresponding to the long-time scale. For the cases of a wide range of ordinate values, the Average of Residuals (ARE) is defined as:

$$ARE = \frac{100}{\mathrm{S}} \sum_{k=1}^{S} abs \left| \frac{(C/C_o)_{\text{calculated}} - (C/C_o)_{\text{experimental}}}{(C/C_o)_{\text{calculated}}} \right| \qquad [4.38]$$

where S is the number of experimental points per isotherm. The ARE function compensate the errors in a wide range of values.

To illustrate this point it is shown the result of the same computer program used to fit a given set of experimental data with both functions (SOR and ARE) used for error minimization. In Figure 4.1a we have plotted the experimental points and the best

fitting results obtained using the ARE and SOR functions. Using the SOR, the fitting of the curve is good for higher values of C/C_o while for smaller values, the computed error is insignificant according to that function. This is also shown in Figure 4.1b where the error for higher times is near zero, while for the initial points is much higher indicating that these points will control the fitting of the curve. A different behavior is presented by the ARE where a more uniform model is obtained in the whole curve, giving more importance to the points in the "Long Time Response" which we are mainly interested in. In Figure 4.1b the error of this function is also shown. It can be noticed that more points contribute to the global error producing a more uniform fitting. For this reason, the ARE method was used for parameter fitting of all ZLC experiments.

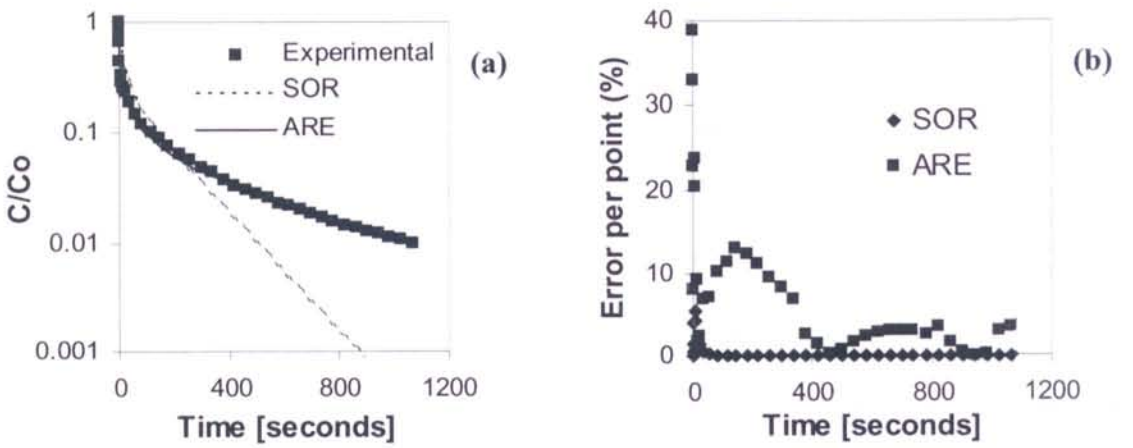

Figure 4.1. (a) Experimental data fitting using the SOR (Square of Residuals) and ARE (Average of Residuals) as minimization functions and (b) the error per point associated to these minimizations.

4.2 Experimental

As mentioned before, in this chapter adsorption kinetics was measured by three different techniques. For the case of ZLC and dilute breakthrough experiments, the equipment used is essentially the same, replacing the ZLC cell by a bigger column completely filled with particles. When this work started, the set-up of the ZLC unit

previously used for other measurements (Da Silva, 1999) was the one employed and is described in Figure 4.2. The GC oven (Carlo Erba 6000, Milan, Italy) has an accuracy of $\pm$ 0.1 K and is used to contain the ZLC cell and the outlet of the cell is sent directly to be analyzed by FID, thus being able only to detect an overall signal corresponding to the hydrocarbon. The scheme limits the use of the unit to pure gas determinations. Also due to this configuration, all the experiments were done at atmospheric pressure.

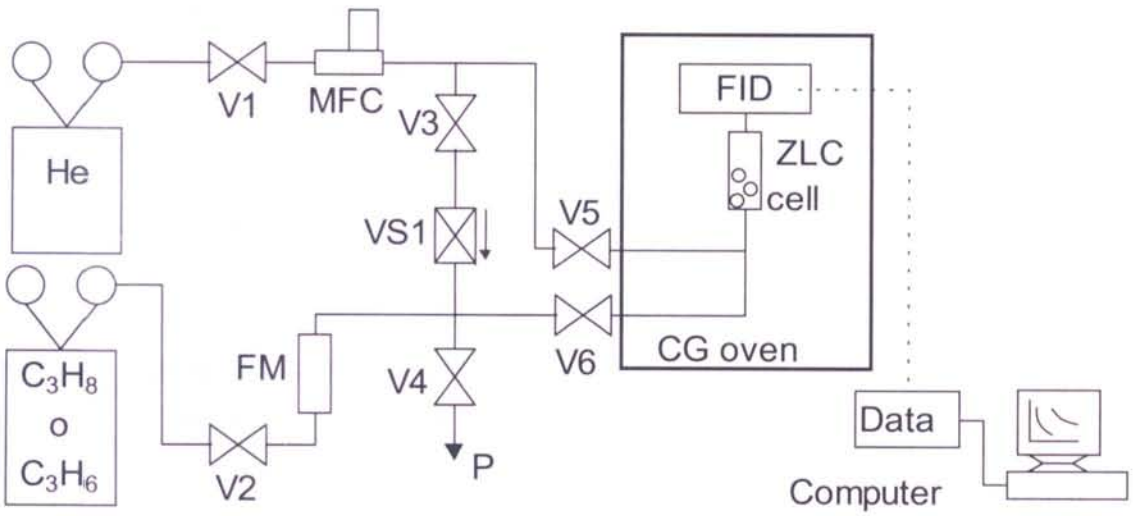

Figure 4.2. Scheme of existing ZLC facility (Da Silva, 1999). V_i are on-off valves, VS1 is a one-way valve, FM is a flowmeter, MFC is a mass flow controller and P is the purge system.

This set-up has the clear advantage of mixing gases on-line, allowing for fast concentration changes when desired. The main problem with this set-up was that constant low concentration of hydrocarbon was very difficult to keep because very small flowrates of hydrocarbon are required and thus any small instability in the needle valve was enough to produce variations in the concentration. The other disadvantage was the large amount of dead-volumes that may produce large errors in very fast runs.

To improve the unit and simplify its set-up, two main modifications were performed. The mixture section was replaced by a single tube where the mixture of inert and hydrocarbon is previously prepared. With this modification, the same concentration

of hydrocarbon was ensured for all the experiments. The second main change was the replacement of two on-off valves by a six-port valve (directly available in the laboratory, otherwise a four-port valve is preferred). With this modification, the dead volumes were reduced drastically and with these two modifications, the cleaning of the ZLC cell was done in less than 3 seconds with a flowrate of 25 cm^3/min at 373 K. The final scheme of the modified unit is shown in Figure 4.3. In the case of ZLC experiments the main interest is the desorption run so the inert gas stream is controlled by a mass flow controller while the saturation stream (inert + hydrocarbon) is regulated by a needle valve. In the case of breakthrough curves, the feed (inert + C_3) is controlled by the mass flow controller and helium (used for activation and desorption) is controlled by the needle valve.

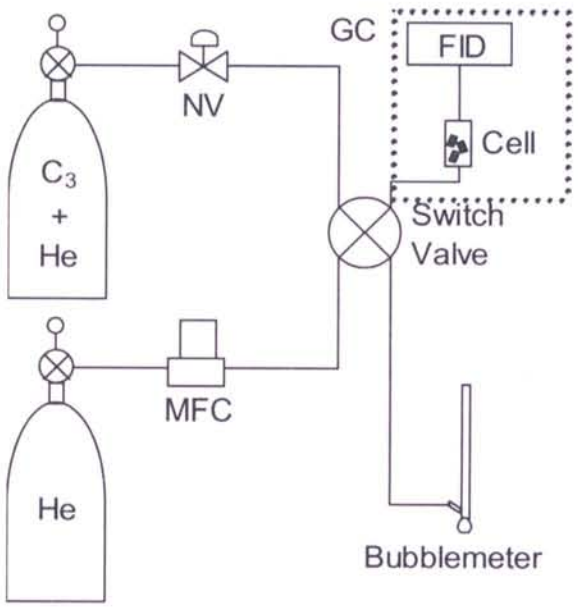

Figure 4.3. Modified ZLC facility. MFC is the mass flow controller and NV is the needle valve used to control flowrate.

Three different ZLC cells were employed according to the size of the particles. In the case of 1/16" diameter extrudates, a Swagelok tube of 1/8" was used. In the case of larger pellets (silica gel) a 1/4" tube was employed. For the case of zeolite crystals a

larger cell with sintered stainless steel filters was used (3/8") because it was directly available in the laboratory (as part of a HPLC column). The size of the sintered filters was not specified. The different ZLC cells (for extrudates and for crystals) are detailed in Figure 4.4.

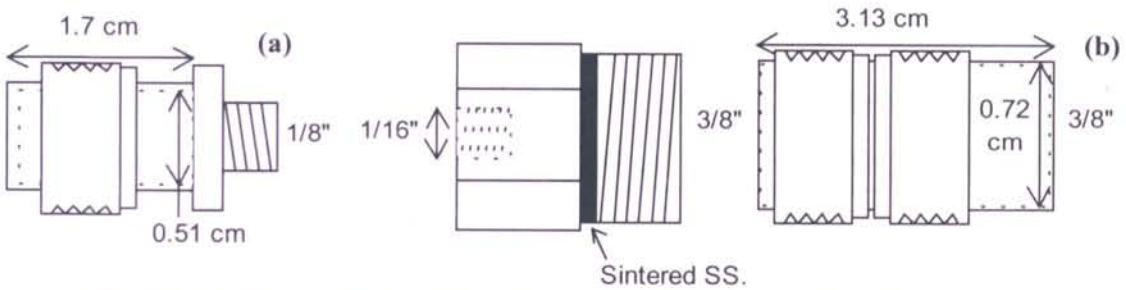

Figure 4.4. ZLC cells for extrudates (a) and for crystals (b). In the case of larger pellets, cell (a) is made with a 1/4" tube instead of a 1/8" tube.

The MIE unit was used to measure the kinetic uptakes of pure gases and the protocol for measurements as well as the experimental set-up was described in Chapter 3. Only the initial uptake was used in this work for diffusivity measurements.

4.3 Adsorbents

Adsorption kinetics was measured in all the adsorbents which adsorption equilibrium was measured as reported in Chapter 2 except for dealuminated mordenite, which has irreversible adsorption isotherms due to propylene oligomerization. The same temperatures were also used.

4.3.1 Silica gel

Adsorption kinetics of pure propane and propylene was measured at 303, 323 and 343 K. Activation of the samples (NSG and WSG) was performed at 423 K for five hours with a heating ramp of 1 K/min with an helium flux of 23 cm^3/min. Helium was

also used as inert purge gas in all the experiments. Inlet concentration of hydrocarbon in the saturation step was never superior to 3% in volume. Diffusivity measurements were carried out using two flowrates of purge gas; 29.3 and 65.0 cm^3/min. Experimental conditions for the ZLC runs are detailed in Table 4.1.

Table 4.1. Experimental conditions for ZLC runs

Adsorbent	NSG	WSG
Cell height [cm]	1.70	1.70
Cell volume [cm^3]	0.27	0.27
Pellet porosity, ε_p	0.40	0.58
Pellet radius R_p [cm]	0.11-0.13*	0.19
Cell porosity, ε_b	0.73	0.68
Adsorbent density, g/cm^3	1.26	0.92

*Variations are due to non-completely spherical shape of the particles.

ZLC desorption curves of propane and propylene in NSG with purge flow rates of 29.3 and 65.0 cm^3/min of helium taken at 303, 323 and 343 K are presented in Figure 4.5. Similar plots for propane and propylene in WSG are presented in Figure 4.6. The reason to use the long time response is because the kinetic curves are very fast and if the complete solution is modeled, many errors due to the washing of the cell and to dead volume effects may hide the real diffusivity values. The plots in semilog scale allow direct calculation of the slope of the long time asymptote that has the information of the pore diffusivity. Figure 4.5a also shows results from simulations with the complete ZLC model using parameters from the long time response. The slopes of the curves (eq. [4.29]) with both flowrates are the same confirming the kinetic control in both cases.

However, the intercept value is different and depends on the purge flowrate. The effect of the different purge flowrates is not very strong because the species are not strongly adsorbed. The slopes of the curves have been calculated with at least five points in the linear asymptote; this was an important point in the analysis of the results.

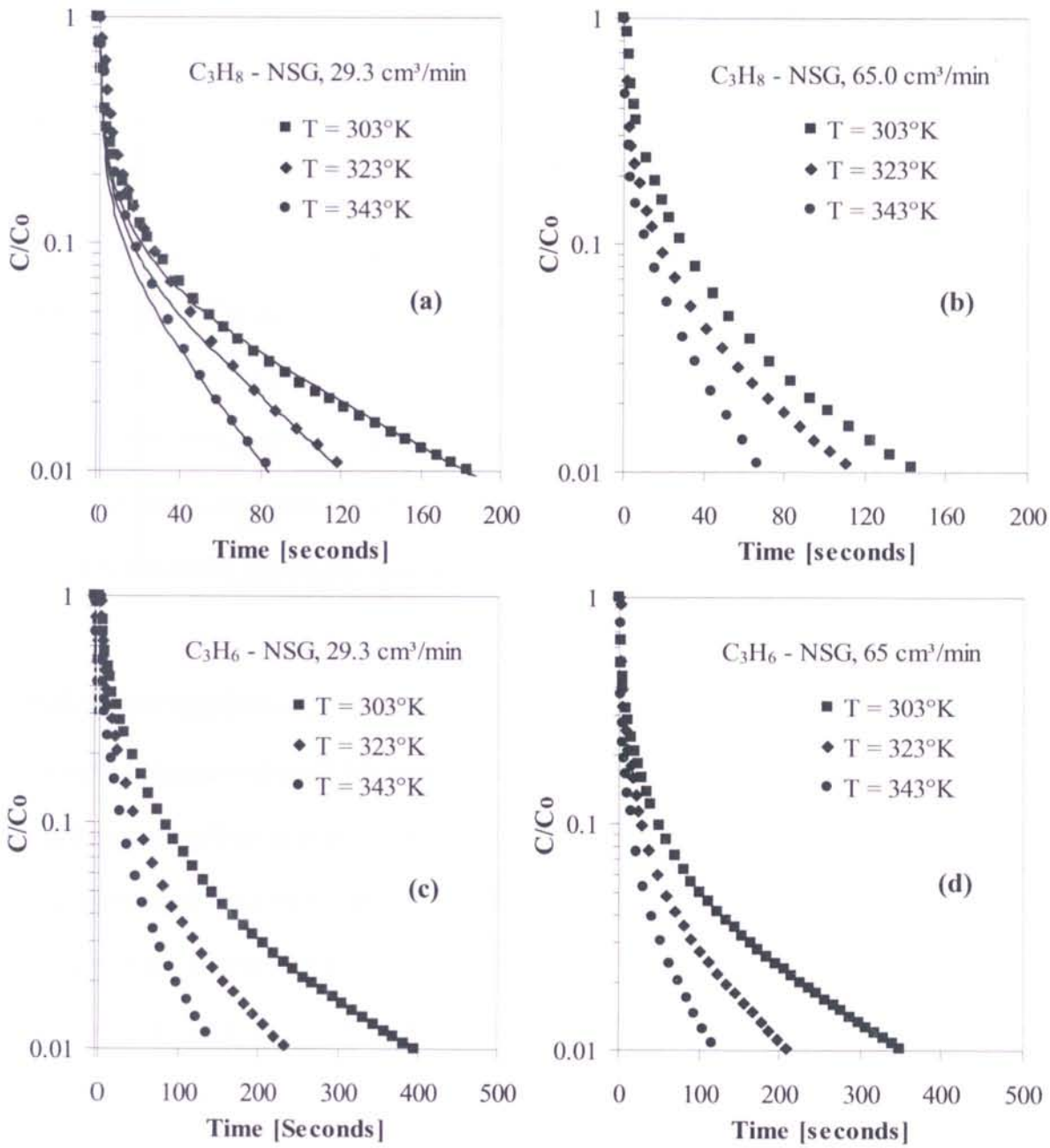

Figure 4.5. ZLC curves for C_3H_6 and C_3H_8 in NSG at 303, 323 and 343 K with different flowrates. Solid lines in (a) are complete ZLC model results using parameters from long time response.

Desorption curves, using nitrogen as purge gas, were measured to assess the importance of surface diffusivity. For both gases in the two samples studied, no surface diffusivity was detected. This was investigated due to some references indicating the importance of surface diffusivity of propane (Schneider and Smith, 1968; Yang, 1987).

The apparent diffusivity D_{ap} obtained using eq. [4.29] is presented in Table 4.2. It has to be pointed that the model for spherical pellets has been used for the narrow silica gel (NSG) pellets, but the pellets used were not exactly spherical. The pore diffusivity D_p has been calculated using the Bosanquet equation as a function of the Knudsen (D_k) and molecular (D_m) diffusion coefficients (equation [4.15]).

The equilibrium constants extracted from the ZLC experiments were comparable to the constants taken from gravimetric measurements when fitted with a thermodynamically correct isotherm in the low-pressure region. The Dubinin equation is not able to fit very low-pressure data because of its incorrect value of the Henry constant. The values of the adsorption constant $K_{eq} = \rho_p H R_g T$ where H is the Henry constant were obtained by fitting the Langmuir equation to the isotherms.

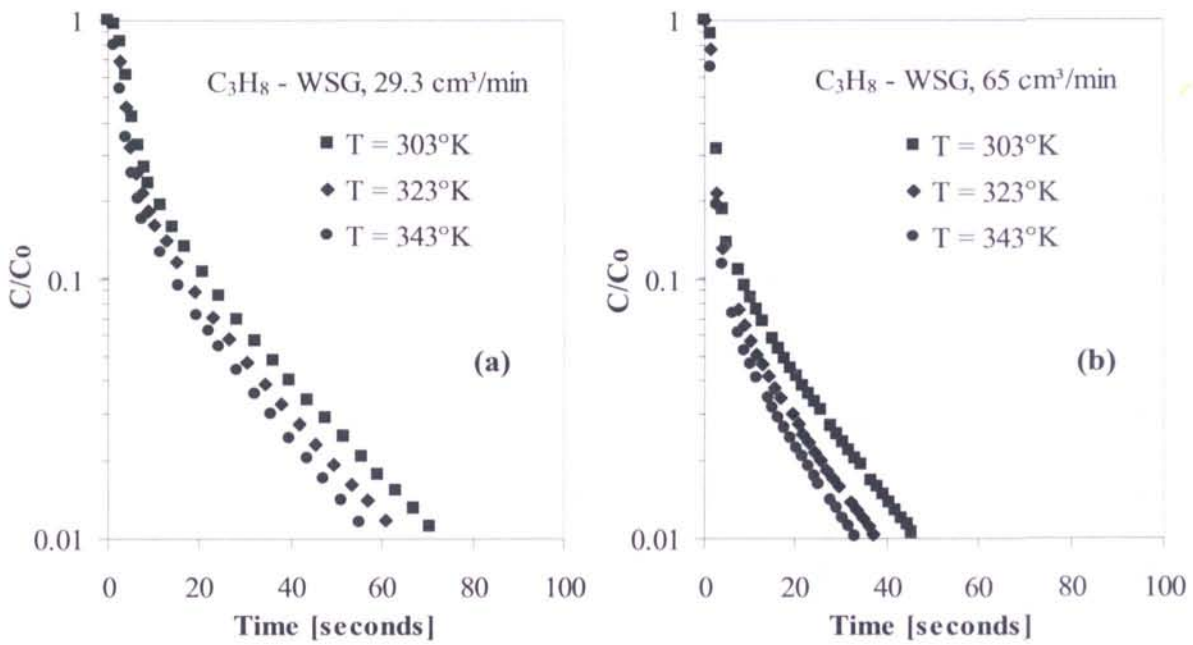

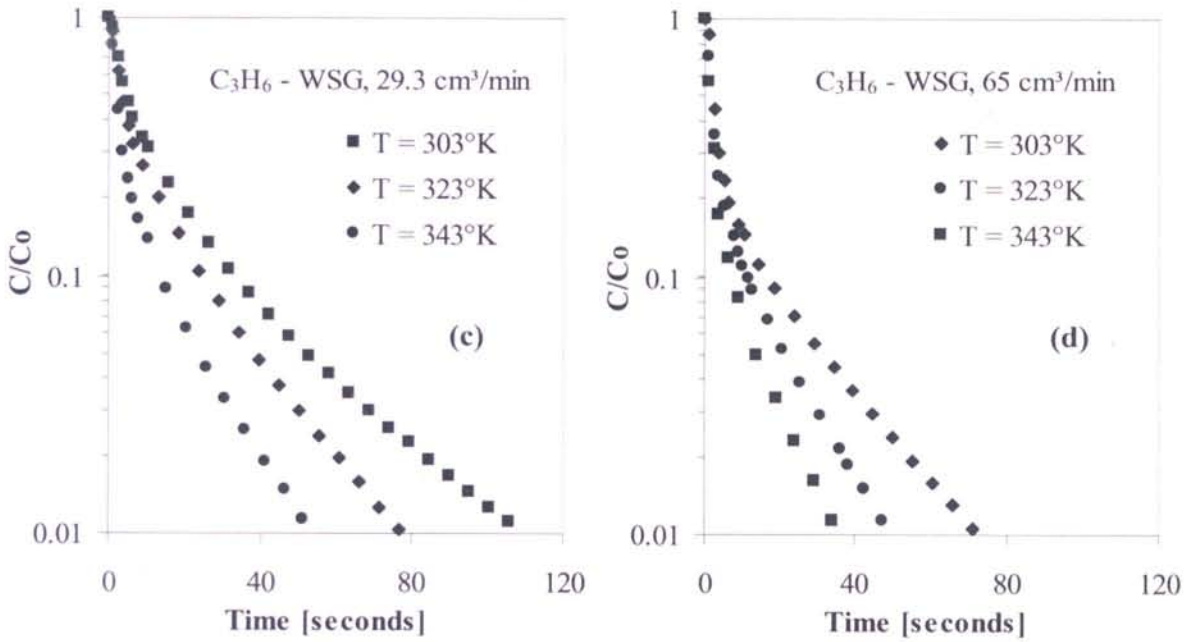

Figure 4.6. ZLC curves for C_3H_6 and C_3H_8 in WSG at 303, 323 and 343 K with different flowrates.

In narrow silica gel (NSG) pellets, the pores are narrow (mean pore diameter: 44 angstroms), so the transport flux should be controlled by Knudsen diffusion or by surface diffusion. Previous experiments with another purge gas, nitrogen, exhibit very different slopes at long times, indicating that surface diffusion is not dominant. Knudsen diffusion, D_k, was calculated using equation [4.17] and values are presented in Table 4.2. From eq. [4.15], without molecular diffusion, the pore diffusivity should be well represented by the Knudsen diffusivity. A plot of (D_K / D_P) for the different experiments, should be an indicative of the tortuosity factor, see Figure 4.7. This plot can also indicate the presence of surface diffusion (Malek and Farooq, 1997). The pore diffusivities determined in the temperature range 303 – 343 K are 2.4×10^{-3} to 2.8×10^{-3} cm²/s and 1.7×10^{-3} to 2.4×10^{-3} cm²/s for propane and propylene. Average tortuosity values ranging from 2 to 6 were reported for silica gel (Yang, 1987). An average

tortuosity value of 2.5 can be estimated from all the experiments made. This is an additional confirmation of the absence of surface diffusion.

Table 4.2. Apparent and pore diffusivities and tortuosity values calculated from ZLC experiments for propane and propylene in NSG.

Temp [K]	D_{ap} *10^5 [cm²/s]	K_{eq}	D_p [cm²/s] (calculated)	D_k [cm²/s] (estimated)	D_m [cm²/s] (estimated)	τ (calculated)
C_3H_8 – NSG, Q_p = 29.3 cm³ He/min						
303	1.9	81.1	0.00236	0.0056	0.390	2.7
323	3.1	58.5	0.00273	0.0058	0.433	2.4
343	4.7	41.6	0.00296	0.0060	0.480	2.3
C_3H_8 – NSG, Q_p = 65 cm³ He/min						
303	2.6	76.7	0.0026	0.0056	0.390	2.1
323	3.2	57.7	0.0024	0.0058	0.433	2.4
343	5.8	37.9	0.0028	0.0060	0.480	2.1
C_3H_6 – NSG, Q_p = 29.3 cm³ He/min						
303	1.0	189.9	0.0024	0.0057	0.429	2.3
323	1.6	109.6	0.0023	0.0059	0.478	2.6
343	2.6	68.4	0.0023	0.0061	0.529	2.6
C_3H_6 – NSG, Q_p = 65 cm³ He/min						
303	0.99	172.1	0.0022	0.0057	0.429	2.6
323	1.5	100.9	0.0020	0.0059	0.478	3.0
343	2.5	55.2	0.0018	0.0061	0.529	3.4

In wide silica gel (WSG) pellets, the mean pore diameter is larger than in NSG (120 Å), and the diffusion can be controlled by a combination of mechanisms (molecular and Knudsen). Molecular diffusion, D_m, was calculated using the Chapman – Enskog equation and is shown in Table 4.3. Pore diffusivities, D_p, were calculated from eq [4.15] without surface diffusion being 6.4×10^{-3} to 9.9×10^{-3} cm²/s for propane and 6.6×10^{-3} to 12.1×10^{-3} cm²/s for propylene. The values are very close to Knudsen

diffusion and for tortuosity calculations, the molecular diffusivity has minor effect. A plot of (D_K / D_P) for WSG is presented in Figure 4.8. The tortuosity has an average value of 2.0 estimated from the complete set of experiments for WSG.

Table 4.3. Apparent and pore diffusivities and tortuosity values calculated from ZLC experiments for propane and propylene in WSG.

Temp [K]	D_{ap} *10^5 [cm²/s]	K_{eq}	D_p [cm²/s] (calculated)	D_k [cm²/s] (estimated)	D_m [cm²/s] (estimated)	τ (calculated)
C_3H_8 – WSG, Q_p = 29.3 cm³ He/min						
303	17.6	56.4	0.0074	0.0153	0.390	2.0
323	19.1	46.5	0.00667	0.0158	0.433	2.3
343	20.6	40.8	0.0064	0.0162	0.480	2.5
C_3H_8 – WSG, Q_p = 65 cm³ He/min						
303	21.5	61.5	0.0099	0.0153	0.390	1.5
323	22.7	43.0	0.0074	0.0158	0.433	2.1
343	24.1	35.7	0.0065	0.0162	0.480	2.4
C_3H_6 – WSG, Q_p = 29.3 cm³ He/min						
303	16.4	73.5	0.0089	0.0156	0.429	1.7
323	22.0	49.2	0.0080	0.0161	0.478	2.0
343	21.7	40.8	0.0066	0.0166	0.529	2.4
C_3H_6 – WSG, Q_p = 65 cm³ He/min						
303	17.0	96.5	0.0121	0.0156	0.429	1.2
323	23.0	55.7	0.0095	0.0161	0.478	1.6
343	25.4	38.2	0.0073	0.0166	0.529	2.2

In both materials, the Knudsen diffusion was the dominant mechanism for mass transfer. These results are consistent with data previously published (Malek and Farooq, 1997). The effects of surface diffusion for both propane and propylene were not detected in all the experiments made using helium or nitrogen as purge gas.

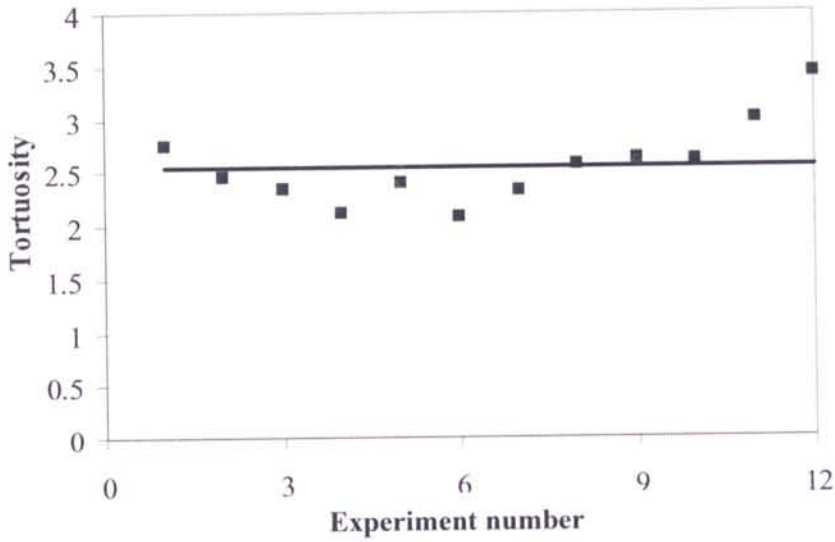

Figure 4.7. Tortuosity of narrow silica gel (NSG) determined by the ZLC method.

The main problem in measuring diffusivities from the desorption curves of these materials is that the response is very fast and the amount adsorbed is not high, so the reproducibility of the results, particularly for the wide silica samples, was around 20%. The other source of error is how many points are considered to be in the "long time region". Large differences in the value of the intercept can be due to this fact. Values reported in Table 4.2 and 4.3 are indicative that variations less than 10% of diffusion coefficients with temperature (expected in the temperature range of 303 – 343 K for Knudsen diffusion control) were within the experimental error.

The larger differences of the pore diffusivities determined from the curves at 65.0 cm^3/min of purge gas when compared with the determined using 29.3 cm^3/min can be because the response of the desorption curve is so fast that make us work in limit conditions where dead volumes and cell washing effects are important. This effect is particularly noticed in WSG.

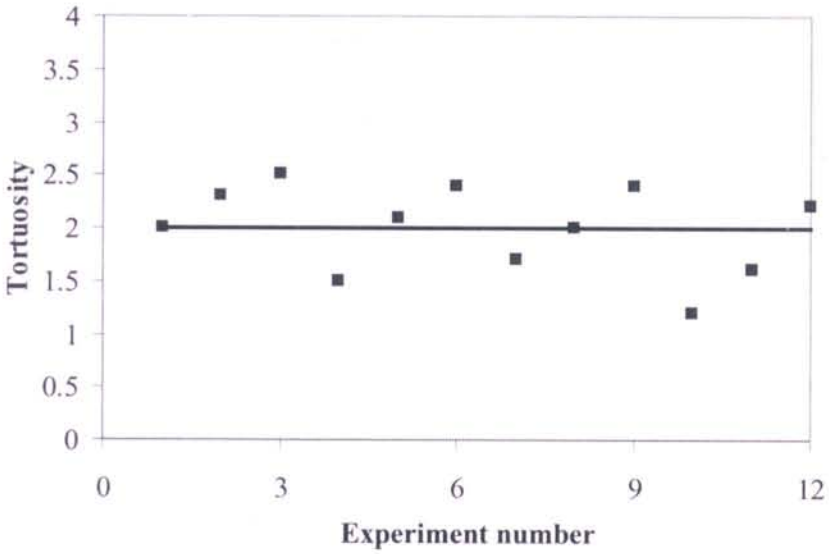

Figure 4.8. Tortuosity of wide silica gel (WSG) determined by the ZLC method.

Once adsorption equilibrium and kinetics are determined, it is possible to predict the column behavior. This is a straightforward method to determine the validity of adsorption equilibrium and kinetic parameters determined independently. In this case, breakthrough curves of pure propane and propylene dilute in helium (1.1 kPa hydrocarbon partial pressure) were performed only in NSG sample. The experimental conditions used in the curves as well as the transport parameters used for simulations are detailed in Table 4.4. Axial dispersion coefficient was calculated using equation [4.35] and film mass transfer coefficient using equation [4.36].

Table 4.4. Experimental conditions of dilute breakthrough curves of propane and propylene in NSG at 303, 323 and 343 K.

Parameter	Value	Parameter	Value
Column length, cm	16.5	Column porosity	0.446
Column radius, cm	0.465	Flowrate, cm^3/min	46.2 (25C, 1 atm)
Adsorbent weight, g	7.819	D_{ax}(303K), cm^2/s	0.608

The breakthrough curves obtained are shown in Figure 4.9 for propylene and propane in NSG. No parameter was used to fit the curves and values determined experimentally were employed. Clearly, the simulations are very close to experimental data indicating the validity of adsorption kinetics and the adsorption equilibrium data in the low-pressure range.

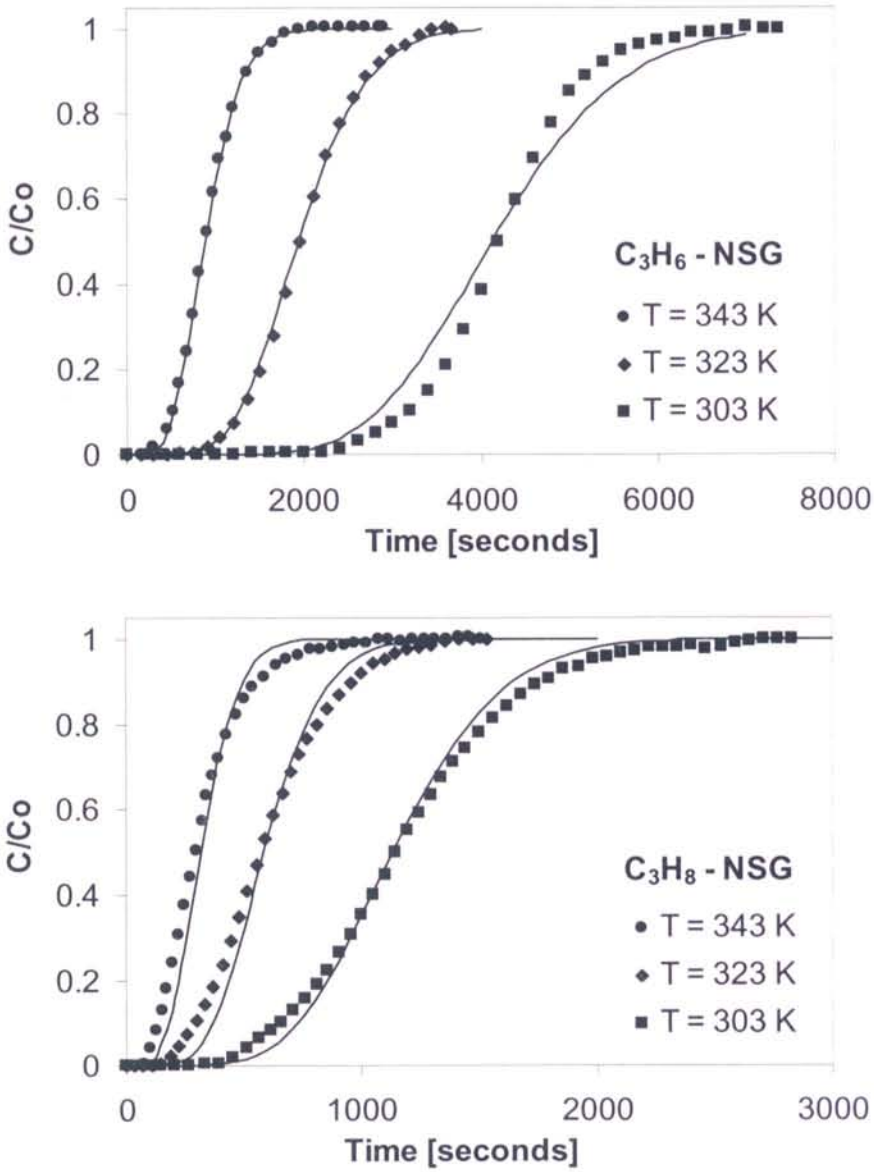

Figure 4.9. Dilute breakthrough curves of propylene and propane on NSG at 303, 323 and 343 K. Solid lines are model using equilibrium parameters determined by gravimetry and kinetic parameters from ZLC (no fitting parameters).

4.3.2 Zeolite 5A pellets and crystals

Adsorption kinetics of pure propane and propylene were measured at 323, 343, 373 and 423 K over zeolite pellets (Grace Davison) and crystals (PQ Corp). To activate both samples, a flow of helium of 14 cm^3/min at 593 K (1K/min heating ramp) was used overnight (10 hours at least). Helium was also used as inert purge gas in all the experiments. Inlet concentration of hydrocarbon in the saturation step was 1% in volume and in these experiments the concentration in all the samples were the same by external preparation of the gas mixture. Experimental conditions for the ZLC runs are detailled in Table 4.5. The cell with sintered filters was used in the case of crystals and the runs were reproducible, so we assume that no crystals passed through the filters.

Table 4.5 – ZLC experimental conditions and adsorbent properties

ZLC characteristics (pellets)	Value	***Adsorbent properties***	Value
Cell height [cm]	1.70	Solid density [g/cm^3]	1.74
Cell volume [cm^3]	0.27	Pellet density [g/cm^3]	1.13
Cell porosity	0.79* – 0.94	Pellet porosity	0.35
Purge flowrate [cm^3/min]	34.3 – 49.5 – 71.0*	Mean pore radius [Å]	500
Pellet diameter [cm]	0.165 – 0.250*	Crystal radius (pellets) [μm]	1.1
		Crystal radius (crystals) [μm]	1.0
		Crystal density [g/cm^3]	1.57[a]

* Values correspond to experiments with big pellets.
[a] Assumed value (Ruthven and Derrah, 1972).

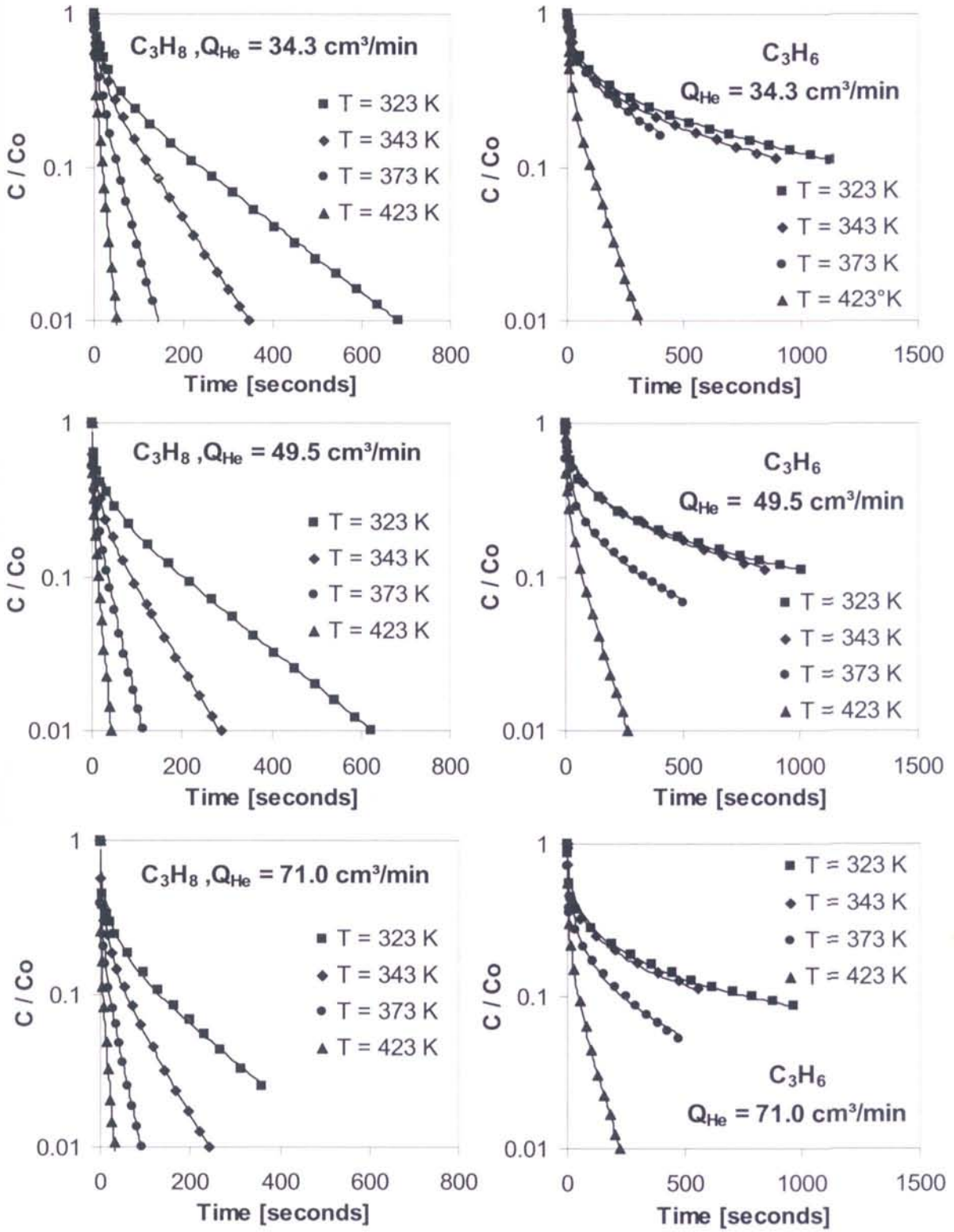

Figure 4.10 –ZLC desorption curves with 34.3, 49.5 and 71.0 cm^3/min of He as inert at 323, 343, 373 and 423 K in pellets of 0.165 cm. Propane (left side) and propylene (right side). Solid lines correspond to the fitting of equation 4.26.

Table 4.6 – Apparent diffusivity of C_3H_8 and C_3H_6 in 5A zeolite determined by ZLC.

	C_3H_8 apparent diffusivity determined by ZLC, cm^2/s			
Flowrate [cm^3/min]	T = 323 K	T = 343 K	T = 373 K	T = 423 K
	LTR	LTR	LTR	LTR
21.0[a]	5.4×10^{-6}	1.0×10^{-5}	2.2×10^{-5}	5.2×10^{-5}
34.3[a]	5.2×10^{-6}	1.1×10^{-5}	2.7×10^{-5}	7.3×10^{-5}
34.3	4.4×10^{-6}	9.7×10^{-6}	2.3×10^{-5}	6.3×10^{-5}
49.5	4.9×10^{-6}	9.3×10^{-6}	2.4×10^{-5}	6.0×10^{-5}
71.0	5.1×10^{-6}	9.5×10^{-5}	2.5×10^{-5}	7.1×10^{-5}
71.0[b]	5.9×10^{-6}	1.1×10^{-5}	2.0×10^{-5}	8.8×10^{-5}
45.0[c]	1.1×10^{-11}	3.2×10^{-11}	4.2×10^{-11}	7.2×10^{-11}
	C_3H_6 apparent diffusivity determined by ZLC, cm^2/s			
Flowrate [cm^3/min]	T = 323°K	T = 343°K	T = 373°K	T = 423°K
	LTR	LTR	LTR	LTR
21.0[a]	8.4×10^{-7}	9.6×10^{-7}	2.1×10^{-6}	9.9×10^{-6}
49.5[a]	7.4×10^{-7}	1.1×10^{-6}	2.1×10^{-6}	1.1×10^{-5}
34.3	7.5×10^{-7}	9.2×10^{-7}	2.7×10^{-6}	9.9×10^{-6}
49.5	6.4×10^{-7}	1.1×10^{-6}	1.9×10^{-6}	9.4×10^{-6}
71.0	9.6×10^{-7}	1.2×10^{-6}	2.1×10^{-6}	9.8×10^{-6}
71.0[b]	1.2×10^{-6}	1.1×10^{-6}	2.7×10^{-6}	7.7×10^{-6}
45.0[c]		2.0×10^{-12}	9.1×10^{-12}	6.3×10^{-11}

[a] Values obtained in the smaller cell with $V_c = 0.06$ cm^3.
[b] Values for pellets with 0.25 cm diameter
[c] Values obtained with PQ Corp. crystals

The ZLC experiments on Grace Davison 5A pellets were carried out also at 323, 343, 373 and 423 K, and using three different purge flow-rates: 34.3, 49.5 and 71.0 cm^3/min. Two pellet sizes, 0.165 and 0.25 cm diameter, were tested although for one diameter (0.250 cm) the experiments were carried out only with a purge flowrate of 71.0 cm^3/min. The experiments with the PQ Corp. crystals were carried out at 45.0 cm^3/min at the same temperatures. The experimental ZLC desorption curves obtained for pellets are presented in Figures 4.10 (0.165 cm pellets) and Figure 4.11 (0.25 cm pellets) and for crystals in Figure 4.12. Solid lines in Figures correspond to the fitting of the complete model (eq. 4.26). Additional experiments were carried out in a second cell (V_c = 0.06 cm^3) to check if the fluid phase volume influenced the results; no variations in the results within experimental error were detected.

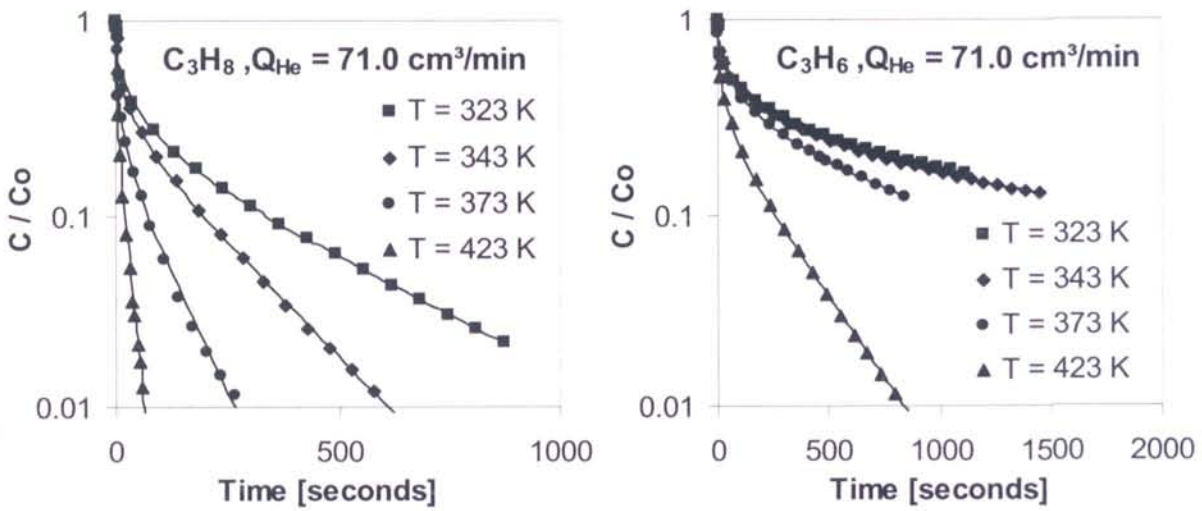

Figure 4.11 –ZLC desorption curves with 71.0 cm^3/min of He as inert at 323, 343, 373 and 423 K in pellets of 0.25 cm diameter. Propane (left side) and propylene (right side).

As an initial estimate, the ZLC data for pellets were fitted with the macropore control model; if the mass transport control was intermediate (macropore and micropore) differences between the experimental and simulated results for the two

pellet sizes would be significant. The values fitted with the complete time response model (CTR) and with the long time response model (LTR) are in good agreement, thus the use of the LTR is recommended because of its simplicity. In Table 4.6 we present the apparent diffusivity obtained from all the experiments. The apparent diffusivity of propane is 6-10 times higher than for propylene and is in the range 0.5 – 7.0 x 10^{-5} cm^2/s while for propylene the values are 0.9 – 9 x10^{-6} cm^2/s. In all pellet calculations, the mean pore radius (500 Å) was used as a first estimate.

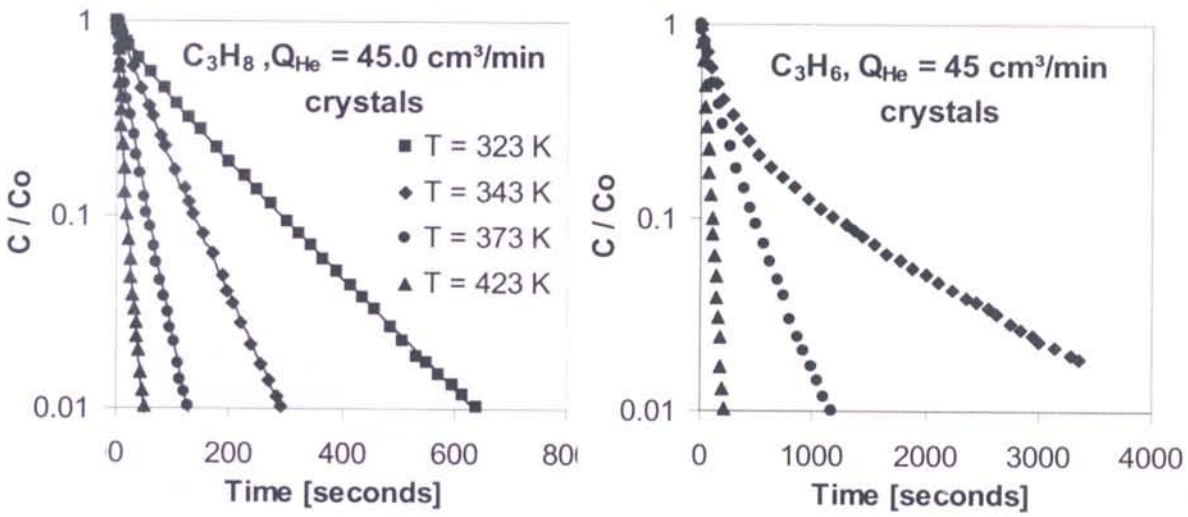

Figure 4.12 –ZLC desorption curves on 5A zeolite crystals (PQ Corp.) with 45.0 cm^3/min of He as inert at 323, 343, 373 and 423 K. Propane (left side) and propylene (right side).

The apparent diffusivities obtained from desorption curves with the larger pellets are in agreement with the curves with smaller pellets showing a R_p^2 dependence. We can conclude that the control mechanism of mass transfer in the pellets is controlled by macropore diffusion in the temperatures studied. This has also been reported for 5A sieves with diffusion measurements (Ruthven and Derrah, 1972) from uptake experiments. Another way to determine the controlling mechanism is to calculate the ratio between the time constants for macropore and micropore diffusion (Silva and Rodrigues, 1996), $\gamma = (D_c/r_c^2)/(D_p/r_p^2)$. The criterion for macropore diffusion control is

$\gamma(K_{eq}+1) > 10$. In all the cases, this value was higher than 15 indicating macropore control. In previous works reported in literature, some differences in the mass transfer control was found (macropore and micropore control) (Antonson and Dranoff, 1969; Ruthven and Derrah, 1972). These differences are explained by the use of different binders and crystal sizes.

The experimental apparent diffusivity shows larger values for propane than for propylene at low temperatures, with smaller difference at high temperatures. Values extracted from the experiments with pellets are given in Table 4.7. From the measurements performed in the crystals, activation energies of 8.3 and 22.4 kJ/mol for propane and propylene were determined respectively; temperature dependence is plotted in Figure 4.13.

Table 4.7 – Henry's constant, Average Pore diffusivity and tortuosity factor estimation of propane and propylene in zeolite 5A pellets.

Temp [K]	K	D_{ap} [cm^2/s].10^5	D_p [cm^2/s]	D_k [cm^2/s]	D_m [cm^2/s]	τ
Propane						
323	2158	0.5	0.022	0.131	0.485	4.7
343	1108	1.0	0.022	0.135	0.537	4.9
373	498	2.3	0.018	0.141	0.615	6.4
423	163	7.0	0.019	0.150	0.764	6.6
Propylene						
323	15912	0.1	0.026	0.135	0.535	4.1
343	12739	0.1	0.025	0.139	0.593	4.5
373	6022	0.2	0.027	0.145	0.683	4.4
423	1043	1.0	0.020	0.154	0.844	6.5

In Table 4.7 the average values of the apparent diffusivity were used to calculate the pore diffusivities using the Henry constants obtained in the ZLC curves. Also, with the calculated values of the Knudsen and molecular diffusion, the tortuosity factors were estimated. The pore diffusivities of both gases are very similar (0.018 – 0.027 cm^2/s) and the average tortuosity factor estimated from 42 experiments was 5.5; this value is comparable to the values reported by Ruthven and Derrah (1972). The values of tortuosity for all the experiments are shown in Figure 4.14.

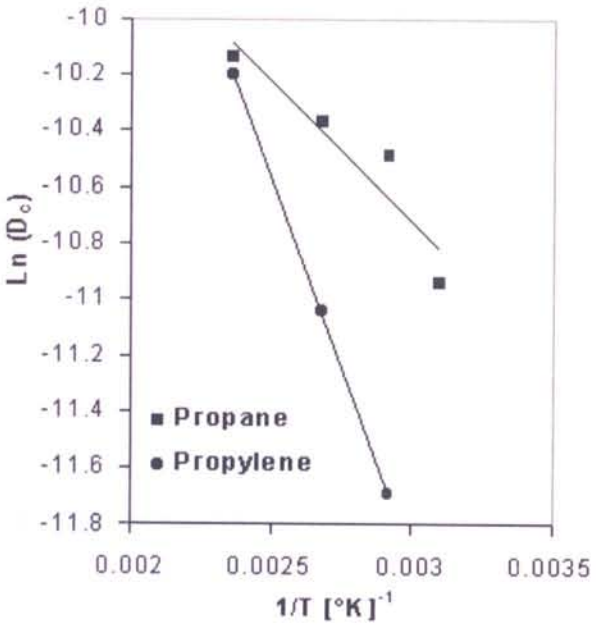

Figure 4.13 – Temperature dependence of crystal diffusivity from ZLC curves for 5A zeolite PQ crystals.

Experiments were carried out in the order 323, 343, 373 and 423 K and then repeated with the same sample. No significant changes were observed. No coke formation at higher temperatures was noticed, otherwise in the second set of experiments the adsorption capacity would has been lower and the kinetic experiments would be different (Silva et al., 2000). Also, the isotherm measurements should not be completely reversible.

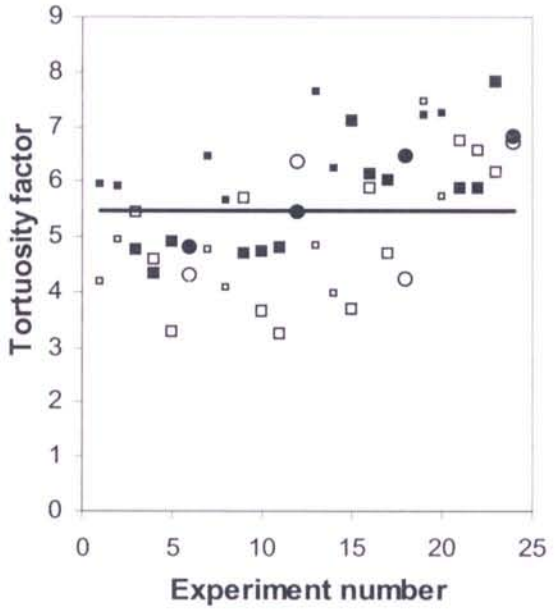

Figure 4.14 – Tortuosity factors obtained in the full set of ZLC experiments done with extrudates (Grace Davison).

4.3.3 Carbon Molecular Sieve

Adsorption kinetics of pure propane and propylene were measured at 343, 373 and 423 K. To activate the samples, a flow of helium of 14 cm^3/min at 523 K (1K/min heating ramp) was used overnight (16 hours at least). The configuration of the ZLC equipment is the same as described in Figure 4.3 but the ZLC experiments were performed in Bahía Blanca, Argentina (PLAPIQUI) using a Perkin Elmer Autosystem 9001 GC. Breakthrough experiments were performed in the same conditions with a larger column and a helium flowrate of 20 cm^3/min for activation. Helium was also used as inert purge gas in all the experiments. Inlet concentration of hydrocarbon in the saturation step was 1.05-1.1% in volume and in these experiments the concentration in all the samples were the same by external preparation of the gas mixture. Experimental conditions for the ZLC and breakthrough runs are detailed in Table 4.8.

Table 4.8 – ZLC and diiute breakthrough curves experimental conditions for propane and propylene onto CMS4A

C_3H_6 and C_3H_8 conc., C_o [% v/v]		1.10 and 1.05	
Pellet radius, R_p [cm]		0.11	
Zero Length Column		***Breakthrough curves***	
C_3H_8 flowrate, Q_p [cm³/min]	30.0	Mass of adsorbent [g]	7.2297
C_3H_6 flowrate, Q_p, [cm³/min]	27.0 – 31.0; 37.0 – 41.0	Flowrate [cm³/min] (100 kPa, 300 K)	62.4
Cell Volume, V_c [cm³]	0.28	C_3 concentration	1.05-1.10 % v/v
Extrudate length, H [cm]	2.3 and 5.0 (small and large extrudates)	Column volume and size [cm³]	11.2 (0.93 x 16.5 cm)
Exttrudate volume, V_s [cm³]	0.061 - 0.057 (small and large extrudates)	Bed porosity	0.283

Zero length column (ZLC) experiments were performed at the same tempœratures of equilibrium measurements (343, 373 and 423 K). The equilibration period was at least one hour. All the runs were duplicated. The experiments for propane desorption are reported in Figure 4.15. A flow around 30 cm³/min was used (see Table 4.9). A very weak dependence with temperature was observed.

The dead volumes of the equipment were highly minimized and the adsorption rate was not extremely fast, so the adsorption step previous to desorption was also measured. As an example, in Figure 4.16 we present the adsorption / desorption steps at 343 K, both in normal scale (Figure 4.16a) as well as in semi-logarithmic scale using the transformation of $1-C/C_o$ for the adsorption curve (Figure 4.16b). The error in the tail of the adsorption curve is higher than in the desorption step due to the lower

sensitivity of the FID detector at higher concentrations. For both curves, the larger errors are presented in the initial portion of the curves probably due to non-uniform size of the micropores in the adsorbent as observed in the characterization reported in Chapter 2. The equilibrium and kinetic parameters for the fitting of both curves were the same. As both curves are symmetrical, we can conclude that we are working in the linear zone of the isotherm.

At the three temperatures the amounts adsorbed in adsorption and desorption steps (obtained by integration of the curve) was the same although only poor agreement is obtained with the manometric data as shown in Table 4.9. These large differences are due to an incomplete integration (the area below C/C_o that is not accounted in some cases should even be higher than the integrated area). In all the cases the differences are higher at lower temperatures confirming this.

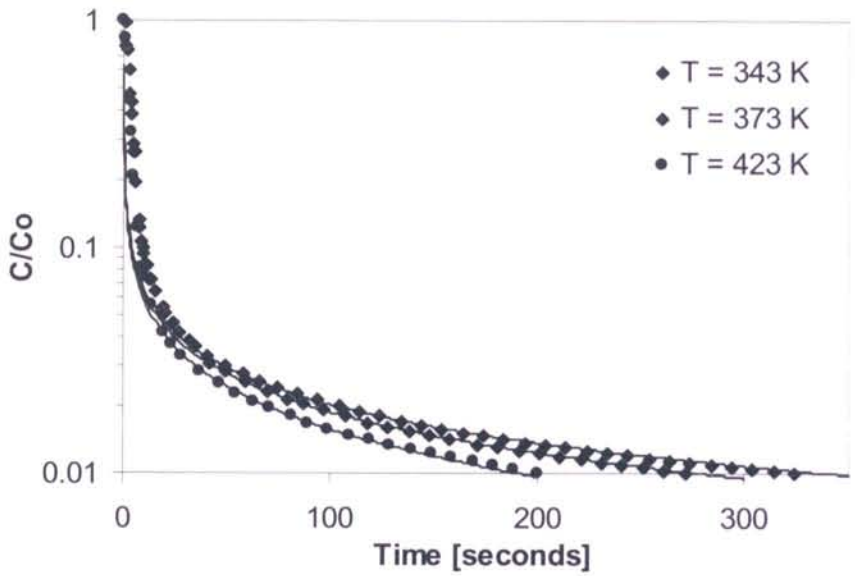

Figure 4.15. Zero Length Column (ZLC) desorption curves of propane in CMS 4A 30 cm^3/min of helium as purge at 343, 373 and 423 K. Solid lines are the complete solution of equation (24) using 150 terms.

The effect of partial activation (Brandani and Ruthven, 1996) is shown in Figure 4.17 for desorption curves at 343 K. If the saturation step is performed for only 250

seconds (equilibrium in the gas phase was apparently reached), the desorption curve has almost the same final slope but the amount adsorbed is clearly not the same giving an underestimate value of the equilibrium constant.

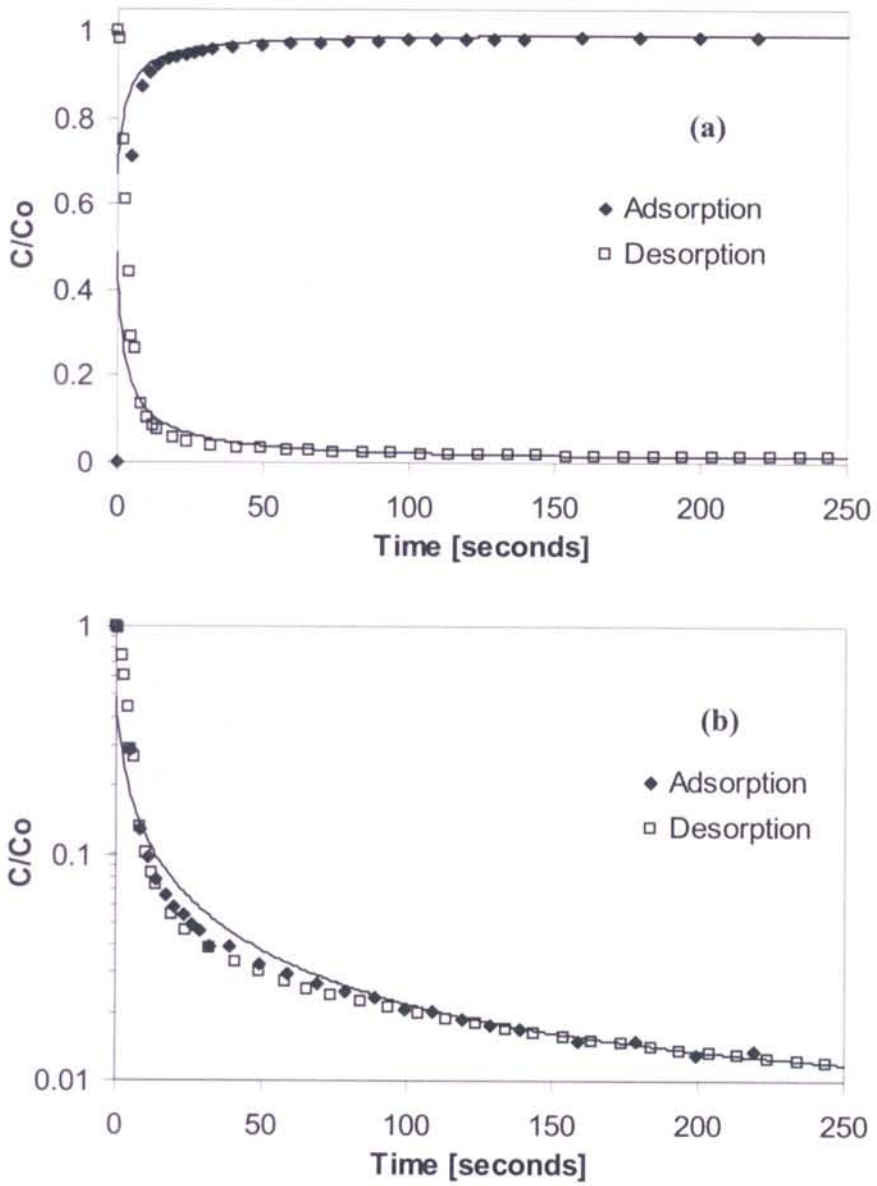

Figure 4.16. Comparison between adsorption and desorption curves of propane in CMS 4A at 343 K obtained by ZLC. (a) Normal scale. (b) Semi-log scale.

As the kinetic diameter of propane is very close to the nominal value of the adsorbent (higher than 3.8Å, which seems to be the demarking limit between propane

and propylene molecules (Padin et al., 2000)), micropore resistances were assumed to control the diffusion process.

Spherical shape was assumed for micropores as a first simplification for data interpretation. We also have to keep in mind that whatever the shape we choose to describe the crystal structure, we are making a gross oversimplification by saying that the radius is uniform in all the structure when it really has large variations as can be seen by SEM images (see Chapter 2). Only few works in literature deal with ZLC experiments with samples with a crystal distribution (Loos et al., 2000; Duncan and Möller, 2001). If a distribution of crystals and/or micropores is present and not considered, the ZLC measured diffusivity will represent only the larger crystals with a higher value of r_c. In this case we have variable-sized micropores in a distribution of crystals of non-uniform shape, a problem that will require many information concerning the structure of the pellet. For this reason a simplification was adopted.

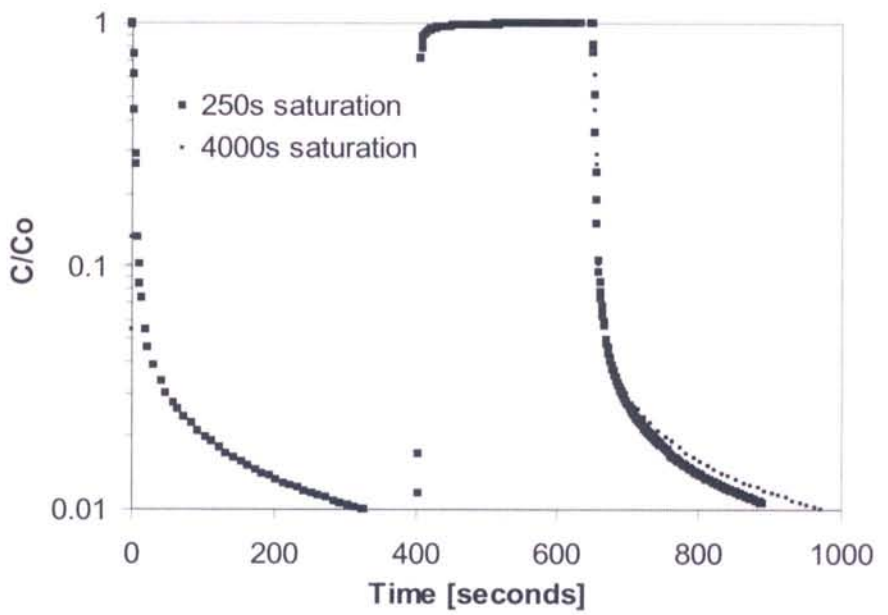

Figure 4.17. Partial activation effect in ZLC desorption curves of propane in CMS4A at 343 K. Q_{He} = 30 cm³/min.

If we look at Figure 4.15 trying to define a slope and intercept needed for the Long Time Response approach, we see that the slope is very difficult to establish. This was also reported in non-uniform crystal structure adsorbents (Duncan and Möller, 2001). For this case, we use the complete solution of equation [4.26] instead of the Long Time Response solution.

The values of the equilibrium constants and the crystal diffusivities are presented in Table 4.9. The long-term behavior is reached for very large values of time. Only using a minimum of 10 terms in the series (see equation [4.26]) the higher-term values of the summation can be neglected. In this work we used at least 100 terms to fit the data.

The micropore model has an exponential dependence with temperature described by equation [4.7]. From the experiments reported in Table 4.9 the activation energy of 33.7 kJ/mol has been calculated which is higher than the value of 29 kJ/mol reported for CMS 5A (Chihara et al., 1978). This indicates that even with a wide micropore distribution, the smaller micropores impose a higher resistance controlling the diffusion step.

Table 4.9 – Propane diffusion and equilibrium parameters in CMS4A obtained by ZLC

Temp. [K]	Flowrate [cm³/min]	K_{eq} [-] Integration	K_{eq} [-] Manometric*	D_c / r_c^2 [s^{-1}]
343	30.1	67.2	269.8	$2.0\ 10^{-5}$
373	30.1	59.9	155.2	$6.0\ 10^{-5}$
423	30.4	58.6	85.5	$1.9\ 10^{-4}$

* Reported in Chapter 2.

Propylene desorption analysis were performed with a flowrate of helium of 27-31 cm³/min (see details in Table 4.10) and the results are shown in Figure 4.18. To confirm the absence of external resistances another set of experiments were performed using a higher flowrate between 37-41 cm³/min (see Figure 4.19). The final slopes in a semi-logarithmic plot are coincident supporting the assumption of no film transfer resistances. These experiments were performed using extrudates of R_p = 0.11 cm and L = 0.5 cm that can be considered as infinite cylinders for macropore diffusion (Antonson and Dranoff, 1969).

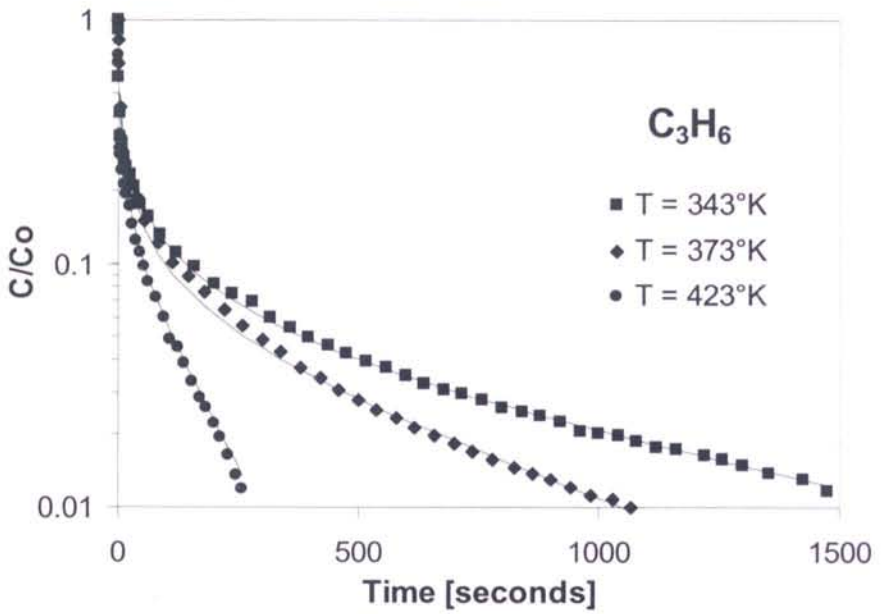

Figure 4.18. ZLC curves of propylene in CMS 4A Takeda at 343, 373, 423 and 448 K measured in the "large extrudates" with smaller helium flowrate: 27-31 cm³/min (see Table 4.10).

In previous literature of propylene diffusion in CMS Takeda 5A, the micropore resistances control the diffusion process (Chihara, 1978). No data were found for the diffusivity of propylene on CMS 4A and in general data with propylene on CMS was found only for the case of wider micropores (Vyas et al., 1994) and for the case of membrane permeation (Fuertez and Menendez, 2002). Of course if the controlling step

is diffusion in the micropores of CMS 5A, we should expect the same tendency in this adsorbent.

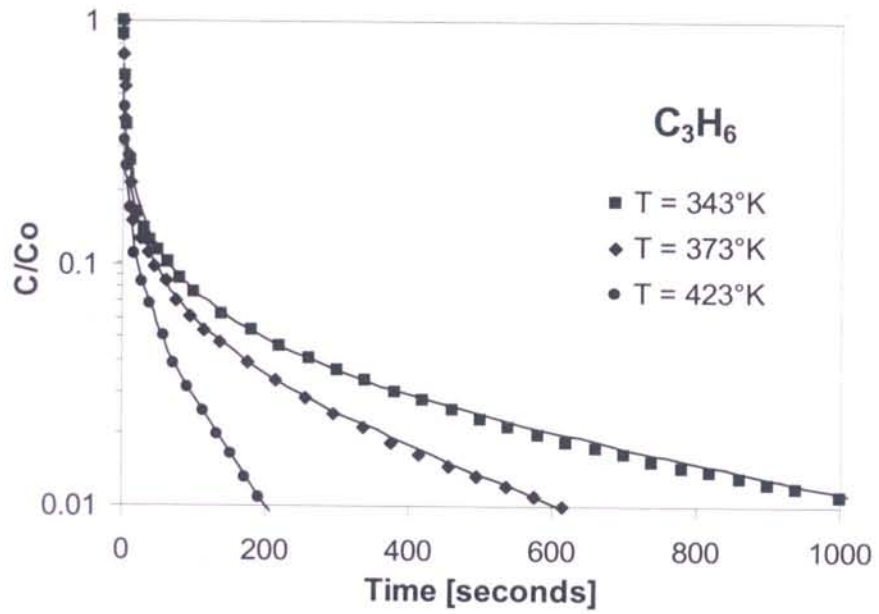

Figure 4.19. ZLC curves of propylene in CMS 4A Takeda at 343, 373 and 423 measured in the "large extrudates" with higher helium flowrate: 37 – 41 cm³/min (see Table 4.10).

As the pellets are extrudates we could not vary the pellet radius because it is constant in all of them. In order to confirm the micropore control, experiments with almost the same mass of adsorbent but with cylinders of different length (0.23 cm) and the same radius (R_p = 0.11 cm) were performed. A reasonable assumption to analyze the data is to consider the shape of the adsorbent as spheres to perform all the calculations. In this "small extrudates" a sphere of equivalent volume can describe the geometry to perform the calculations. If the control step is in the macropores, some differences in the slope will be observed (in fact to keep the same pore diffusivity, as the roots of equations [4.28] are different, a different value of apparent diffusivity should be obtained). If diffusion in micropores is the controlling step, no difference should be observed in the curves (within the accuracy of the measurements). Desorption curves obtained with these "small extrudates" are shown in Figure 4.20. The flowrate used was

also 37-41 cm³/min (see Table 4.10), a flowrate where no film mass transfer was observed in the larger extrudates. The slope of the desorption curves is similar indicating that no variation occurs when we change the external geometry of the pellet, confirming the micropore control of the propylene diffusion in this CMS sample.

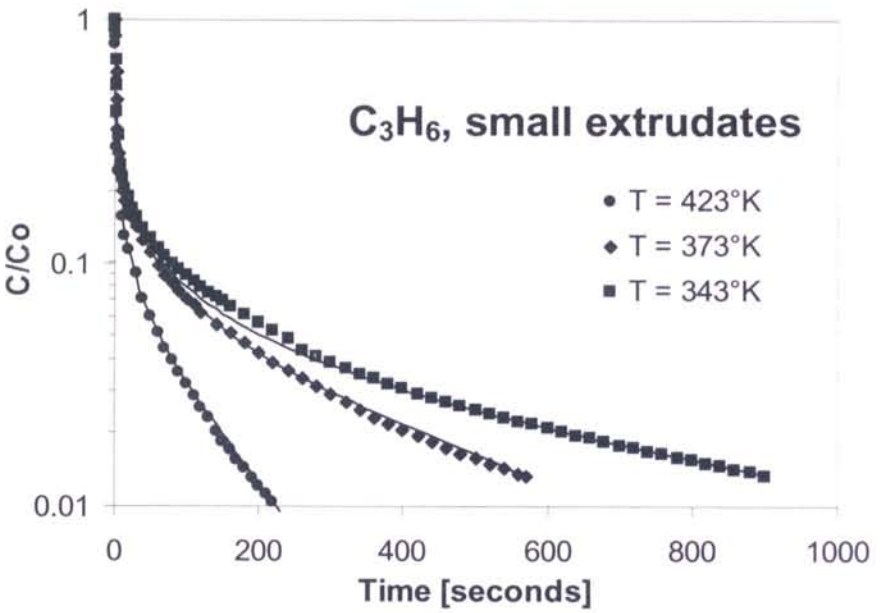

Figure 4.20. ZLC desorption curves of propylene in CMS 4A Takeda at 343, 373 and 423 measured in the "small extrudates". Helium flowrate is 37 – 41 cm³/min (Table 4.10).

The equilibrium constant and the micropore diffusivity parameters obtained in all the experiments are shown in Table 4.3..9. In the fitting of equation [4.26] also 100 terms were employed.

From the experiments reported in Table 4.10 the activation energy of 30.8 kJ/mol has been calculated which is a little higher than the 29 kJ/mol reported for CMS 5A (Chihara et al., 1978), but is clearly within the error of the measurements. In the case of CMS 5A no distinction between propane and propylene were noticed in the energy of activation, but in this case, with narrow micropores, some difference was detected (propane has more difficulty to penetrate the narrower micropores).

Table 4.10 – Propylene diffusion parameters in CMS4A obtained by ZLC

	Temp. [K]	Flowrate [cm³/min]	K_{eq} [-]	D_c / r_c^2 [s^{-1}]
Large extrudates	343	27.8	708.6	$1.2\ 10^{-4}$
	373	29.1	497.5	$2.0\ 10^{-4}$
	423	31.8	196.6	$9.5\ 10^{-4}$
	343	38.0	593.0	$1.4\ 10^{-4}$
	373	41.3	402.4	$2.8\ 10^{-4}$
	423	40.5	155.6	$9.7\ 10^{-4}$
Small extrudates	343	38.0	572.4	$1.4\ 10^{-4}$
	373	41.3	468.3	$2.8\ 10^{-4}$
	423	40.5	133.3	$1.1\ 10^{-3}$

The manometric – chromatographic equipment presented in detail in Chapter 3 is a powerful method to determine pure component and binary adsorption equilibrium. In this equipment there is a compromise between the pressure range and the pressure accuracy in the low-pressure range. The Henry constant is obtained as H = q/P. In the measurement of the pressure we have an error of 0.5 kPa, which in measurements of pressures around 2 kPa translates an error of 75% in the estimation of the Henry constant. To avoid a poor extrapolation of the Henry constant from the manometric data, breakthrough curves were measured using a 1% concentration of hydrocarbon, which can be considered in the linear zone of the isotherm and gives a reliable value of

the Henry constant needed to predict the binary equilibrium with confidence (Talu, 1998).

After obtaining the experimental data, the first thing to do is to calculate the stoichiometric time to compare with the capacity obtained by the dynamic method with the manometric one (even knowing that large differences may occur). The calculation of the stoichiometric time, $\bar{t}$, as made by Ruthven (Ruthven, 1984) is:

$$\bar{t} = \frac{L_c}{u_i}\left[1 + \left(\frac{1-\varepsilon_c}{\varepsilon_c}\right)H\right] = \int_0^\infty \left(1 - \frac{C}{C_o}\right)dt \qquad [4.39]$$

where L_c is the length of the column, u_i is the interstitial gas velocity, H is the Henry constant and ε_c is the porosity of the column. Note that we have used the linear isotherm expression for the calculation of the stoichiometric time, due to the very low pressure of hydrocarbon used. The comparison between the Henry constant obtained from the integration of the stoichiometric time and the manometric value is performed in Table 4.11 for propane and propylene. Note that in the Henry constant determined in the manometric unit there is not a specific value but a range of values, which includes the error associated with each measurement. In the case of propylene, all the values determined from the breakthrough curves are inside the range determined in the manometric equipment. In the case of propane the difference between the two Henry values increase with the temperature. This is because the first manometric measurement at 373 K and 423 K were only at 6 and 8 kPa, a point out of the linear zone of equilibrium with a slope smaller than the Henry constant.

A general model, including macropore, micropore and film resistances was developed and tested in this system. This model was selected because in the search of a proper adsorbent for the propane / propylene separation, some adsorbents studied have macropore resistances (Grande and Rodrigues, 2001; Grande et al., 2002) while others,

like CMS4A have micropore control (Grande et al., 2003a). In order to fill the parameters of the bidisperse model a pore diffusivity has to be given. To do this, we assume a tortuosity factor of 6 (Yang, 1987) and the pore diffusivity D_p has been calculated using the Bosanquet equation (eq. 4.15).

Table 4.11 – Henry constant of propane and propylene in CMS4A comparison between manometric and dynamic (breakthrough) methods

Temp. [K]	$\bar{t}$ [s] $[C_3H_8] - [C_3H_6]$	H [mmol/g.kPa] C_3H_8		H [mmol/g.kPa] C_3H_6	
		Dynamic	Manometric	Dynamic	Manometric
343	5478.3 – 12716.6	0.277	0.16-0.27	0.643	0.77-0.40
373	3337.2 – 7750.3	0.167	0.10-0.14	0.392	0.47-0.23
423	1622.0 – 2687.1	0.082	0.03-0.04	0.136	0.15-0.11

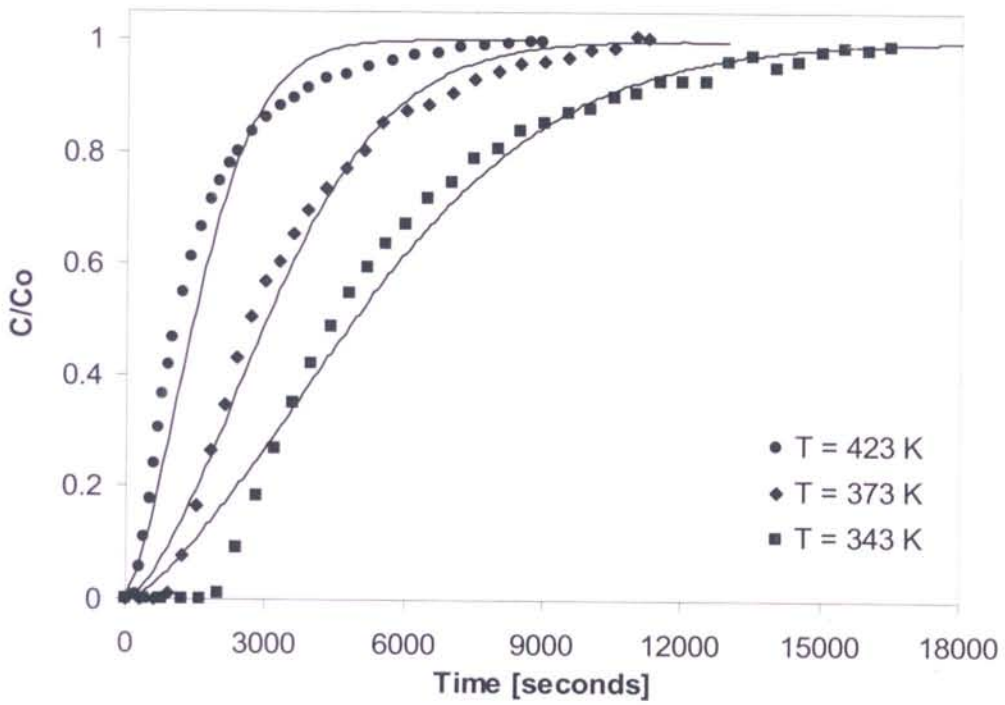

Figure 4.21. Propane breakthrough curves in CMS4A at 343, 373 and 423 K. Solid lines represent the bidisperse model of equations (4.30-4.37).

The experimental breakthrough curves measured are shown in Figures 4.21 and 4.22 for propane and propylene, respectively. The experimental conditions of measurement of these curves are detailed in Table 4.8. The solid lines represent the fitting with the bidisperse model.

The crystal diffusivity parameters used for the fitting of both gases are listed in Table 4.12. In all the cases we have verified that the mass transfer coefficient calculated from equation [4.36] is too large and we can consider that film mass transfer resistance is negligible. Also, the macropore diffusion was changed (simulating a tortuosity factor up to 12) and no variations were observed. So we confirmed that the control of the diffusion mechanism is really in the micropores for both gases.

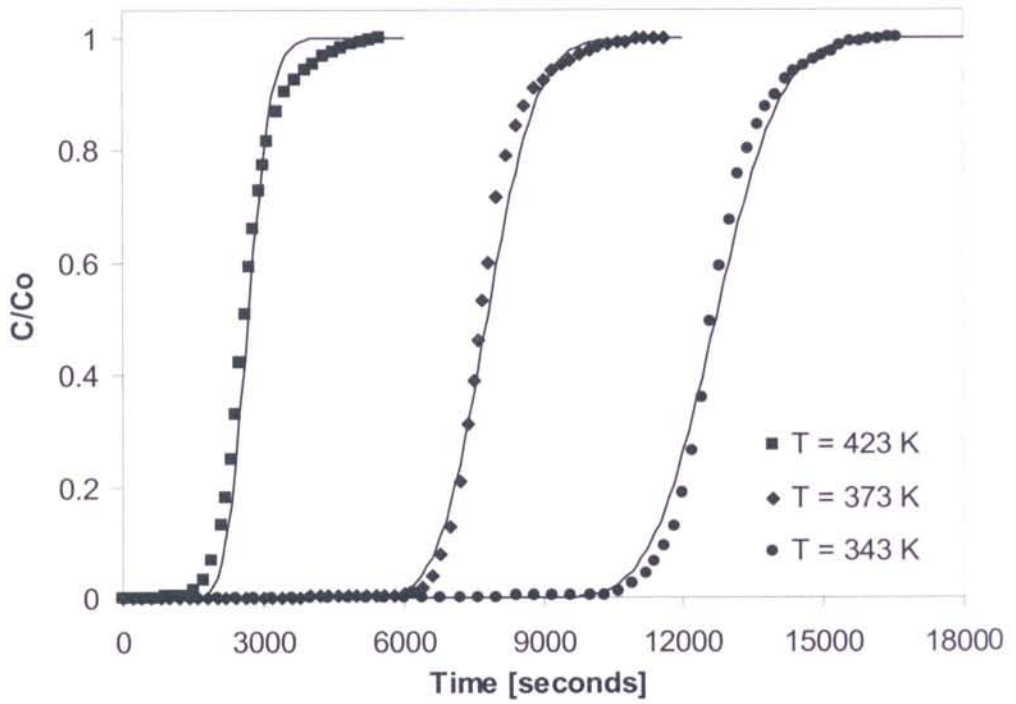

Figure 4.22. Propylene breakthrough curves at 343, 373 and 423 K. Solid lines represent the bidisperse model of equations (4.30-4.37).

Table 4.12 – Diffusion parameters and energy of activation of propane and propylene adsorption in CMS4A determined from breakthrough curves.

Gas	Temperature [K]	D_c/r_c^2 [s^{-1}]	E_a [kJ/mol]
C_3H_8	343	$8.4\ 10^{-5}$	23.39
	373	$2.2\ 10^{-4}$	
	423	$4.0\ 10^{-4}$	
C_3H_6	343	$6.0\ 10^{-3}$	16.57
	373	$1.1\ 10^{-2}$	
	423	$1.6\ 10^{-2}$	

Note that the diffusivity parameters obtained from the ZLC and the dynamic methods have large deviation between them, i.e., a factor of 2-4 for propane and 15-50 for propylene. As we reported in the adsorbent characterization, the adsorbent has a distribution of "crystal" sizes which is better detected in the breakthrough curves than in the ZLC experiments, where the largest particles are responsible for the final response of the desorption curves. To that, we have to add the micropore size distribution, already mentioned in the equilibrium section and that in this case of molecular sieving may affect more one of the gases, in this case propylene. This distribution can be reflected in the calculation of the activation energy of diffusion. From the ZLC experiments, values from 33-30 kJ/mol for propane and propylene were calculated and from dynamic experiments values of 23-16 kJ/mol. Clearly the ZLC experiments are indicating a major difficulty of the molecules to adsorb and also the difference between the gases is smaller than the values calculated from breakthrough curves. Also, the effect of axial dispersion in the breakthrough curves is negligible and resistance to diffusion is controlled only by micropores. With those considerations, we can consider

that the micropore diffusivity values obtained from the breakthrough curves are more representative and will be used in further experiments with this adsorbent.

4.3.4 Zeolite 4A

Adsorption kinetics of pure propane and propylene were measured at 373, 423 and 473 K over zeolite extrudates. This sample was analyzed using the three techniques (uptake curves, ZLC and dilute breakthrough) for comparison purposes.

Activation of the sample was performed at 593 K for 24 hours with a heating ramp of 1 K/min. In the case of batch adsorption, activation was made in vacuum ($<10^{-5}$ kPa), while for the other techniques a small constant flow of helium at atmospheric pressure was used. Inlet concentration of hydrocarbon in the ZLC and breakthrough curves was 1.1% in volume. Experimental conditions for the ZLC and breakthrough runs are detailed in Table 4.13. The uptake curves used for kinetic determinations correspond to the first points of equilibrium shown in Chapter 2.

Propylene experiments at 423 and 473K using two different flowrates (41.6 and 65.6 cm^3/min) of helium as purge gas are presented in Figures 4.23 and 4.24. The initial portion of the desorption curve is very fast and for a better visualization the plots are presented from $C/C_o = 0.1$ instead of the initial value of 1. Propane desorption is not possible to analyze by this technique because the curves were extremely fast falling to $C/C_o = 0.001$ nearly in the same time as the blank essay. As expected, varying the flowrate does not have influence in the final slope of the curves. Average propylene diffusivity determined in these experiments is: 6.07×10^{-12} cm^2/s at 423 K and 1.17×10^{-11} cm^2/s at 473 K. Detailed results from each experiment are listed in Table 4.14. These values are in accordance with values determined previously for this system (Da Silva and Rodrigues, 1999; Rege et al., 1998).

Table 4.13. Experimental conditions of Zero Length Column (ZLC) and breakthrough curve experiments of propane and propylene in zeolite 4A (CECA).

Zero Length Column (ZLC) experiments	
Cell volume [cm^3]	0.28
Pellet volume [cm^3]	0.03
Gas flowrate [cm^3/min]	45.6; 61.6
Breakthrough curve experiments	
Column length [cm]	16.5
Column diameter [cm]	0.93
Flowrate [cm^3/min]	32.0; 46.2; 62.5
C_3H_6 partial pressure in feed [kPa]	1.0-1.1
Column porosity [-]	0.336
Total pressure [kPa]	101.3
Adsorbent properties: zeolite 4A (CECA)	
Adsorbent density [g/cm^3]	1.21
Adsorbent porosity [-]	0.315
Zeolite crystal radius [cm]	1.9×10^{-4}
Extrudate diameter [cm]	0.055

Propylene breakthrough experiments were performed in the same temperatures and with the same dilute mixture (1.1% v/v of propylene in helium) used for ZLC experiments. Also in these experiments the amount adsorbed at very low pressures was determined with good accuracy.

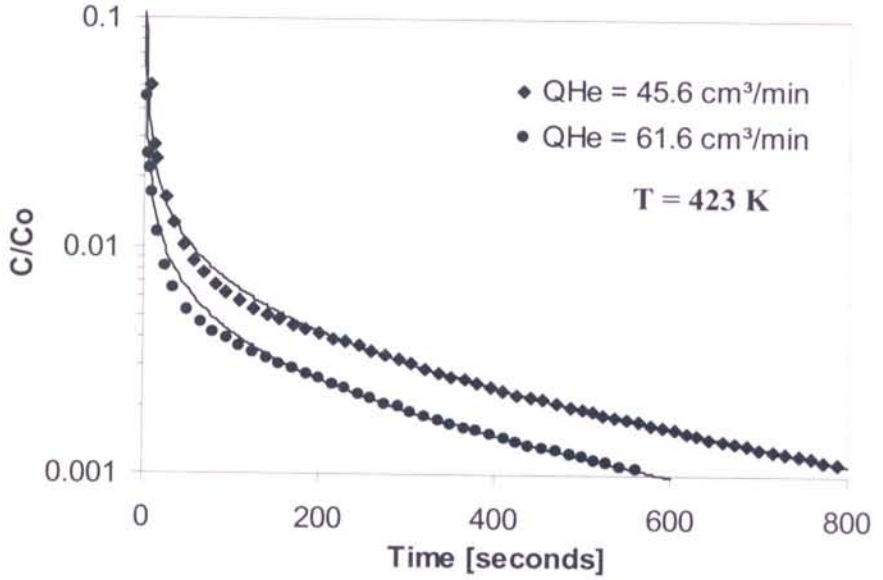

Figure 4.23. ZLC desorption curve of propylene in zeolite 4A at 423 K using 45.6 and 61.6 cm³/min of inert gas (Helium).

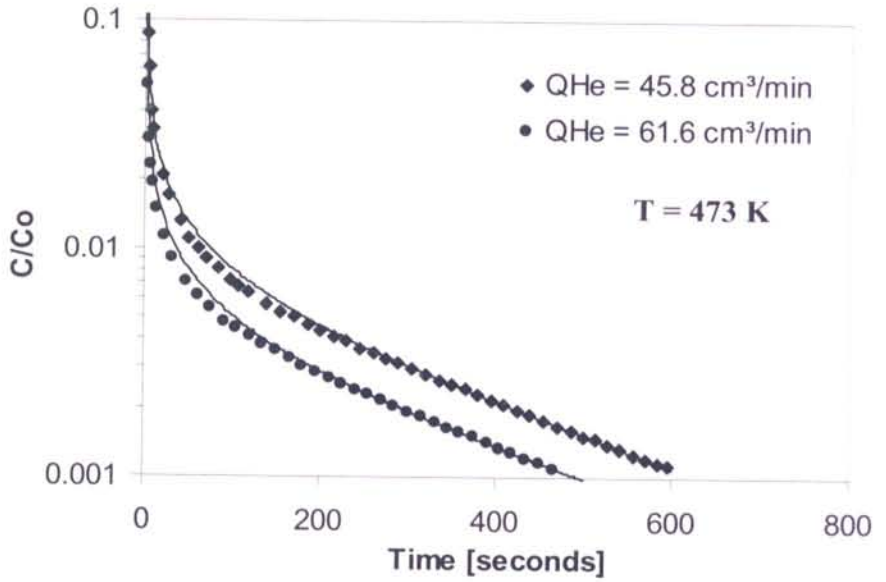

Figure 4.24. ZLC desorption curve of propylene in zeolite 4A at 473 K using 45.8 and 61.6 cm³/min of inert gas (Helium).

The results obtained at 423 and 473 K using a total flowrate of 62.5 cm³/min are shown in Figure 4.25. The stoichiometric time together with the kinetic parameters are reported in Table 4.15 The amount adsorbed calculated by the overall mass balance is in

agreement with values determined manometrically and fitted with the multi-site Langmuir isotherm as shown in Chapter 2 (Grande et al., 2003a). To confirm the values of the kinetic parameters at 473 K we have also measured breakthrough curves at other two flowrates: 46.2 and 32.0 cm³/min. Breakthrough curves at 473 K with these three flowrates are shown in Figure 4.26.

Table 4.14. Kinetic parameters of propylene diffusion in zeolite 4A determined from ZLC experiments.

Temperature [K]	Flowrate [cm³/min]	D_c [cm²/s]
423	45.6	6.10×10^{-12}
	61.6	6.04×10^{-12}
473	45.8	1.20×10^{-11}
	61.6	1.15×10^{-11}

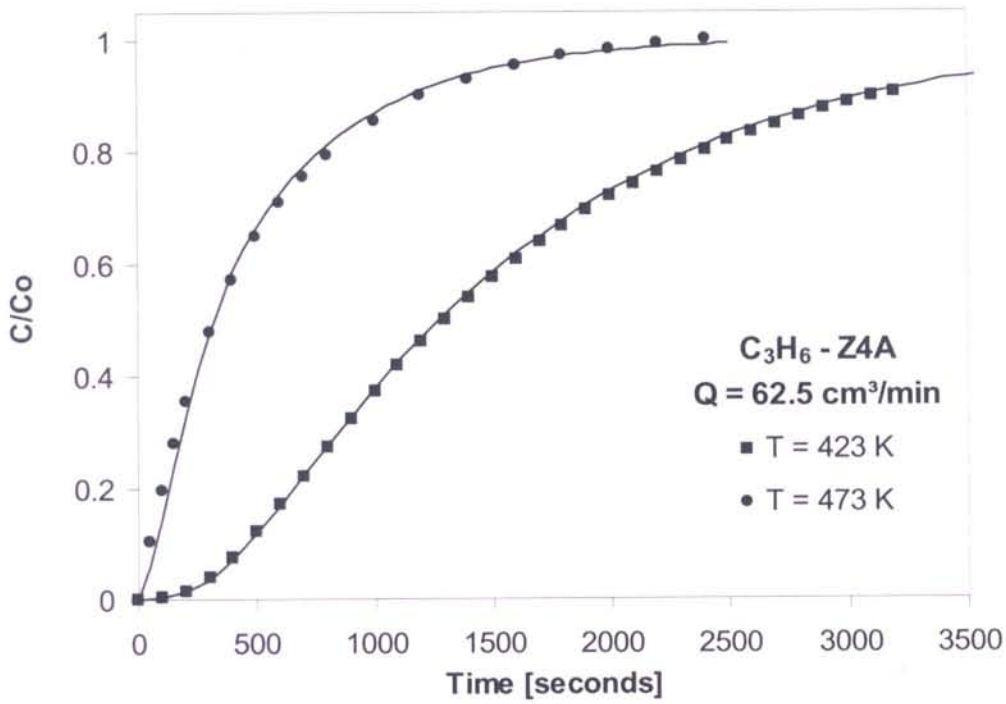

Figure 4.25. Propylene breakthrough curve in zeolite 4A at 423 K and 473 K using 62.5 cm³/min of mixture (C_3+He).

From the set of experiments performed, average diffusivity values of 5.8 and $9.1.10^{-12}$ cm²/s were obtained for 423 and 473 K, respectively. These values are in good agreement with the values obtained in the ZLC experiments (difference around 10% between both methods). The curves at 473 K provide the required tools to determine the micropore control against axial dispersion, macropore diffusion and film mass transfer by the momentum theory (Ruthven, 1984).

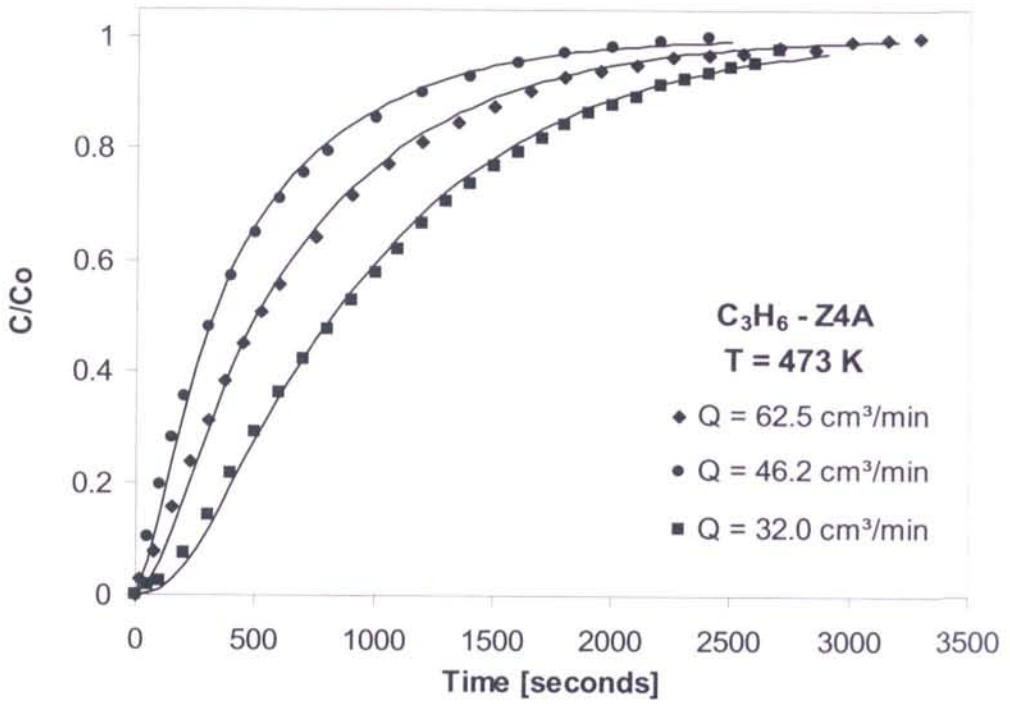

Figure 4.26. Propylene breakthrough curve in zeolite 4A at 473 K using 32.0, 46.2 and 62.5 cm³/min of mixture (C_3+He).

Table 4.15. Adsorption equilibrium and kinetic parameters of propylene adsorption in zeolite 4A CECA determined from breakthrough experiments.

T [K]	Flowrate [ml/min]	K_{eq} [-]	D_c [cm²/s]	D_{ax} [cm²/s]	k_f [cm/s]
423	62.5	311.1	$5.8\ 10^{-12}$	0.53	18.32
473	62.5	106.0	$9.4\ 10^{-12}$	0.65	20.53
	46.2	114.9	$9.0\ 10^{-12}$	0.54	20.48
	32.0	110.9	$9.1\ 10^{-12}$	0.45	20.44

Assuming that the species is strongly adsorbed, $K_{eq} >> \varepsilon_p$ and that the film mass transfer and macropore resistances are negligible (only mass transfer resistance in the micropores is important) the following expression relates the first and second moments with the equilibrium and kinetic parameters (Ruthven, 1984):

$$\frac{\sigma^2}{\mu^2} = \frac{2D_{ax}}{u_i L_c} + \frac{2u_i}{L_c}\left(\frac{\varepsilon_c}{1-\varepsilon_c}\right)\frac{r_c^2}{15K_{eq}D_c} \qquad [4.40]$$

where D_{ax} is the axial dispersion coefficient, u_i is the interstitial velocity of the gas, K_{eq} the equilibrium constant, L_c the length of the column, r_c is the crystal radius and D_c the crystal diffusivity. Equation [4.40] indicates that from a single breakthrough curve, only combined information of mass transfer resistance by micropores and axial dispersion can be obtained.

An alternative arrangement of equation [4.40] is:

$$\frac{\sigma^2}{\mu^2}u_i L_c = 2D_{ax} + 2\left(\frac{\varepsilon_c}{1-\varepsilon_c}\right)\frac{r_c^2}{15KD_c}u_i^2 = A + Bx \qquad [4.41]$$

with $x = u_i^2$. In equation [4.41] we can see that if different experiments are performed varying only the velocity of the gas, a linear relation can be obtained ($x = u_i^2$) and the axial dispersion and crystal diffusivity coefficients can be separately obtained from the slope and intercept of $\sigma^2 u_i L_c / \mu^2$ versus x. This is only true when the axial dispersion coefficient does not vary significantly with the velocity (mainly controlled by the molecular diffusion term in equation 4.35) and can be considered as constant. The linearized plot is shown in Figure 4.27. The axial dispersion coefficient obtained by this way is in good agreement with the ones obtained by equation [4.35].

The propane breakthrough on zeolite 4A at 423 and 473 K also using 1.1% (v/v) of hydrocarbon dilute in helium are shown in Figure 4.28. The flowrate used in these experiments was 23 cm³/min, near half of the used for propylene experiments. Even

through, breakthrough was very fast. These results are consistent with that previous observation; the diffusion coefficient is very small and thus the breakthrough is very fast. To approach equilibrium the tail of the dynamic response has to be very large as observed in Figure 4.28.

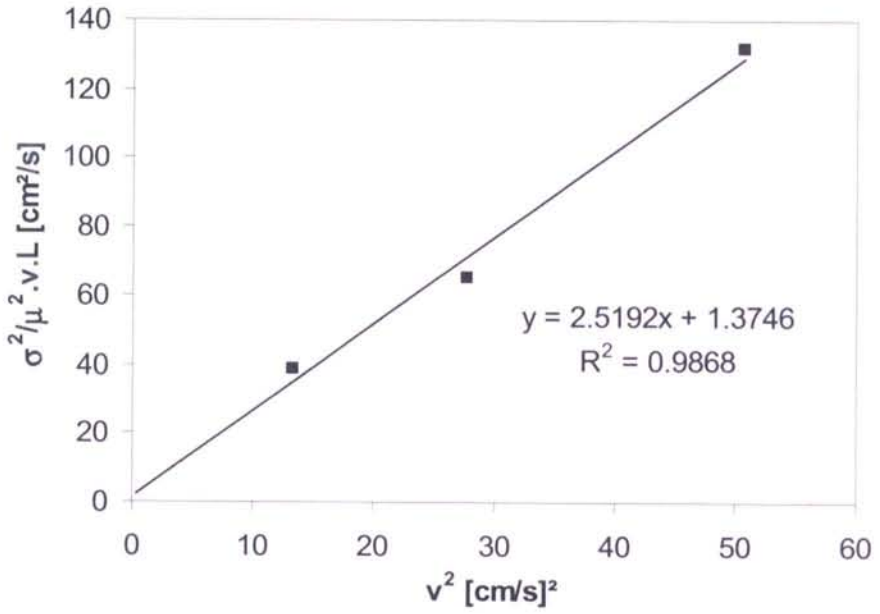

Figure 4.27. Moments analysis of propylene breakthrough: $\sigma^2 u_i L / \mu^2$ **versus** $x = u_i^2$

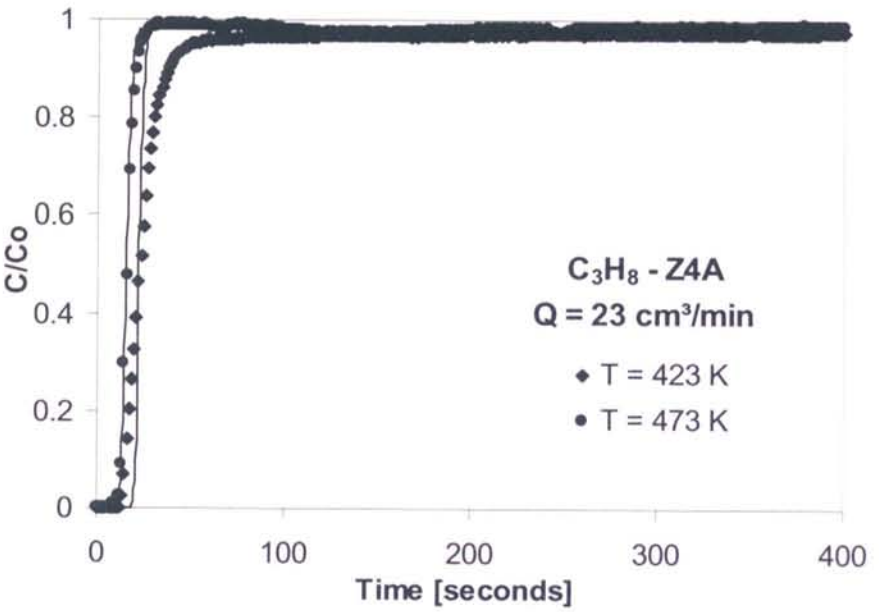

Figure 4.28. Propane breakthrough curves in zeolite 4A at 423 and 473 K using 23 cm³/min of mixture (C_3+He).

Another employed technique to analyze the adsorption equilibrium data was the batch adsorption by measuring the adsorption uptake. For the low-pressure equilibrium points, the pressure decrease was monitored in all the equilibration time. The initial batch experiment of propane adsorption uptake in zeolite 4A at 473 K is presented in Figure 4.29. In the same plot we show the pressure decrease of the system while gas is adsorbing. The solid lines represent the model described by equations [4.1-4.23]. No temperature changes were observed in the experiment as confirmed by simulations.

The crystal diffusivity of propane was estimated from the fractional uptake curves by matching the experimental data to equation [4.25]. The average crystal radius of the zeolite crystals is 1.9 μm determined by Scanning Electron Microscopy. The uptake curves at 423 and 473 K used for kinetic measurements together with the fitting are plotted in Figure 4.30. Propane experiments at 423 and 473 K have been fitted using crystal diffusivities of 2.7 and 5.5×10^{-14} cm²/s, respectively. The model described by equations [4.1-4.23] is coincident with the theoretical solution for finite batch isothermal systems with linear isotherm (Grande et al., 2003a). The constants to describe crystal diffusion by equation [4.7] are $D_c^o = 2.26.10^{-15}$ cm²/s and $E_a = 23.67$ kJ/mol. These two values were determined only with two temperatures and are thus subjected to large errors. This value is one order of magnitude different from other values previously reported of 1.7×10^{-17} m²/s at 424 K (Khodakov and Rees, 1995), although the activation energy of 23.7 kJ/mol is comparable with the 24.5 kJ/mol value also reported in that work. Similar discrepancies in diffusivity values with constancy in the activation energy were also reported for smaller molecules in this zeolite (Ruthven, 2001).

When we consider the kinetic diameter of the propane molecule and the opening of the zeolite structure, we are assuming that the molecules as well as the zeolite

channels are rigid (Xiao and Wei, 1992). With the equilibrium results shown here is clear that propane passes through the zeolite channels, but we still do not known the mechanism of diffusion.

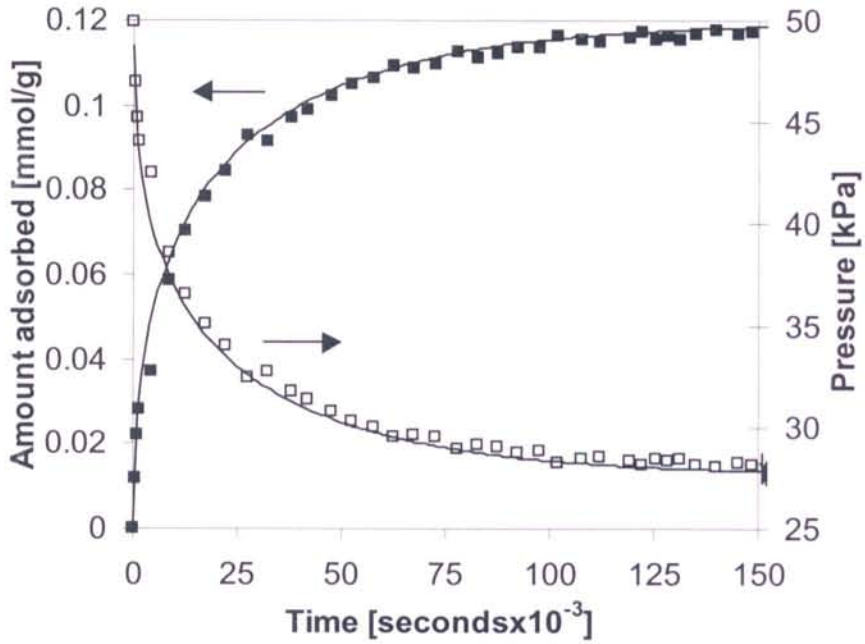

Figure 4.29. Uptake curve and pressure change with time for propane adsorption on zeolite 4A at 473 K.

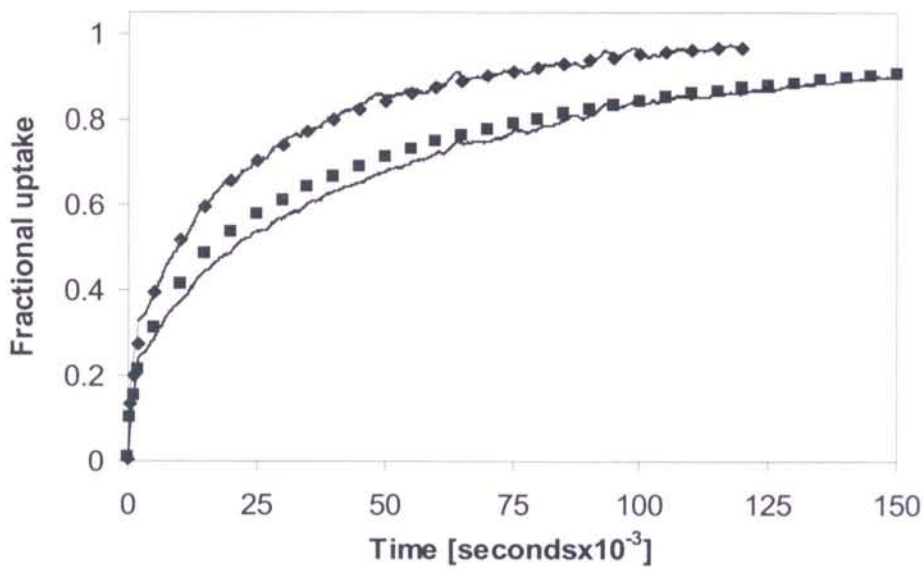

Figure 4.30: Fractional uptake curves of propane on zeolite 4A. Symbols: ■ T = 423 K and ◆ T = 473 K.

The equivalent experiments for propylene adsorption in zeolite 4A at 373, 423 and 473 K are presented in Figures 4.31-4.33 (Grande and Rodrigues, 2003). The temperature variations when adsorption was taking place are also shown in Figures 4.31-4.33. The experiments at 423 and 473 K were initialized with a propylene pressure of 25 kPa while the one at 373 K was initialized with 50 kPa of propylene. Lower pressure cannot be used because the pressure decrease due to adsorption leads to a final pressure within the error of the pressure transducer. In these cases, the initial pressures used fall in the non-linear region of the isotherm and no theoretical solutions can be applied to the data. Also, the temperature increase in the initial moments of the adsorption is within 2-4 K for the different experiments and isothermal operation can be no longer assumed. In Figures 4.31-4.33 the solid line is the temperature of the solid while the dotted line is the temperature of the gas phase. A priori we did not know the exact location of the thermocouple that was sensing the temperature but is clear that is in contact with the adsorbent surface.

The analysis of these experiments to determine the crystal diffusivity at the three different temperatures is not as easy as the other methods presented in this work. Temperature is not constant and both parameters D_c^o and E_a of equation [4.7] should be determined directly from the set of experiments. Also, the mass transfer film resistance and other parameters are varying with temperature. To simplify the model, the mass and heat transfer coefficients were assumed constant in all the experiment. The film mass transfer for the propylene experiments was calculated for a pressure of 10 kPa and 30 kPa were used for propane calculations. In both set of experiments if we neglect the fluid film mass transfer resistance the effects in the crystal diffusivity are not significant (in all cases the Biot number was higher than 10) but if we neglect the temperature

effects, the crystal diffusivity parameters were an order of magnitude higher (10^{-11} cm²/s). In both cases lower activation energy was observed.

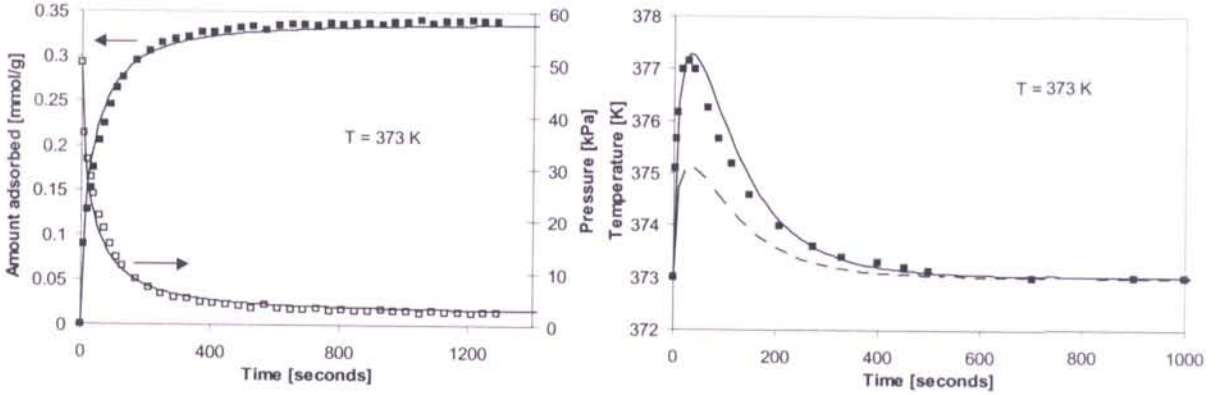

Figure 4.31. Static – batch propylene adsorption on zeolite 4A at 373 K: (a) uptake curve and pressure change; (b) temperature evolution in the gas (dashed line) and solid phase (solid line).

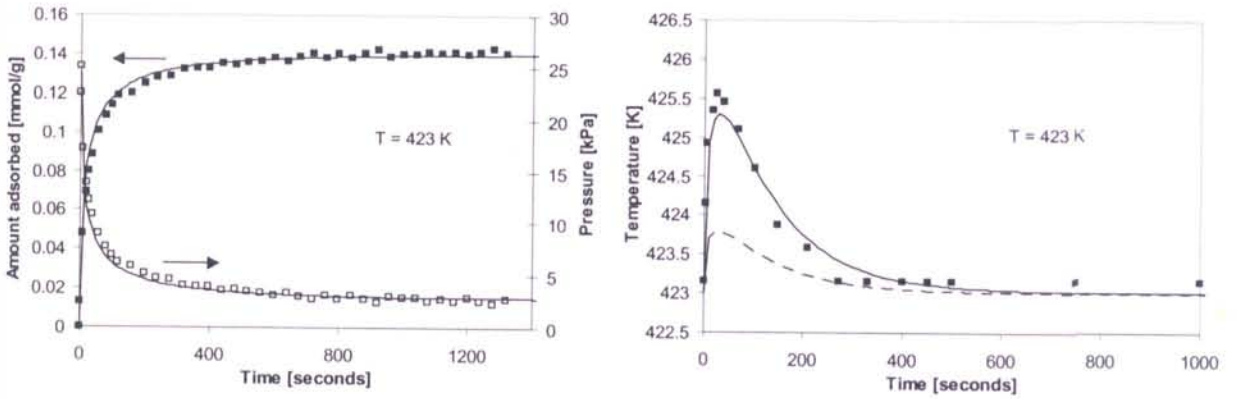

Figure 4.32. Static – batch propylene adsorption on zeolite 4A at 423 K: (a) uptake curve and pressure change; (b) temperature evolution in the gas (dashed line) and solid phase (solid line).

The constants to describe crystal diffusion by equation [4.7] are $D_c^o = 4.66.10^{-10}$ cm²/s and E_a = 15.61 kJ/mol. The energy of activation as determined from these three values is in agreement with 17 kJ/mol reported in literature (Rege et al., 1998). A comparison between the data obtained in this work and the ones previously published is

shown in Figure 4.34 (Kubota et al., 1989; Rege et al., 1998; Da Silva and Rodrigues, 1999) where D_c (cm²/s) is plotted in semi-log scale as a function of 1000/T with T expressed in Kelvin degrees. As we can see, the values obtained in this work compare fairly well with previous data.

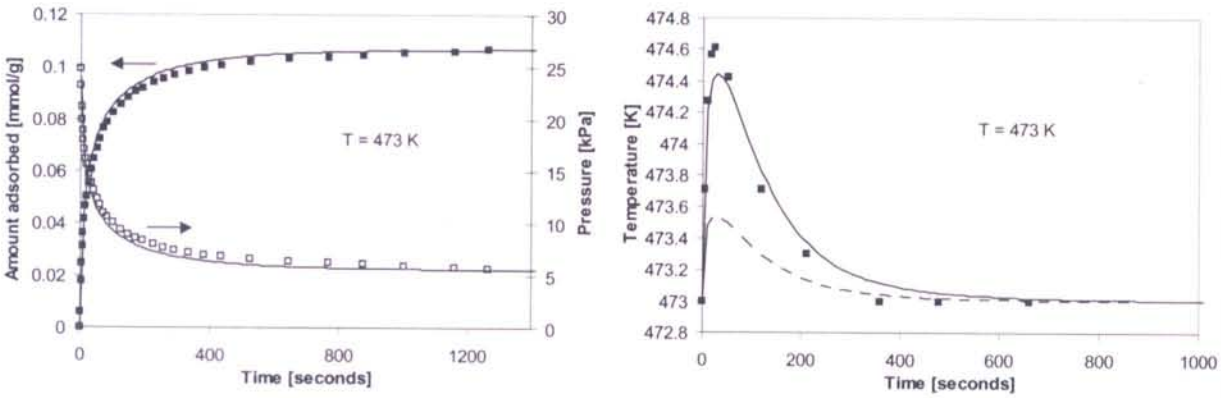

Figure 4.33. Static – batch propylene adsorption on zeolite 4A at 473 K: (a) uptake curve and pressure change; (b) temperature evolution in the gas (dashed line) and solid phase (solid line).

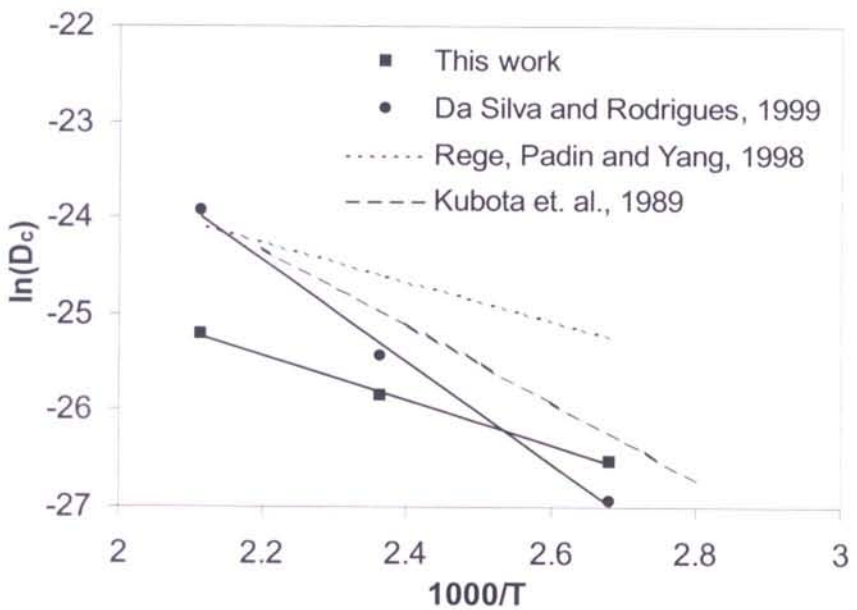

Figure 4.34. Propylene crystal diffusivity in zeolite 4A; comparison with literature.

It is clear that the model described by equations [4.1-4.23] fit the data correctly predicting well the temperature rise in the propylene experiments and also confirming the isothermal behavior of the propane uptake.

Determination of diffusivity coefficients by static-batch technique is possible; although it is not as easy as the other techniques employed in this work, particularly for strong adsorbed species, the use of eq. [4.7] instead of a single parameter is mandatory so a very good initial estimative is needed. Here, the parameters determined from ZLC and dynamic methods were used but if these values are not available, the assumptions of isothermal behavior and linear isotherm (with theoretical solution) are a good choice. The experiments of strong adsorbed species have the advantage of direct confirmation of the heat of adsorption estimated from the equilibrium data. A good value of the heat of adsorption is very important for the design of a PSA operation for gas separation.

4.4 Conclusions

In this chapter, adsorption kinetics of pure propane and propylene in several commercial adsorbents was studied. Three different techniques were used for diffusivity determinations: Zero Length Column, dilute breakthrough curves and adsorption uptakes at low pressures. The diffusion of both hydrocarbons in silica gel samples (wide pore and narrow pore) as well as in zeolite 5A pellets was controlled by macropore diffusion in the Knudsen regime. In the case of carbon molecular sieve 4A and zeolite 4A extrudates the diffusion of propane and propylene were controlled by micropore diffusion. In both molecular sieves, the energy of activation of the diffusion process was higher for propane than for propylene.

The adsorption equilibrium characterization together with the kinetic measurements performed in this chapter allows the modeling and simulation of a

Pressure Swing Adsorption (PSA) unit. In order to select a good adsorbent for this process, a difference in adsorption equilibrium capacity or in adsorption rate of both hydrocarbons should exist. The equilibrium selectivity of all adsorbents tested here was not large and thus none of them can perform a good separation purely by adsorption equilibrium differences. In the case of carbon molecular sieve 4A and zeolite 4A the differences in crystal diffusion of propylene in comparison to propane are higher than 10, which may allow the kinetic separation of the mixture propane – propylene. For this reason in the chapter dealing with PSA experiments, only these two adsorbents will be used.

Nomenclature

a	number of neighboring sites occupied in the Nitta model
C	bulk molar concentration of component i in the gas phase, mol/m^3
C_o	initial hydrocarbon bulk molar concentration, mol/m^3
C_{eq}	hydrocarbon bulk molar concentration in equilibrium with an adsorbed concentration q_s given by the isotherm model, mol/m^3
C_p	hydrocarbon bulk molar concentration in the pores of the adsorbent, mol/m^3
C_{ps}	constant pressure specific heat capacity of the adsorbent, J/kg.K
C_{vg}	constant volume specific heat capacity of the gas mixture, J/mol.K
D_{aa}	self diffusivity of the adsorbate, m^2/s
D_{ap}	apparent diffusivity parameter, m^2/s
D_{ax}	axial dispersion coefficient, m^2/s
D_k	Knudsen diffusivity, m^2/s
D_c	crystal diffusivity, m^2/s

D_c^o	limiting crystal diffusivity at high temperatures, m^2/s
D_m	molecular diffusivity, m^2/s
D_p	pore diffusivity, m^2/s
E_a	activation energy of crystal diffusion, J/mol
H	Henry equilibrium constant
h_f	film heat transfer between the gas and the adsorbent, W/m^2K
h_w	film heat transfer between the gas and the column wall, W/m^2K
J_o	Bessel function of first kind and zero order
J_1	Bessel function of first kind and first order
k_b	micropore barrier mass transfer coefficient, m/s
k_f	film mass transfer coefficient, m/s
k_g	Gas thermal conductivity, W/m.K
K_{eq}	equilibrium constant, kPa^{-1}
K_{eq}^o	equilibrium constant at the limit $T \rightarrow \infty$, kPa^{-1}
ℓ	representative spatial dimension of the pellet, m
L_c	column length in breakthrough experiments, m
L	ZLC parameter defined by eq. [4.27]
M_w	molecular weight, kg/mol
P	hydrocarbon pressure, kPa
P_c	critical pressure for self-diffusivity calculations, atm
P_p	pressure of hydrocarbon in the macropores, kPa
P_o	initial pressure of hydrocarbon, kPa
q	adsorbed phase concentration of hydrocarbon, mol/kg
$\bar{q}$	crystal averaged amount adsorbed phase concentration, mol/kg
$\langle \overline{q_i} \rangle$	particle averaged adsorbed phase concentration of hydrocarbon, mol/kg

q_{max}	maximum adsorbed phase concentration, mol/kg
q_s	adsorbed phase concentration in the crystal surface, mol/kg
r_c	crystal radius, m
R_g	ideal gas constant, 8.314 J/mol.K
r_p	mean macropore radius for D_k calculations, m
R_p	pellet radius, m
R_w	radius of the static- batch column, m
$\bar{t}$	stoichiometric time, s
T	gas temperature, K
T_c	critical temperature of adsorbate for self-diffusivity calculations, K
T_s	solid temperature, K
T_w	temperature of the column wall in static-batch experiments, K
u_i	interstitial velocity, m/s
V_o	void space volume in the MIE experiments, m^3
V_r	reference (initial) volume in the MIE experiments, m^3
ω_s	adsorbent weight, kg

Greek Letters

β_n	root of elemental eq. [4.28]
ρ_p	adsorbent density, kg/m^3
$(-\Delta H)$	heat of adsorption, J/mol
ε_c	column cell void fraction in breakthrough experiments
ε_p	porosity of the pellet
Λ	concentration variation parameter
τ_p	pore tortuosity
μ_g	gas viscosity, Pa.s

References

Antonson, C. R.; Dranoff, J. S. Nonlinear Equilibrium and Particle Effects in Intraparticle Diffusion Controlled Adsorption, *Chem. Eng. Prog. Symp. Ser.*, **1969**, 65(96), 20-26.

Bird, R. B.; Stewart, W. E.; Lightfoot, E. N. *Transport Phenomena* (2nd edition), Wiley International, Singapore, **2002**.

Brandani, S.; Ruthven, D. M. Analysis of ZLC Desorption Curves for Gaseous Systems. *Adsorption,* **1996**, 2, 133-143.

Carslaw H. S.; Jaeger, J. C. *Conduction of Heat in Solids*. Clarendon Press, Oxford, **1959**.

Cavalcante, C.; Azevedo, D.; Souza, I.; Silva, C.; Alsina, O.; Lima, V.; Araujo, A. Sorption and diffusion of p-xylene and o-xylene in aluminophosphate molecular sieve AlPO4-11. *Adsorption,* **2000**, 6(1), 53-60.

Chihara, K.; Suziki, M.; Kawazoe, K. Adsorption Rate on Molecular Sieving Carbon by Chromatography. *AIChE J.*, **1978**, 24, 237-246.

Da Silva, F. A. *Cyclic Adsorption Processes: Application to Propane / Propylene Separation*. Ph.D. Dissertation, University of Porto, Portugal, **1999**.

Da Silva, F. A.; Rodrigues A. E. Adsorption equilibria and kinetics for propylene and propane over 13X and 4A zeolite pellets. *Ind. Eng. Chem. Res.*, **1999**, 38, 2434-2438.

Duncan, W. L.; Möller, K. P. The effect of a crystal size distribution on ZLC experiments. *Chem. Eng. Sci.*, **2002,** 57, 2641-2652.

Eic, M.; Ruthven, D. M. A New Experimental Technique for Measurement of Intracrystalline Diffusivity. *Zeolites,* **1988**, 8, 40-45.

Fuertez, A. B.; Menendez, I. Separation of Hydrocarbon Gas Mixtures Using Phenolic Resin-Based Carbon Membranes. *Sep. Purif. Technol.*, **2002**, 28, 29-41.

Grande, C. A.; Rodrigues, A. E. Adsorption Equilibria and Kinetics of Propane and Propylene in Silica Gel. *Ind. Eng. Chem. Res.*, **2001**, 40, 1686-1693.

Grande, C. A.; Gigola, C.; Rodrigues, A. E. Adsorption of Propane and Propylene in Pellets and Crystals of Zeolite 5A, *Ind. Eng. Chem. Res.*, **2002**, 41, 85-92.

Grande, C. A.; Silva, V. M. T. M.; Gigola, C.; Rodrigues, A. E. Adsorption of Propane and Propylene onto Carbon Molecular Sieve, *Carbon,* **2003a**, 41(13), 2533-2545.

Grande, C. A.; Gigola, C.; Rodrigues, A. E. Propane-Propylene Binary Adsorption on Zeolite 4A, *Adsorption*, **2003b**, 9, 321-329.

Grande, C. A.; Rodrigues, A. E. Adsorption Kinetics of Propane and Propylene in Zeolite 4A, *Trans. Inst. Chem. Eng. A, Chem. Eng. Res. Dev.*, **2004**, in press.

Hufton, J. R.; Ruthven, D. M. Diffusion of Light Alkanes in Silicalite Studied by the Zero Length Column Method. *Ind. Eng. Chem. Res.*, **1993**, 32, 2379-2386.

Kärger, J.; Ruthven, D. M. *Diffusion in Zeolites and Other Microporous Solids,* Wiley, London, **1992**.

Khodakov, A. Y.; Rees, L. V. C. Effect of Propane on the Kinetics of Carbon Dioxide Adsorption in NaA Zeolites, *Gas Sep. Purif.,* **1995**, 9, 253-257.

Kubota, K.; Nakajima, K.; Ono, Y.; Hayashi, S. Adsorption Characteristics of Propylene on Molecular Sieve 4A, *Sep. Sci. and Techn.*, **1989**, 24, 709-719.

Loos J-B. W. P.; Verheijen, P. J. T.; Moujlin, J. A. Improved Estimation of Zeolite Diffusion Coefficients from Zero-Length Column Experiments. *Chem. Eng. Sci.*, **2000**, 55, 51-65.

Malek, A.; Farooq, S. Kinetics of Hydrocarbon Adsorption on Activated Carbon and Silica Gel, *AIChE J.*, **1997**, 42, 761-775.

Morgan, S. S. *A comparison of Simplex Method Algorithms*, Ms Thesis, Univ. of Florida, **1997** (www.cise.ufl.edu/~davis/Morgan/index.htm).

Nitta, T.; Shigetomi, T.; Kuro-Oka, M.; Katayama, T. An adsorption isotherm of multi-site occupancy model for homogeneous surface. *J. Chem. Eng. Japan*, **1984**, 17, 39-45.

Padin, J., Rege, S. U., Yang, R. T. and Cheng, L. S. Molecular-Sieve Sorbents for Kinetic Separation of Propane/Propylene, *Chem. Eng. Sci.*, **2000**, 55, 4525-4535.

Qinglin, H.; Sundaram, S. M.; Farooq, S. Revisiting Transport of Gases in the Micropores of Carbon Molecular Sieves. *Langmuir*, **2003**, 19, 393-405.

Ramachandran, R.; Dao, L. H.; Brooks, B. *Method of Producing Unsaturated Hydrocarbons and Separating the Same from Saturated Hydrocarbons*, U.S. Patent 5,365,011, **1994**.

Rege, S. U.; Padin, J.; Yang, R. T. Olefin/Paraffin Separations by Adsorption - Pi-Complexation vs. Kinetic Separation, *AIChE J.*, **1998**, 44, 799-809.

Ruthven, D. M. *Principles of adsorption and adsorption processes*, Wiley, New York, USA, **1984**.

Ruthven, D. M.; Derrah, R. I. Sorption in Davison 5A Molecular Sieves. *Can. J. Chem. Eng.*, **1972**, 50, 743-747.

Ruthven, D. M. Short Communication: Diffusion of Simple Molecules in 4A Zeolite, *Adsorption*, **2001**, 7, 301-304.

Ruthven, D. M.; Xu, Z. Diffusion of Oxigen and Nitrogen in 5A Zeolite Crystals and Commercial 5A Pellets. *Chem. Eng. Sci.*, **1993**, 48, 3307-3312.

Schneider, P.; Smith, J. M. Adsorption Rate Constants from Chromatography. *AIChE J.*, **1968**, 17, 762-771.

Schröter H. J. Carbon Molecular Sieves for Gas Separation Processes. *Gas Sep. and Purif.*, **1993**, 7(4), 247-251.

Silva, J.A.C. *Separation of n/iso – Paraffins by Adsorption Process,* Ph.D. Dissertation University of Porto, Portugal, **1998**.

Silva, J. A. C.; Rodrigues, A. E. Analysis of ZLC Technique for Diffusivity Measurements in Bidisperse Porous Adsorbent Pellets, *Gas Sep. Purif.*, **1996**, 10, 207-224.

Silva, J. A. C.; Mata, V. G.; Dias, M. M.; Lopes, J.C.; Rodrigues, A. E. Effect of Coke in the Equilibrium and Kinetics of Sorption on 5A Molecular Sieve Zeolites, *Ind. Eng. Chem. Res.*, **2000**, 39, 1030-1034.

Sircar, S. Influence of Adsorbate Size and Adsorbent Heterogeneity on IAST, *AIChE J.*, **1995**, 41, 1135-1145.

Sircar, S., Measurement of Gibbsian Surface Excess, *AIChE J.*, **2001**, 47, 1169-1176.

Talu, O. Needs, Status, Techniques and Problems with Binary Gas Adsorption Experiments, *Adv. Col. Interf. Sci.*, **1998**, 76-77, 227-269.

Vyas, S. N.; Patwardhan, S. R.; Vijayalakshmi, S.; Sri Ganesh, K. Adsorption of Gases on Carbon Molecular Sieves. *J. Col. Interf. Sci.*, **1994**, 168, 275-280.

Xiao, J.; Wei, J. Diffusion Mechanism of Hydrocarbons in Zoelites-I. Theory, *Chem. Eng. Sci.*, **1992**, 47, 1123-1141.

Yang, R. T. *Gas Separation by Adsorption Processes.* Butterworths, Boston, **1987**.

5. Adsorption Equilibrium and Kinetics on Laboratory-Made Adsorbents

In previous chapters we have studied adsorption equilibrium (single and binary) and adsorption kinetics of available commercial adsorbents. Except for the results for zeolite 4A and carbon molecular sieve 4A, all other sorbents tested did not have good equilibrium or either kinetic selectivity. Also in zeolite 4A the difference of diffusivities is large with good selectivity, but the diffusivity of propylene is still small producing dispersed concentration fronts inside the columns of the PSA unit. Modifications of the crystal size may improve the PSA performance.

In this chapter we report adsorption properties (adsorption equilibrium and kinetics) of three different kinds of sorbents produced in laboratory. Initially, with the aim of studying the effects of crystal size on the performance of PSA units we have measured adsorption equilibrium and kinetics of pure gases on four different crystals of zeolite 4A with average size: 0.3, 1.9, 10.0 and 22.0 μm. Also, searching for a new adsorbent, a study performed on Cuban natural zeolites (clinoptilolites) exchanged with different materials is also presented. On the other side, the π-complexation adsorbents for increasing propylene selectivity using transition metals (in this case Ag^{+}) were prepared in a mesoporous silica matrix, SBA-15 using two different loadings of silver.

5.1 Zeolite 4A crystals

5.1.1 Background

Adsorption of propane and propylene on zeolite 4A has been extensively investigated in literature due to partial exclusion of the propane molecule compared to

propylene adsorption either experimentally (Kubota et al., 1989; Järvelin and Fair, 1993; Rege et al., 1998; Da Silva and Rodrigues, 1999; Patiño-Iglesias et al., 2004) or by molecular simulations (Zhang et al., 2003). In all these works, propane was only slightly adsorbed. As reported in chapter 2, adsorption of propane measured in this work was much higher (Grande et al., 2003) with a very small diffusivity coefficient consistent with other reported value (Khodakov and Rees, 1995). However, in Chapter 4 we have shown that propylene diffusivity has the same order of magnitude in most of these works.

The molecules of both hydrocarbons are shown in Figure 5.1. If the molecules are treated as having a single kinetic diameter, it is clear that propane has a slightly larger diameter, enough to be excluded from the channels and adsorbing only on the crystal surface (Zhang et al., 2003). When we consider the kinetic diameter of the propane molecule and the opening of the zeolite structure, we are assuming that the molecules as well as the zeolite channels are rigid (Xiao and Wei, 1992) and this may not be strictly the case of this systems, although microscopic techniques may give us a better understanding of the diffusion mechanism.

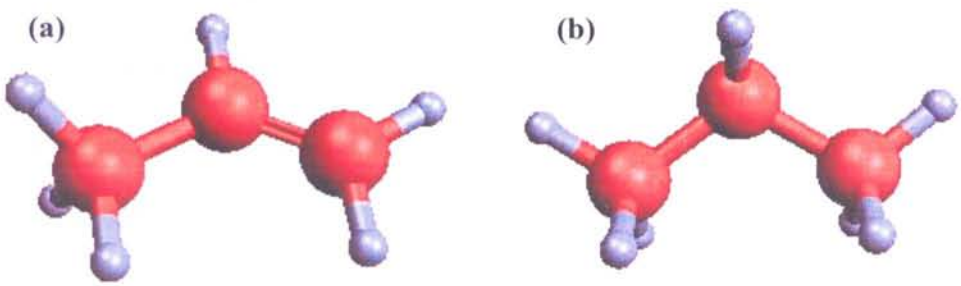

Figure 5.1. Propylene (a) and propane (b) molecules in gas phase at 298 K.

Even with a large difference in diffusion velocities, the diffusivity coefficient of propylene is small when compared to other systems used in PSA and this reason was

mentioned in some reports as the problem to look at with this material (Järvelin and Fair, 1993). The parameter that is important to understand the adsorption / desorption kinetics is not the diffusivity coefficient but the ratio D_c/r_c^2 where r_c is the crystal radius. Nothing can be done to diminish the diffusivity coefficient without changing the zeolite structure, but the size of the zeolite crystal can always be modified.

As shown in previous chapters, the size of the zeolite crystals in the commercial sample used is 3.8 μm. This diameter is close to other works (Da Silva, 1999) and may be due to the optimum size of zeolite 4A used for detergent applications, that is around 3.5 μm (Ullman´s Encyclopedia, 2003). Before studying the possibility of changing the crystal size of the zeolite in the PSA process, it is interesting to know if the adsorption equilibrium of the commercial sample was modified in the pelletization process. If the pelletization process destroys or modifies the adsorption equilibrium, less amount of hydrocarbon will be adsorbed in the laboratory samples. Similar variations can happen in the adsorption kinetics of propane and propylene. For this purpose we have measured adsorption equilibrium and kinetics of propane and propylene on four laboratory-made samples of zeolite 4A having different crystal diameters: 0.3, 1.9, 10.0 and 22.0 μm.

5.1.2 Zeolite 4A synthesis and characterization

Elena I. Basaldella at CINDECA (La Plata, Argentina) synthesized all the samples. Zeolite crystals were prepared by batch hydrothermal crystallization. The different batch experiments were carried out in closed polypropylene containers, at 365 ± 1 K, without stirring. The raw materials used were: NaOH (Carlo Erba, analytical reagent), commercial sodium aluminate [Al_2O_3 (36.5%), Na_2O (29.6%), H_2O (33.9%)], soluble water-glass with SiO_2 / Na_2O = 3.18 (w/w) (density equal to 1.36 g/ml) and distilled water. Triethanolamine, TEA, (Anedra, analytical reagent) was incorporated in

variable quantities to obtain the different crystal sizes. This product increases the density of the liquid phase inhibiting crystal growth and creating more nucleation points.

Products were characterized by X-Ray Diffraction (XRD). The diffraction patterns were obtained in a Philips PW 1732/10 equipment using CuKα radiation and a Ni filter, at a rate of 2°/min. The diffraction diagrams of the zeolite samples were identified by comparison with those detailed in the literature (Breck, 1974).

The zeolite crystal size diameter was obtained by scanning electron microscopy (SEM) observations in a JEOL, JSM-6301F (Centro de Materiais da Universidade do Porto, CEMUP) where an X-ray spectrometer (NORAN-VOYAGER) is coupled to determine chemical composition. Morphology and crystal size of the samples observed by SEM can be seen in Figure 5.2. The crystal sizes of the samples are 0.3, 1.9, 10.0 and 22.0 μm, although some crystal size distribution was observed. In the larger crystals (10 and 22 μm samples) some coalescence between two or more crystals was also found.

5.1.2 Adsorption equilibrium

Adsorption of propane and propylene was measured at 373, 423 and 473 K in the MIE equipment described in previous chapters and used to measure adsorption equilibrium of the commercial sample of zeolite 4A. The wet mass of adsorbent used for each experiments was 0.609 g. After activation in vacuum ($< 10^{-5}$ kPa) and high temperature, the samples lost around 20% in weight (air + pre-adsorbed moisture). Using an activation temperature of 593 K (with a heating ramp of 1K/min) that was recommended for zeolites (Breck, 1974) the isotherms were non-reproducible and the amount adsorbed of propylene was very low in the initial measurements. This difficulty was solved using an activation temperature of 673 K.

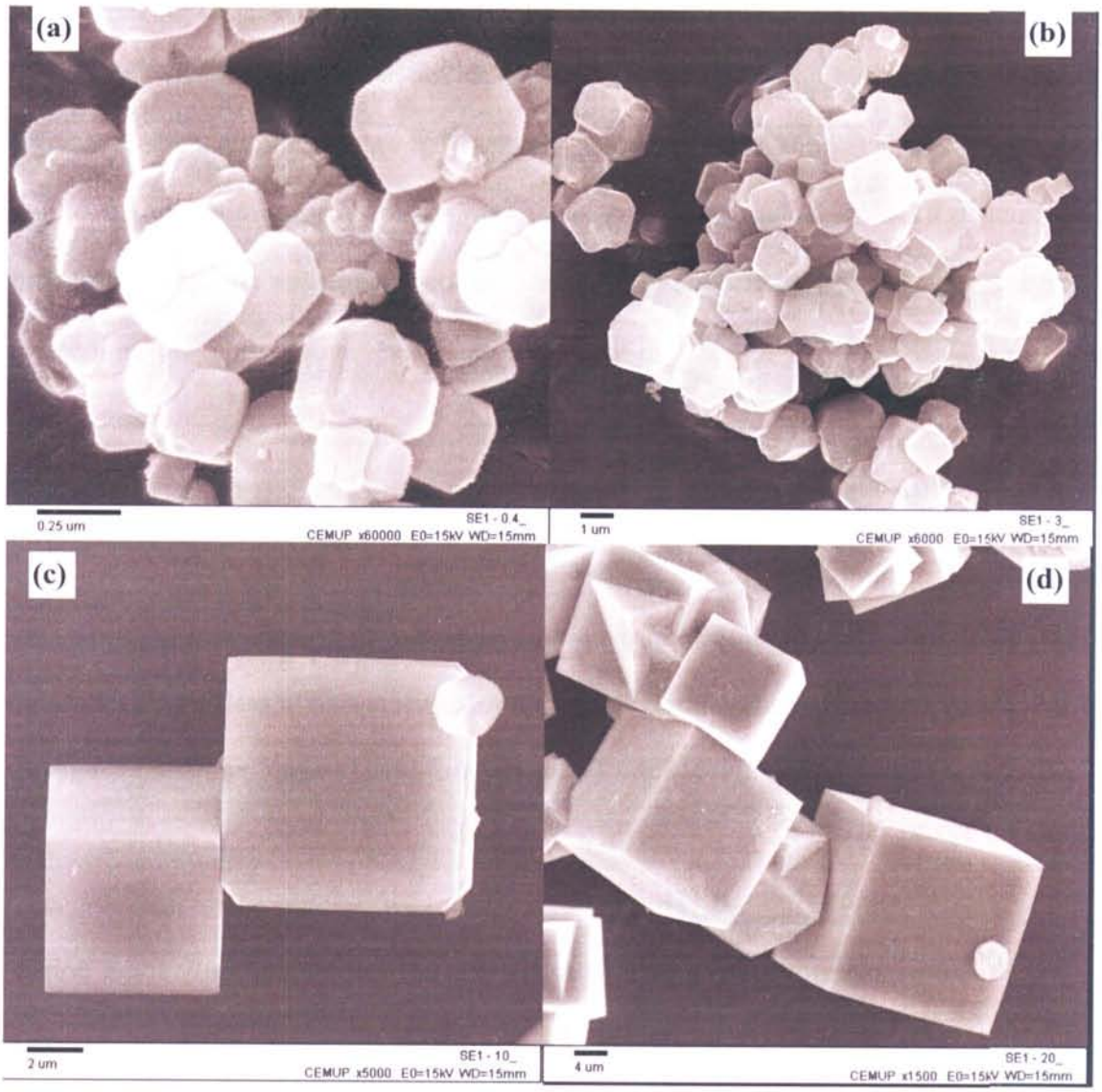

Figure 5.2. SEM images of the four different samples of crystals of zeolite 4A: (a) 0.3 μm, (b) 1.9 μm, (c) 10 μm and (d) 22 μm.

The propylene isotherms measured in the four samples of zeolite 4A crystals (represented in wet weight basis) are shown in Figure 5.3. In the same figure, data on the commercial sample fitted with the multi-site Langmuir model is presented for comparison showing good agreement. If we assume that the amount adsorbed of propylene is the same in the pellet sample as in the crystal samples studied here, we can conclude that the amount of inert binder in the zeolite extrudates is 20%.

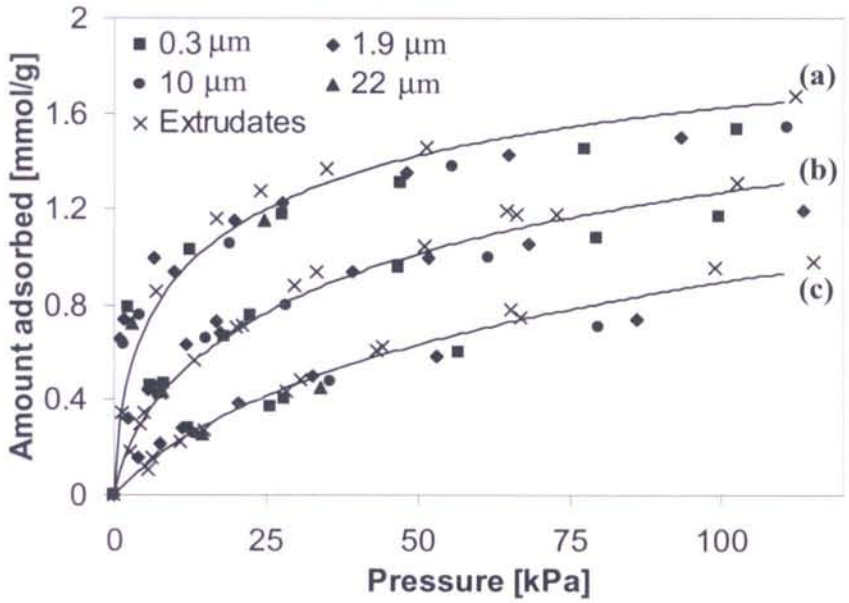

Figure 5.3. Adsorption equilibrium of propylene on zeolite 4A crystals of 0.3, 1.9, 10 and 22 µm. Points (x) correspond to adsorption equilibrium measured in zeolite 4A extrudates (CECA) at the same temperature. Solid line is the multisite Langmuir model fitting: (a) 373 K; (b) 423 K; (c) 473 K.

Propane isotherms were measured in the 0.3 µm sample and only some points were recorded with the 1.9 µm sample. As a result of the lower values of propane diffusivity, three days are needed to reach a single equilibrium point in the zeolite with 3.8 µm crystal diameter and thus it will take more than a week per point in the larger crystals. As the propylene loading of all the crystal samples is the same, with some confidence we can assume that the propane adsorption will be also the same in the larger crystals. Results obtained at 423 and 473 K are presented in Figure 5.4. Results are also compared with data obtained in commercial extrudates fitted with the multi-site Langmuir model showing also good agreement.

We have compared the adsorption equilibrium of propane and propylene on four samples of zeolite 4A of very different crystal size diameter made in laboratory, with

the commercial zeolite sample reported in Chapter 2. With that basis, we can conclude that the adsorption capacity of zeolite 4A for propane and propylene was the same for all crystal sizes, and no strange effects appeared in the larger and in the smaller crystals due to the preparation protocol. Indirectly, we can also conclude that the pelletization process did not alter adsorption equilibrium capacity of C_3 hydrocarbons on the crystals located in the commercial extrudates reported in Chapter 2. This means that the parameters obtained in Chapter 2 for adsorption equilibrium can be used in further works using zeolite 4A with different size diameters.

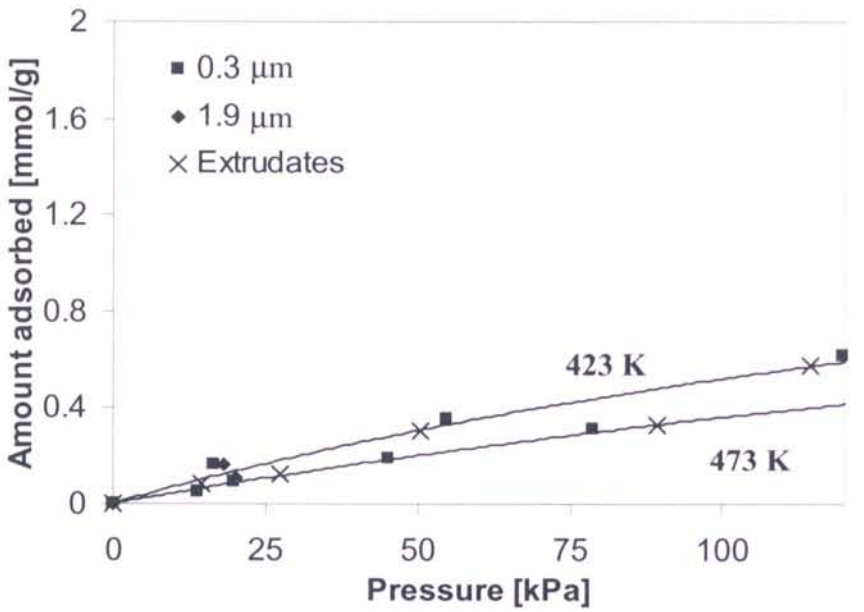

Figure 5.4. Adsorption equilibrium of propane on zeolite 4A crystals of 0.3 and 1.9 μm. Points (x) correspond to adsorption equilibrium measured in zeolite 4A extrudates (CECA) at the same temperature. Solid line is the multisite Langmuir model fitting.

5.1.2 Adsorption kinetics

The same crystals used for equilibrium determination were employed for breakthrough curve measurements. To activate the samples, a flow of helium of 15 cm^3/min at 673 K (1K/min heating ramp) was used overnight. Details of the

breakthrough experiments are listed in Table 5.1. Only the smaller crystals were used for propane measurements.

Table 5.1 – Basic physical properties of zeolite 4A crystals and breakthrough curves conditions

Crystal diameter [μm]	0.3; 1.9; 10.0; 22.0
Crystal density [g/cm³] [(a)]	1.57
Column length [cm]	3.13
Column diameter [cm]	0.69
Flowrate [cm³/min] [(b)]	35.0-38.0
C_3 partial pressure [kPa]	1.1
Column porosity [-]	0.412

[(a)] Assumed value from Ruthven and Derrah, 1972.

[(b)] Measured at laboratory temperature (295K)

Adsorption experiments of propylene in the 0.3 μm sample at 373, 423 and 473 K are shown in Figure 5.5. The solid lines represents the breakthrough model described in Chapter 4. The experiments were performed using such a flowrate to ensure isothermal behavior (experimentally confirmed at the outlet of the column). As the samples were crystals, the only possible resistances are crystal diffusivity, film mass transfer and axial dispersion. As the flowrate was high the film mass transfer resistance was neglected. The variations of crystal diffusivity affect only slightly the tail of the curve, confirming that the parameter D_c/r_c^2 is high and thus the crystal diffusivity and the axial dispersion share the control of the curve. The values used for the fitting of the curves in Figure 5.5 are reported in Table 5.2.

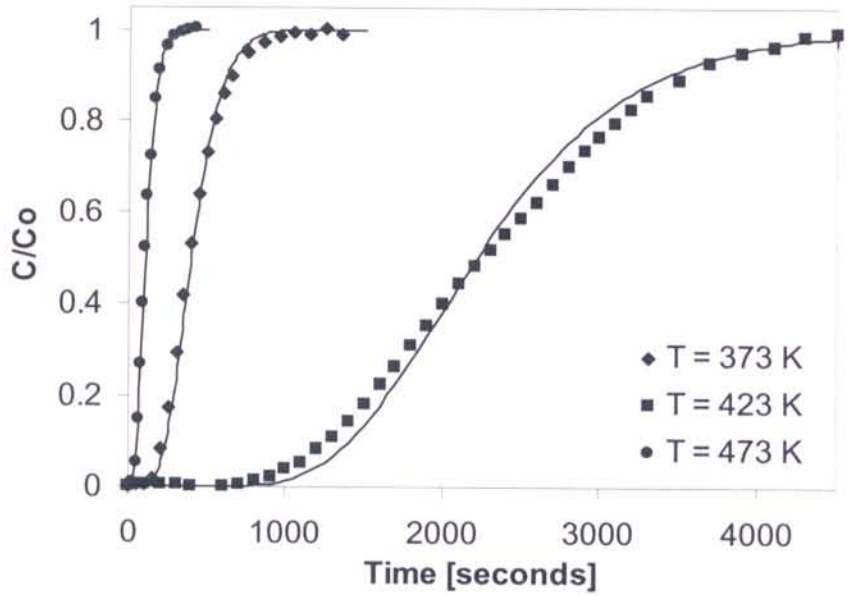

Figure 5.5. Dilute breakthrough experiments of propylene in zeolite 4A crystals with 0.3 μm average diameter at 373, 423 and 473 K.

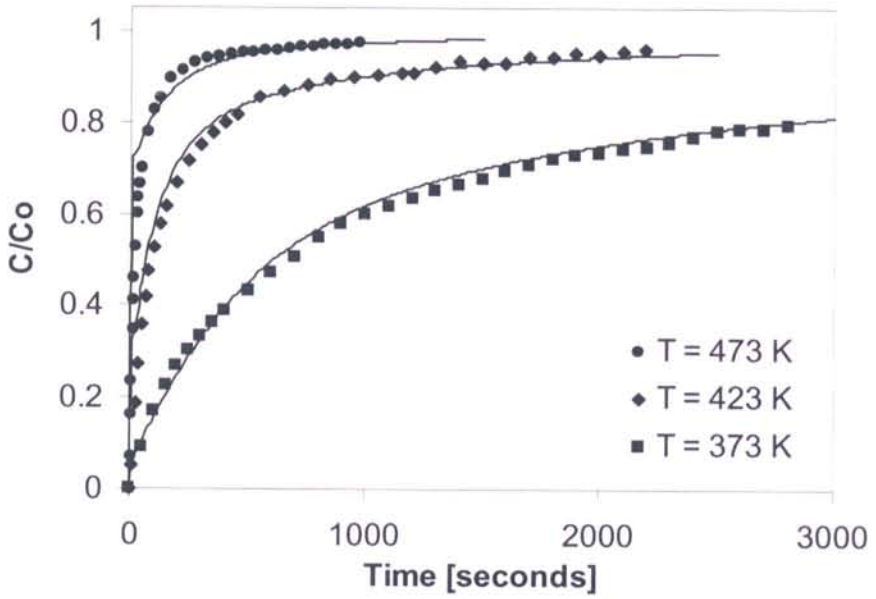

Figure 5.6. Dilute breakthrough experiments of propylene in zeolite 4A crystals with 10 μm average diameter at 373, 423 and 473 K.

Breakthrough experiments in the same conditions (mass of adsorbent and flowrate) at 373, 423 and 473 K were performed for the crystals of 10 μm. The experimental data together with the fitting of the model are shown in Figure 5.6. In this

case the outlet concentration profile is much more dispersed. The diffusivities (and axial dispersion coefficients) used for fitting the simulation to the experimental results are also reported in Table 5.2.

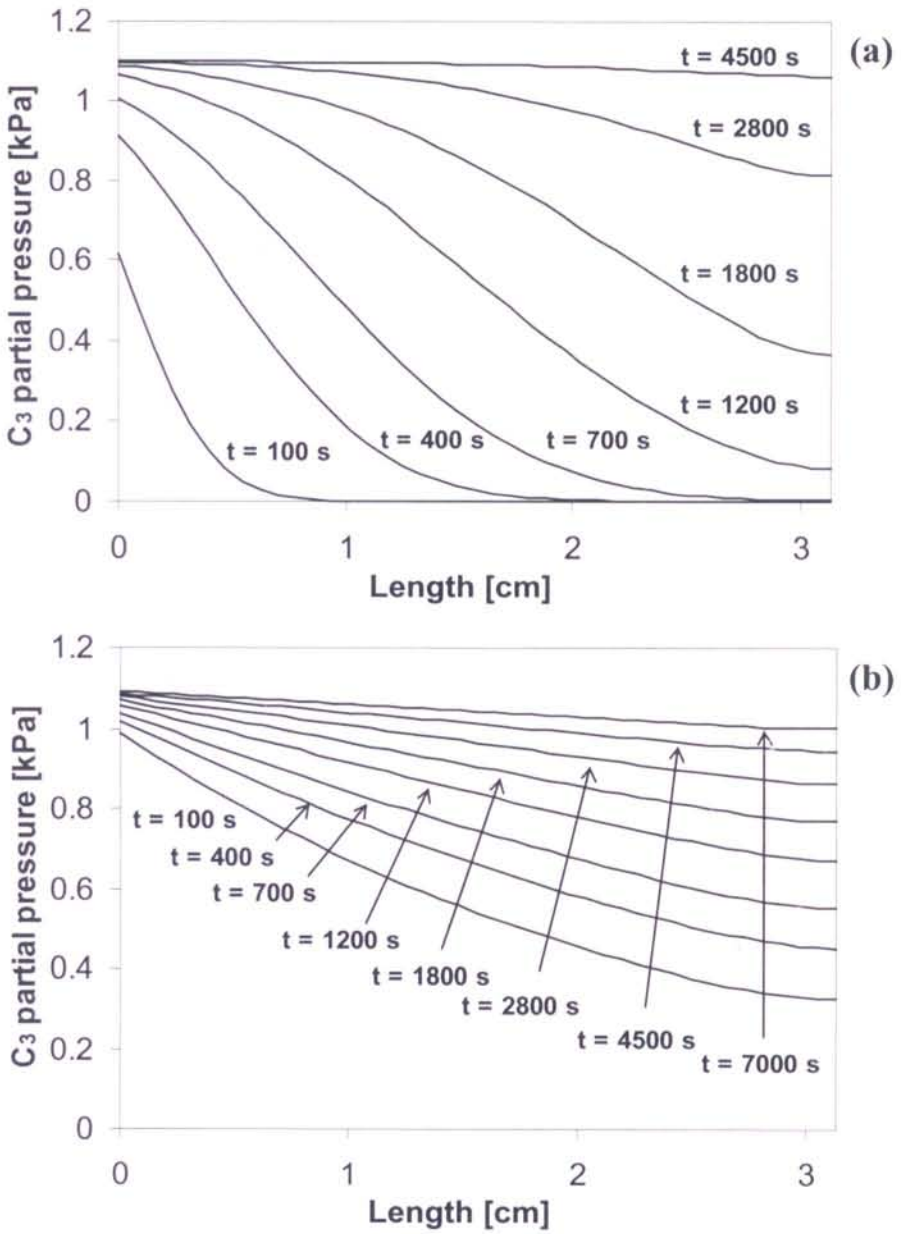

Figure 5.7. Concentration profiles of propylene inside the column at 373 K for the 0.3 μm crystals (a) and for the 10 μm crystals (b) of zeolite 4A.

The concentration profiles inside the column with these two different samples are shown for T = 373 K in Figure 5.7. Clearly in the case of the larger sample the concentration profile is much more dispersed than in the small one.

Table 5.2 – Crystal diffusivity of propane and propylene in zeolite 4A, D_c [cm²/s], obtained from fitting of breakthrough curves

Gas	T, [K]	0.3 μm	1.9 μm	10.0 μm	22.0 μm
C_3H_6	373	$3.1x10^{-12}$	--	$3.3x10^{-12}$	--
	423	$6.4x10^{-12}$	$6.8x10^{-12}$	$7.4x10^{-12}$	$7.1x10^{-12}$
	473	$9.8x10^{-12}$	--	$9.4x10^{-12}$	--
C_3H_8	373	--			
	423	$3.6x10^{-14}$			
	473	$6.8x10^{-14}$			

Breakthrough experiments on the other crystals (1.9 and 22 μm) were performed only at 423 K. These breakthrough curves are shown in Figure 5.8. Again, in the larger crystals the effect of crystal size distribution is pronounced. The diffusivity values used for the fitting are also reported in Table 5.2. As can be seen, the values reported for all the crystals are within 15% and the difference is not large when compared with the results obtained in extrudates and reported in Chapter 4.

One of the main advantages of having very small crystals of zeolite 4A is that it allows more accurate measurements of the propane diffusivity; i.e., adsorption equilibrium in the smaller samples was obtained only after 2 hours of adsorbate – adsorbent contact. Even with the very small crystal size of one of the samples, extremely fast curves are expected for Zero Length Column (ZLC) measurements. Breakthrough curves of propane at 423 and 473 K measured in the 0.3 μm sample are shown in Figure 5.9. In this case also, the process was isothermal. The solid line

corresponds to the model described in Chapter 4. The diffusivity values used to fit the experimental data to the model are also reported in Table 5.2.

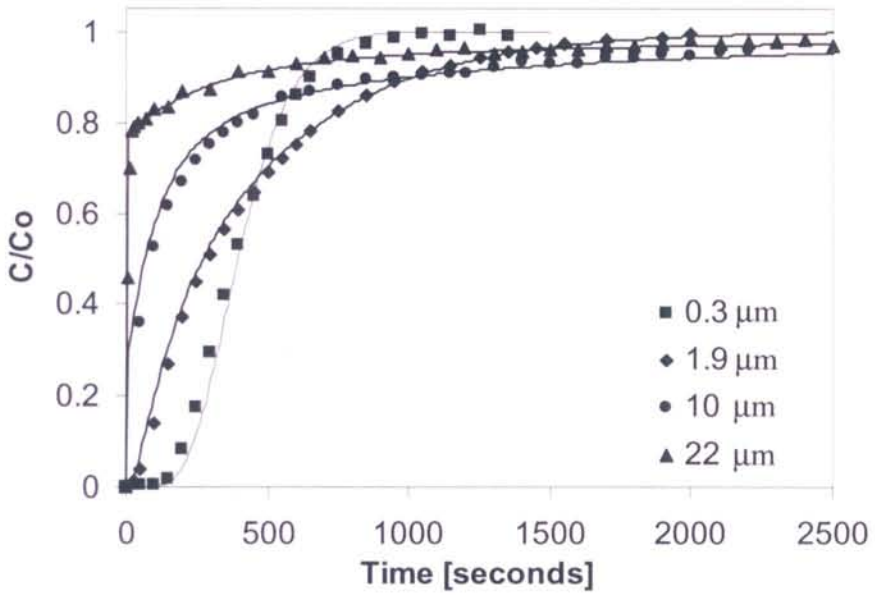

Figure 5.8. Dilute breakthrough experiments of propylene in zeolite 4A crystals at 423 K with 0.3, 1.9, 10 and 22 μm average diameter.

The adsorption diffusivity of propylene was measured in four different crystal sizes of laboratory-prepared zeolite 4A while propane experiments were performed only in the smaller crystals. The diffusivity values obtained from the fitting of the diffusion model confirm at least, the order of magnitude of previous reported values for extrudates with crystal size diameter of 3.8 μm.

These results show that the crystal diffusivity for each hydrocarbon was approximately the same in all the samples and furthermore the pelletization process does not affect seriously the diffusion of these gases. Large differences ($D_c^{crystals}/D_c^{pellets}$ = 6 to 8) was reported for ethane in crystals and pellets of zeolite 4A indicating some damage of the crystals during pelletization (Kondis and Dranoff, 1971). With these results we can have the possibility of "adsorbent design" for a targeted separation, in

this case, propane-propylene varying the crystal size according to convenient results in VSA-PSA unit.

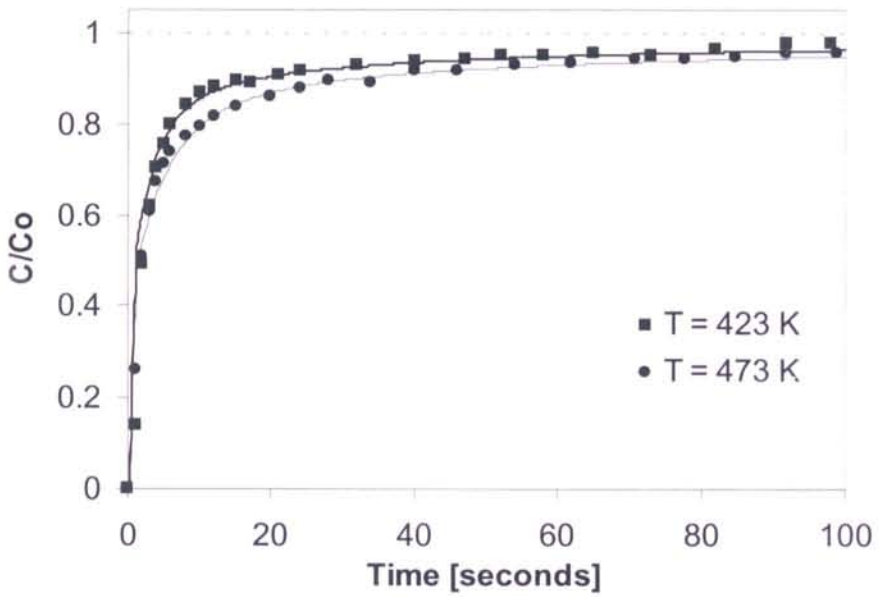

Figure 5.9. Dilute breakthrough experiments of propane in zeolite 4A crystals with 0.3 μm average diameter at 423 and 473 K.

5.2 Exchanged natural zeolites

Natural zeolites like clinoptilolites, mordenites and erionites are natural compounds that are frequently found in United States, Mexico and Cuba. In natural zeolites the positive charges are equilibrated with different cations and so in the same sample, sodium, calcium, potassium and other metals can be found. With this cation distribution, the pore size of the zeolites and its 3-dimensional structure are rather random, reasons why natural zeolites are not used in any industrial process in large scale, even with their low price. A possibility to reduce these defects is to treat the zeolite in laboratory and exchange it with a single cation to homogenize its structure and properties. All these zeolites have small micropores arranged in either bi or tri-dimensional sequence. The structures of mordenite and clinoptilolite are shown in

Figure 5.10. In this work, again due to collaboration with other research teams that form the CYTED V.8, we have obtained from the group of Miguel Autié, different samples of Cuban zeolites exchanged in laboratory. Two samples of natural mordenite, exchanged with different cations, copper (CuMOR) and silver (AgMOR) were employed for the measurements. Also a sample of clinoptilolite exchanged with zinc was analyzed. Approximately one gram of zeolite was received in small particles with sizes around 0.5 mm and without a defined shape (samples crushed from natural zeolites and not pelletized).

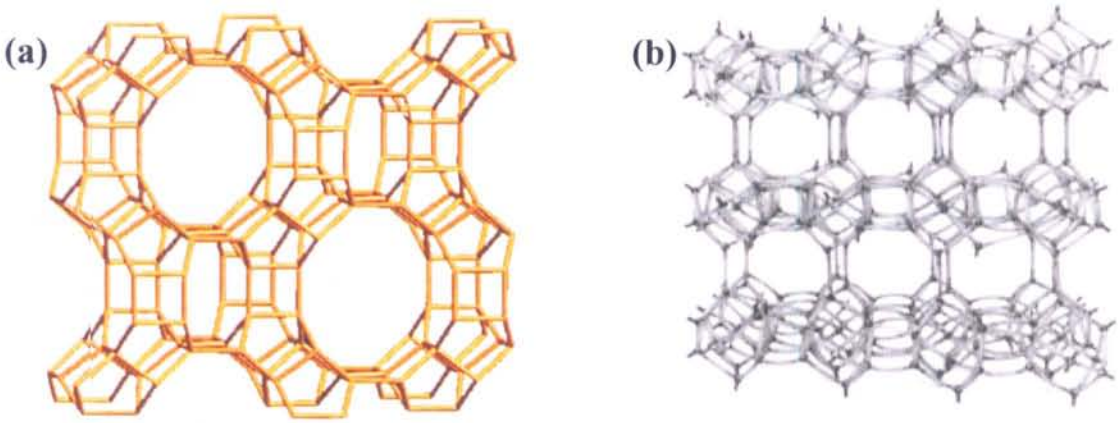

Figure 5.10. Mordenite (a) and clinoptilolite (b) structures.

The samples were packed in a column of 0.69 cm diameter and 3.13 cm length for breakthrough experiments. A mixture with 4% propylene diluted with helium was used. All the experiments were performed at 323 K with a previous activation of the sample using 15 cm^3/min of pure helium at 593 K overnight. The temperature of 593 K was reached with a heating ramp of 1 K/min, as recommended for zeolites (Breck, 1974). The analysis were performed in the modified unit for ZLC and diluted breakthrough measurements. The humid weight of sample used for each sample was: AgMOR = 1.0207 g; CuMOR = 1.0783 g; HZn = 1.1696 g.

Propylene adsorption breakthroughs on AgMOR at 323 K are presented in Figure 5.11. The initial adsorption curve showed a high retention of propylene that decreases in successive experiments. After the third experiment, the amount retained is very low. Desorption curves are also plotted in this figure. If no reaction takes place in the adsorbent, the adsorption and desorption curves should be symmetrical which is clearly not this case.

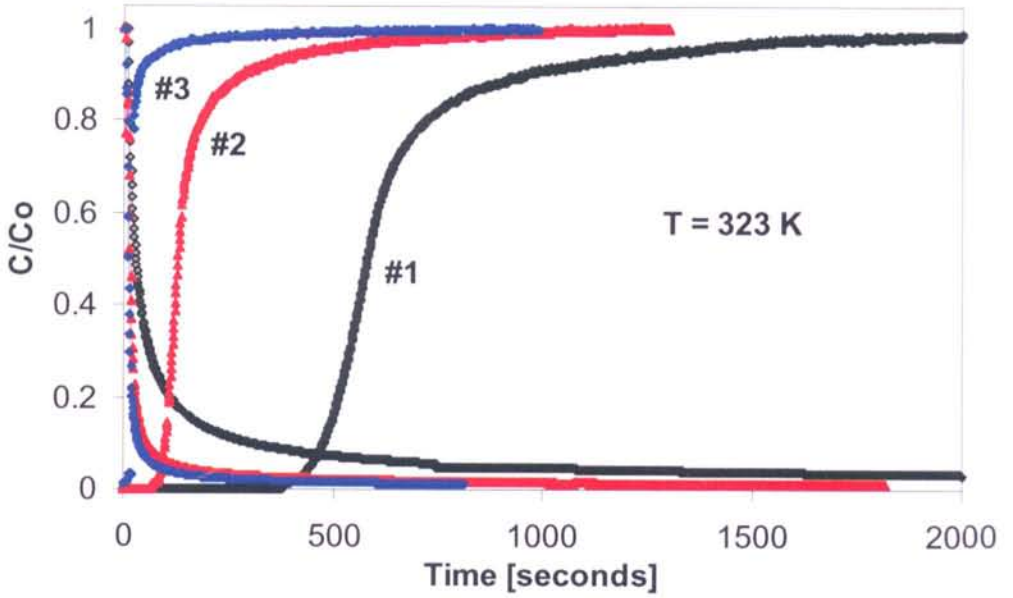

Figure 5.11. Consecutive propylene dilute breakthrough curves on AgMOR at 323 K.

The adsorption/desorption breakthrough curves of propylene on the CuMOR samples are shown in Figure 5.12 presenting the same behavior. In this CuMOR case, prior to the third measurement, the sample was heated to 473 K for 15 minutes until it releases some extra propylene.

In all the samples it is clear that the amount retained in the adsorption step is not released in the desorption step. As we have propylene at lower temperatures we may assume that a previously reported mechanism is occurring: allylic carbocations were produced and these species are irreversibly adsorbed producing coke when temperature

is increased by a Brønsted-induced mechanism (Chiapetta et al., 1999). This mechanism was proposed for three H-mordenites with Si/Al ranging from 6.5 to 24 and was the same situation that the one reported in Chapter 2 with commercial acid mordenite, but in this case with a much lower Si/Al ratio.

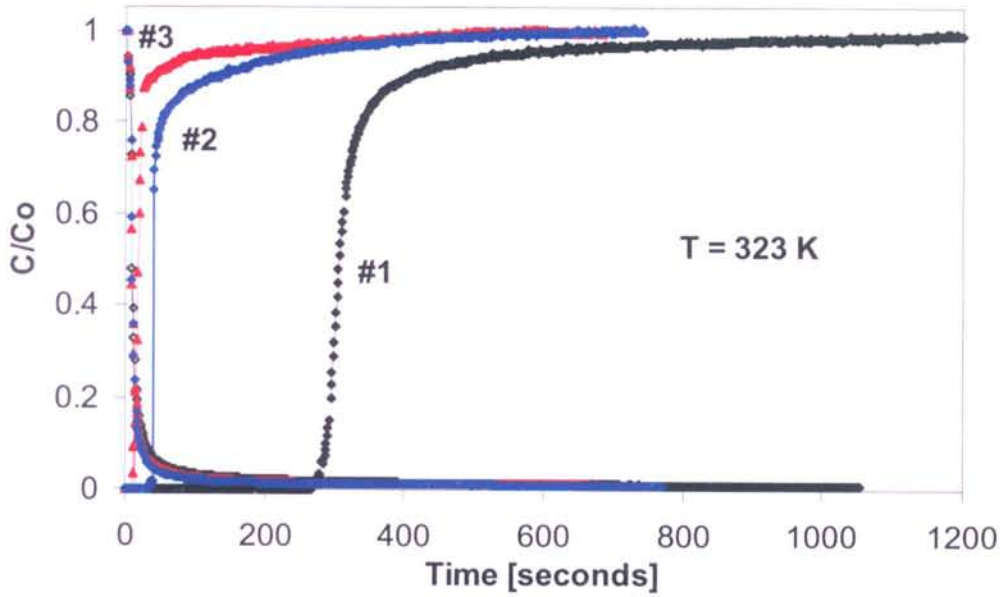

Figure 5.12. Consecutive propylene dilute breakthrough curves on CuMOR at 323 K.

Clinoptilolite adsorbents were previously reported to have good selectivity for the CH_4/N_2 separation due to partial or total size exclusion of the methane molecule (Ackley and Yang, 1991; Jayaraman et al., 2004). With that information, we measured the breakthrough curves of propylene without knowing whether the molecule will penetrate into the pores or not. The same routine of measurements was performed and the results are shown in Figure 5.13. In this case, the first desorption run was finished after three hours when the second run starts. Apparently, there exists some irreversible adsorption of propylene as in the other samples. The difference is that in this case if the column is left overnight with a flow of helium, the same results as in the first day are obtained. This is the indication that propylene has serious problems to penetrate the

micropore channels of this zeolite. As the diffusivity of propylene in this sample is extremely small, the adsorbent will not be used for further experiments on propane-propylene separation.

Unfortunately, none of the three adsorbents tested gave good results only with propylene adsorption so it was not worthy either to analyze the data presented in the figures and to measure adsorption equilibrium using propylene or propane.

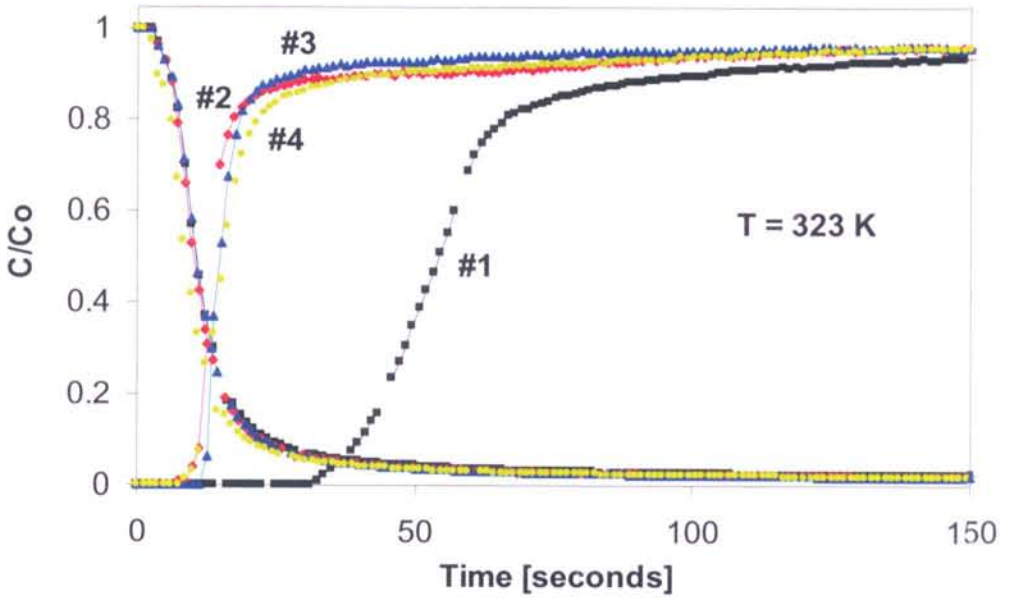

Figure 5.13. Consecutive propylene dilute breakthrough curves on ZnCLT at 323 K.

5.3 SBA-15 and silver exchanged SBA-15

The group of professor Ralph T. Yang followed the research line of π-bonds formation between olefins and some transition metal ions and reported many adsorbents applied to olefin-paraffin separation (Yang and Kikkinides, 1995; Cheng and Yang, 1995; Rege et al., 1998; Padin et al., 2000). In their papers, different matrices (polymeric resins, silica, Al_2O_3, Y-zeolites, pillared clays, MCM-41) were used to disperse silver and copper (Cu^+) by several techniques, like cation exchange, thermal dispersion and incipient wetness. Also, proprietary adsorbent (Olesorb-1), a dispersion

of silwer nitrate in bentonite clay with some promoters, were employed (Cho et al., 2001; Choudary et al., 2002). Other works involving the use of supported silver and cuprous ions have been published mainly in the field of membranes (Teramoto et al., 2002; Kim et al., 2000a; Kim et al, 2000b; Jose et al., 2001).

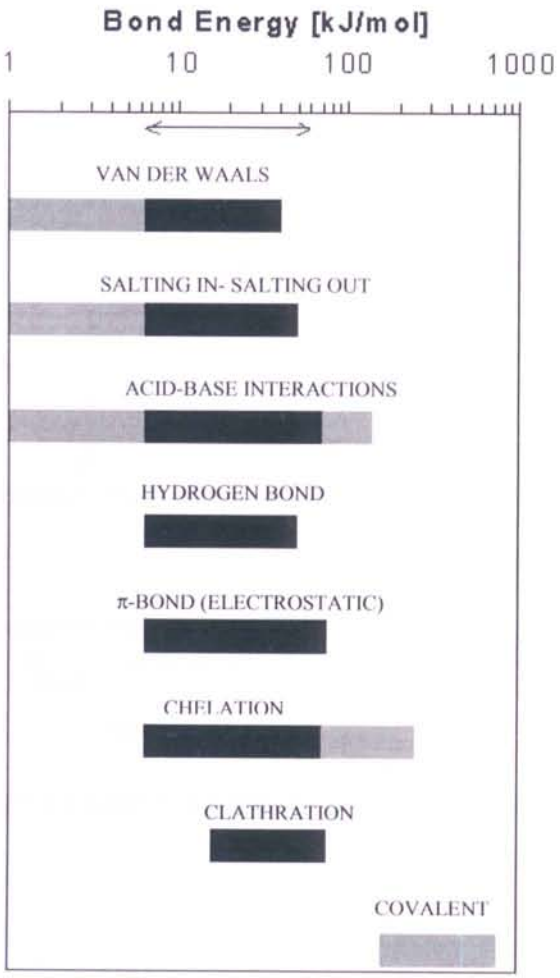

Figure 5.14. Bond energies for adsorption. Range marked in black is in the optimal range for reversible complexation. Figure adapted from Humphrey and Keller (1997).

The idea of forming π-complexation bonds between the olefin and a transition metal ion is to obtain a strong enough bond between the olefin and the adsorbent to provide high selectivity but not too strong to allow desorption of the olefin to desorb it by changing the operating conditions (temperature or pressure). As shown in Figure

5.14, from the different kind of adsorption forces, the π-bond formation lies in the optimal range of bond strengths to be used in adsorption processes (Humphrey and Keller, 1997).

SBA-15 is a novel ordered mesoporous silica (Zhao et al., 1998) that has already been used for many applications including protein adsorption (Jun et al., 2000), preparation of nanostructured carbon materials (Han et al., 1999). It was also evaluated for the separation of C_2-C_3 olefin-paraffin systems (Newalkar et al., 2002; Newalkar et al., 2003). This material has many advantages like robust synthesis conditions, large surface area per mass of adsorbent, pore size tuning according to preparation and hydrothermal stability.

In this work we have coupled the use of SBA-15 as a large surface area matrix to deposit silver for π-bond formation between propylene and the transition metal ion and explore the selectivity towards propylene for propane-propylene separation purposes. The effects of silver loading were assessed employing two different metal loadings. The silver containing adsorbents were prepared by incipient wetness. All the materials reported in this section were synthesized by Elena Basaldela and Norberto Firpo at CINDECA (LaPlata, Argentina) and were characterized and studied for propane / propylene separation at the LSRE. Adsorption equilibrium and kinetics of propane and propylene in the three adsorbents (pure SBA-15 and two samples with different amounts of silver deposition) was studied at three different temperatures: 323, 343 and 373 K.

5.3.1 SBA-15 synthesis and characterization

SBA-15 was prepared using tetraethyl orthosilicate TEOS (Aldrich) and poly(ethylene glycol) - block-poly(propylene glycol) - block-poly(ethylene glycol), H(-

$OCH_2CH_2)_x[-OCHCH_3CH_2-]_y(-OCH_2CH_2-)_zOH$ (average M_w = 5800, Aldrich) as the organic structure–directing agent. A gel having the appropriate composition (Zhao et al., 1998) was stirred overnight at 308 K and submitted to hydrothermal conditions at 353 K for 16 h. The resulting solid phase was filtered and washed, then dried at 383 K and finally heated at 763 K in air for a period of 6 h.

The silver adsorbents were prepared by incipient wetness impregnation on SBA-15 support with an aqueous solution of $AgNO_3$ (Aldrich Co., 99.9%) using distilled deionized water followed by drying and calcination at 473 K in nitrogen flow for 12 h. In this way, two $AgNO_3$ / SBA-15 samples with different silver/substrate ratios were prepared: Ag/SBA-15 = 0.5 and Ag/SBA-15 = 1.0.

Samples were characterized by X-ray diffraction (XRD), scanning electron microscopy (SEM) and transmission electron microscopy (TEM). Semi quantitative chemical analysis was carried out by X ray dispersion (EDAX). XRD patterns were recorded with a Philips APD 1700 diffractometer, using CuKα radiation, at 40 Kv, 30mA, 0.02 step size and 1s step time. Size and morphology of solid particles were observed by SEM using a Philips 505 microscope. Transmission Electron Microscopy (TEM) images were recorded in a Carl Zeiss unit. Textural properties were determined by nitrogen isotherms at 77 K measured with a Micromeritics Accusorb 2100E.

The chemical composition analysis carried out with the EDAX electronic microprobe indicated that the impregnated samples Ag/SBA-15 = 1.0 and Ag/SBA-15 = 0.5 contained a Ag/Si ratio of about 1.09 (w/w) and 0.54 (w/w), respectively. Initially, nitrogen adsorption experiments were measured on the different samples to determine the area of the base material (SBA-15) and its reduction with the introduction of different amounts of silver. The area of SBA-15 is 996 m^2/g while Ag/SBA-15 = 0.5 has 594 m^2/g and Ag/SBA-15 = 1.0 has 297 m^2/g. Clearly the introduction of higher

amounts of silver produced a significant decrease in the adsorbent area. The reduction in the area can be due to a reduction of the diameter of the mesopores due to silver ions deposition or by partial (or total) blocking of them either by silver ions or even metallic silver.

The XRD patterns (range $5° < 2\theta < 60°$) of Ag/SBA-15 samples (see Figure 5.15) showed some reflections corresponding to the $AgNO_3$ used for impregnation. These reflections are very weak in the pattern of Ag/SBA-15 = 0.5. In the small angle region the peaks of ordered mesoporous material SBA-15 were identified in all the samples, although an equipment with higher resolution is required to locate them with more accuracy to determine the solid wall thickness.

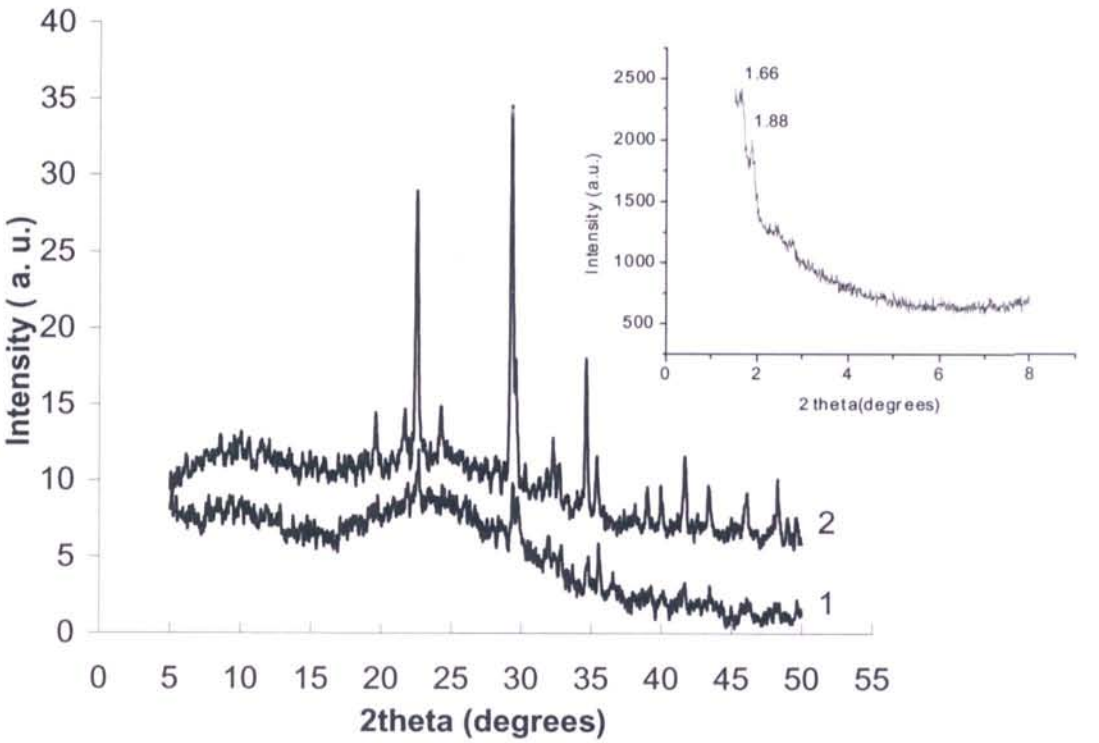

Figure 5.15. XRD pattern of the samples. (1) Ag/SBA-15 = 0.5 and (2) Ag/SBA-15 = 1.0. The small plot corresponds to the detection of ordered mesoporous material formation in the case of SBA-15 (Zhao et al., 1998).

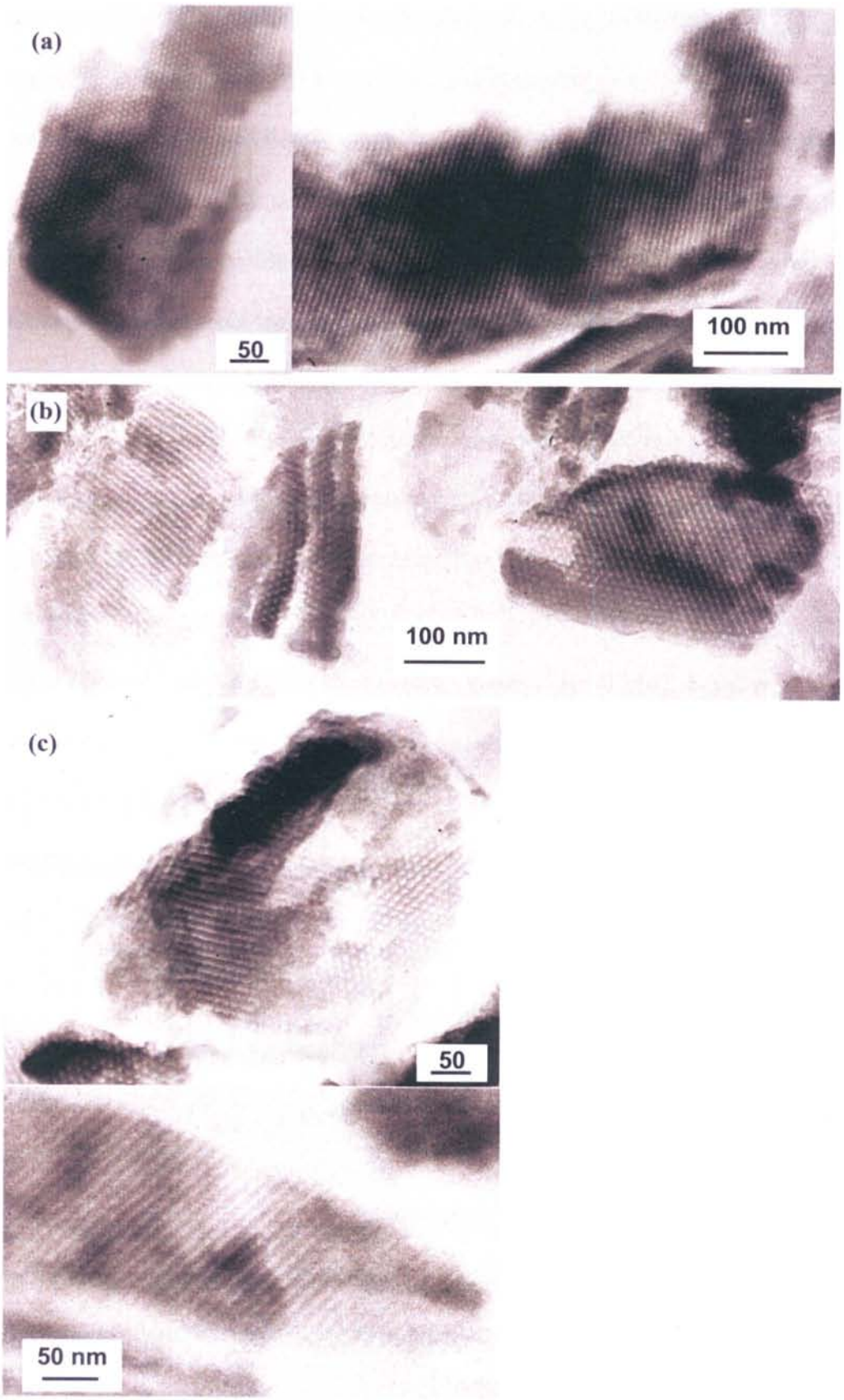

Figure 5.16. TEM images of the SBA-15 and Ag/SBA-15: (a) SBA-15; (b) Ag/SBA-15 = 0.5; (c) Ag/SBA-15 = 1.0.

Transmission Electron Microscopy (TEM) analyses were performed in all the samples. Images with the results for the three samples are shown in Figure 5.16. The typical ordered structure reported for these mesoporous materials was found (Choi and Yang, 2003; Janssen et al., 2002; Zhu et al., 2003). Two general conclusions can be taken from these pictures. The first one is that the amount of metallic silver is very small in the Ag/SBA-15 = 1.0 and was not detectable in the Ag/SBA-15 = 0.5. The other observation is that the diameter of the mesopores decreases in the modified samples, but the ordered shape of the pores remained constant when compared to the original SBA-15 sample. The pore diameters of the samples are: 8 nm (SBA-15), 6 nm (Ag/SBA-15 = 0.5) and 4 nm (Ag/SBA-15 = 1.0).

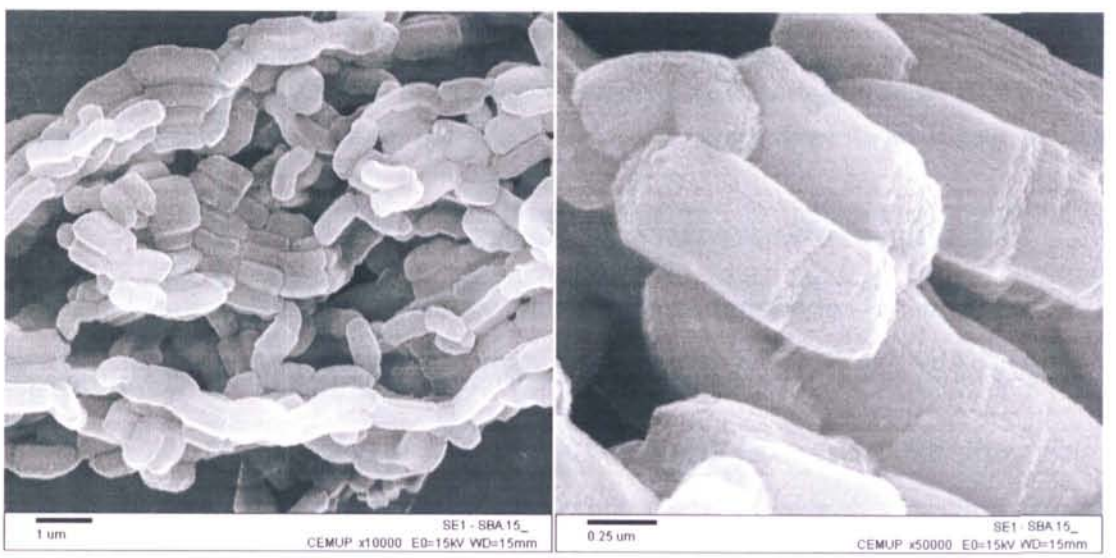

Figure 5.17. SEM images of the pure SBA-15 sample.

Finally, in Figure 5.17 the morphology of SBA-15 determined by Scanning Electron Microscopy (SEM) is shown, to be used in the kinetic model. Cylinders of 1.1 μm with 0.4 μm diameter were found. The size distribution of these cylinders is also very narrow. In Figure 5.18 SEM images of the impregnated samples are also shown. It can be seen that the crystal structure also was not altered by the impregnation, although

some traces containing higher amounts of ionic silver were found in the Ag/SiO_2 = 1.0 sample. The characterization of the materials showed a good silver dispersion with no detectable metallic silver, even after propane and propylene adsorption experiments.

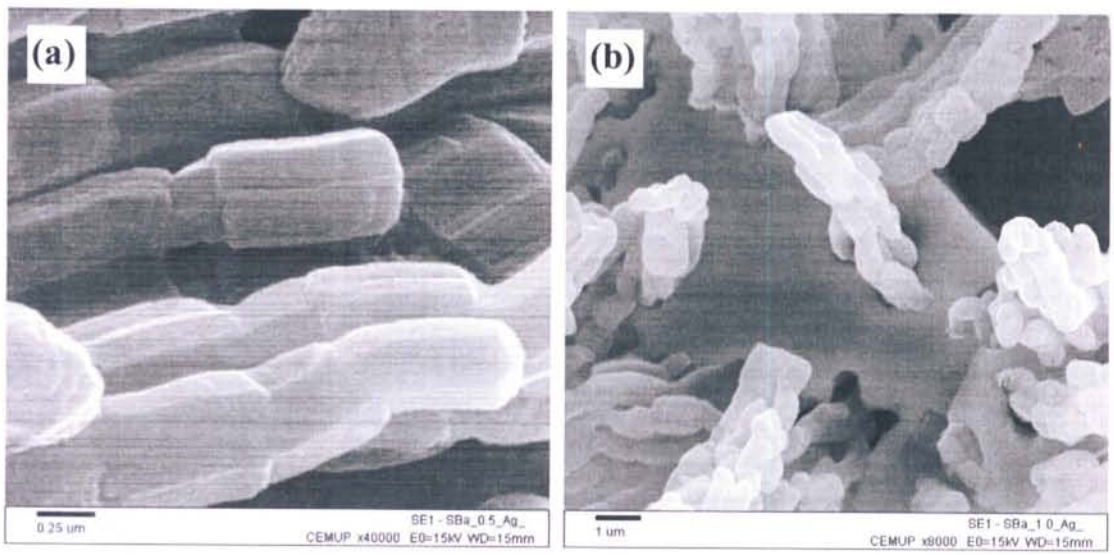

Figure 5.18. SEM images of the Ag/SBA-15 = 0.5 (a) and Ag/SBA-15 = 1.0 (b) samples.

5.3.2 Adsorption equilibrium of pure gases

In the analysis of adsorption equilibrium, we have to consider a model that takes account of physical adsorption and also the enhanced adsorption due to chemisorption. In this work, the Toth model (Toth, 1971) was used to describe physical adsorption while π-complexation was described with a Langmuir model assuming that adsorption sites have a uniform energy distribution (Yang and Kikkinides, 1995). The complete model is:

$$q = \frac{q_m K_{eq}{}^{1/n} P}{\left[1 + KP^n\right]^{1/n}} + \frac{q_{mc}}{2s} \ln\left[\frac{1 + b_c Pe^{s}}{1 + b_c Pe^{-s}}\right] \qquad [5.1]$$

where K_{eq} is the physical adsorption constant, q_m and q_{mc} are the maximum adsorbed phase concentrations of physical adsorption and chemisorption, respectively, b_c is the chemisorption constant and s is the spread of energy distribution. Although the nature of

the Toth model is empirical, it offers several advantages: it has a large flexibility to describe experimental data and a direct extension to multicomponent predictions. These two properties are very important in PSA (Pressure Swing Adsorption) modeling.

The adsorption constants have Arrhenius dependence in the form:

$$K_{eq} = K_{eq}^{\,o} \exp\left(\frac{-\Delta H}{R_g T}\right)$$
$$b_c = b_c^{\,o} \exp\left(\frac{\Psi}{R_g T}\right) \qquad [5.2]$$

where K_{eq}^{o} and b_c^{o} are the infinite adsorption constants, $(-\Delta H)$ is the enthalpy of adsorption and Ψ is the mean variance of the uniform energy distribution (Yang and Kikkinides, 1995).

This description of adsorption equilibrium involves many parameters. The parameters of the Toth equation (q_m, K_{eq}^{o}, $-\Delta H$ and n) were determined fitting the Toth model to the propane adsorption equilibrium data alone. In the case of propylene, the same parameters were used for physical adsorption while the chemisorption parameters (q_{mc}, b_c^{o}, Ψ and s) were determined from the best data fitting (Yang and Kikkinides, 1995).

Pure propane and propylene adsorption equilibrium was measured using a Rubotherm microbalance device operated in closed system. Activation of the samples was performed at 385 K overnight under vacuum ($< 10^{-5}$ kPa).

Adsorption equilibrium isotherms of propane and propylene measured at 323, 343 and 373 K on the SBA-15 sample are shown in Figure 5.19. The amount adsorbed of both hydrocarbons is very similar indicating that the adsorbent has a very small selectivity. Adsorption and desorption points were coincident indicating that the isotherms are completely reversible. The propylene data are in very good agreement with other published data, although propane was slightly more adsorbed in this sample

(Newalkar et al., 2002; Newalkar et al., 2003). Propane isotherms are in good agreement with the ones measured in silica gel with large surface area and narrow pores (NSG) as reported in Chapter 2.

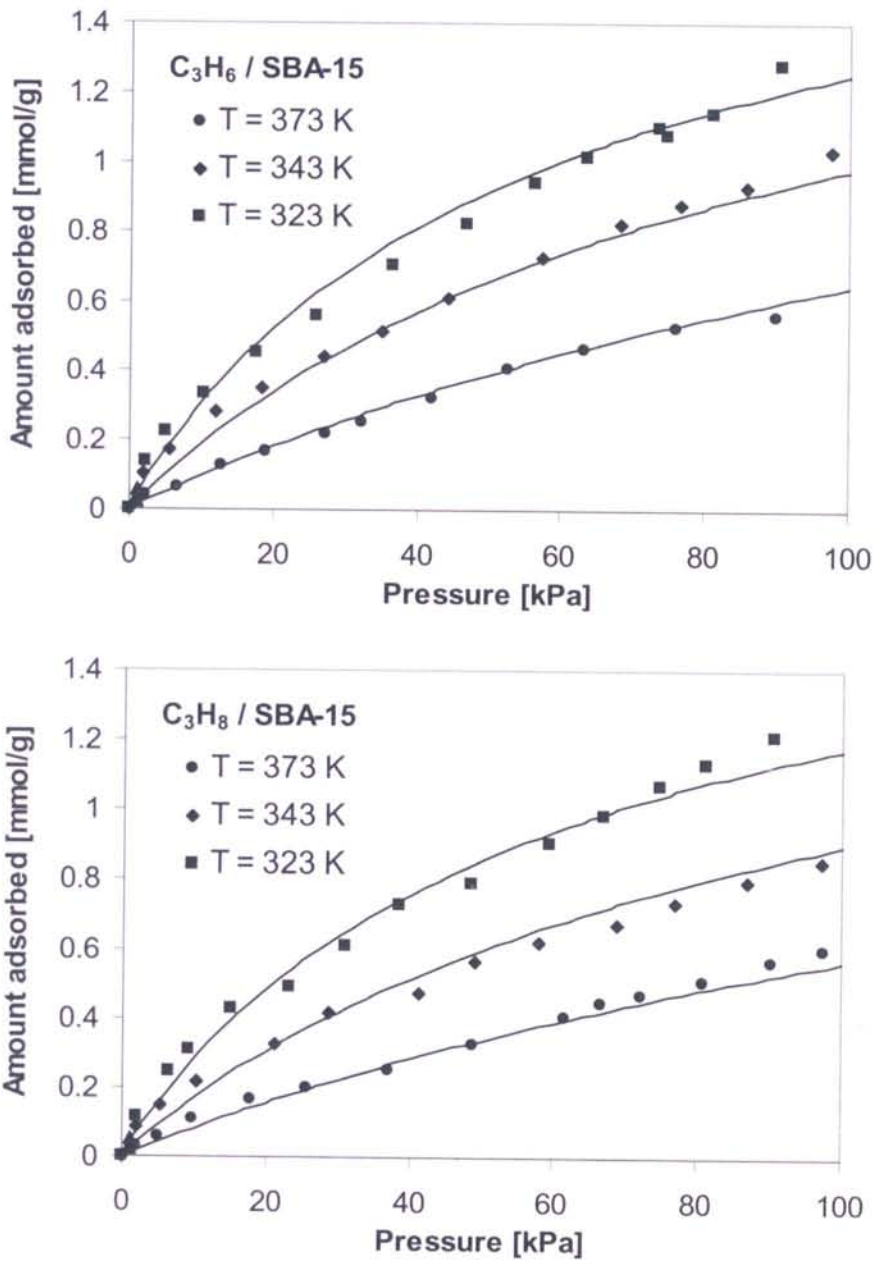

Figure 5.19. Adsorption equilibrium of propane and propylene on SBA-15 at 323, 343 and 373 K. Solid lines are the Toth model fitting.

The adsorption isotherms of propane and propylene measured at 323, 343 and 373 K in SBA-15 with Ag/SBA-15 = 0.5 are shown in Figure 5.20. The amount of

propylene adsorbed is much larger than the adsorbed in the pure sample, particularly at lower pressures. On the other side, the amount of propane adsorbed has decreased significantly and now the ratio of propylene and propane adsorbed concentration is around 15 at 100 kPa.

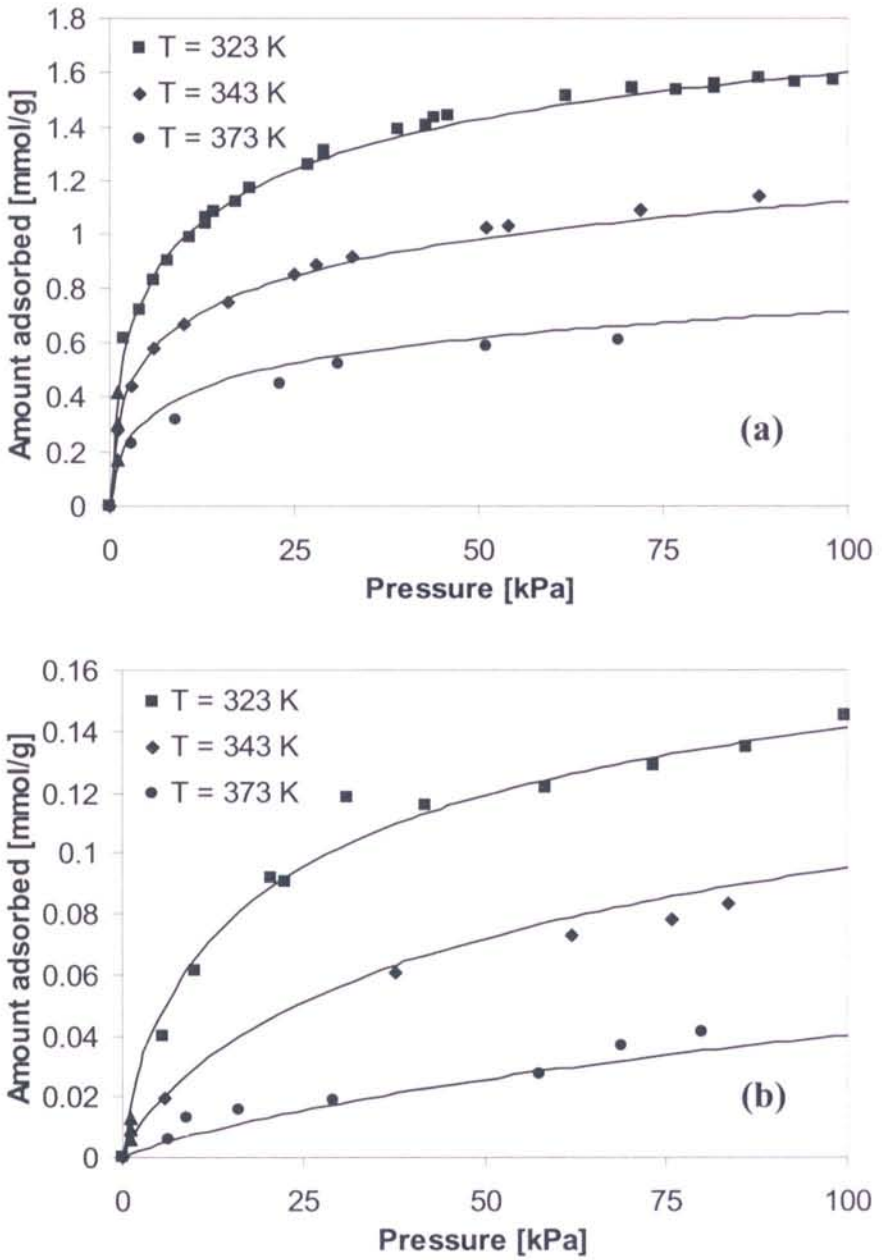

Figure 5.20. Adsorption equilibrium of propylene (a) and propane (b) on Ag/SBA-15=0.5 at 323, 343 and 373 K. Solid lines correspond to fitting of model described above.

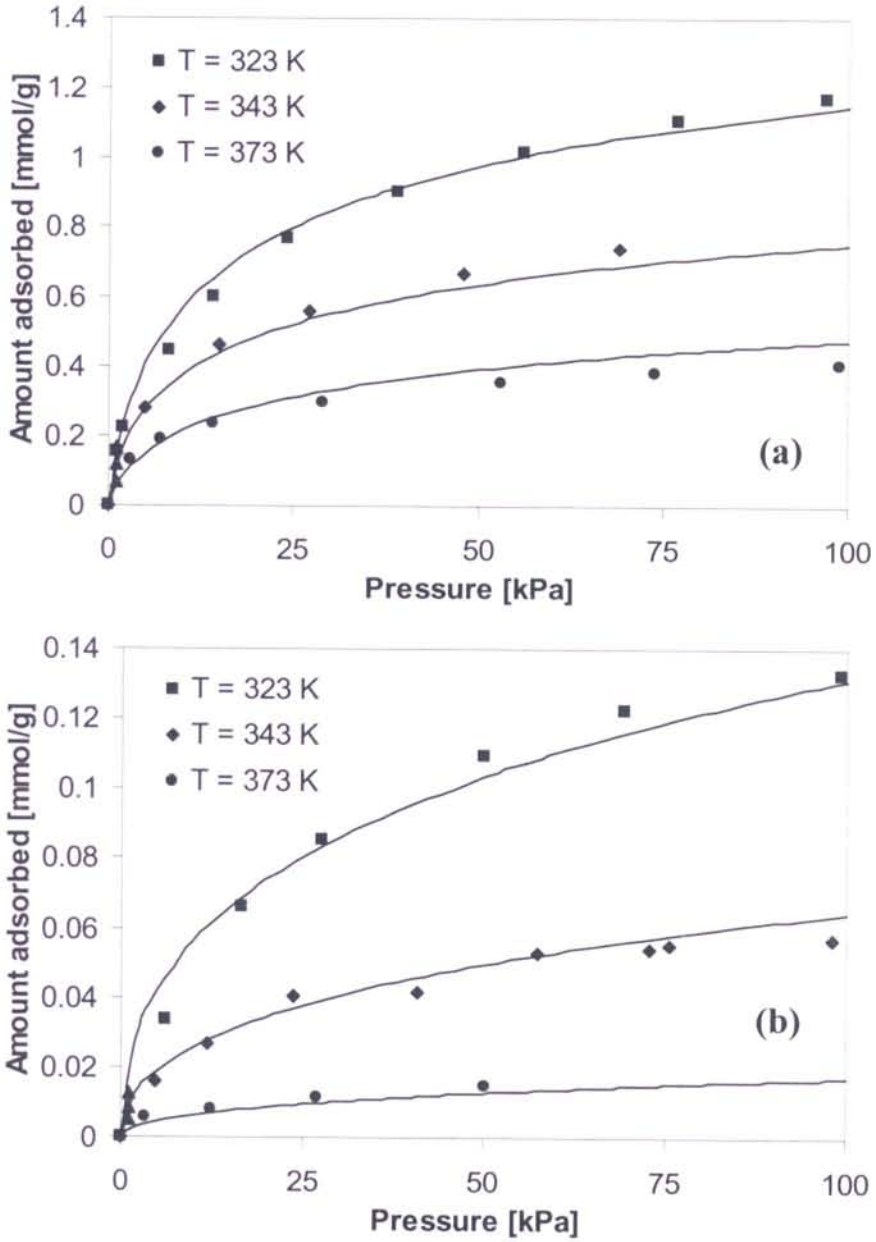

Figure 5.21. Adsorption equilibrium of propylene (a) and propane (b) on Ag/SBA-15=1.0 at 323, 343 and 373 K. Solid lines correspond to fitting of model described above.

The corresponding isotherms measured in the sample Ag/SBA-15 = 1.0 are shown in Figure 5.21. In this case, the concentration of propane adsorbed is quite similar with the other modified SBA (Ag/SBA-15 = 0.5), but the concentration of propylene adsorbed has decreased. Even though, in this sample the ratio of propylene to propane adsorbed concentration is still high.

We have seen that the dispersion of silver ions (Ag/SBA-15 = 0.5 and 1) reduces the area available in factors of 2 and 4, approximately. In the case of the Ag/SBA-15 = 0.5 sample, the area reduction is counterbalanced by an increase of the amount of propylene adsorbed. On the other way, the amount of propane adsorbed decreases around ten times. When the proportion of silver ions is increased (Ag/SBA-15 = 1.0) the amount of propane remains essentially constant although the propylene adsorbed amount is slightly lower. This indicates that for propane there may be a limiting amount adsorbed (the one observed in these two samples) while for propylene there is an optimum amount of silver loading and this optimum is near 0.54 and below 1.09.

Solid lines in Figures 5.19 represent the fitting of the data using the Toth model. In this case of pure SBA, independent parameters were obtained for propane and propylene. They are reported in Table 5.3. The parameters of both gases are very similar; for that reason propane parameters will be assumed valid for physical adsorption of both gases. We can see that the heat of adsorption of both gases is around 24 kJ/mol indicating that the SBA-15 has the same kind of interactions with both gases. This value is larger than 14.8 kJ/mol previously reported for this material (Newalkar et al., 2002), but are in good agreement with values obtained for silica gel and reported in Chapter 2.

The fitting of Ag/SBA-15 = 0.5 and Ag/SBA-15 = 1.0 was performed in the same way: physical adsorption parameters were estimated by fitting propane data and used in the propylene data to fit only the chemisorption parameters (see equations [1-2]). The parameters obtained with this routine are also reported in Table 5.3. We should note that the in the case of physical adsorption, the heat of adsorption has increased a little when compared with the pure matrix but remained almost constant for both salt-dispersed materials. Also, the degree of heterogeneity (given by the decrease in

BIBLIOTECA F.E. PORTO

parameter n) increased when increasing the silver content. In the case of chemisorption, the mean variance of the energy distribution is almost the same in both samples with a value around 76 kJ/mol.

Table 5.3 – Adsorption equilibrium parameters (Toth model) for propane and propylene adsorption on SBA-15 and Ag-modified SBA-15 samples.

Sorbent	Gas	q_m [mmol/g]	K_{eq}^{o} [1/kPa]^n	$(-\Delta H)$ [kJ/mol]	n [-]	q_{mc} [mmol/g]	b_c^{o} [1/kPa]	Ψ [kJ/mol]	s [-]
SBA-15	C_3H_6	2.041	$3.55.10^{-6}$	24.240	0.87	-	-	-	-
	C_3H_8	2.062	$3.55.10^{-6}$	23.885	0.91	-	-	-	-
Ag/SBA-15 = 0.5	C_3H_6	0.221	$1.04.10^{-6}$	34.028	0.53	-	-	-	-
	C_3H_8	0.221	$1.04.10^{-6}$	34.028	0.53	1.870	$2.0x10^{-14}$	-78.352	3.58; 5.52; 6.91
Ag/SBA-15 = 1.0	C_3H_6	0.189	$1.04.10^{-6}$	36.866	0.36	-	-	-	-
	C_3H_8	0.189	$1.04.10^{-6}$	36.866	0.36	1.475	$2.0x10^{-14}$	-75.893	2.66; 4.84; 6.45

Clearly from the results shown in Figures 5.19-5.21, the best adsorbent for propane-propylene separation is Ag/SBA-15 = 0.5. To see the ideal equilibrium selectivity of the adsorbents, the ratio q_{C3H6}/q_{C3H8} at 343 K is plotted in Figure 5.22. Note that in the case of a PSA operating between 10-100 kPa, the selectivity of Ag/SBA-15 = 0.5 is between 22 and 13.

Results for these adsorbents have to be compared with previously published data to see whether the performance of the adsorbent compensate its high cost or not. Other silver-based π-complexation adsorbents were used for that purpose (Padin et al., 2000; Choudary et al., 2002). A silver modified clay (Choudary et al., 2002) has a much lower adsorption capacity than both modified samples reported here due to a smaller

superficial area available for adsorption (165 m^2/g). Even though, propane adsorption is higher than in our samples indicating a low selectivity of such adsorbent with respect to the ones reported in this work. When comparing with silica substrate, propylene adsorption capacity of Ag/SBA-15 = 0.5 at 343 K is very similar to the previously reported (Padin et al., 2000), although again, the amount of propane adsorbed in our adsorbents is 3 times smaller. It is interesting to notice that in the preparation of silver-modified SiO_2, MCM-41 (Padin et al., 2000) and SBA-15 (for Ag/SBA-15 = 0.5), the area reduction with respect to the original material is 38-40%.

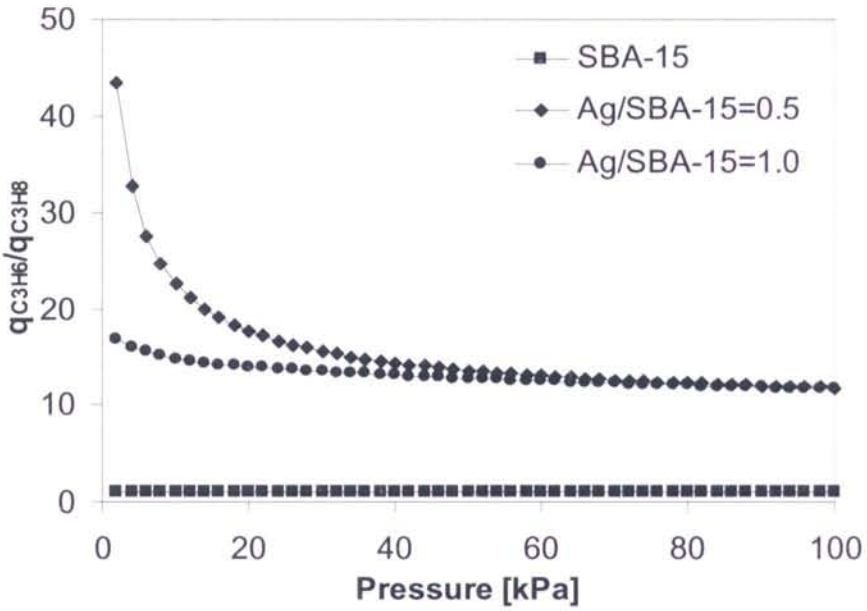

Figure 5.22. Propylene / propane ratio of amount adsorbed at 343 K.

5.3.3 Adsorption kinetics of pure gases

The kinetics of adsorption of propane and propylene in the three samples analyzed above was determined by diluted breakthrough curves in the same temperature range (323, 343 and 373 K). Mixtures of helium/C_3 were prepared in a bottle and both mixtures have a concentration of 1.1% of hydrocarbon. The column has 3.13 cm length with 0.69 cm internal diameter. Flowrates and mass of adsorbent used for each

experiment are shown in Table 5.4. The analysis of the curves was done with the model described in Chapter 4.

Table 5.4 – Experimental conditions (mass of adsorbent and flowrate) for breakthrough curves, stoichiometric time and adsorbed phase concentration of propane and propylene in SBA-15 and Ag/SBA-15.

Adsorbent	Gas	Temp [K]	Flow* [cm³/s]	$\bar{t}$ [s]	q [mmol/g]
SBA-15 Pure sample m_{ads} = 0.134 g	C_3H_6	323	0.85	24.3	0.059
		343	0.91	14.4	0.037
		373	0.85	9.1	0.021
	C_3H_8	323	0.99	17.2	0.049
		343	0.88	12.8	0.034
		373	0.69	9.3	0.020
SBA-15 Ag/SBA-15 = 0.5 m_{ads} = 0.311 g	C_3H_6	323	0.39	822.6	0.420
		343	0.39	591.6	0.302
		373	0.37	351.1	0.167
	C_3H_8	323	0.43	21.9	0.013
		343	0.44	15.9	0.009
		373	0.43	12.8	0.006
SBA-15 Ag/SiO_2 = 1.0 m_{ads} = 0.422 g	C_3H_6	323	0.88	198.1	0.166
		343	0.88	141.3	0.118
		373	0.85	85.8	0.069
	C_3H_8	323	0.64	21.6	0.013
		343	0.56	16.4	0.008
		373	0.51	12.3	0.005

*Flowrate measured at 298 K.

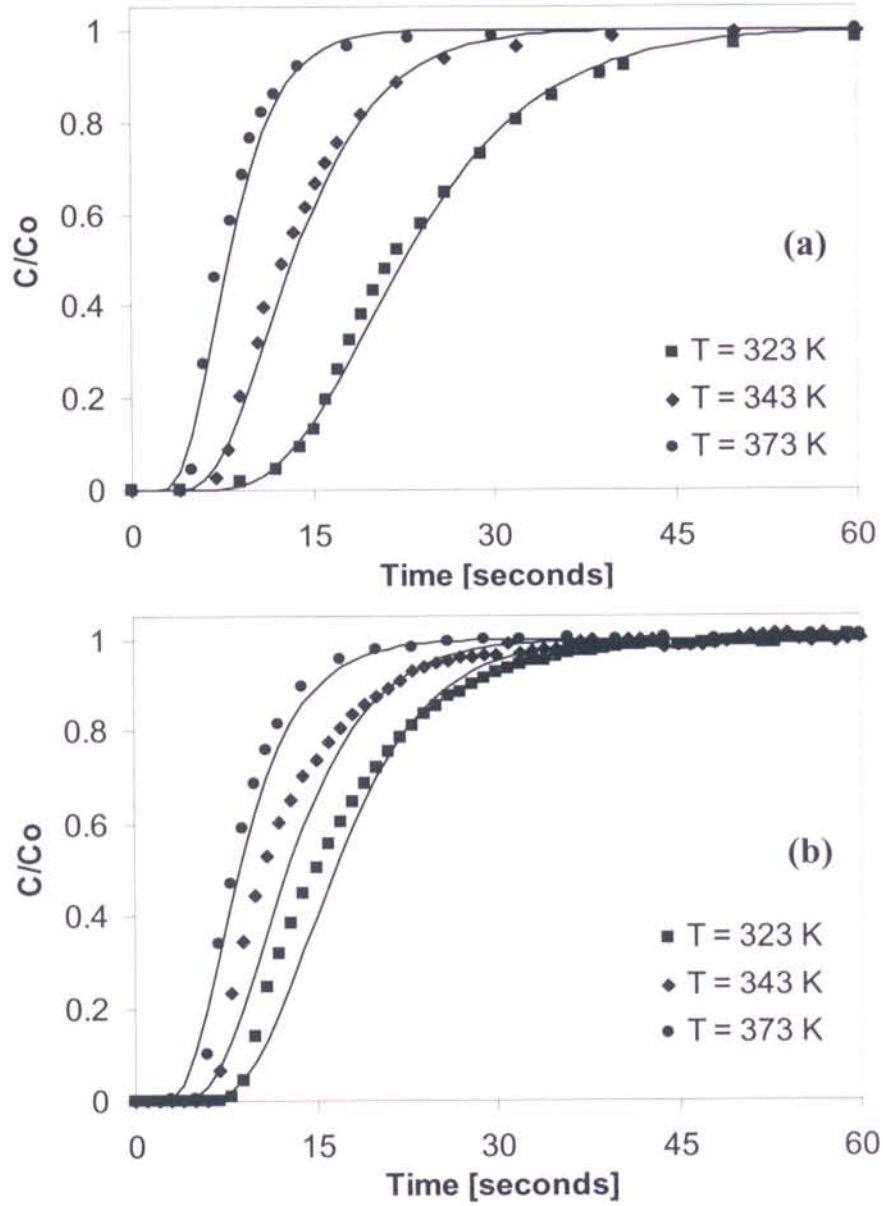

Figure 5.23. Adsorption breakthrough curves of propylene (a) and propane (b) in SBA-15 at 323, 343 and 373 K.

Results obtained for the base material (SBA-15) for propylene and propane are shown in Figure 5.23. As can be noticed, the diffusion of both gases is very fast. Similar curves for Ag/SBA-15 = 0.5 and Ag/SBA-15 = 1.0 are reported in Figures 5.24 and 5.25, respectively. All the curves shown here were measured under isothermal conditions. The adsorbed phase concentration determined from breakthrough curves was in all the cases consistent with the gravimetric data (although hard to see because

concentration is 1.1 kPa). The amount adsorbed determined by breakthrough experiments together with the stoichiometric times are reported in Table 5.4.

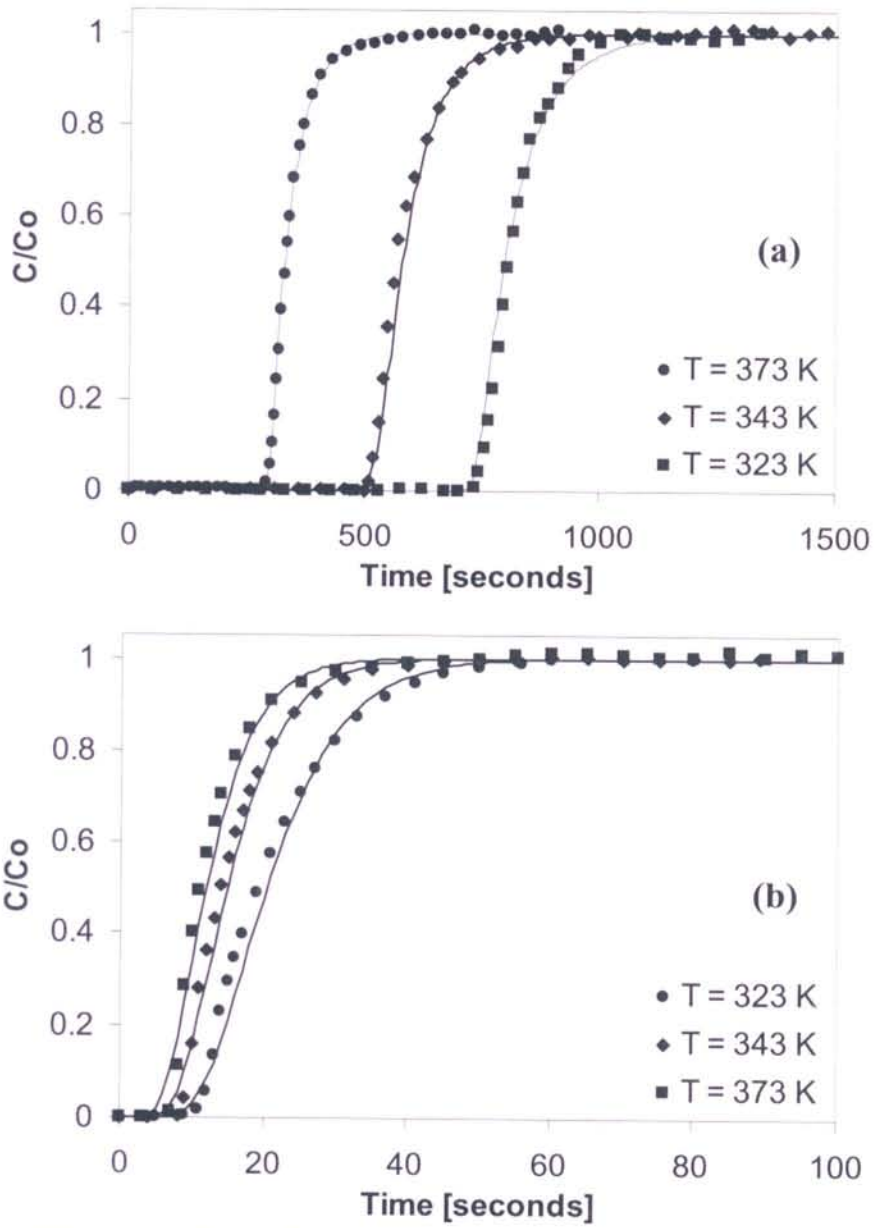

Figure 5.24. Adsorption breakthrough curves of propylene (a) and propane (b) in Ag/SBA-15=0.5 at 323, 343 and 373 K.

Diffusivities obtained from fitting the model of diluted breakthrough curves described in Chapter 4 (solid lines in Figures 5.23-5.25) are reported in Table 5.5. For the calculation of the pore diffusivity, the Bosanquet equation has been used. In this case, as verified by TEM, the channels are straight which means that the tortuosity

factor (τ_p) is 1. In Table 5.5 we are also reporting the axial dispersion (D_{ax}) calculated with (Ruthven, 1984)

$$D_{ax} = (0.45 + 0.55\varepsilon_c)D_m + \gamma_2 2R_p u_i \qquad [5.3]$$

where ε_c is the porosity of the column, R_p is the particle radius, $\gamma_2 = 0.5$ and u_i is the interstitial gas velocity. Although the differences are small (only due to molecular diffusion), the same axial dispersion values were used for propane and propylene.

Table 5.5 – Adsorption kinetic parameters determined from breakthrough curves.

Adsorbent	Gas	T [K]	D_m [cm²/s]	D_K [cm²/s]	D_p [cm²/s]	D_{ax} [cm²/s]
SBA-15 Pure sample	C_3H_6	323	0.563	0.0107	0.0106	0.75
		343	0.624	0.0111	0.0109	0.95
		373	0.718	0.0116	0.0114	1.05
	C_3H_8	323	0.480	0.0105	0.0103	0.75
		343	0.532	0.0108	0.0106	0.95
		373	0.612	0.0113	0.0111	1.05
SBA-15 Ag/SBA-15 = 0.5	C_3H_6	323	0.563	0.0081	0.0080	0.55
		343	0.624	0.0083	0.0082	0.60
		373	0.718	0.0087	0.0086	0.65
	C_3H_8	323	0.480	0.0079	0.0078	0.55
		343	0.532	0.0081	0.0080	0.60
		373	0.612	0.0085	0.0084	0.65
SBA-15 Ag:SiO_2 = 1.0	C_3H_6	323	0.563	0.0054	0.0053	0.75
		343	0.624	0.0055	0.0055	0.95
		373	0.718	0.0058	0.0058	1.05
	C_3H_8	323	0.480	0.0053	0.0053	0.75
		343	0.532	0.0054	0.0054	0.95
		373	0.612	0.0056	0.0056	1.05

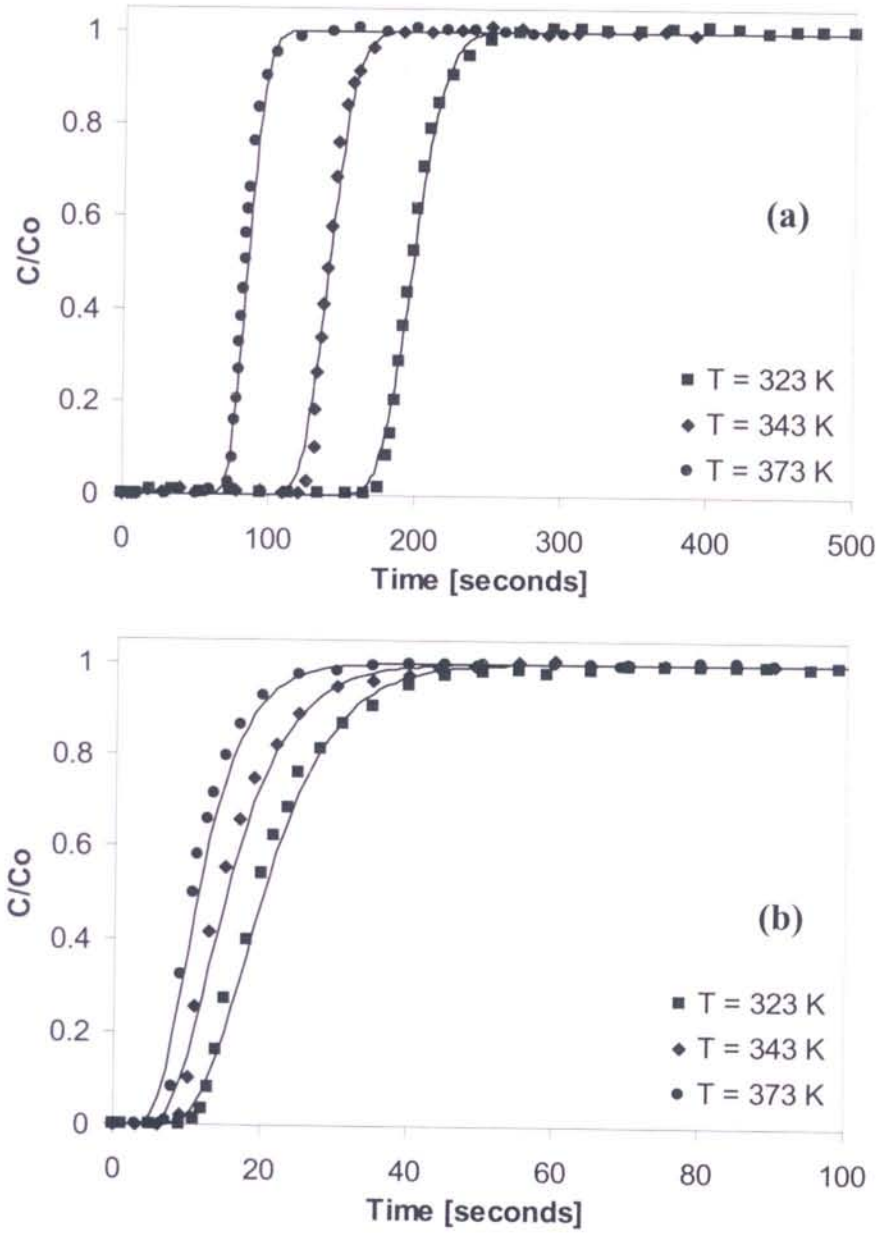

Figure 5.25. Adsorption breakthrough curves of propylene (a) and propane (b) in Ag/SBA-15=1.0 at 323, 343 and 373 K.

In all cases, the control of the breakthrough curves was shared by pore diffusion and axial dispersion. For these curves, film mass transfer resistance was neglected because the particles have a very small diameter and this resistance will not influence the simulation results. In the fitting of these curves, no adjustable parameter was employed and the predicted curves are in very good agreement with the experimental

ones. Although a very precise value of the pore diffusivity of the hydrocarbons cannot be extracted from these curves, the interesting fact is that the pore diffusivity of both gases, propylene and propane, have high values. In the case of propylene, also a self-sharpening of the concentration wave was observed due to the strongly non-linearity of the adsorption isotherms, even at this very low partial pressure of propylene.

5.4 Conclusions

In this chapter we have measured adsorption equilibrium and kinetics of pure propane and propylene in seven samples; four samples of zeolite 4A with different crystal size and pure SBA-15 and two samples of silver-loaded SBA-15. Also, adsorption tests on natural zeolites were performed, unfortunately with poor results for propane / propylene separation by PSA.

The study of adsorption of pure gases using different sized zeolite 4A crystals, showed that pure gas adsorption equilibrium and kinetic parameters (reported in previous chapters) can be applied to simulations of a PSA process with zeolite 4A whatever the size of the crystals. Indirectly we have determined that the adsorption equilibrium and kinetic properties of the commercial sample was not deteriorated in the pelletization process.

Using SBA-15 as starting material, a very poor selectivity for propane-propylene separation was obtained. Both silver-modified materials reported here have very good selectivity towards propylene. The material having a ratio Ag/SBA-15 = 0.5 presented the best selectivity: $q_{C3H6}/ q_{C3H8} \approx 13$ at 100 kPa. When the amount of silver is doubled, the decrease in surface area is detrimental to the adsorption of propylene, while the adsorption of propane remains constant, giving a lower selectivity factor towards propylene.

Nomenclature

b_c	chemisorption constant, kPa^{-1}
b_c	infinite chemisorption constant, kPa^{-1}
D_{ax}	axial dispersion coefficient, m^2/s
D_c	crystal diffusivity, m^2/s
D_m	molecular diffusivity, m^2/s
K_{eq}	equilibrium constant, $kPa^{-1/n}$
K_{eq}^{o}	equilibrium constant at the limit $T \rightarrow \infty$, $kPa^{-1/n}$
n	Heterogeneity parameter for physical adsorption (Toth model)
P	pressure, kPa
q	adsorbed phase concentration, mol/kg
q_m	maximum adsorbed phase concentration by physical interactions, mol/kg
q_{mc}	maximum adsorbed phase concentration by chemical interactions, mol/kg
R_g	ideal gas constant, 8.314 kJ/mol.K
R_p	particle radius, m
s	spread of energy distribution in chemisorption model
T	temperature, K
u_i	interstitial velocity, m/s

Greek Letters

$(-\Delta H)$	heat of physical adsorption, kJ/mol
Ψ	heat of chemical adsorption, kJ/mol

References

Ackley, M. W.; Yang, R. T. Diffusion in ion-Exchanged Clinoptilolites. *AIChE J.*, **1991**, 37(11), 1645-1656.

Breck, W. D. *Zeolite Molecular Sieves*. Wiley, New York, **1974**.

Cheng, L. S.; Yang, R. T. Monolayer Cuprous Chloride Dispersed on Pillared Clays fo Olefin – Paraffin Separations by π-Comlexation. *Adsorption*, **1995**, 1, 61-75.

Chiappetta, R.; Bodoardo, S.; Geobaldo, F.; Fajula, F.; Garrone, E. Propane Adsorption and Reaction on Zeolites and Pillared Clays. *Res. Chem. Interm.*, **1999**, 25, 111-129.

Cho, S. H.; Han, S. S.; Kim, J. N.; Choudary, N. V.; Kumar, P.; Bhat, S. G. T. *Adsorbents, Method for the Preparation and Method for the Separation of Unsaturated Hydrocarbons for Gas Mixtures*. U.S. Patent, 6,315,816, **2001**.

Choudary, N. V.; Kumar, P.; Bhat, S. G. T.; Cho, S. H.; Han, S. S.; Kim, J. N. Adsorption of Light Hydrocarbon Gases on Alkene – Selective Adsorbent. *Ind. Eng. Chem. Res.*, **2002**, 41, 2728-2734.

Da Silva, F. A. *Cyclic Adsorption Processes: Application to Propane / Propylene Separation*. Ph.D. Dissertation, University of Porto, Portugal, **1999**.

Da Silva, F. A.; Rodrigues A. E. Adsorption equilibria and kinetics for propylene and propane over 13X and 4A zeolite pellets. *Ind. Eng. Chem. Res.*, **1999**, 38, 2434-2438.

Grande, C. A.; Gigola, C.; Rodrigues, A. E. Propane-Propylene Binary Adsorption on Zeolite 4A, *Adsorption*, **2003**, 9, 321-329.

Grande, C. A.; Araujo, J. D. P.; Cavenati, S.; Firpo, N.; Basaldella, E.; Rodrigues, A. E. New PI-Complexation Adsorbents for Propane/Propylene Separation, *Langmuir*, **2004,** 20, 5291-5297.

Grande, C. A.; Basaldella, E. I.; Rodrigues, A. E. Crystal Size Effect in Vacuum Pressure Swing Adsorption for Propane / Propylene Adsorption, *Ind. Eng. Chem. Res.*, **2004**, 43, 7557-7565.

Han, Y.-J.; Stucky, G. D.; Butler, A. Mesoporous Silicate Sequestration and Release of Proteins*J. Am. Chem. Soc.*, **1999**, 121, 9897-9898.

Humphrey, J. L.; Keller, G. E. II. *Separation Process Technology*, McGraw-Hill, New York, **1997**.

Järvelin, H.; Fair, J. R. Adsorptive Separation of Propane – Propylene Mixtures. *Ind. Eng. Chem. Res.*, **1993**, 32, 2201-2207.

Jayaraman, A.; Hernandez-Maldonado, A. J.; Yang, R. T.; Chinn, D.; Munson, C. L.; Mohr, D. H. Clinoptilolites for Nitrogen / Methane Separation. *Chem. Eng. Sci.*, **2004**, 59(12), 2407-2417.

Jose, B.; Ryu, J. H.; Lee, B. G.; Lee, H.; Kang, Y. S.; Kim, H. S. Effect of Pthalates on the Stability and Performance of AgBF4-PVP Membranes for Olefin/Paraffin Separation, *Chem. Commun.*, **2001**, 15, 2046-2047.

Jun, S.; Joo, S. H.; Ryoo, R.; Kruk, M.; Jaroniec, M.; Liu, Z.; Ohsuna, T.; Terasaki, O. Synthesis of New Nanoporous Carbon with Hexagonally Ordered Mesostructure. *J. Am. Chem. Soc.*, **2000**, 122, 10712-10713.

Khodakov, A. Y.; Rees, L. V. C. Effect of Propane on the Kinetics of Carbon Dioxide Adsorption in NaA Zeolites, *Gas Sep. Purif.*, **1995**, 9, 253-257.

Kim, H. S.; Ryu, J. H.; Kim, H.; Ahn, B. S.; Kang, Y. S. Reversible Olefin Complexation by Silver Ions in Dry Poly(Vinyl Methyl Ketone) Membrane and Its Application to Olefin / Paraffin Separations. *Chem. Commun.*, **2000**, 14, 1261-1262.

Kim, Y. H.; Ryu, J. H.; Bae, J. Y.; Kang, Y. S.; Kim, H. S. Reactive Polymer Membranes Containing Cuprous Complexes in Olefin / Paraffin Separation. *Chem. Commun.*, **2000**, 14, 195-196.

Kondis E. F.; Dranoff J. S. *Kinetics of Ethane Sorption on 4A Molecular Sieve Crystal Powder and Pellets*. In Molecular Sieve Zeolites II Adv. Chem. Ser. 102, Gould RF (ed.), Washington, **1971**; 171-183.

Kubota, K.; Nakajima, K.; Ono, Y.; Hayashi, S. Adsorption Characteristics of Propylene on Molecular Sieve 4A, *Sep. Sci. and Techn.*, **1989**, 24, 709-719.

Newalkar, B. L.; Choudary, N. V.; Kumar, P.; Komarneni, S.; Bhat, T. S. G. Exploring the Potential of Mesoporous Silica, SBA-15, as an Adsorbent for Light Hydrocarbon Separation. *Chem. Mater.*, **2002**, 14, 304-309.

Newalkar, B. L.; Choudary, N. V.; Turaga, U. T.; Vijayalakshmi, R. P.; Kumar, P.; Komarneni, S.; Bhat, T. S. G. Potential Adsorbent for Light Hydrocarbon Separation: Role of SBA-15 Framework Porosity. *Chem. Mater.*, **2003**, 15, 1474-1479.

Padin,J.; Rege, S. U.; Yang, R. T.; Cheng, L. S. Molecular-Sieve Sorbents for Kinetic Separation of Propane/Propylene. *Chem. Eng. Sci.*, **2000**, 55, 4525-4535.

Patiño-Iglesias, M. E.; Aguilar-Armenta, G.; Jimenez-Lopez, A.; Rodrigues-Castellón, E. Kinetics of the Total and Reversible Adsorption of Propylene and Propane on Zeolite 4A (CECA) at Different Temperatures. *Col. Surf. Sci. A.*, **2004**, 237(1-3), 73-77.

Rege, S. U.; Padin, J.; Yang, R. T. Olefin/Paraffin Separations by Adsorption - Pi-Complexation vs. Kinetic Separation. *AIChE J.*, **1998**, 44, 799-809.

Ruthven, D. M.; Derrah, R. I. Sorption in Davison 5A Molecular Sieves. *Can. J. Chem. Eng.*, **1972**, 50, 743-747.

Teramoto, M.; Takeuchi, N.; Maki, T.; Matsuyama, H. Ethylene / Ethane Separation by Facilitated Transport Membrane Accompanied by Permeation of Aqueous Silver Nitrate Solution. *Sep. & Purif. Technol.*, **2002**, 28, 117-124.

Toth, J. State equations of the solid – gas interface layers. *Acta Chim. Acad. Sci. Hung.*, **1971**, 69, 311-328.

Ullmann's Encyclopedia of Industrial Chemistry; 7ª Edition, Wiley-VCH, Verlag GmbH & Co..KGaA, **2003**.

Xiao, J.; Wei, J. Diffusion Mechanism of Hydrocarbons in Zoelites-I. Theory. *Chem. Eng. Sci.*, **1992**, 47, 1123-1141.

Yang R. T. *Adsorbents. Fundamentals and Applications,* New Jersey: J. Wiley, **2003**.

Yang, R. T., Kikkinides, E. S. New Sorbents for olefin / paraffin separations by Adsorption via π-Complexation. *AIChE J.*, **1995**, 41, 509-517.

Zhao, D.; Feng, J.; Huo, Q.; Melosh, N.; Fredrickson, G. H.; Chmelka, B. F.; Stucky, G. D. Triblock Copolymer Syntheses of Mesoporous Silica with Periodic 50 to 300 Angstrom Pores. *Science*, **1998**, 279, 548-552.

Zhang, Y.; Furukawa, S-I; Nitta, T. Molecular Simulation Studies on Adsorption of Propane / Propylene in NaA Zeolite by Using a Monte Carlo Technique. *J. Chem. Eng. Japan*, **2003**, 36(9), 1085-1094.

6. Adsorption of Propane and Propylene in Zeolite 4A Honeycomb Monolith

One of the developments in separation technologies by adsorption is the use of new shaped materials offering some attractive properties relative to fixed bed behavior. Monolithic adsorbents offer the possibility of operating with small pressure drop, minimize the attrition and in some cases produce better separation results than in fixed bed packed with particles.

It is the purpose of this chapter to measure adsorption equilibrium and kinetics of pure propane and propylene in a square honeycomb monolith where zeolite 4A crystals were inserted in the structure by extrusion.

6.1 Introduction

The word Monolith has Greek origins: "mono lithos", which means single stone. For engineering applications, monolithic materials are solids that are composed by a bundle of channels that can have straight shape or not. When the monolith has straight parallel channels, the final shape of the material resembles a honeycomb structure reason why they are normally termed "honeycomb monoliths".

Monolithic materials had its first application as three–way catalytic converters in NO_x reduction in the automotive industry (Gulati, 1998). Several advantages make them preferable to fixed bed of pellets. In a car, the attrition of the catalyst can be very severe, particularly for low-density pellets, which are lighter for transport. The monolithic adsorbents have good attrition properties (compact shape) and also very important is that the pressure drop of the gas is much lower than in a fixed bed allowing a good

combustion process in the motor. An additional benefit of the monolith is that the "light-off" temperature is achieved faster (Gulati, 1998).

Even when most of the studies published in literature dealing with monoliths are related to NO_x elimination, many other applications were found (Irandoust and Anderson, 1988), including catalytic combustion (Lopez et al., 2001; Groppi et al., 2000), affinity chromatography (Golay, 1958; Martin del Valle et al., 2003) and 3-phase processes (Heibel et al., 2003). In this work we deal only with ceramic honeycomb monoliths (Gulati, 1998), although other materials like carbon honeycombs (Gadkaree, 1998) or metal monoliths can be found in other chemical applications (Irandoust and Anderson, 1988; Boger et al., 2004).

In stationary sources, the attrition of particles when compared to vehicle applications is much smaller and as engines are not initiated randomly, the light-off temperature is not so critical. From the many advantages offered by monoliths, when compared with packed beds, the most important one is the pressure drop. Low-pressure drop is very important in some adsorption processes, like Rapid Pressure Swing Adsorption (Kopaygorodsky et al., 2004) or when the separation process produces an important pressure drop and the product requires recompression.

For gas phase adsorption purposes, monolithic applications were only limited to a few systems. Up to September 2004, experimental data on gas phase adsorption in monolithic materials was reported for the following systems where in some cases, more than one research groups over the world is working with: n-butane on carbon coated ceramic support (Valdes-Solis et al., 2004); air separation (Li, Perera and Crittenden, 1998; Shen et al., 2002); air separation with NaX and LiX- alumina (Jain et al., 2001); ammonia on activated carbon for refrigeration (Critoph, 2002); VOC's removal with carbon (Yates et al.,2003; Yu et al., 2002); NOx removal with zeolite Na-Y (Brilhac et

al., 2002); methane storage on carbon (Lozano-Castello et al., 2002); VOC´s adsorption (Gadkaree, 1997; Lee et al., 2000; Kim et al., 2004); CO_2 and H_2S on CMS fibers composite material (Burchell et al., 1997); CO_2 and N_2 separation on activated carbon-graphite (Menard et al., 2003); water adsorption on zeolite 4A-polymer (Gorbach et al., 2004);

In this chapter, a zeolite 4A honeycomb monolith prepared by extrusion is characterized and adsorption equilibrium and kinetics of propane and propylene are measured by gravimetric and dynamic methods. Experimental equilibrium data was measured at 423 and 473 K and between 0-100 kPa. Breakthrough curves of propylene were measured at atmospheric pressure with a partial pressure of hydrocarbon of: 1.5, 5.6 and 10.0 kPa.

6.2 Experimental

Propane and propylene adsorption equilibrium was measured using a Rubotherm microbalance device operated in closed system. Activation of the samples was performed at 593 K overnight under vacuum. The gravimetric unit operation is similar to the one used for SBA-15 measurements reported in Chapter 5 and its operation is given elsewhere (Cavenati et al., 2004). In this work no buoyancy correction was performed because at low pressures (0 – 100 kPa) this correction can be neglected. The adsorption uptake for kinetic determination was automatically measured by the program controlling the Rubotherm unit (MessPro) collecting points each 20 seconds in the initial adsorption equilibrium measurement at the different temperatures. While using the initial adsorption equilibrium point, the effect of non-linearity of the isotherm in the diffusivity parameter determination can be neglected (Ruthven, 1984). ZLC experiments were also performed using a scheme like the one described in Chapter 4,

but using a new gas chromatograph (Danni, GC1000, Italy) and a six-port valve (Vici, Valco, England) located inside the GC oven to minimize as maximum as possible dead volumes.

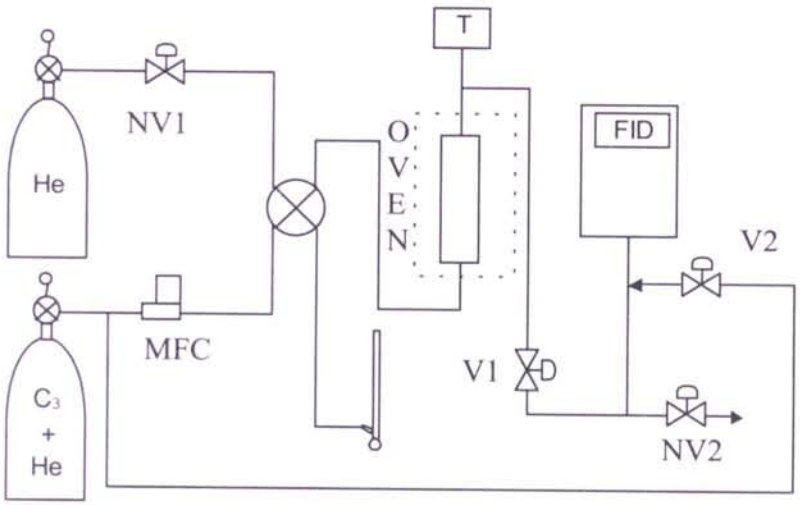

Figure 6.1. Scheme of the experimental set-up used for monolith breakthrough curves measurements.

Adsorption breakthrough curves of propylene were measured using the fixed bed equipment shown in Figure 6.1. The column was placed in an oven (Termolab, Portugal), which controls temperature within ± 1K. After the monolith (0.2 cm above the end of the honeycomb) a thermocouple is placed. The flowrate of the mixture (helium + hydrocarbon) is controlled with a mass flow controller (MFC) Hastings from 0-300 cm^3/min in standard conditions. The needle valve NV1 controls the flowrate of helium, used as inert gas in all the experiments. The valves V1 and V2 were used to switch the inlet of the GC to obtain the feed composition signal for normalization. The flowrate entering the gas chromatograph detector cannot exceed 100 ml/min. The other needle valve NV2 was opened when measuring the more concentrated breakthrough curves to avoid FID saturation.

A detailed internal view of the square column and how the monolith was inserted in it is shown in Figure 6.2a. In Figure 6.2b the interior dimensions of the column are given. As can be seen, the honeycomb monolith is square shape with a length of 20 cm and 900 channels (30x30) with a side length of 3.7 cm (424 cells per square inch, cpsi). The 900 square channels of the honeycomb are almost all the same size, except the ones near the exterior walls that are slightly smaller. At the entrance of the column, a distance of 2 cm was left. In the initial portion of this void space, some glass spheres were inserted up to a distance of near 1.0 cm where the gases can be accommodated to pass from a small bed of glass spheres to the square ducts of the monolith. After the bed of glass spheres there is an empty space of 1 cm. Empty spaces before honeycomb monoliths helps to homogenize the velocity distribution over the channels producing a flatter profile (Valdés-Solís et al., 2004).

Before inserting the monolith in the column, it was isolated with Interam 100 ® from 3M Corporation kindly offered by 3M Portugal. The insulation is to fill the interstitial space between the column diameter and the honeycomb diameter and avoid lateral flows bypassing the monolith, but also results in thermal insulation of the adsorbent. This insulating material offers unique properties that allow the operation at high temperatures adapting two materials (stainless steel of the column and ceramic material used in the monolith preparation), which have very different thermal expansion coefficients (Langer and Marlor, 1981). Actually this material is being used in automobile monoliths for NO_x reduction with the same purposes of insulation, but paying more attention to thermal insulation.

The view of the monolith is shown in Figure 6.3. The Interam material used to cover the honeycomb is also shown. Once the monolith is placed in the column this material is slightly compressed taking a final thickness of 0.15 cm. This compression is

reduced at high temperature when the metal of the column expands more than the ceramic monolith.

As explained before, the Interam insulating material was used to cover the honeycomb. In the first experimental arrangement, to avoid possible leaks, the insulation was covered with Teflon strip. Once the adsorbent was activated at 593 K, a strange and intense smell comes out from the column. This smell, similar to the smell of the "green oil" present in acetylene hydrogenation due to polymerization reactions, was accompanied with a brown liquid that resembles the "green oil". The column was opened and it was verified that the Teflon coverage disappeared and that the structure of the honeycomb (initially white) was also brown. This behavior was not expected because the melting point of Teflon is near 670 K, but it can happen that a catalytic reaction produces a hot spot and in a system without high pressure imposed, the Teflon can creep and after the zeolite material made some catalytic decomposition.

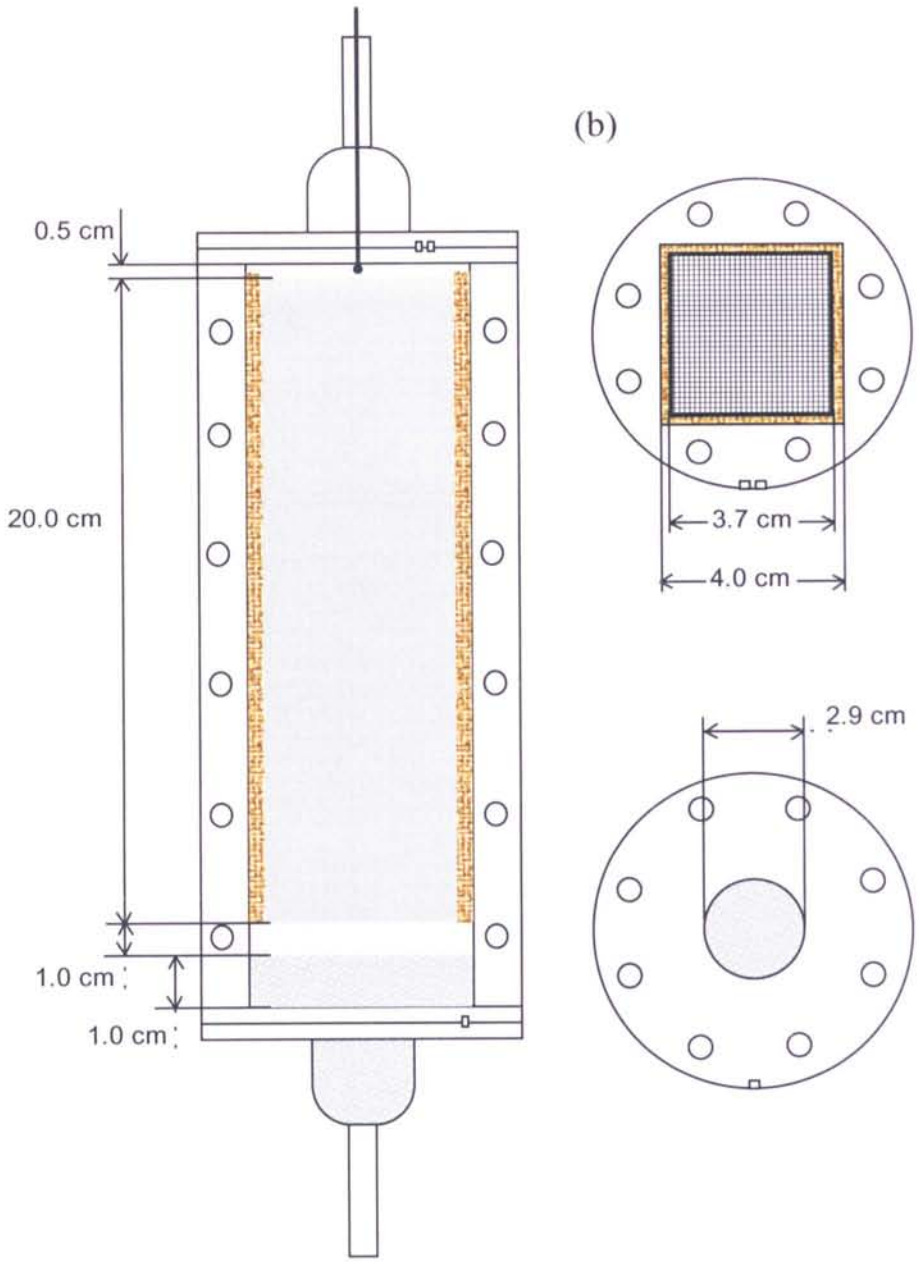

Figure 6.2. Detailed view of the column where the monolith was placed for breakthrough experiments: (a) picture of the column and (b) dimensions of the inner parts.

A small piece of this material was removed from the honeycomb and treated with a stream of purified air (ArK, Air Liquide, Portugal) at 673 K for 6 hours and after with a small stream of hydrogen for 30 minutes at the same temperature. This thermal treatment proves to remove severe coking formations in acetylene hydrogenation catalysts (Grande and Gigola, 1999). This sample was exposed to atmospheric

conditions for one week and after used in the adsorption equilibrium and kinetic measurements. Also, Scanning Electron Microscopy (SEM) coupled with an EDAX analysis characterization was performed on this sample showing no traces of carbon, meaning that coking was removed. Adsorption breakthrough experiments were performed using a second honeycomb structure with the same dimensions. The column was prepared using the same procedure explained before without the Teflon strip.

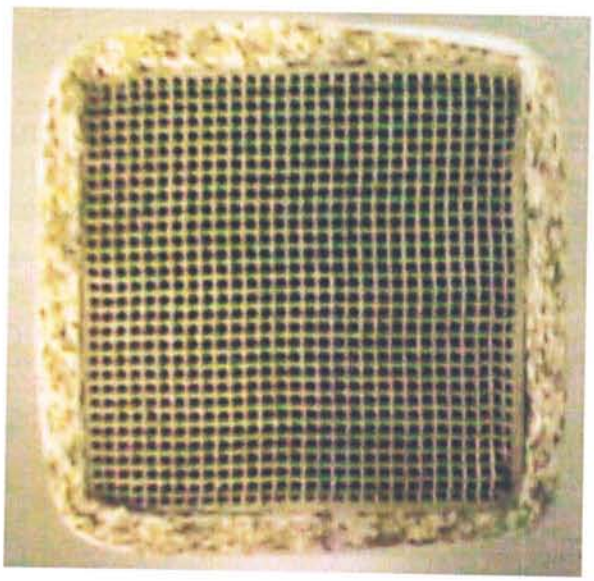

Figure 6.3. Detailed view of the square honeycomb structure of the monolith.

6.3 Adsorbent characterization

Two monoliths containing zeolite 4A were kindly supplied by Prof. Dr.-Ing. H.-G. Fritz from the University of Stuttgart. In order to know some details about the adsorbents, Scanning Electron Microscopy and EDAX analyses were done to a portion of one of the monoliths.

The Scanning Electron Microscopy (SEM) images were collected in order to identify the average diameter of the crystal zeolite 4A and also possible additional resistances due to fabrication of the honeycomb. The observations were performed in a

JEOL, JSM-6301F (Centro de Materiais da Universidade do Porto, CEMUP) where an X-ray spectrometer (NORAN-VOYAGER) is coupled to determine chemical composition. Several images were taken to show in detail the structure of the adsorbent.

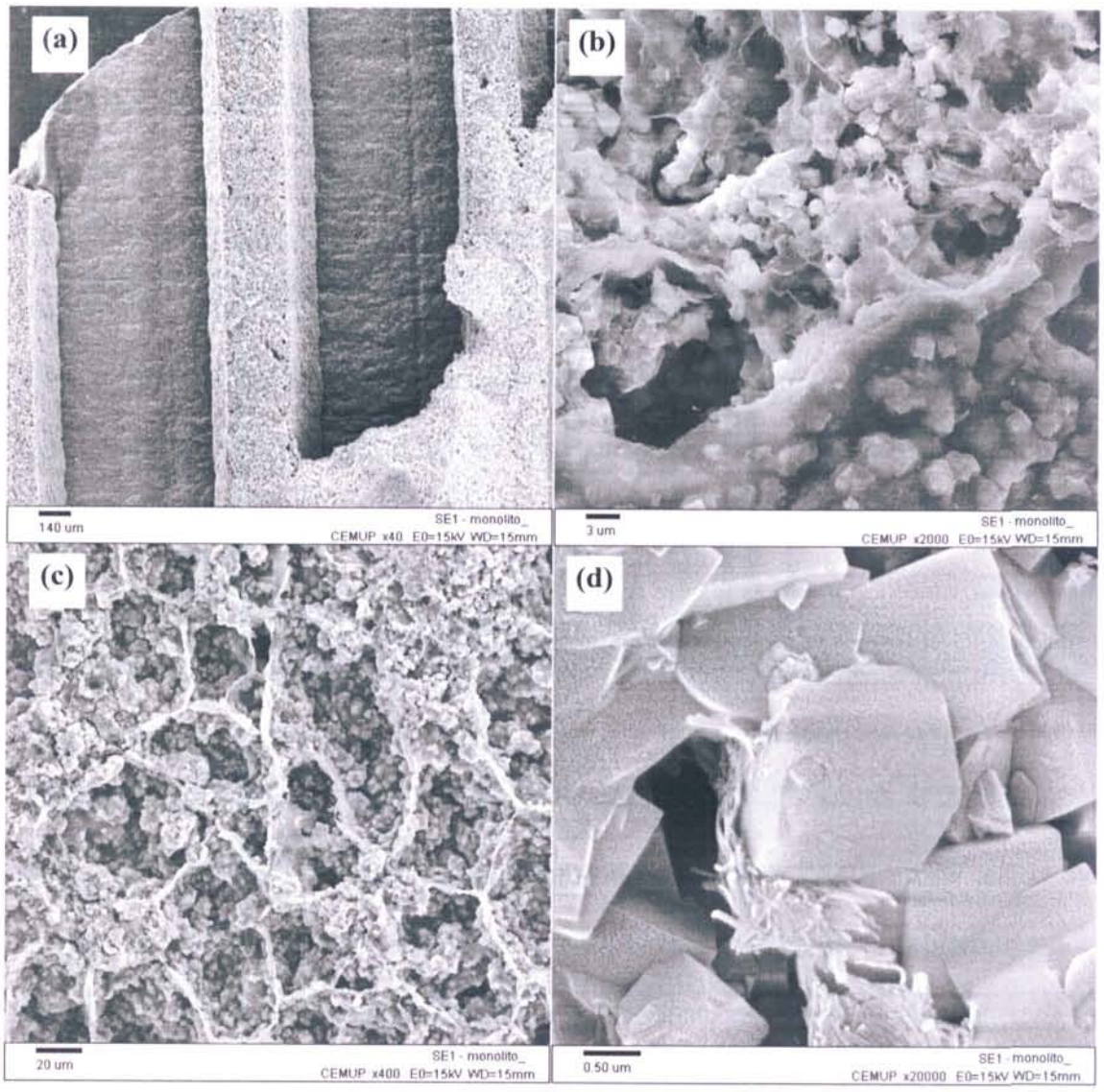

Figure 6.4. Morphology of the zeolite 4A monolith: (a) channel dimensions; (b) sided image showing the external surface of the channel and the internal structure of the walls; (c) frontal view of the interior of the wall showing large macroporosity channels; (d) zeolite 4A crystals.

Figure 6.4 shows the morphology of the material starting from the size homogeneity of the channels to the narrow distribution of crystal sizes. The internal diameter of the channel detected by SEM is 850 μm with a wall thickness of 320 μm (see Figure 6.4a). These dimensions were found to be very regular in the four channels analyzed over a length of 0.5 cm. In Figure 6.4c it is also seen that except the channels in the corners of the external walls, the channel diameters are very homogeneous. In the internal surface of the monolith channels the zeolite crystals are covered with a thin film of the binder material. In Figure 6.4b the interface between the external surface (below) and the internal structure of the material (above) are shown. Even though, this structure is very porous as the internal parts of the wall (Figure 6.4c). In Figure 6.4d the crystals of zeolite 4A are shown. The crystal diameter in the entire analyzed sample is very homogeneous and with more than 25 measurements the value of 1.4 ± 0.1 μm was determined.

When the chemical structure of the material is analyzed we have to consider that this is a bidisperse material and if a general spectra is measured, a combination of results will be obtained. For this reason, in Figure 6.5 we show a SEM image indicating two points where EDAX measurements were locally performed. In the spectra of the zeolite particle (P2) the typical composition of zeolite 4A was observed. In the case of the measurement in the binder material (b2) a different spectra containing magnesium and much less sodium and aluminium was obtained. Even though, as the penetration of EDAX is around 1 μm (with 15 kV of energy used for the measurements), we cannot determine that the spectra is purely of the binder material, while for the crystals with a larger diameter, this spectra can be considered only as being from the zeolite material.

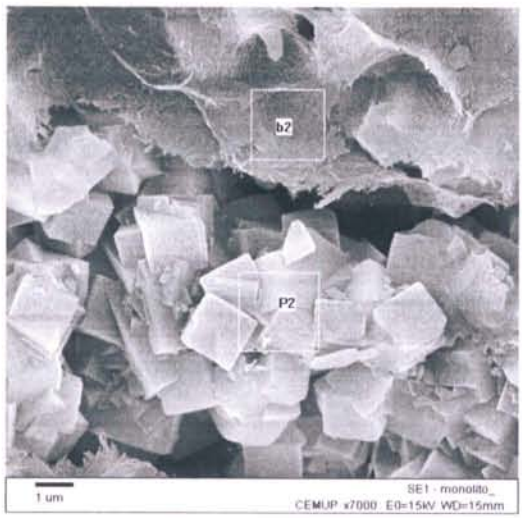

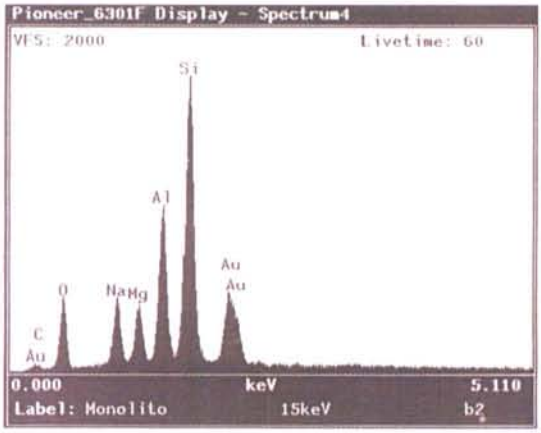

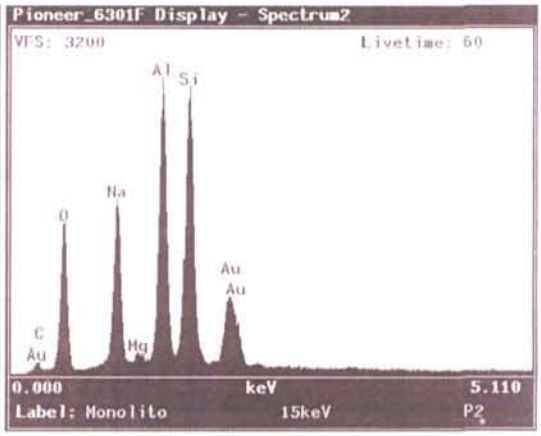

Figure 6.5. Chemical analysis in two different points of the zeolite 4A monolith: zeolite crystals (P2) and binder material (b2).

6.4 Theoretical analysis of adsorption equilibrium and kinetics

Modeling of the adsorption of a mixture of gases in a honeycomb monolith will be treated in this section.

To solve the equations of a packed bed, the bed porosity is considered constant and the mass balance for all components is solved. In a honeycomb monolith, a bundle of parallel channels form the structure. The monolith is also isolated (for mass and heat transfer) while packing it in the column. In this work the assumption of "complete

uniformity" in the channels was assumed (Groppi et al., 2000) being able to describe the behavior of the honeycomb. By complete uniformity we understand that the internal diameter and wall thickness is uniform in all the length of the monolith and the same for all channels and also that the amount of zeolite is also constant in the entire volume of the adsorbent. The graphical representation of this uniformity as well as the location of the axis of coordinates for a single channel is shown in Figure 6.6.

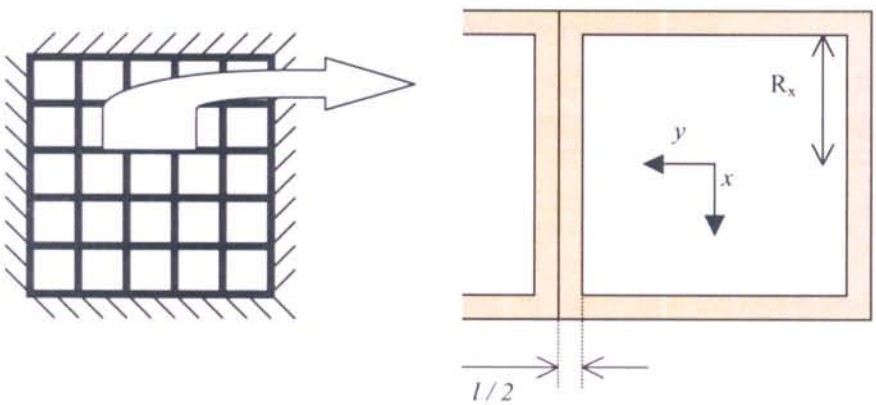

Figure 6.6. Geometrical description and location of the axis of coordinates in a single channel of the monolith.

With this equivalence some parameters have to be defined (Shah et al., 1996):

$$R_x = R_y = \sqrt{\frac{\varepsilon_m}{\pi n_d}} \qquad [6.1]$$

$$v_z = \frac{Q/A}{n_d} \qquad [6.2]$$

where Q is the total gas flowrate entering the column where the monolith is placed and A is the sectional area of the monolith (which is not the same as the column area because of the insulating material), v_z is the velocity of the gas in each channel, R_x and R_y are the half-length of a single channel in coordinates x and y, respectively, n_d is the number of channels per unit area and ε_m is the porosity of the monolith. Note that equation [6.1] is only valid for square shape channels.

In the accumulation of momentum the axial pressure variation as well as convection and the friction losses due to radial velocity are included. In dealing with bulk adsorption, the possibility of changes in the density of the gas due to adsorption also has to be taken into account. With these considerations, the momentum equation in Cartesian coordinates for a single adsorbate can be written as [Bird et al., 2002]:

$$\frac{\partial(\rho v_z)}{\partial t} = \mu_g \left[\frac{\partial^2 v_z}{\partial x^2} + \frac{\partial^2 v_z}{\partial y^2} + \frac{\partial^2 v_z}{\partial z^2} \right] - v_z \frac{\partial(\rho v_z)}{\partial z} - \frac{\partial P}{\partial z} \qquad [6.3]$$

where $P(z)$ is the gas pressure, $\rho(x,y,z)$ is the gas density and $v_z(x,y,z)$ is the axial gas velocity in the channel.

The momentum equation is coupled to the continuity equation, which is a statement of mass conservation in terms of density and velocity changes:

$$\frac{\partial \rho}{\partial t} + \rho \frac{\partial v_z}{\partial z} = 0 \qquad [6.4]$$

To write both momentum equations we have assumed that velocities in the x and y direction can be neglected, situation that may not be true for very strongly adsorbed and fast diffusing species at high concentrations.

The experiments are always started after passing the same flowrate of inert gas through the column so the initial velocity of the experiment is known. According to the geometry defined in Figure 6.6, the boundary conditions are given by:

$$v_z(t=0) = v_{z,feed} \qquad [6.5]$$

$$v_z(x=R_x, y, z) = 0 \qquad [6.6]$$

$$v_z(x, y=R_x, z) = 0 \qquad [6.7]$$

$$\left.\frac{\partial v_z}{\partial x}\right|_{(x=0,y,z)} = 0 \qquad [6.8]$$

$$\left.\frac{\partial v_z}{\partial y}\right|_{(x,y=0,z)} = 0 \qquad [6.9]$$

$$P(z = L_c) = P_f \qquad [6.10]$$

where P_f is the pressure at the end of the channel imposed by the back-pressure controller, or atmospheric pressure in case of a channel open to atmosphere.

The ideal law of the gases gives the relation between the density of the gas and the total pressure of the system:

$$\rho = \frac{M_w}{R_g T_g} P \qquad [6.11]$$

where M is the molecular weight of the gas, R_g is the universal gas constant and $T_g(x,y,z)$ is the temperature of the gas.

The mass balance for component i in the gas phase (continuity equation) is:

$$\frac{\partial C_i}{\partial t} + a'\left(\frac{1-\varepsilon_m}{\varepsilon_m}\right) k_f \left(C_i - C_i^*\right) = -\frac{\partial (v_z C_i)}{\partial z} + D_m\left[\frac{\partial^2 C_i}{\partial x^2} + \frac{\partial^2 C_i}{\partial y^2} + \frac{\partial^2 C_i}{\partial z^2}\right] \qquad [6.12]$$

where $C_i(x,y,z)$ is the bulk gas concentration of component i, $C_i^*(x,y,z)$ is the gas concentration of component i at the channel walls surface, a' is the area to volume ratio of the monolith channel, k_f is the film mass transfer resistance in the boundary layer surrounding the channel walls and D_m is the molecular diffusivity of the gas.

The initial condition for the mass balance equation is:

$$C_i(t = 0) = 0 \qquad [6.13]$$

The boundary conditions of this equation are given by the symmetry condition at the middle of the channel and the mass transfer to the film mass transfer resistance near the channel walls:

$$C_i(x, y, z = 0) = C_{i,feed} \qquad [6.14]$$

$$\left.\frac{\partial C_i}{\partial z}\right|_{(x,y,z=L_c)} = 0 \qquad [6.15]$$

$$\left.\frac{\partial C_i}{\partial x}\right|_{(x=0,y,z)} = 0 \qquad [6.16]$$

$$\left.\frac{\partial C_i}{\partial y}\right|_{(x,y=0,z)} = 0 \qquad [6.17]$$

$$D_m \left.\frac{\partial C_i^*}{\partial x}\right|_{(x=R_x,y,z)} = D_{p,i} \left.\frac{\partial C_{pi}}{\partial x}\right|_{(x=R_x,y,z)} \qquad [6.18]$$

$$D_m \left.\frac{\partial C_i^*}{\partial y}\right|_{(x,y=R_y,z)} = D_{p,i} \left.\frac{\partial C_{pi}}{\partial y}\right|_{(x,y=R_y,z)} \qquad [6.19]$$

where $C_{i,feed}$ is the feed concentration of component i in the feed stream, R_x and R_y are the channel half side in the x and y coordinates and L_c is the monolith length.

The transport of mass into the wall is given by the continuity equations (eqns. 6.18 and 6.19), which are also used as boundary equations for the mass balance in the element of the wall.

The mass balance in an element of the monolith wall is represented by:

$$\varepsilon_w \frac{\partial C_{pi}}{\partial t} + \rho_w \frac{\partial \overline{q_i}}{\partial t} = \varepsilon_w D_{p,i} \left[\frac{\partial^2 C_{pi}}{\partial x^2} + \frac{\partial^2 C_{pi}}{\partial y^2} + \frac{\partial^2 C_{pi}}{\partial z^2} \right] \qquad [6.20]$$

where $C_{pi}(x,y,z)$ is the gas concentration inside the pore network, $D_{p,i}$ is the pore diffusion coefficient of component i, ε_w is the porosity of the channel walls, ρ_w is the density of the channel walls and $\overline{q}_i(x,y,z)$ is the average amount adsorbed in the crystals. The initial condition is expressed by:

$$C_{pi}(\mathrm{t}=0)=0 \qquad [6.21]$$

and the boundary conditions are:

$$C_{pi}(x,y,z=0) = C_{i,feed} \qquad [6.22]$$

$$\left.\frac{\partial C_{pi}}{\partial z}\right|_{(x,y,z=L_c)} = 0 \qquad [6.23]$$

$$\left.\frac{\partial C_{pi}}{\partial x}\right|_{(x=R_x+\ell/2,y,z)} = 0 \qquad [6.24]$$

$$\left.\frac{\partial C_{pi}}{\partial y}\right|_{(x,y=R_x+\ell/2,z)} = 0 \qquad [6.25]$$

where $\ell/2$ is the half thickness of the channel wall.

Finally, to describe the Fickian diffusion in a spherical zeolite crystal (where micropores are located) is

$$\frac{\partial q_i}{\partial t} = \frac{1}{r^2}\frac{\partial}{\partial r}\left[D_{c,i} r^2 \frac{\partial q_i}{\partial r}\right] \qquad [6.26]$$

where $D_{c,i}$ is the crystal diffusivity of component i and $q_i(r,x,y,z)$ is the amount adsorbed of component i in the zeolite crystals placed in the walls of the channel. This equation has to be solved with the following initial and boundary conditions

$$q_i(t=0)=0 \qquad [6.27]$$

$$\left.\frac{\partial q_i}{\partial r}\right|(r=0,x,y,z)=0 \qquad [6.28]$$

$$q_i(r=r_c,x,y,z)=q_{s,i}=f(C_{pi}) \qquad [6.29]$$

where r_c is the crystal radius and $q_{s,i}$ is the amount adsorbed of component i in equilibrium with the gas phase given by the adsorption equilibrium equation.

The crystal diffusivity was assumed constant with concentration and having an exponential dependence with temperature described by an Arrhenius law:

$$D_{c,i} = D_{c,i}^{0}.\exp(-E_{a,i}/R_g T_s) \qquad [6.30]$$

where $D_{c,i}^{0}$ is the limiting diffusivity at infinite temperature, $E_{a,i}$ is the activation energy and $T_s(x,y,z)$ is the temperature of the wall.

Equation [6.29] is the condition of adsorption equilibrium at the surface of the crystal. In this work, the isotherm model used was the multisite Langmuir model (Nitta, 1984):

$$\left(\frac{q_{s,i}}{q_{max,i}}\right) = K_{eq,i} P_i \left[1 - \sum\left(\frac{q_{s,i}}{q_{max,i}}\right)\right]^{a_i} \qquad [6.31]$$

where $q_{max,i}$ is the maximum amount adsorbed of component i, a_i is number of neighboring sites occupied by the molecule of component i and $K_{eq,i}$ is the adsorption constant for component i which has an Arrhenius exponential temperature dependence as:

$$K_{eq,i} = K_{eq,i}^{\ 0} \exp\left(-\Delta H_i / R_g T_s\right) \qquad [6.32]$$

where $K_{eq,i}^{\ 0}$ is the adsorption constant at the limit of $T \to \infty$ and $(-\Delta H_i)$ is the isosteric heat of adsorption of component i at zero coverage.

In the energy equation the radial dispersion terms were eliminated and the energy balance for the fluid phase is:

$$\varepsilon_m \rho c_p \frac{\partial T_g}{\partial t} = \lambda\left[\frac{\partial^2 T_g}{\partial x^2} + \frac{\partial^2 T_g}{\partial y^2} + \frac{\partial^2 T_g}{\partial z^2}\right] + \varepsilon_m R_g T_g \frac{\partial C_i}{\partial t} - \varepsilon_m \rho c_p v_z \frac{\partial T_g}{\partial z} - (1-\varepsilon_m)\, a'\, h_f \left(T_g - T_s\right) \qquad [6.33]$$

where c_p is the heat capacity of the gas phase, λ is the thermal conductivity of the gas and T_g and T_s are the temperature of the gas phase and the solid phase of the monolith, respectively.

Initial and boundary conditions for the energy balance in the gas phase are:

$$T_g(t=0) = T_{feed} \qquad [6.34]$$

$$T_g(x, y, z=0) = T_{feed} \qquad [6.35]$$

$$\left.\frac{\partial T_g}{\partial z}\right|_{(x,y,z=L_r)} = 0 \qquad [6.36]$$

$$\left.\frac{\partial T_g}{\partial x}\right|_{(x=0,y,z)} = 0 \qquad [6.37]$$

$$\left.\frac{\partial T_g}{\partial y}\right|_{(x,y=0,z)} = 0 \qquad [6.38]$$

$$\lambda \left.\frac{\partial T_g}{\partial x}\right|_{(x=R_x,y,z)} = h_f \left(T_g|_{(x=R_x,y,z)} - T_g^*|_{(x=R_x,y,z)} \right) \qquad [6.39]$$

$$\lambda \left.\frac{\partial T_g}{\partial y}\right|_{(x,y=R_y,z)} = h_f \left(T_g|_{(x,y=R_y,z)} - T_g^*|_{(x,y=R_y,z)} \right) \qquad [6.40]$$

where $T_g^*(x, y, z)$ is the temperature at the gas – solid interface.

In the adsorbent wall the energy balance is:

$$(1-\varepsilon_m)\rho_w c_{ps} \frac{\partial T_s}{\partial t} = \lambda_s \left[\frac{\partial^2 T_s}{\partial x^2} + \frac{\partial^2 T_s}{\partial y^2} + \frac{\partial^2 T_s}{\partial z^2} \right] + (1-\varepsilon_m)\, a'\, h_f \left(T_g - T_s\right) + \rho_w (-\Delta H) \frac{\partial \overline{\langle q_i \rangle}}{\partial t} \qquad [6.41]$$

where c_{ps} is the heat capacity of the material of the monolith, λ_s is the thermal conductivity of the solid, h_f is the film heat transfer coefficient between the gas phase and the solid phase. No heat transfer was considered to the column wall because the monolith was covered with an isolating material to avoid lateral passage resulting also in heat insulation.

The boundary conditions are expressed by the continuity of heat fluxes in the interface between the boundary layer of gas and the wall and also by considering the channel of the monolith as isolated. Initial and boundary conditions are given by:

$$T_s(t=0) = 0 \qquad [6.42]$$

$$T_s(x, y, z=0) = T_{feed} \qquad [6.43]$$

$$\left.\frac{\partial T_s}{\partial z}\right|_{(x,y,z=L_c)} = 0 \qquad [6.44]$$

$$\lambda \left.\frac{\partial T_g^*}{\partial x}\right|_{(x=R_x,y,z)} = \lambda_s \left.\frac{\partial T_s}{\partial x}\right|_{(x=R_x,y,z)} \qquad [6.45]$$

$$\lambda \left.\frac{\partial T_g^*}{\partial y}\right|_{(x,y=R_x,z)} = \lambda_s \left.\frac{\partial T_s}{\partial y}\right|_{(x,y=R_x,z)} \qquad [6.46]$$

$$\left.\frac{\partial T_s}{\partial x}\right|_{(x=R_x+\ell/2,y,z)} = 0 \qquad [6.47]$$

$$\left.\frac{\partial T_s}{\partial y}\right|_{(x,y=R_x+\ell/2,z)} = 0 \qquad [6.48]$$

SIMPLIFICATIONS TO THE COMPLETE MODEL

The set of equations presented above is the complete model describing the adsorption of a single adsorbate in a honeycomb monolith structure. The set of equations describe in three spatial coordinates, three resistances to diffusion (film mass transfer, macropore and micropore diffusion). The possibility of density variations due to bulk adsorption and its effects in the momentum transfer have also been considered and also the energy balances were included in case of non-isothermal (adiabatic) operation.

From an engineering point of view, solving the equations presented above requires large computational effort, particularly if the results of this model have to be applied to a Pressure Swing Adsorption (PSA) system where boundary conditions are changing cyclically in each step. In this work two different simplifications to the complete model will be described. The first one is for the case of dilute adsorbate where the equations of the complete model might be largely simplified and the second one is a

more overall description of the phenomena of adsorption considering variations only in the axial direction. This simplification is commonly known as lumped parameter model.

Case 1: Complete model for dilute single adsorbate

When the amount of adsorbate is small compared to the total stream fed to the column, the system can be considered as dilute. In this case, two main simplifications can be done in the complete model (Ruthven, 1984): the velocity inside the column can be considered constant in the z-direction and also, the density of the gas is constant. An additional simplification is that, even when the system is isolated, the temperature increase is small and thus the system can be considered as isothermal, excluding the energy balances from the model.

As the density of the gas is constant the continuity equation simplifies to $\partial v_z / \partial z = 0$ and also equation [6.3] can be simplified to:

$$\rho \frac{\partial v_z}{\partial t} = \mu_g \left[\frac{\partial^2 v_z}{\partial x^2} + \frac{\partial^2 v_z}{\partial y^2} \right] - \frac{\partial P}{\partial z} \qquad [6.49]$$

with $v_z(x,y)$ is the axial gas velocity in the channel constant in the axial direction. The adsorption experiments started by passing a stream of inert gas and at time zero switching to the dilute stream. If we neglect the entrance effects in the channel and considered that the velocity profile is completely developed in the entire length of the channel, the term $\partial v_z / \partial t = 0$ vanishes and an analytical expression for the velocity can be obtained (Bird et al., 2002 p. 106):

$$v_z = \frac{\Delta P R_x^{\,2}}{4 \mu_g L_c} \left\{ 1 - \left(\frac{x}{R_x} \right)^2 \right\} \left\{ 1 - \left(\frac{y}{R_x} \right)^2 \right\} \qquad [6.50]$$

where ΔP is the difference of pressure between the inlet and the outlet of the monolith structure and μ is the gas viscosity. The mass balance in the gas phase is also simplified:

$$\frac{\partial C_i}{\partial t} + a'\left(\frac{1-\varepsilon_m}{\varepsilon_m}\right)k_f\left(C_i - C_i^*\right) = -v_z\frac{\partial C_i}{\partial z} + D_m\left[\frac{\partial^2 C_i}{\partial x^2} + \frac{\partial^2 C_i}{\partial y^2} + \frac{\partial^2 C_i}{\partial z^2}\right] \qquad [6.51]$$

Note that in equation [6.49] the velocity can be now substituted by the expression of equation [6.50]. In the set of equations presented above only the macropore and micropore resistances equations remain because as the system is isothermal, the temperature is the same for the entire column. Recasting, the complete model (7 PDE balances: 2 for momentum, 3 for mass and 2 for energy transfer) is now simplified to a set of 3 PDEs (mass transfer balances) decreasing the computing time. Another important reduction is the number of mass and energy transport parameters of the system. In the dilute case, the parameters that have to be determined are the film mass transfer and macropore – micropore resistances.

Case 2: Lumped parameter model

In the theoretical treatment given before, the mass and energy balances were derived from separate elements in gas and solid phases in Cartesian coordinates. Another approach can be done using a differential element over the entire area of the channel for the gas phase. This difference between the differential elements used in the distributed model (explained above) and this new simplification given in this section (called as lumped model), is shown in Figure 6.7.

Note that for the lumped model (Figure 6.7b), there is no differential volume element in the solid phase. In order to simplify the diffusion into the solid to a single dimension problem, the adsorption was considered to happen in an infinite slab of dimensions $R_x < R < R_x + \ell/2$. This is equivalent to say that the thickness of the wall is very small compared to the channel diameter available for mass transfer ($R_x >> \ell$) and that we are including the effects of the corners in a generic parameter, the pore

diffusivity, D_p. As we will estimate the pore diffusivity with the Bosanquet equation, the effects of the corners are being neglected. This approximation may not be valid for very fast diffusing species.

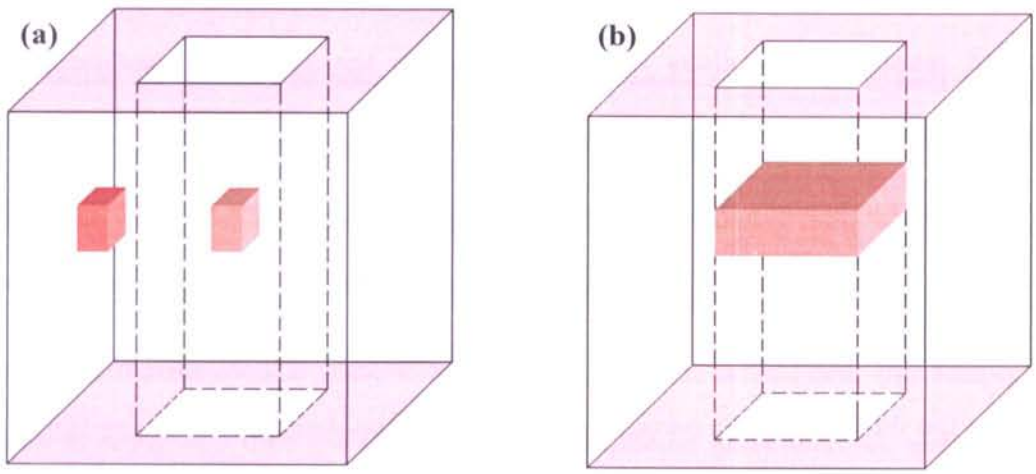

Figure 6.7. Differential elements in the gas phase for the distributed parameter model (a) and for the lumped parameter model (b).

With the lumped parameter model, the equations to describe the adsorption phenomena are derived over a single dimension, the channel length. This simplification does not reduce the number of partial differential equations but produces a significant reduction in the number of elements per matrix of each variable. The disadvantage is that the description is now made by average variables over the x and y dimensions. This analysis is the most applied in literature dealing with monoliths for catalysis and adsorption (Tronconi and Forzatti, 1992; Shah et al., 1996; Gulati, 1998; Valdés-Solís et al., 2004).

The mass balance for component i in the channels is given by:

$$\frac{\partial C_i}{\partial t}+\left(\frac{1-\varepsilon_m}{\varepsilon_m}\right)\rho_w\frac{\partial\langle\overline{q_i}\rangle}{\partial t}=-v_z\frac{\partial C_i}{\partial z}+D_{ax}\left[\frac{\partial^2 C_i}{\partial z^2}\right] \qquad [6.52]$$

where $C_i(z)$ is the area averaged concentration for a certain position in the axial coordinate, $v_z(z)$ is the area average velocity, $\langle \overline{q_i} \rangle$ is the area averaged amount adsorbed in the solid walls and D_{ax} is the axial dispersion coefficient where all effects of flow pattern were lumped.

The initial and boundary conditions are the same as the applied in the complete model, but now only for the axial direction:

$$C_i(t=0)=0 \qquad [6.53]$$

$$C_i(z=0)=C_{i,feed} \qquad [6.54]$$

$$\left.\frac{\partial C_i}{\partial z}\right|_{(x,y,z=L_c)}=0 \qquad [6.55]$$

Equations for mass transport in the macro and micropores are expressed now in terms of averaged concentrations and amounts adsorbed in a plane of the axial coordinate:

$$\varepsilon_w \frac{\partial C_{pi}}{\partial t}+\rho_w \frac{\partial \overline{q_i}}{\partial t}=\varepsilon_w D_{p,i}\left[\frac{\partial^2 C_{pi}}{\partial R^2}\right] \qquad [6.56]$$

where $C_{pi}(R,z)$ is the averaged gas concentration inside the pore network and $\overline{q}_i(R,z)$ is the averaged amount adsorbed in the crystals. The initial and boundary conditions are expressed by:

$$C_{pi}(\mathrm{t}=0)=0 \qquad [6.57]$$

$$D_m \left.\frac{\partial C_i}{\partial R}\right|_{(R=R_s,z)}=D_p \left.\frac{\partial C_{pi}}{\partial R}\right|_{(R=R_s,z)} \qquad [6.58]$$

$$\left.\frac{\partial C_{pi}}{\partial R}\right|_{(\mathrm{R}=\mathrm{R}_s+\ell/2,z)}=0 \qquad [6.59]$$

The description of diffusion in a spherical zeolite crystal is given by equations 6.26 – 6.29 replacing $q_i(r,x,y,z)$ by $q_i(r,R,z)$.

When equation 6.50 was written, the radial diffusion limitations were neglected because the following condition was fulfilled in all the experiments performed in this work (Taylor, 1954):

$$D_m \frac{L_c}{4R_x^{\,2} v_z} \gg \frac{1}{56} \qquad [6.60]$$

Also, the axial dispersion coefficient is calculated using the Taylor correlation with the molecular diffusivity contribution (Aris, 1956; Hoebink and Marin, 1998):

$$D_{ax} = D_m + \frac{4R_x^{\,2} v_z^{\,2}}{192 D_m} \qquad [6.61]$$

Transport studies in regular channels of honeycomb structures were already studied theoretically (Young and Finlayson, 1974). Experimentally the work of Hawthorn is one of the most used in NOx applications (Hawthorn, 1974) and was also used in adsorption studies (Perera and Crittenden, 1998; Valdés-Solís et al., 2004). The equation used to describe the dependency of the Sherwood number is:

$$Sh = \frac{2k_f R_x}{D_m} = 2.796\left(1 + 0.190\,\mathrm{Re}\,Sc\frac{R_x}{L_c}\right)^{0.45} \qquad [6.62]$$

where $\mathrm{Re} = 2\rho v_z R_x / \mu$ is the Reynolds number and $Sh = \mu / \rho D_m$ is the Schmidt number. This equation shows that even with a very small velocity a limiting value of k_f can be obtained for a pre-defined geometry. In the case of liquid systems, the molecular diffusivity of the adsorbate will be small and thus the film mass transfer resistance cannot be previously ignored, but in gas systems where the molecular diffusivity is much larger there might be a situation where micropore or macropore or a combination of both were much more important and film mass transfer resistance can be ignored.

Energy balances are written with similar simplifications averaging gas and solid temperatures in the area of the gas and solid phases, respectively. The energy balance equations for gas and solid phases with initial and boundary conditions are given below:

$$\varepsilon_m \rho_b c_v \frac{\partial T_g}{\partial t} = \delta\left[\frac{\partial^2 T_g}{\partial z^2}\right] + \varepsilon_m R_g T_g \frac{\partial C_i}{\partial t} - \varepsilon_m \rho_b c_p v_z \frac{\partial T_g}{\partial z} - (1-\varepsilon_m)\, a'\, h_f \left(T_g - T_s\right) \quad [6.63]$$

$$T_g(t=0) = T_{feed} \quad [6.64]$$

$$T_g(z=0) = T_{feed} \quad [6.65]$$

$$\left.\frac{\partial T_g}{\partial z}\right|_{(z=L_c)} = 0 \quad [6.66]$$

$$\rho_b c_{ps} \frac{\partial T_s}{\partial t} - = \delta\left[\frac{\partial^2 T_s}{\partial z^2}\right] + (1-\varepsilon_m)\, a'\, h_f \left(T_g - T_s\right) + \rho_b (-\Delta H_i) \frac{\partial \langle \overline{q_i} \rangle}{\partial t} \quad [6.67]$$

$$T_s(t=0) = 0 \quad [6.68]$$

$$T_s(z=0) = T_{feed} \quad [6.69]$$

$$\left.\frac{\partial T_s}{\partial z}\right|_{(z=L_c)} = 0 \quad [6.70]$$

where $T(z)$ is the area averaged temperature of the gas, ρ_b is the bulk density of the column and δ is the axial thermal dispersion of the column.

The simplifications of the complete model (case 1 for dilute systems and lumped model for concentrated mixtures) were solved using gPROMS (PSA Enterprise, UK). The orthogonal collocation method on finite elements (OCFE) was used in all cases with two interior collocation points per element. For the dilute system 25 elements were used in the axial dimension and 8 elements in the x and y dimensions and in the zeolite crystal. For the case of the lumped parameter model, also 25 elements were used in the axial dimension while 8 elements were used both in the wall and in the crystals.

6.5 Adsorption equilibrium and kinetics of propane and propylene

The first step in adsorbent characterization for a specific separation is the measurement of adsorption equilibrium of pure components. Adsorption equilibrium of propane and propylene were measured gravimetrically in the Rubotherm unit previously used for measurements in SBA-15 crystals as detailed in Chapter 5. The amount of wet sample used was 1.890g, which corresponds to a section of the monolith carefully removed from the honeycomb structure. The activation of the sample was performed overnight at 593 K under vacuum (< 10^{-5} kPa), similarly to the activation protocol used in zeolite 4A extrudates. The weight loss during activation was 18.1%.

The gravimetric procedure to measure adsorption equilibrium was the same used in Chapter 5. Isotherms at 423 and 473 K were measured for propane and propylene up to 100 kPa. All isotherms were reversible and this was confirmed by measuring some desorption points. Adsorption equilibrium of propylene and propane at 423 and 473 K in the monolith material is shown in Figure 6.8. In this figure data collected in the manometric unit (see Chapter 4) on the zeolite 4A commercial extrudates (CECA) are also shown at the same temperature. It can be seen that for both gases, data are coincident in the initial portion of the isotherms (P < 20 kPa) while for higher pressures the total capacity of the monolith is somewhat higher. Adsorption equilibrium data were fitted with the multisite Langmuir model (solid line in Figure 6.8). As these data at low pressures are very similar to the values reported in extrudates, the adsorption equilibrium constants as well as the number of neighboring sites used for adsorption in extrudates was used (Grande et al., 2003a) and differences between adsorption equilibrium of the zeolite 4A monolith and zeolite 4A commercial were only accounted by using a different saturation capacity, that is slightly larger in the monolith material. The saturation capacity of propane is larger than the one of propylene because of the

constraint $a_i q_{\max,i} = \text{constant}$ (Sircar, 1995) to satisfy a material balance of sites in the adsorbent.

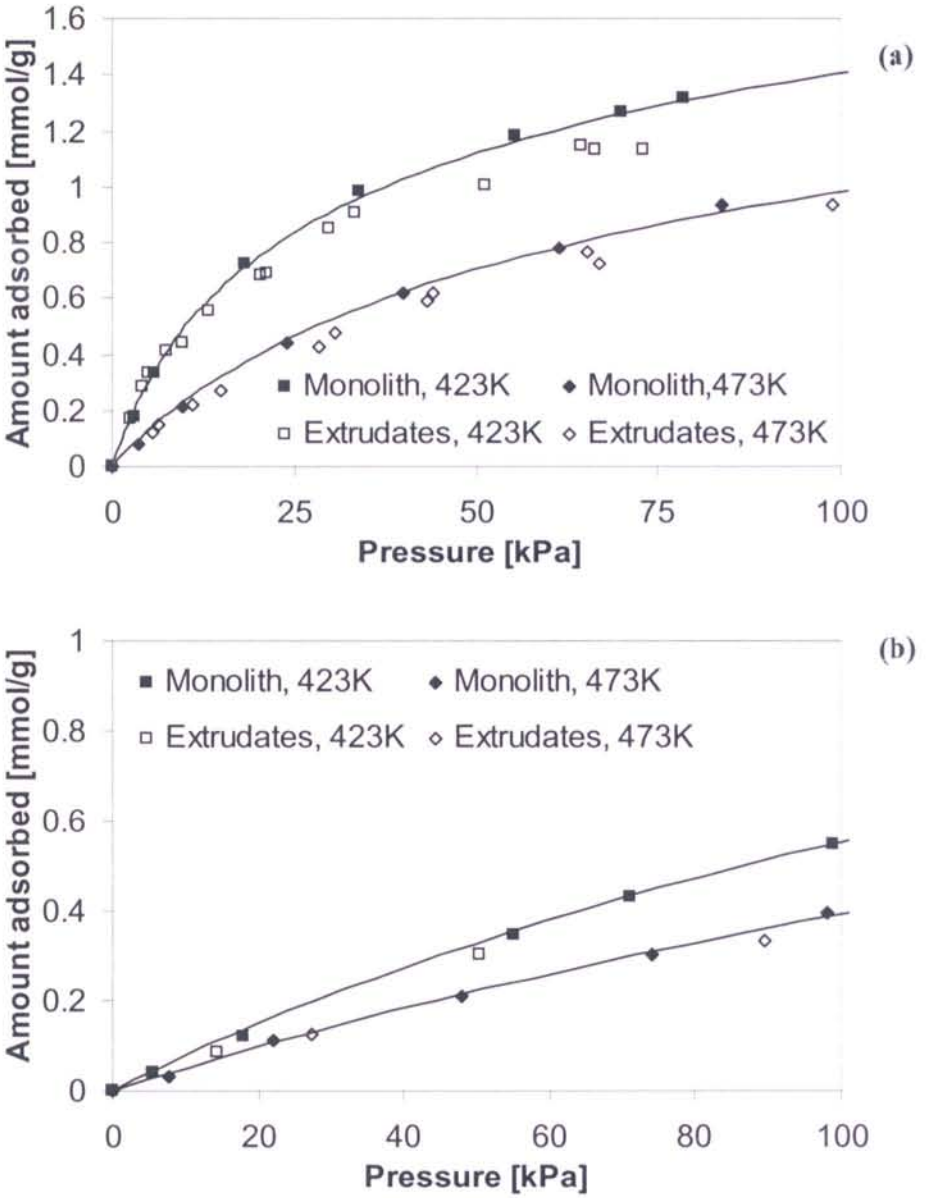

Figure 6.8. Adsorption equilibrium of propylene (a) and propane (b) at 423 and 473 K in the zeolite 4A monolith (solid points). Adsorption equilibrium on commercial sample is shown for comparison (empty points). Solid line – multisite Langmuir model fitting.

Table 6.1. Fitting parameters of the multisite Langmuir model of Nitta for propylene and propane adsorption equilibrium at 423 and 473 K.

Gas	q_{mi} [mmol/g]	a_i [-]	K_i(423 K) [kPa^{-1}]	K_i(473 K) [kPa^{-1}]
C_3H_6	2.857	2.612	0.0288	0.0103
C_3H_8	3.409	2.189	0.0024	0.0015

When measuring adsorption equilibrium in the Rubotherm unit, a signal reporting the difference of weight allows us to see the adsorption uptake while the experiment is running. In previous experiments in zeolite 4A with extrudates, the uptake for propylene took thirty minutes and was controlled by crystal diffusion. It was expected that the uptake in the monolith was faster; however, the complete uptake took around two hours indicating a very low diffusivity of propylene. The uptakes of propylene at 423 and 473 K are shown in Figure 6.9. The solid line corresponds to the model for uptake in finite volume previously used for propane adsorption in zeolite 4A (see Chapter 4). The initial part of the curve is shown in detail in Figure 6.9. If we consider that the concentration of the gas phase will be constant in the initial moments of the experiment such that the infinite medium condition can be satisfied, the uptake is plotted as C/C_0 versus the square root of time and the initial slope is proportional to (Ruthven, 1984):

$$Slope = \frac{6}{\sqrt{\pi}}\left(\frac{D_c}{r_c^{\,2}}\right)^{0.5} \qquad [6.71]$$

The crystal diffusivities of propylene at 423 and 473 K fitted with the complete model (see Chapter 4, equation 4.23) were: $D_c(423) = 1.5\text{x}10^{-17}$ m^2/s and $D_c(473) = 6.3\text{x}10^{-17}$ m^2/s. Using the approximation of the initial slope the values were: $D_c(423) =$

2.3×10^{-17} m²/s and $D_c(473) = 5.7 \times 10^{-17}$ m²/s. The main difference of these values is due to the consideration of infinite volume for the estimation of diffusivity using the initial slope (concentration variation of 5% were observed in the first 150 s) while the complete curve uses the more realistic scenario of pressure changes due to adsorption in a finite volume. The importance of the results using the initial slope is not the diffusivity value obtained; in other materials it was shown that if an additional resistance (surface barrier at the mouth of the micropores) is present, such plot will have a very smaller slope than the one considering only micropore resistances (Grande et al., 2004; Qinglin et al., 2003).

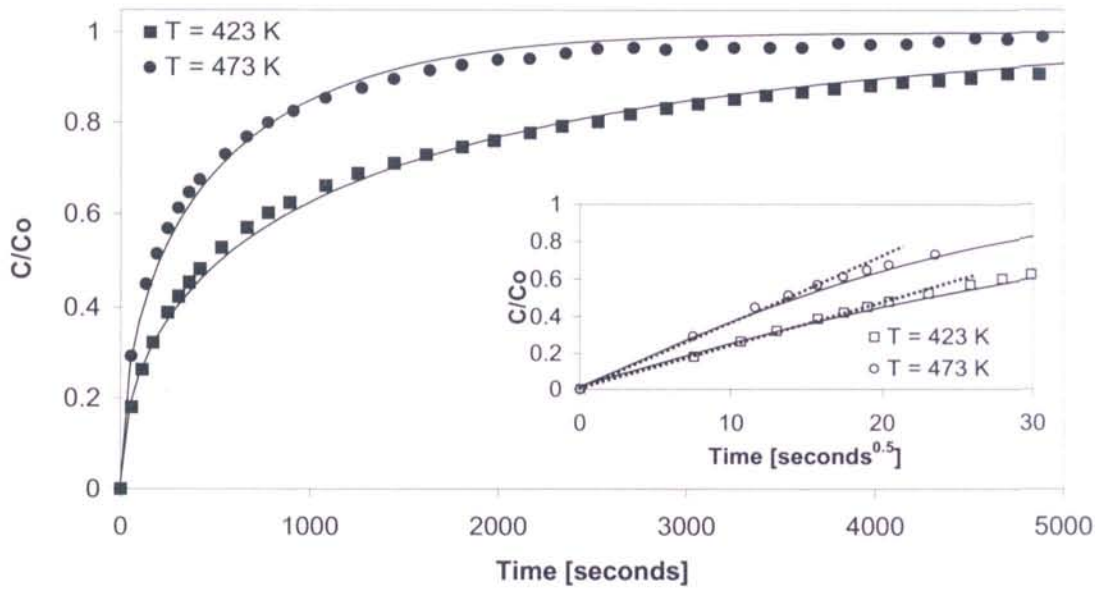

Figure 6.9. Adsorption uptakes of propylene at 423 and 473 K at low partial pressure (less than 3 kPa). Solid lines are the complete model for uptake analysis. Dotted line in the initial portion of the curve is the approximation for diffusivity estimation using the initial slope.

The reasons behind the large difference between the diffusivity values obtained for commercial and laboratory prepared crystals shown in Chapter 5 and the values reported here must be discussed.

If we consider that diffusion of propylene in zeolite 4A has a unique value previously determined in this work, an additional resistance to diffusion is present in this monolithic material and has to be measured. From the SEM images shown in Figure 6.4, the external layer of the channel (interface gas – solid) seems to have a "film" of the binder that may offer some resistance. To determine if this film produces an additional resistance to diffusion, Zero Length Column (ZLC) curves were done.

To measure ZLC curves, pieces of material taken from the faces that composes the square channels were used (slab geometry). The sample of humid material used was 132 mg and the helium flowrate were 40 cm^3/min (measured at 297 K). After experiments at 423 and 473 K, the sample was crushed with a spoon until a fine dust was obtained (no size measurements were performed) and experiments with the same helium flowrate were repeated. If there is an additional resistance in the external layer of the slabs used in the initial experiments such that it controls the propylene diffusion, some difference should be observed when making experiments in the crushed sample.

In Figure 6.10 we show the experiments of slab particles ($2R_x$ side, ℓ thickness and 1 cm length) and crushed sample of the monolith material measured at 423 and 473 K. As can be seen, no noticeable difference was observed. Also the decay of the curve is very fast indicating a very low diffusivity coefficient. This clearly indicates that the resistance of diffusion is located in the crystals of zeolite 4A. These experiments were not analyzed to determine a value of diffusivity and equilibrium constant because the experimental data are collected near to the baseline of the FID (Flame Ionization Detector) so large errors (particularly in the intercept) are expected.

A similar effect of very low diffusion of propylene was previously observed when experiments were performed in sample of zeolite 4A named as CECA1 (see Chapter 2) and also in crystals prepared in laboratory (see Chapter 5). In those cases the

adsorption equilibrium was also affected, but the values of propylene diffusivity were very small. With the zeolite 4A crystals this phenomenon was corrected by activating the sample at higher temperature, reason why 673 K was the temperature used. In this case, the sample stored in the Rubotherm unit was again activated, but using the higher temperature of 673 K. In this case, the results obtained as measured by the gravimetric unit are shown in Figure 6.11. It can be seen that no significant difference was observed with this sample, and analyzing the new data a value of $D_c = 1.7x10^{-17}$ cm²/s can be obtained, which means that the activation temperature did not improve, in this case, the adsorption diffusivity of propylene.

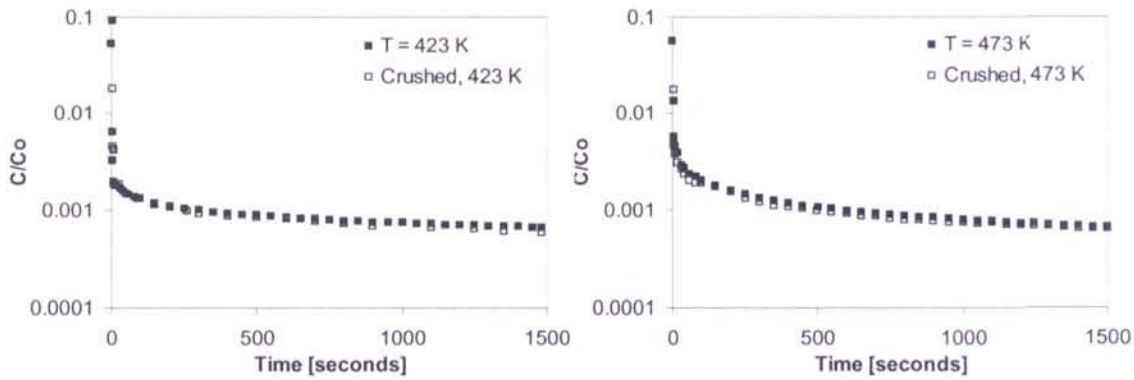

Figure 6.10. ZLC desorption curves of propylene in monolith adsorbent at 423 and 473 K using 40 cm³/min of helium (measured at 297 K). Sample was activated at 593 K overnight in flow of helium.

Adsorption kinetics of propane was also recorded for the points at low pressure. The uptakes of propane at 423 and 473 K are shown in Figure 6.12. The solid line corresponds to the model for uptake in finite volume previously used in Chapter 4. In this figure the values of diffusivity used were: $D_c(423) = 0.70x10^{-18}$ m²/s and $D_c(473) = 1.5x10^{-18}$ m²/s. These values have the same order of magnitude of those determined for propane adsorption in zeolite 4A extrudates (CECA), but they are also four times

smaller, indicating that also for the propane molecule the path in the zeolite channels is more tight in the 4A crystals contained in the monolith.

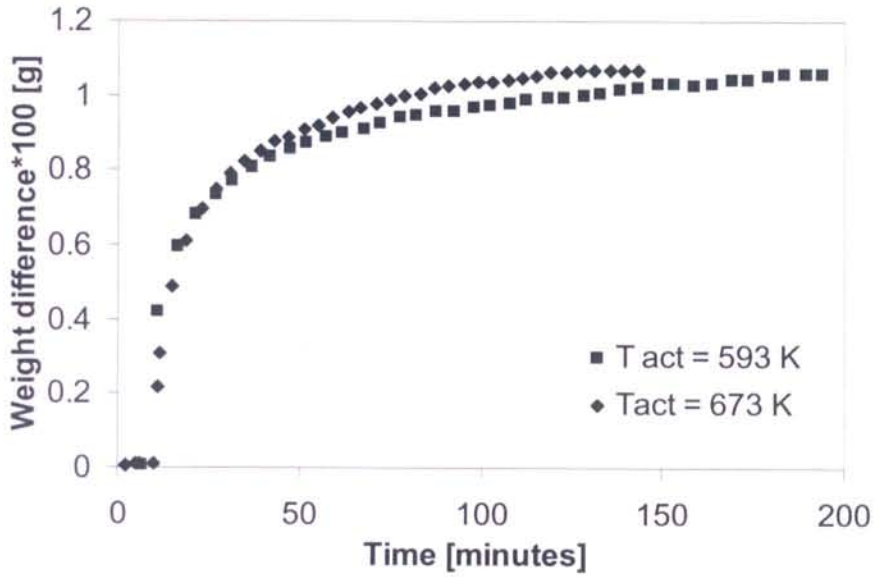

Figure 6.11. Adsorption of propylene at 473 K on the monolith of zeolite 4A with activation at 593 K and at 673 K under vacuum (>10^{-5} kPa).

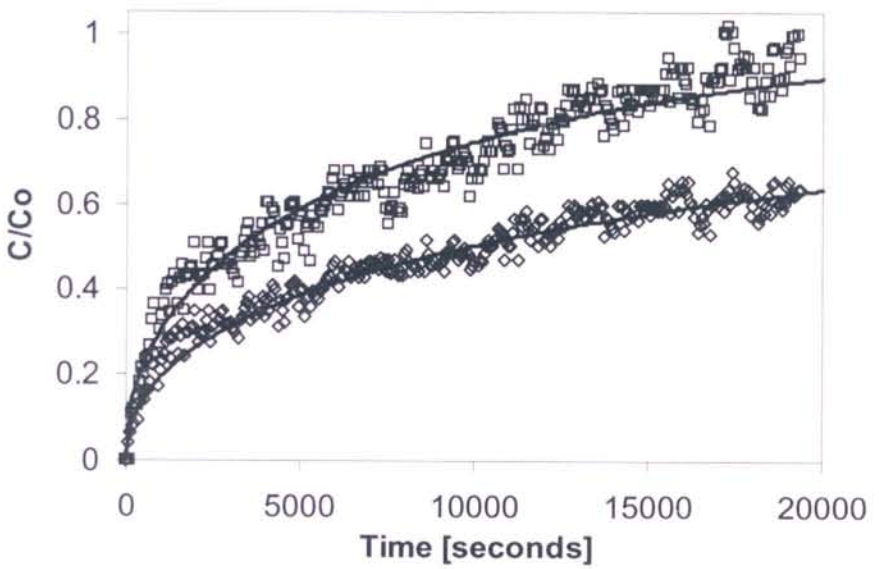

Figure 6.12. Adsorption uptakes of propane at 423 and 473 K at low partial pressure (less than 10 kPa). Solid lines are the complete model for uptake analysis.

6.6 Fixed bed adsorption experiments

Once adsorption equilibrium and kinetics of both gases were characterized from independent techniques, the breakthrough analysis using low partial pressures of hydrocarbons will allow us to confirm the values obtained before and also to have a more realistic value of the diffusivity coefficients than the one from batch studies where other phenomena, can occur in parallel giving us an overall diffusion coefficient. Also the experiments reported here were done in the second honeycomb monolith having a mass of adsorbent much higher than the one used for adsorption equilibrium and kinetic measurements.

The activation of the monolith was performed at 673 K for 24 hours, even when the results obtained in the adsorption equilibrium measurements did not show significant differences between activation at 593 and 673 K. This temperature was achieved with a heating ramp of 1K/min under a flow of 50 cm^3/min of helium. This large amount of helium was used to ensure no condensation of water in the colder parts outside the monolith. Also the column outlet was not connected to the GC during activation. This disconnection was done well above the column to send the water vapor out of the experimental set-up and not to condensate in the tee above the column and fall into the monolith structure.

The initial experiments performed here were the dilute breakthrough curves of propylene with 1.2 kPa partial pressure at 423 and 473 K at atmospheric pressure. Experimental conditions of the curves are detailed in Table 6.2.

Once experimental data were recorded and analyzed, the first thing to do is to analyze the stoichiometric time to compare the capacity of the sample obtained by gravimetry and by the dynamic method. The stoichiometric time of the samples were calculated by (see Chapter 4):

$$\bar{t} = \frac{L}{u_i}\left[1 + \left(\frac{1-\varepsilon_m}{\varepsilon_m}\right)\frac{q_{si}}{C_i}\right] = \int_0^\infty \left(1 - \frac{C}{C_o}\right) dt \qquad [6.72]$$

where $q_{s,i}$ is the amount adsorbed of component i in equilibrium with the gas phase concentration of this component C_i and u_i ($=Q/A\varepsilon_m$) is the interstitial velocity calculated for the entire monolith.

Table 6.2. Experimental conditions for breakthrough experiments of propylene – helium mixtures in zeolite 4A monolith at 423 and 473 K.

Monolith weight (humid), g	187.5
Monolith length, cm	20.0
Zeolite crystal diameter, μm	1.4
Hydrocarbon partial pressure, kPa	1.5; 5.6; 10.0
Feed flowrate (measured at 297 K), cm^3/min	46.15; 85.71
Monolith porosity	0.70
Bulk monolith density, g/cm^3	1.306

The experimental data are integrated and an experimental value of the stoichiometric time is obtained. Then the adsorption equilibrium is calculated and this value is the one compared with the gravimetric data. The Henry constant determined by the gravimetric and dynamic methods is reported in Table 6.3. Note that the error is less than 10%.

Diffusivity determinations can be done once capacity is checked. The experimental results obtained using a partial pressure of propylene of 1.5 kPa are presented in Figure 6.13. Solid lines in this figure correspond to the complete model simplified for dilute systems also assuming isothermal behavior (simplification

described as Case 1). This model was used in order to build a package able to solve the adsorption of a gas in a monolith column where a bidisperse adsorbent is placed and a combination of different resistances may happen. For the case when only micropore resistances control the diffusion process, it was reported before that, the monolith adsorbent and a fixed bed have the same overall behavior (Shah et al., 1996). In these curves, the diffusivity parameter was also considered as a fitting variable. The values that best fit the experimental data were: $D_c(423) = 0.56 \times 10^{-17}$ m²/s and $D_c(473) = 2.00 \times 10^{-17}$ m²/s for the lower flowrate (46.15 cm³/min) and $D_c(423) = 0.49 \times 10^{-17}$ m²/s and $D_c(473) = 1.70 \times 10^{-17}$ m²/s for the higher flowrate (85.71 cm³/min).

Table 6.3. Henry constants for propylene adsorption equilibrium on zeolite 4A monolith at 423 and 473 K.

T, K	Flowrate*, cm³/min	$H_{dynamic}$, mmol/g.kPa	$H_{gravimetric}$#, mmol/g.kPa	Difference, %
423	46.15	0.0633	0.0591	6.6
	85.71	0.0658		10.2
473	46.15	0.0208	0.0219	5.3
	85.71	0.0228		3.9

*Flowrate measured at 297 K

First gravimetric point measured in the linear zone of the isotherms

The values have only the same order of magnitude of those found in the adsorption uptake, but there is a factor of four between these values. Even though, the values obtained in the fixed bed analysis using two different flowrates are consistent. No variation in the temperature (within experimental error) was found. For these measurements we are assuming that the experimental error is within ± 0.3 K.

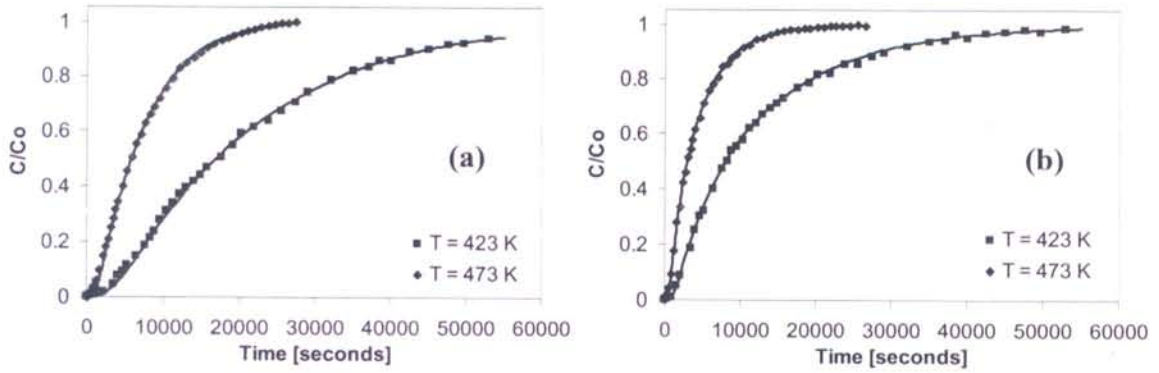

Figure 6.13. Dilute breakthrough curves of propylene (1.5 kPa partial pressure) in zeolite 4A honeycomb monolith at 423 and 473 K at different total flowrates: (a) 46.15 cm³/min, (b) 85.71 cm³/min measured at 297 K. Full experimental conditions are given in Table 6.2. Solid lines correspond to the complete model simplified for dilute systems using bidisperse adsorbents.

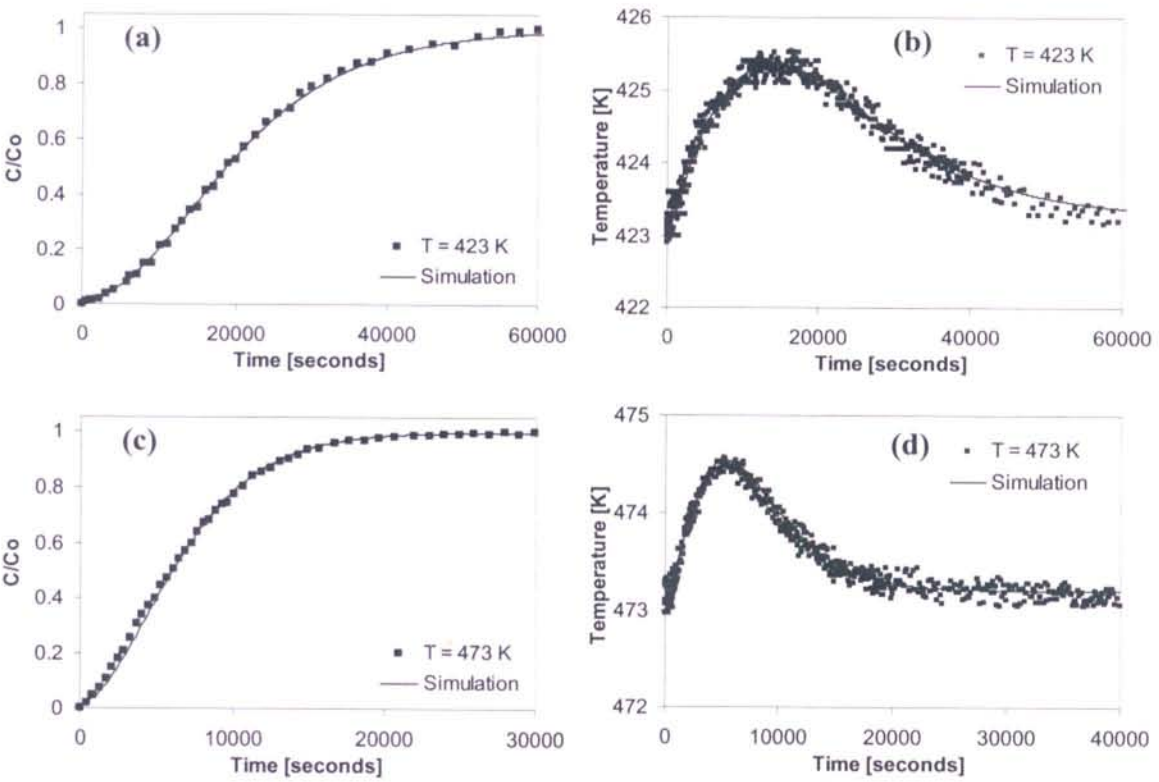

Figure 6.14. Breakthrough curves of propylene (partial pressure of 5.63 kPa) in zeolite 4A honeycomb monolith at 423 and 473 K with a total flowrate of 46.15 cm³/min measured at 297 K: (a, b) T = 423 K, (c, d) T = 473 K. Solid lines correspond to the lumped parameter model for bidisperse adsorbents.

As no strange effects were observed in the dilute experiments, using higher concentrations the experiments were measured only using the lower flowrate (46.15 cm^3/min measured at 297 K). Experiments at 423 and 473 K done with a hydrocarbon partial pressure of 5.63 kPa are reported in Figure 6.14. Experimental conditions are the same as the ones for dilute system (except the propylene partial pressure). Experiments with a propylene partial pressure of 10.0 kPa are reported in Figure 6.15 using the same total flowrate (46.15 cm^3/min measured at 297 K). In both figures, the solid lines are the ones simulated with the lumped parameter model. Using these higher concentrations it can be seen a temperature increase due to the release of the heat of adsorption. Parameters of energy and mass transfer used for the simulations are given in Table 6.4.

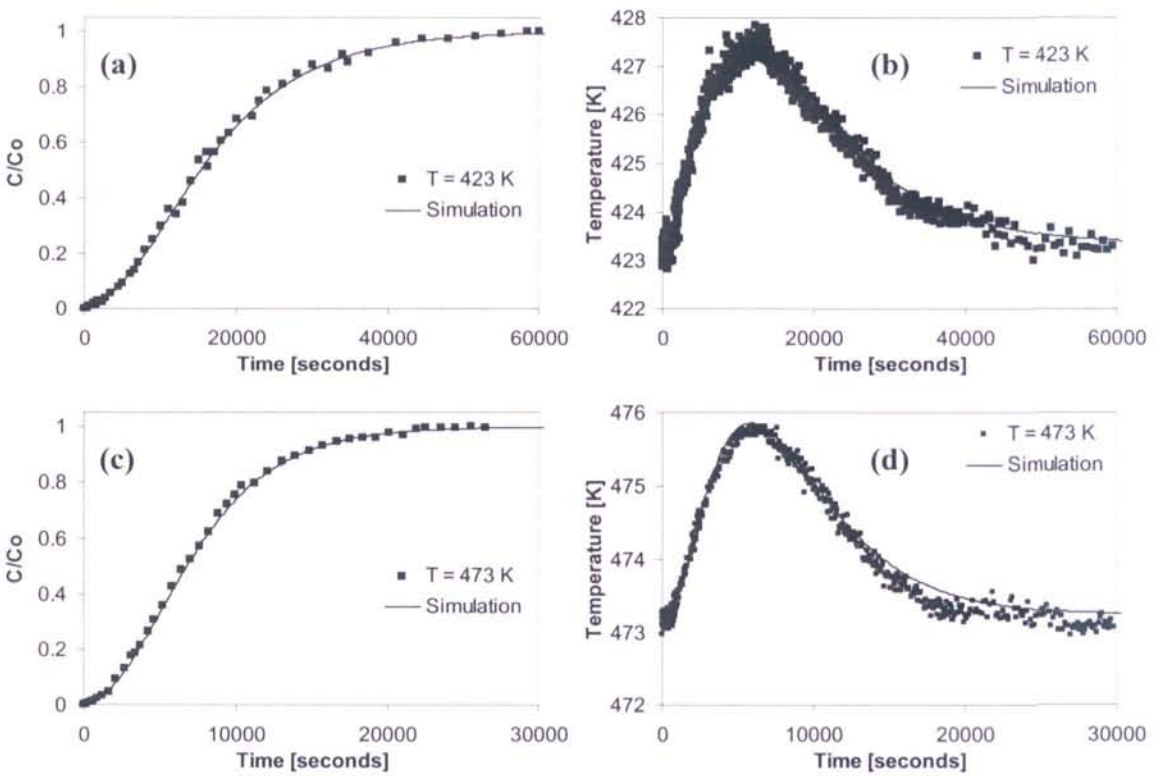

Figure 6.15. Breakthrough curves of propylene (partial pressure of 10.0 kPa) in zeolite 4A honeycomb monolith at 423 and 473 K with a total flowrate of 46.15 cm^3/min measured at 297 K: (a, b) T = 423 K, (c, d) T = 473 K. Solid lines correspond to the lumped parameter model for bidisperse adsorbents.

With the results from these breakthrough curves another adsorption equilibrium points can be obtained, which must be comparable (within experimental error) with the previous adsorption equilibrium data measured by other technique. The adsorption equilibrium points determined from breakthrough curves (solid points) together with the equilibrium points determined by gravimetric analysis (empty points) are shown in Figure 6.16. Also, these values, together with the crystal diffusivities used to fit the curves are tabulated in Table 6.5.

Table 6.4. Mass and energy transport parameters used for simulations of propylene breakthrough curves in zeolite 4A monolith.

	T = 423 K			T = 473 K		
Propylene pressure, kPa	1.5	5.6	10.0	1.5	5.6	10.0
Molecular diffusivity, cm^2/s	0.8862			1.0681		
Axial dispersion, cm^2/s	0.8866	0.8863	0.8863	1.0685	1.0682	1.0682
Reynolds number	0.020	0.013	0.016	0.019	0.013	0.015
Schmidt number	0.712	0.569	0.471	0.699	0.559	0.462
Film mass transfer, cm/s	29.15	29.15	29.15	29.15	29.15	29.15
Thermal axial dispersion, W/cm K	0.8866	0.8863	0.8863	1.0685	1.0682	1.0682
Heat capacity of solid	1.046 J/g K *					
Solid thermal conductivity	4.18×10^{-3} J/cm s K *					

* The value used was the one reported for extruded cordierite (Gulati, 1998).

The crystal diffusivity of propylene measured in all the dynamic experiments is around the same value, which is four times smaller than the crystal diffusivity

determined in uptake adsorption curves. Even though, the adsorption equilibrium capacity determined from dynamic and gravimetric methods seems to be the same. As explained before, the sample used for gravimetric measurements was previously treated with air and hydrogen.

Table 6.5 Propylene amount adsorbed and crystal diffusivity in zeolite 4A monolith determined from breakthrough curves.

T, K	Q, cm^3/min	P, kPa	q_{si}, mmol/g	D_c, cm^2/s
423	46.15	1.5	0.0949	$0.50x10^{-13}$
	85.71	1.5	0.0989	$0.53x10^{-13}$
	46.15	5.6	0.3494	$0.60x10^{-13}$
	46.15	10.0	0.5165	$0.64x10^{-13}$
473	46.15	1.5	0.0312	$1.50x10^{-13}$
	85.71	1.5	0.0342	$1.70x10^{-13}$
	46.15	5.6	0.1107	$1.90x10^{-13}$
	46.15	10.0	0.2223	$1.80x10^{-13}$

The difference between the samples used in the gravimetric and dynamic experiments was the thermal treatment prior to the experiments, which may produce some changes in the crystal of zeolite 4A such that the entrance of the molecules is different. Even though, the diffusivities determined in these monolithic samples were much smaller than the ones obtained in commercial pellets and in crystals prepared in laboratory, as shown in previous chapters. The reason of the difference of diffusivities is not known and is located in the crystals of zeolite 4A and not in the monolith structure, as probed by the ZLC experiments with crushed samples.

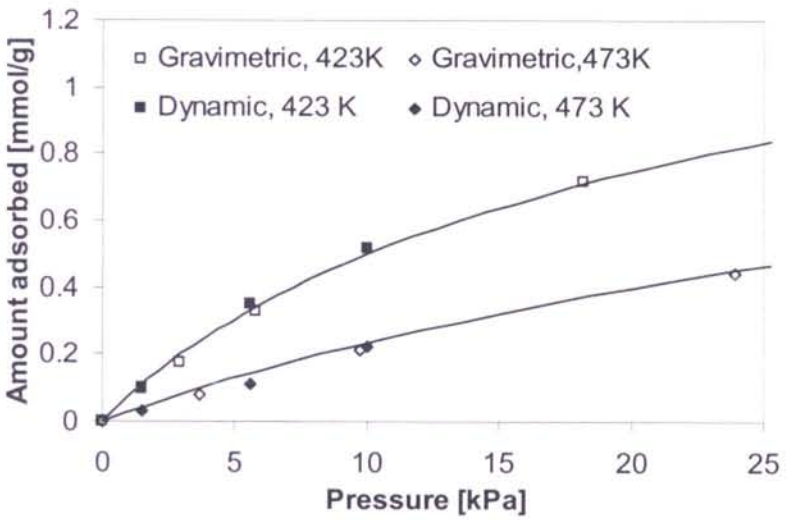

Figure 6.16. Adsorption equilibrium of propylene in zeolite 4A monolith. Comparison between gravimetric (empty points) and dynamic (solid points) data. Solid line correspond to the fitting of the gravimetric data using the Nitta model

6.8 Conclusions

Adsorption equilibrium of propane and propylene was measured in a honeycomb monolith where zeolite 4A crystals were mixed with an inert material by extrusion. The data were collected at 423 and 473 K and in a pressure range from 0-100 kPa. Adsorption equilibrium was measured using a gravimetric Rubotherm unit and some points determined from breakthrough curves were also determined for comparison. Adsorption equilibrium data of both gases were comparable with the previous data obtained in zeolite 4A commercial extrudates, indicating that the amount of inert in the honeycomb structure is around 20%.

Adsorption kinetics was also studied by differential uptakes and by breakthrough curves. The average diameter of the zeolite crystals is 1.4 μm determined from SEM measurements. In all the experiments the diffusion process was controlled by crystal diffusion. The diffusivity of both hydrocarbons is lower than previous values obtained

other zeolite 4A materials (commercial extrudates and laboratory prepared crystals). In the case of propylene, the difference is large being of an order of magnitude. The propylene diffusivities obtained in differential uptakes is also four times higher from those obtained from breakthrough curves: $D_c(423K) = 0.50\text{-}0.64 \times 10^{-13}$ cm²/s by dynamic experiments against $D_c(423K) = 1.50\text{-}2.30 \times 10^{-13}$ cm²/s from differential uptakes. This difference may be due to different thermal treatment prior to the experiments, although more studies are required to confirm this.

Nomenclature

a_i	number of neighboring sites occupied in the Nitta model
a'	area to volume ratio, m^{-1}
A	sectional area of the monolith, m^2
C_i	bulk molar concentration of component i in the gas phase, mol/m^3
C_i^*	molar concentration of component i in the gas phase at the channel wall surface, mol/m^3
$C_{i,feed}$	gas molar concentration of component i in the feed stream, mol/m^3
c_p	heat capacity of the gas phase, J/kg K
C_{pi}	gas molar concentration of component i in the macropores of the channel wall, mol/m^3
c_{ps}	heat capacity of the material of the monolith, J/kg K
D_{ax}	axial dispersion coefficient, m^2/s
$D_{c,i}$	crystal diffusivity of component i, m^2/s
$D_{c,i}^o$	limiting crystal diffusivity of component i at infinite temperature, m^2/s
D_m	molecular diffusivity of the gas, m^2/s
$D_{p,i}$	pore diffusivity of component i, m^2/s

$E_{a,i}$	activation energy of crystal diffusion for component *i*, J/mol
h_f	film heat transfer between the gas and the channel wall, W/m² K
$K_{eq,i}$	equilibrium constant of the component *i*, kPa^{-1}
$K_{eq,i}^{o}$	equilibrium constant of component *i* at the limit T → ∞, kPa^{-1}
k_f	film mass transfer coefficient, m/s
ℓ	thickness of the monolith channel wall, m
L_c	length of the monolith channel, m
M_w	molecular weight, kg/mol
n_d	number of channels per unit area
P	gas pressure, kPa
P_f	gas pressure at the end of the channel, kPa
q_i	adsorbed phase concentration of hydrocarbon, mol/kg
$\overline{q}_i$	crystal averaged amount adsorbed phase concentration, mol/kg
$\langle \overline{q_i} \rangle$	averaged adsorbed phase concentration of hydrocarbon, mol/kg
$q_{max,i}$	maximum adsorbed phase concentration of component *i*, mol/kg
$q_{s,i}$	adsorbed phase concentration of component *i* in the crystal surface, mol/kg
Q	total gas flowrate used in breakthrough experiments, m³/s
r_c	crystal radius of zeolite 4A, m
R	spatial coordinate inside the adsorbent in the simplified model (case 2: lumped parameter model), m
R_x	half-length of a single channel in the *x* spatial coordinate
R_y	half-length of a single channel in the *y* spatial coordinate
T_{feed}	gas temperature of the feed stream, K
T_g	gas temperature, K

T_s	solid temperature, K
v_z	velocity of the gas in each channel, m/s
$v_{z,feed}$	velocity of the gas in each channel for z=0 (entrance of the monolith), m/s
u_i	overall interstitial velocity of the gas ($Q/A\varepsilon_m$), m/s

Greek Letters

$(-\Delta H_i)$	heat of adsorption of component *i*, J/mol
ΔP	pressure drop in the monolith channel, kPa
λ	thermal conductivity of the gas, W/m.K
λ_s	thermal conductivity of the solid, W/m K
ρ	gas density, kg/m^3
ρ_b	bulk density of the monolith column, kg/m^3
ρ_w	density of the channel wall, kg/m^3
δ	thermal axial dispersion, W/m K
ε_m	monolith porosity
ε_w	porosity of the channel walls
μ_g	gas viscosity, Pa.s

References

Bird, R.B.; Stewart, W.E; Lightfoot, E.N. *Transport Phenomena*, 2nd edition, Wiley International, Singapore, **2002**.

Boger, T.; Heibel, A. K.; Sorensen, C. M. Monolith Catalysts for the Chemical Industry. *Ind. Eng. Chem. Res.*, **2004**, 43, 4602-4611.

Brilhac, J. F.; Sultana, A.; Gilot, P.; Martens, J. A. Adsorption and Pressure Swing Desorption of NOx in Na-Y Zeolite: Experiments and Modelling. *Environ. Sci. Technol.*, **2002**, 36, 1136-1140.

Burchell, T. D.; Judkins, R. R.; Rogers, M. R.; Williams, A. M. A Novel Process and Material for the Separation of Carbon Dioxide and Hydrogen Sulfide Gas Mixtures. *Carbon*, **1997**, 35, 1279-1294.

Cavenati, S.; Grande, C. A.; Rodrigues, A. E. Adsorption Equilibrium of Methane, Carbon Dioxide and Nitrogen on Zeolite 13X at High Pressures. *J. Chem. Eng. Data*, **2004**, 49, 1095-1101.

Critoph, R. E. Multiple Bed Regenerative Adsorption Cycle Using the Monolithic Carbon-Ammonia Pair. *Applied Thermal Engng.*, **2002**, 22, 667-677.

Da Silva, F. A. *Cyclic Adsorption Processes: Application to Propane / Propylene Separation*. Ph.D. Dissertation, University of Porto, Portugal, **1999**.

Eic, M.; Ruthven, D. M. A New Experimental Technique For Measurement of Intracrystalline Diffusivity. *Zeolites* **1988**, 8, 40-45.

Eldridge, R. B. Olefin/Paraffin Separation Technology: a Review. *Ind. Eng. Chem. Res.*, **1993**, 32, 2208-2212.

Fedorov, A. G.; Viskanta, R. Analysis of Transient Heat/Mass Transfer and Adsorption/Desorption Interactions. *Int. J. Heat Mass Transfer*, **1999**, 42, 803-819.

Groppi, G; Tronconi, E.; Berg, M.; Forzatti, P. Development and Application of Mathematical Models of Pilot-Scale Catalytic Combustors Fueled by Gasified Biomass. *Ind. Eng. Chem. Res.*, **2000**, 39, 4106-4113.

Gadkaree, K. P. *System and Method for Adsorbing Contaminants and Regenerating the Adsorber*. U.S. Patent 5,658,372, **1997**.

Gorbach, A. B.; Stegmaie, M.; Eigenberger, G.; Hammer, J.; Fritz, H.-G. *Compact Pressure Swing Adsorption Processes – Impact and Potential of New – Type Adsorbent – Polymer Monoliths*. FOA 8, Sedona (USA) 23-28 May, **2004**.

Grande, C. A.; Gigola, C. E. *Activity and Selectivity of Commercial Catalysts for Acetylene Removal* (*in Spanish*), XXI Congreso Argentino de Catálisis, San Luis (Argentina) 28-30 September **1999**.

Grande, C. A.; Cavenati, S.; Rodrigues, A. E. *Carbon Molecular Sieves for Hydrocarbon Separations by Adsorption*. CARBON 2004, Rhode Island (United States), 11-16 July, **2004**.

Gulati, S. T. *Ceramic Catalyst Supports for Gasoline Fuel. in Structured Catalysts and Reactors* (Editors: A. Cybulski and J. A. Moulijn), Marcel Dekker, New York, **1998**.

Gupta, N.; Balakotaiah, V. Heat and Mass Transfer Coefficients in Catalytic Monoliths. *Chem. Eng. Sci.*, **2001**, 56, 4771-4786.

Hawthorn, R. D.; Afterburner Catalysts. Effect of Heat and Mass Transfer Between Gas and Catalytic Surface. *AIChE Symp. Ser.*, **1974**, 137, 428-437.

Heibel, A. K.; Vergeldt, F. J.; Van As, H.; Kapteijn, F.; Moulijn, J.; Boger, T. Gas and Liquid Distribution in the Monolith Film Flow Reactor. *AIChE J.*, **2003**, 49, 3007-3017.

Irandoust, S.; Anderson, B. Monolithic Catalysts for Nonautomobile Applications. *Catal. Rev. Sci. Eng.*, **1988**, 30, 341-392.

Jain, R.; LaCava, A. I.; Maheshwary, A.; Ambriano, J. R.; Acharya, D. R.; Fitch, F. R. *Air Separation Using Monolith Adsorbent Bed*. U. S. Patent, 6,231,644, **2001**.

Kim, D. J.; Kim, J. W.; Yie, J. E.; Moon, H. Temperature-Programmed Adsorption and Characteristics of Honeycomb Hydrocarbon Adsorbers. *Ind. Eng. Chem. Res.*, **2002**, 41, 6589-6592.

Kopaygorodsky, E. M.; Guliants, V. V.; Krantz, W. B. Predictive Dynamic Model of Single-Stage Ultra-Rapid Pressure Swing Adsorption. *AIChE J.*, **2004**, 50, 953-962.

Langer, R. L.; Marlor, A. J. *Intumescent Sheet Material*. U.S. Patent 4,305,992, **1981**.

Lee, L. Y.; Perera, S. P.; Crittenden, B. D.; Kolaczkowski, S. T. Manufacture and Characterization of Silicalite Monoliths. *Adsorp. Sci. Technol.*, **2000**, 18, 147-170.

Li, Y. Y.; Perera, S. P.; Crittenden, B. D.; Brisgwater, J. The Effect of Binder on the Manufacture of a 5A Zeolite Monolith. *Powder Technology*, **2001**, 116, 85-96.

Li, Y. Y.; Perera, S. P.; Crittenden, B. D. Zeolite Monoliths for Air Separation. Part 2: Oxygen Enrichment, Pressure Drop and Pressurization. *Trans IchemE*, **1998**, 76, 931-941.

Lopez, E.; Schbib, N. S.; Gigola, C. E.; Bucala, V. Influence of the methane combustion kinetic model on the operating conditions of an autothermal catalytic reactor. *Ind. Eng. Chem. Res.*, **2001**, 40, 5199-5205.

Lozano-Castello, D.; Cazorla-Amoros, D.; Linares-Solano, A.; Quinn, D. F. Activated Carbon Monoliths for Methane Storage. Influence of Binder. *Carbon*, **2002**, 40, 2817-2825.

Martin del Valle, E.; Galan Serrano, M. A.; Cerro, R. L. Use of Ceramic Monoliths as Stationary Phase in Affinity Chromatography. *Biotechnol. Prog.*, **2003**, 19, 921-927.

Pinkas, P.; Snita, D.; Kubicek, M.; Marek, M. Modelling of Spatiotemporal Patterns in a Sequence of Catalytic Monolith Reactors. *Chem. Eng. Sci.*, **1996**, 51, 3157-3162.

Ramachandran, R.; Dao, L. H.; Brooks, B. *Method of Producing Unsaturated Hydrocarbons and Separating the Same from Saturated Hydrocarbons*. U.S. Patent 5,365,011, **1994**.

Ruthven, D. M., Farooq, S., Knaebel, K. S. *Pressure Swing Adsorption*, VCH Publishers, New York, **1994**.

Schnidt, L. D.; Bodke, A. *Process for the Production of an Oxidation Catalyst On-line.* U.S. Patent 6,365,543, **2002**.

Shah, D. B.; Perera, S. P.; Crittenden, B. D. *Adsorption Dynamics in a Monolithic Adsorbent*. Fundamentals of Adsorption (Editor: M. D. LeVan), Kluwer Academic Publishers, Boston, USA, **1996**.

Shen, D. Jale, S. R.; Fitch, F. R.; Jain, R.; Shirley, A. I.; Lu, Y.; Acharya, D. R. *Activation Process for Monolith Adsorbents*. U. S. Patent 6,409,801, **2002**.

Silva, J. A. C. *Separation of n/iso – Paraffins by Adsorption Process.* Ph.D. Dissertation, University of Porto, Portugal, **1998**.

Tronconi, E.; Forzatti, P. Adequacy of Lumped Parameter Models for SCR Reactors with Monolith Structure. AIChE J., **1992**, 38, 201-210.

Ullmann's Encyclopedia of Industrial Chemistry; 7ª Edition, Wiley-VCH, Verlag GmbH & Co..KGaA, **2003**.

Valdes-Solis, T.; Linders, M. J. G.; Kapteijn, F.; Marban, G.; Fuertes, A. B. Adsorption and Breakthrough Performance of Carbon-Coated Ceramic Monoliths at Low Concentration of n-Butane. *Chem. Eng. Sci.*, **2004**, 59, 2791-2800.

Yang, R. T. *Gas Separation by Adsorption Processes.* Butterworths, Boston, **1987**.

Yang R.T. *Adsorbents. Fundamentals and Applications,* New Jersey: J. Wiley, **2003**.

Yates, M.; Blanco, J.; Martin-Luengo, M. A.; Martin, M. P. Vapour Adsorption Capacity of Controlled Porosity Honeycomb Monoliths. *Micropor. Mesopor. Mater.*, **2003**, 65, 219-231.

Yu, F. D.; Luo, L. A.; Grevillot, G. Adsorption Isotherms of VOCs Onto an Activated Carbon Monolith: Experimental Measurement and Correlation with Different Models. *J. Chem. Eng. Data.*, **2002**, 47, 467-473.

7. Separation of Propane and Propylene by Pressure Swing Adsorption, PSA

When dealing with adsorption processes for gas separation, Pressure Swing Adsorption, PSA is the most industrialized technology of this category (Sircar, 2002).

It is the purpose of this Chapter to present the performance evaluation of a PSA unit for propane – propylene separation with some of the adsorbents used in the previous chapters. Only the more selective adsorbents were selected to perform PSA experiments and / or simulations. Carbon molecular Sieve 4A (Takeda Corporation) and zeolite 4A (CECA) were used for PSA experiments while only simulations were performed with the silver impregnated mesoporous SBA-15. We used two different compositions for experiments: 85 / 15 and nearly equimolar mixtures: 52 / 48 for CMS 4A and 54 / 46 for zeolite 4A (propylene to propane ratio). This mixture is an intermediate value (between refinery grade propylene and propylene stream coming from the propane dehydrogenation unit) used as example of the PSA behavior when using a more diluted mixture.

7.1 PSA Propane – propylene separation: state of the art

Pressure Swing Adsorption is an alternative gas separation process that relies on the use of a surface where selectively one or more components of a gaseous mixture are preferentially adsorbed while other(s) are not preferentially adsorbed. This selective surface is helpful to increase the separation factor in cases of difficult separations, saving energy. But the decision whether to use this process or other is always mainly based on separation costs. In the case of air separation for N_2 supply this technology is favourable for feed flowrate in the range 100-1000 m^3/h (Mersmann et al., 2000). In the

case of propane – propylene separation, the savings in energy can be considerable, at least theoretically, when comparing to distillation.

Pressure Swing Adsorption is used since 1960 when the first patent of air separation by PSA cycle was filled (Skarstrom, 1960). An alternative process using vacuum desorption blowdown was filled in 1964 (Guerin de Montgareuil and Domine, 1964). Since that time PSA technology is commercially used in many industrial applications. It is commercially applied in n-iso paraffin separation (Silva and Rodrigues, 1998), hydrogen purification (Ruthven et al., 1994), nitrogen production from air using carbon molecular sieves (Ruthven et al., 1986; Schröter and Jüntgen, 1988), methane enrichment from natural gas (Engelhard, 2001) and oxygen recovery for human breathing (Teague and Edgar, 1999; Jee et al., 2001). On research stages are many other systems including flue gas treatment (Na et al., 2002; Ko et al., 2003) and gasoline desulphuration (Yang, 2003). Other new applications of PSA technology in Japan have been also discussed (Izumi, 2004).

The propane / propylene separation by PSA is still in research stage and some processes dealing with specific adsorbents have been patented (Cheng et al., 2001; Yang et al., 2002; Cho et al., 2001; Reyes et al., 2003; Kuznicki and Bell, 2003; Olson, 2002; Choudary et al., 2003). Many available commercial adsorbents were previously evaluated for this separation (Järvelin and Fair, 1993; Rege et al., 1998; Da Silva and Rodrigues, 1999; Grande et al., 2003b; Yang, 2003). From all the commercial adsorbents, zeolite 4A presented a very high selectivity towards propylene (Järvelin and Fair, 1993; Da Silva and Rodrigues, 1999; Rege et al., 1998). In fact a PSA process (BOC PETROFIN®) using this zeolite as adsorbent was patented (Ramachandran et al., 1994). Even when, in most of the works, propylene with high purity is obtained with zeolite 4A, there are large differences in the recovery of propylene obtained in this

patent and other works (Ramachandran et al., 1994; Da Silva and Rodrigues, 2001; Cheng et al., 2002; Yang et al., 2001). For this particular mixture, as propylene is strongly adsorbed by zeolite 4A the blowdown step has to be done in vacuum so the process can be called VSA-PSA (Vacuum Pressure Swing Adsorption).

When trying to present a VSA-PSA process for propylene separation, three different propylene / propane ratios can be typically found in industry according to the upstream process and / or propylene sources. The stream with more propylene (85 / 15 propylene to propane) comes from the FCC (Fluid Catalytic Cracking) unit which accounts for already 30% of the propylene production. The other common source of propylene found in industry is the "refinery grade propylene" which has a lower content of propylene (67 / 33 propylene to propane ratio) and came from naphta reforming, which is the main source of propylene. The other less found source of propylene (2-4% of total production) is the more diluted one that is coming from the propane dehydrogenation unit (40 / 60 propylene to propane ratio).

Actually in industry, these three streams are used for polymer grade propylene production using distillation columns. The most common name of the distillation column that performs the propane – propylene separation is C_3 – splitter and is located in the separation train of the plant (Ullman's Encyclopedia, 2003).

The conditions used in distillation columns depend on the particular industry where the separation is carried out. Two situations are the most common ones in industry. The first one is that conditions depend on the heat network developed in the plant (mostly for petrochemical operations where propylene and polypropylene production run together). The second case is when no complex heat network is available (mainly in industries where separation of methane and ethane is not important). In this last case the conditions can be chosen as trade – off situation of energy consumption

and process productivity. The size of the column also depends on the composition and flowrates used but also depend on some particular variables like tray design and compacting options and atmospheric conditions (in windy regions the column is divided in two smaller ones). The number of trays in this column is large and with the trays designed by UOP (MD ™ multiple downcorner distillation trays) the distance between them can be diminished and thus the total unit is more compact. Even with that technology, a normal process to treat a feed stream of 100 tons per hour has 232 trays (operating at 313 – 333 K and 25 bars), which means one distillation tower with 70 meters tall. In windy regions a normal solution is to split the C_3 splitter into two different columns in series, with the additional benefit of having chemical grade propylene available at the outlet of the first column.

7.2 Adsorbent selection

In previous chapters, adsorption equilibrium of propane and propylene were measured on several adsorbents. All of them were selective to propylene and also the kinetics of propylene adsorption was faster than that of propane in all of them. There are many parameters used in literature to establish a selective adsorbent for a given separation (Yang, 2003). In this paper we have used the most basic one given before relating the difference in the product amount adsorbed divided by the contaminant and less adsorbed species amount adsorbed. This ratio will be called the equilibrium selectivity factor, β_{EQ}. When this ratio is multiplied by the ratio of the square root of the diffusivities, which results from a simplification of the adsorption uptake at short times (Habgood, 1958), we obtain the kinetic selectivity factor, β_{SEL}, that is defined by:

$$\beta_{SEL} = \frac{\Delta q_{C3H6}}{\Delta q_{C3H8}} \sqrt{\frac{D_{C3H6}}{D_{C3H8}}} = \beta_{EQ} \sqrt{\frac{D_{C3H6}}{D_{C3H8}}} \qquad [7.1]$$

where Δq_{C3H6} and Δq_{C3H8} are the difference of the adsorption equilibrium amounts adsorbed at the partial pressure of the feed and of the counter-current blowdown. Note that we have indicated the diffusivity of both gases simply with a value that can be macropore or micropore diffusivity depending on the adsorbent. It has to be mentioned that other selection factors were evaluated in literature (Rege and Yang, 2001)

In Chapters 2 and 4 we have measured adsorption equilibrium and kinetics of pure components on several commercial adsorbents. The adsorption equilibrium was measured for a range of pressures while adsorption kinetics was only measured for diluted hydrocarbon partial pressures. For this reason we will first calculate the equilibrium selectivity factor (β_{EQ}) for the adsorbents tested. The equilibrium selectivity factor for the four commercial samples tested in this work (narrow pore silica gel, zeolite 5A, carbon molecular sieve 4A and zeolite 4A) at the intermediate temperature used for adsorption equilibrium measurements are shown in Figure 7.1. In this figure the zone below 10 kPa is not plotted because a reasonable blowdown pressure for the VSA-PSA unit is 10 kPa (lower will be unrealistic from an industrial point of view).

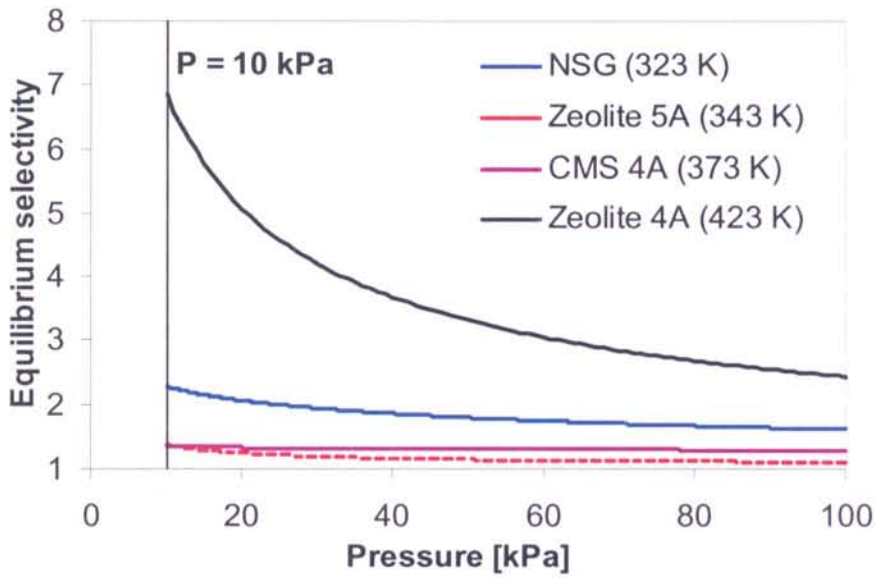

Figure 7.1. Equilibrium selectivity factor of four commercial adsorbents: narrow pore silica gel (NSG), zeolite 5A, carbon molecular sieve 4A and zeolite 4A.

Figure 7.1 shows that none of the adsorbents has equilibrium selectivity over 3 at partial pressures around 100 kPa. That means that in all these adsorbents a separation based in differences of adsorption equilibrium could not be performed. One of the ways to improve propane – propylene separation (the research line followed by the groups of prof. Ralph Yang and also the group of Indian petrochemicals) is to enhance this equilibrium selectivity by impregnation of a transition metal salt to form a π-complexation bond as explained in Chapter 5 (Yang et al., 2001; Cho et al., 2001). With this technique, equilibrium selectivity factors around 35 can be found at pressures higher than 10 kPa. Another approach is the kinetic selectivity improvement. The group of Dr. Kuznicki at Engelhard Corporation successfully followed this research line in many gas separation processes like methane purification (Engelhard, 2001) and more recently in a patent with a material for propane – propylene separation (Kuznicki and Bell, 2003), although technology was not analyzed neither tested in this case. They use fine pore tunable titanosilicates (ETS – 4, Engelhard titanosilicates). At the beginning of this work, the two approaches were scheduled. The reason of measuring adsorption data on silica gel was its future impregnation with silver for π-complexation bond forming with propylene. After some years it was reported that these materials have many drawbacks when used in industrial operations (acetylene and H_2S are poisons for silver and the presence of H_2 reduces the silver deactivating the adsorbent), which lead us to slow down this research line even with the optimistic results obtained from silver impregnated SBA-15 samples reported in Chapter 5. From the kinetic point of view the 4A molecular sieves were considered. As explained in previous chapters, both materials are supposed to have pores that allow propylene adsorption excluding the propane molecule. It was demonstrated in Chapter 2 that propane adsorbs in this material and in Figure 7.1 we can see that the equilibrium selectivity is not very large. Even though the

difference in the diffusivity of propylene and propane is ≈ 100 in zeolite 4A (at 423 K) and ≈ 40 in CMS 4A (at 373 K). This selectivity factor is higher than those of other adsorbents (NSG and zeolite 5A) where the difference in diffusivity of both gases is not large. For this reason these "*kinetic materials*" were chosen to test in PSA experiments for propane – propylene separation, with separation purely based in adsorption kinetic difference between both gases. Also the silver impregnated SBA-15 was considered to run some PSA simulations (experiments were not done because only two grams of material were prepared in powder form and at least 200 grams of pelletized material are required to be used in the PSA column).

7.3 Experimental

The PSA laboratory unit used in this work was already installed in our laboratory for hydrocarbon gas separation (Silva, 1998; Da Silva, 1999). The operating ranges of the equipment are 313-673 K, 10-700 kPa, 0.1-6 SLPM (standard liters per minute at 273 K and 1 bar). The inlet gas and/or the outlet column gas can be analyzed via a multi-port valve system where 11 samples can be stored for subsequent analysis with FID (flame ionization detector) in a Chrompack 9001 gas chromatograph. The analysis of each sample takes 3 minutes so after one cycle is monitored, the loops can be refilled only after 37 minutes (4 minutes for trash-loop analysis + 33 of sample analysis). In practice this means that after sampling the first cycle, the next one is only cycle 8 or 9, depending on the cycle step times. A full description of the unit (operation instructions and control set-up) was given elsewhere (Da Silva, 1999). In Figure 7.2 a simplified scheme of the equipment is shown. In this experimental array, the following variables were recorded and stored in the computer: pressure at the inlet (PT, pressure

transducer) and outlet of the column (BPR, back-pressure regulator), thermocouples (TT1, TT2, TT3) and mass flow controllers (MFC1 to MFC4).

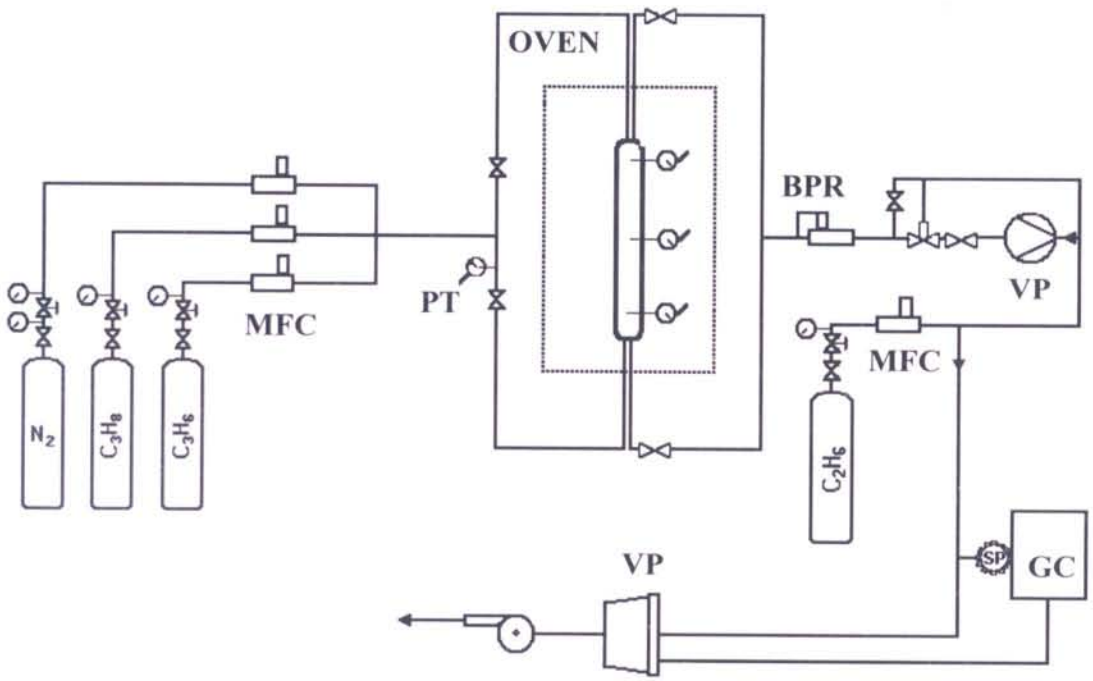

Figure 7.2- Flow diagram of the laboratory PSA unit used in this work: PT, pressure transducer; BPR, back pressure regulator; MFC mass flow controllers; GC, gas chromatograph; VP, vacuum pump.

The experiments reported in this work were performed at different temperatures depending on the adsorbent used: 343 – 423 K for CMS 4A and 423 – 463 K for zeolite 4A. The total high pressure was also varied in the experiments while intermediate and blowdown pressures were always kept at 50 and 10 kPa, respectively in both adsorbents used. Adsorbent activation was done using a flow of nitrogen at the same high temperatures mentioned in Chapters 2-4: 523 K for CMS 4A and 593 K for zeolite 4A. Prior to the activation protocol, the loaded column was kept 18 hours under a small flow of nitrogen and only after, the heating ramp (1K/min) to achieve the activation high temperatures mentioned before started. The samples were kept 24 hours at the high temperature and after that initial treatment, no other high temperature treatment was

performed. Even though, the column was kept with a small flow of nitrogen to avoid air / humidity adsorption that may change the adsorbent properties, when no PSA cycles were run.

Air Liquide provided all gases used in this work: propane N35, propylene N24-(N25) and nitrogen 50 (purity greater than 99.95, 99.4 (99.5) and 99.999% respectively). Propylene N24 was used for zeolite 4A experiments while N25 was used for CMS 4A (Air Liquide only supply propylene N25 from 2003 in Portugal).

7.4 Theoretical

The zeolitic adsorbents are bidisperse materials consisting in an inert matrix (clay binder) that contains the zeolite crystals. For this reason, macro and mesopores of the inert binder may control the mass transfer or this process can be controlled by intracrystalline diffusion in the channels of the zeolite crystals, or even by a combination of both resistances. Also, a film mass transfer resistance may exist in the layer surrounding the pellet. A model to describe breakthrough curves of propane or propylene or binary mixture must contain these resistances. Also the gas-phase axial dispersion would be lumped into a single parameter, the axial dispersion parameter.

As we are working in bulk separations, due to the heat of adsorption / desorption, non-isothermal behavior is expected and the heat balance has to be included in the model. Also due to bulk adsorption, the velocity along the column length will vary and so there will be a net pressure drop, reason why the momentum balance has also to be included in the analysis.

The assumptions for the model that will be used below are the following:

1- Ideal gas behavior

2- Heat, mass and momentum transport in the radial direction of the column are neglected and only axial coordinate is considered.

3- Meso-macropore resistances are lumped in a single parameter, the macropore diffusivity that is obtained relating the Knudsen and molecular diffusion via the Bosanquet equation.

4- Macropore and micropore diffusion equations are described by the LDF (linear driving force) model instead of the mass balances in the macropores and in the zeolite crystals. This assumption has a large impact in computational time.

5- Macropore diffusivity value is not a function of the adsorbed phase concentration. Micropore diffusivity dependence with concentration is described by the Darken law.

6- The void fraction is uniform in the entire column.

With these assumptions the fixed-bed model is described by the following equations (mass, energy and momentum balances). The component mass balance on the column is:

$$\varepsilon_c \frac{\partial C_i}{\partial t} = \varepsilon_c \frac{\partial}{\partial z}\left(D_{ax,i} C_T \frac{\partial y_i}{\partial t} \right) - \frac{\partial (u_i C_i)}{\partial z} - (1-\varepsilon_c)\frac{a' k_{fi}}{Bi_i + 1}\left(C_i - \overline{c_i}\right) \qquad [7.2]$$

where C_i is the gas-phase concentration, $D_{ax,i}$ is the axial dispersion coefficient, u_i is the interstitial velocity, ε_c is the column porosity, y_i is the molar fraction, k_{fi} is the film mass transfer resistance, $\mathrm{Bi}_i = R_p k_{fi} / (5\varepsilon_p D_{p,i})$ is the Biot number and $\overline{c_i}$ is the averaged concentration in the macropores, all valid for component i, while C_T is the total gas concentration and a' is the pellet specific area.

The momentum balance is the balance of forces acting in a reference control volume. In this model we will only consider the terms of pressure drop and velocity changes, and relate them by the Ergun equation, defined by:

$$\frac{\partial P}{\partial z} = -\frac{150\,\mu_g\,(1-\varepsilon_c)^2}{\varepsilon_c^{\,3}\,d_p^{\,2}}u_i + \frac{1.75\,(1-\varepsilon_c)\rho_g}{\varepsilon_c^{\,3}\,d_p}|u_i|\,u_i \qquad [7.3]$$

where P is the total pressure, μ_g is the gas viscosity, d_p is the pellet diameter and ρ_g is the gas density.

As expressed above, we will assume a LDF model for the mass transfer rate from the gas phase to the macropores:

$$\varepsilon_p \frac{\partial \overline{c_i}}{\partial t} + \rho_p \frac{\partial \langle \overline{q_i} \rangle}{\partial t} = \varepsilon_p \frac{15\,D_{p,i}}{R_p^{\,2}} \frac{Bi_i}{Bi_i + 1}\left(C_i - \overline{c_i}\right) \qquad [7.4]$$

where $D_{p,i}$ is the pore diffusivity, R_p is the pellet radius, ρ_p is the particle density, ε_p is the pellet porosity, w_c is the adsorbent weight and $\langle \overline{q_i} \rangle$ is the pellet averaged adsorbed phase concentration.

The LDF equation for the crystals averaged over the entire pellet is expressed by:

$$\frac{\partial \langle \overline{q_i} \rangle}{\partial t} = \frac{15\,D_{c,i}}{r_c^{\,2}}\left(q_i^{\,*} - \langle \overline{q_i} \rangle\right) \qquad [7.5]$$

where $D_{c,i}$ is the crystal diffusivity, r_c is the crystal radius and $q_i^{\,*}$ is the adsorbed phase concentration in the equilibrium state. In the case of zeolite 4A, the adsorption equilibrium was described previously with the multisite Langmuir model (Grande et al., 2003a).

The energy balance will take into account the three phases present: gas, solid and column wall. The gas phase energy balance is:

$$\varepsilon_c C_t \widetilde{C}_v \frac{\partial T_g}{\partial t} = \frac{\partial}{\partial z}\left(\lambda \frac{\partial T_g}{\partial z}\right) - u_t C_t \widetilde{C}_p \frac{\partial T_g}{\partial z} + \varepsilon_c R_g T_g \frac{\partial C_t}{\partial t} - (1-\varepsilon_c) a' h_f (T_g - T_s) - \frac{2 h_w}{R_w}(T_g - T_w) \quad [7.6]$$

where $\widetilde{C}_v$ is the molar constant volume specific heat of the gas mixture, T_g is the temperature of the gas-phase, λ is the axial heat dispersion, $\widetilde{C}_p$ is the molar constant pressure specific heat of the gas mixture, R_g is the universal gas constant, h_f is the film heat transfer coefficient between the gas and the solid phase, T_s is the solid temperature (extrudates), h_w is the film heat transfer coefficient between the gas phase and the column wall, R_w is the column radius and T_w is the wall temperature.

The solid phase energy balance is expressed by:

$$(1-\varepsilon_c)\left[\varepsilon_p \sum_{i=1}^{n} \overline{c_i}\, \widetilde{C}_{vi} + \rho_p \sum_{i=1}^{n} \left\langle \overline{q_i} \right\rangle \widetilde{C}_{v,ads,i} + \rho_p \widetilde{C}_{ps}\right] \frac{\partial T_s}{\partial t} = (1-\varepsilon_c)\varepsilon_p R_g T_s \frac{\partial \overline{c_i}}{\partial T} + \rho_b \sum_{i=1}^{n} (-\Delta H_i) \frac{\partial \left\langle \overline{q_i} \right\rangle}{\partial t} + (1-\varepsilon_c) a' h_f (T_g - T_s) \quad [7.7]$$

where ρ_b is the bulk density of the column and $(-\Delta H_i)$ is the isosteric heat of adsorption of component *i*.

Finally, the wall energy balance can be expressed by:

$$\rho_w \widetilde{C}_{pw} \frac{\partial T_w}{\partial t} = \alpha_w h_w (T_g - T_w) - \alpha_{wl} U (T_w - T_\infty) \quad [7.8]$$

with:

$$\alpha_w = \frac{D_w}{e(D_w + e)} \quad [7.9]$$

$$\alpha_{wl} = \frac{1}{(D_w + e)\ln\left(\frac{D_w + e}{D_w}\right)} \quad [7.10]$$

where α_w is the ratio of the internal surface area to the volume of the column wall, α_{wl} is the ratio of the logarithmic mean surface area of the column shell to the volume of the

column wall, D_w is the internal diameter of the column, e is the wall thickness, $\hat{C}_{pw}$ is the specific heat of the column wall, U is the global external heat transfer coefficient and T_∞ is the oven constant set-point temperature.

The model described in this work was previously used in our laboratory for propane-propylene separation in a Pressure Swing Adsorption (PSA) unit, and even the notation was almost kept invariant (Da Silva, 1999).

Equations [7.2-7.8] are partial differential equations; they need boundary and initial conditions. Such conditions depend on the conditions applied to the column. In a PSA unit, the same column is exposed to various different steps that require different conditions. For this purpose, we will mention the different steps that were used in this work together with the initial and boundary conditions.

Adsorption equilibrium of pure components and the binary mixtures were determined in a previous work (Grande et al., 2003a). The multisite Langmuir model will be used in this work. The parameters for propane and propylene are given in Table 2. Nitrogen is assumed to be a non-adsorbing gas at the operating temperature. The multisite Langmuir model is expressed by (Nitta, 1984):

$$\frac{q_i^*}{q_{\max,i}} = K_{\mathrm{eq},i}\, y_i P \left(1 - \sum \frac{q_i^*}{q_{\max,i}} \right)^{a_i} \qquad [7.11]$$

where $q_{max,i}$ is the maximum amount adsorbed, a_i is the number of sites occupied per molecule and with an exponential temperature dependence for the adsorption constant $K_{eq,i}$ described as:

$$K_{eq,i} = K_{eq,i}{}^{0} \exp\left(\frac{-\Delta H_i}{R_g T_s} \right) \qquad [7.12]$$

where $K_{eq,i}{}^{0}$ is the infinite adsorption constant and $(-\Delta H_i)$ is the isosteric heat of adsorption, both for component i.

The crystal diffusivity of propane and propylene at infinite dilution is a function of temperature described by:

$$D^{\infty}_{c,i} = D^{\infty}_{c,i,0}.\exp(-E_a/R_g T) \quad [7.13]$$

where $D^{\infty}_{c,i,0}$ is the limiting diffusivity at high temperatures and E_a is the activation energy. The micropore diffusivity as used in the LDF constant (eq. 7.5) also depends on concentration. In this work we described this dependency by the Darken´s model (Do, 1998):

$$D_{c,i} = D^{\infty}_{c,i} \frac{d\ln(P_i)}{d\ln(q_i)} \quad [7.14]$$

As noted from the theoretical model, some transport parameters are needed. They were calculated from the relations presented below.

The pore diffusivity was calculated with the Bosanquet equation:

$$\frac{1}{D_{p,i}} = \tau_p \left(\frac{1}{D_{m,i}} + \frac{1}{D_{k,i}} \right) \quad [7.15]$$

where $D_{m,i}$ is the molecular diffusivity, $D_{k,i}$ is Knudsen diffusivity, both for component i and τ_p is the pore tortuosity. The molecular diffusivity for the mixture was approximated with:

$$D_{m,i} = \frac{1 - y_i}{\sum_{\substack{j=1 \\ j \neq i}}^{n} \frac{y_i}{D_{ij}}} \quad [7.16]$$

where the binary molecular diffusivity D_{ij} was calculated with the Chapman-Enskog equation (Bird, 2002). The Knudsen diffusivity is calculated by

$$D_{k,i} = 9700 r_p \sqrt{\frac{T_g}{M_w}} \quad [7.17]$$

where r_p is the mean pore radius (cm) and M_w is the molecular weight of the adsorbate.

The axial mass and heat dispersion coefficients as well as the mass transfer and heat convective coefficient were calculated using the Wakao and Funazkri correlations (Wakao and Funazkri, 1978; Yang, 1987, Da Silva, 1999):

$$\frac{\varepsilon D_{ax,i}}{D_{m,i}} = 20 + 0.5 Sc_i Re \qquad [7.18]$$

$$\frac{\lambda}{k_g} = 7 + 0.5 PrRe \qquad [7.19]$$

$$Sh_i = 2.0 + 1.1 Re^{0.6} Sc_i^{1/3} \qquad [7.20]$$

$$Nu = 2.0 + 1.1 Re^{0.6} Pr_i^{1/3} \qquad [7.21]$$

The axial coefficient relations are valid for the range 3<Re<10,000. The dimensional parameters are defined by:

Schmidt number: $Sc_i = \frac{\mu_g}{\rho_g D_{m,i}}$ for component *i*, [7.22]

Reynolds number: $Re = \frac{\rho_g u_i d_p}{\mu_g}$, [7.23]

Prandtl number: $Pr = \frac{\hat{C}_{pg} \mu_g}{k_g}$, [7.24]

Sherwood number: $Sh_i = k_{fi} d_p / D_{m,i}$ for component *i*, [7.25]

Nusselt number: $Nu = h_f d_p / k_g$. [7.26]

In these equations, d_p is the pellet diameter. The global heat transfer coefficient, U, was calculated according to (Incropera and Witt, 1996):

$$\frac{1}{U} = \frac{1}{h_w} + \frac{e d_{in}}{\lambda_w d_{\ln}} + \frac{d_{in}}{d_{ex} h_{ex}} \qquad [7.27]$$

where e is the wall thickness, d_{in} is the internal diameter of the column, λ_w is the wall conductivity, d_{ex} is the external diameter of the column, $d_{\ln} = \frac{(d_{ex} - d_{in})}{ln(d_{ex} - d_{in})}$, h_w is the

internal heat transfer coefficient and h_{ex} is the external convective heat coefficient. The internal convective heat transfer coefficient h_w between gas and the wall column can be estimated with Wasch e Froment correlation (Wasch e Froment, 1972):

$$\frac{h_w d_{in}}{k_g} = 140 + 0.013396 \frac{d_{in}^2}{d_p k_g} Re \qquad [7.28]$$

where h_w is expressed in W/m²K, d_{in} is in m, k_g is the gas conductivity in W/mK and d_p is the pellet diameter in m. The external convective heat transfer coefficient was estimated with the Churchill and Chu correlation (Incropera and Witt, 1996):

$$\frac{h_{ex} L}{k_{g,ex}} = 0.68 + \frac{0.67 Ra^{1/4}}{\left[1 + \left(\frac{0.492}{\mathrm{Pr}}\right)^{9/16}\right]^{4/9}} \qquad [7.29]$$

where the sub-index *ex* represent the properties of the external gas surrounding the column. The Rayleigh number is defined by: $Ra = Gr\,\mathrm{Pr}$ and the Grashof number is: $Gr = \frac{g\beta(T_w - T_\infty)L^3}{\nu\alpha}$ where g = 9.8 m²/s, ν is the kinematic viscosity of the external gas, α is the external thermal diffusivity and β is the thermal expansion coefficient. The properties of the external gas are evaluated at the film temperature: $T_{film} = (T_w - T_\infty)/2$.

General properties of the gases, like density, viscosity, and thermal conductivity were calculated according to Bird, Stewart and Lightfoot, 2002.

The initial conditions are considered only as the initial clean state of the column before the cyclic process starts because the initial conditions of the process once started corresponds to the final stage of the previous step. From the basic point of view in terms of PSA process, the most common steps employed are (Ruthven et al., 1994); pressurization, feed, rinse with product, depressurization, counter-current blowdown and counter-current purge. Depending on the objective of the PSA unit (recovery of the less adsorbed compound or the heavy one) the pressurization step can be performed

with feed or in counter-current fashion with the less adsorbed compound. A brief schematic diagram of these steps is given below, together with the corresponding boundary equations.

Pressurization with feed 	***Inlet, z = 0*** Pressure: $P(0) = P_{inlet}$ Composition: $-\frac{\varepsilon D_{ax,i}}{u_i(0)}\frac{\partial y(i,0)}{\partial z}\Big\|_{z^+} + y(i,0)\|_{z^+} - y(i,0)\|_{z^-} = 0$ Temperature: $-\lambda\frac{\partial T_g(0)}{\partial z}\Big\|_{z^+} + u_i C_t \widetilde{C}_p T_g(0)\|_{z^+} - u_i C_t \widetilde{C}_p T_g(0)\|_{z^-} = 0$ ***Outlet, z = L*** Pressure: $u_i(L) = 0$ Composition: $\frac{\partial y(i,L)}{\partial z}\Big\|_{z^-} = 0$ Temperature: $\frac{\partial T_g(L)}{\partial z}\Big\|_{z^-} = 0$

Pressurization with less adsorbed compound

z = 0

Pressure: $u_t(0) = 0$

Composition: $\left.\frac{\partial y(i,0)}{\partial z}\right|_{z^-} = 0$

Temperature: $\left.\frac{\partial T_g(0)}{\partial z}\right|_{z^-} = 0$

***Inlet*, z = L**

Pressure: $P(L) = P_{inlet}$

Composition: $-\frac{\varepsilon D_{ax,i}}{u_t(L)}\left.\frac{\partial y(i,L)}{\partial z}\right|_{z^-} + y(i,L)\big|_{z^-} - y(i,L)\big|_{z^+} = 0$

Temperature: $\lambda\left.\frac{\partial T_g(L)}{\partial z}\right|_{z^-} + u_t C_t \widetilde{C}_p T_g(0)\big|_{z^-} - u_t C_t \widetilde{C}_p T_g(0)\big|_{z^+} = 0$

Feed step

***Inlet*, z = 0**

Molar flowrate: $u_t(0)C(i,0)\big|_{z^+} = u_t(0)C(i,0)\big|_{z^-}$

Composition: $-\frac{\varepsilon_c D_{ax,i}(i)}{u_t(0)}\left.\frac{\partial y(i,0)}{\partial z}\right|_{z^+} + y(i,0)\big|_{z^+} - y(i,0)\big|_{z^-} = 0$

Temperature: $-\lambda\left.\frac{\partial T_g(0)}{\partial z}\right|_{z^+} + u_t C_t \widetilde{C}_p T_g(0)\big|_{z^+} - u_t C_t \widetilde{C}_p T_g(0)\big|_{z^-} = 0$

***Outlet*, z = L**

Pressure: $P(L) = P_{exit}$

Composition: $\left.\frac{\partial y(i,L)}{\partial z}\right|_{z^-} = 0$

Temperature: $\left.\frac{\partial T_g(L)}{\partial z}\right|_{z^-} = 0$

Rinse with product (propylene)

Inlet, z = 0

Molar flowrate: $u_i(0)C(i,0)\big|_{z^+} = u_i(0)C(i,0)\big|_{z^-}$

Composition: $-\dfrac{\varepsilon_c D_{ax,i}(i)}{u_i(0)}\dfrac{\partial y(i,0)}{\partial z}\bigg|_{z^+} + y(i,0)\big|_{z^+} - y(i,0)\big|_{z^-} = 0$

Temperature: $-\lambda\dfrac{\partial T_g(0)}{\partial z}\bigg|_{z^+} + u_i C_t \widetilde{C}_p T_g(0)\big|_{z^+} - u_i C_t \widetilde{C}_p T_g(0)\big|_{z^-} = 0$

Outlet, z = L

Pressure: $P(L) = P_{exit}$

Composition: $\dfrac{\partial y(i,L)}{\partial z}\bigg|_{z^-} = 0$

Temperature: $\dfrac{\partial T_g(L)}{\partial z}\bigg|_{z^-} = 0$

Co-current depressurization

z = 0

Molar flowrate: $u_i(0) = 0$

Composition: $\dfrac{\partial y(i,0)}{\partial z}\bigg|_{z^-} = 0$

Temperature: $\dfrac{\partial T_g(0)}{\partial z}\bigg|_{z^-} = 0$

Outlet, z = L

Pressure: $P(L) = P_{exit}$

Composition: $\dfrac{\partial y(i,L)}{\partial z}\bigg|_{z^-} = 0$

Temperature: $\dfrac{\partial T_g(L)}{\partial z}\bigg|_{z^-} = 0$

Counter-current blowdown

Outlet, z = 0

Molar flowrate: $P(0) = P_{exit}$

Composition: $\left.\frac{\partial y(i,0)}{\partial z}\right|_{z^-} = 0$

Temperature: $\left.\frac{\partial T_g(0)}{\partial z}\right|_{z^+} = 0$

z = L

Pressure: $u_i(L) = 0$

Composition: $\left.\frac{\partial y(i,L)}{\partial z}\right|_{z^-} = 0$

Temperature: $\left.\frac{\partial T_g(L)}{\partial z}\right|_{z^-} = 0$

Counter-current purge (propane)

Outlet, z = 0

Molar flowrate: $P(0) = P_{exit}$

Composition: $\left.\frac{\partial Y(i,0)}{\partial z}\right|_{z^-} = 0$

Temperature: $\left.\frac{\partial T_g(0)}{\partial z}\right|_{z^-} = 0$

Inlet, z = L

Pressure: $u_i(L)C(i,L)\big|_{z^+} = u_i(L)C(i,L)\big|_{z^-}$

Composition: $-\frac{\varepsilon_c D_{ax,i}}{u_i(L)}\left.\frac{\partial y(i,L)}{\partial z}\right|_{z^-} + y(i,L)\big|_{z^-} - y(i,L)\big|_{z^+} = 0$

Temperature: $\lambda\left.\frac{\partial T_g(L)}{\partial z}\right|_{z^-} + u_i C_t \widetilde{C}_p T_g(0)\big|_{z^-} - u_i C_t \widetilde{C}_p T_g(0)\big|_{z^+} = 0$

The order of the steps as well as its numbering / sequence depends on the specific application of the PSA unit. In this case we are interested in separating propylene, which is the most adsorbed gas in all the adsorbents studied. The arrangement of steps was previously chosen for this separation and is described as follows (Da Silva, 1999): pressurization with feed to a high pressure, P_{high}; feed at constant pressure P_{high}; rinse with product at P_{high}; co-current depressurization to an intermediate pressure P_{inter}; counter-current blowdown to low pressure P_{low}. The choice of the steps was defined because we are interested in the recovery of the most adsorbed gas at a high purity of 99.5% or higher. For this reason, after feed, two different "purification" steps were included. First the rinse with propylene is to displace the propane in the voidage of the column and some of the larger macropores. For the smaller micropores the co-current depressurization intends to desorb more of the less adsorbed compound (propane) and also decrease total pressure to improve propylene desorption also increasing its purity. As the low pressure used in this work is around 10 kPa we have called this process as Vacuum Pressure Swing Adsorption, VSA – PSA. Other alternative configurations tested are discussed for each particular adsorbent.

The performance of the different experiments and simulations was evaluated according to three basic parameters: purity of product, recovery of product and productivity of the PSA. They are defined by (Rota and Wankat, 1990; Da Silva, 1999):

$$PURITY = \frac{\int_0^{tblow} C_{C3H6} u_i\big|_{z=0} dt}{\left(\int_0^{tblow} C_{C3H6} u_i\big|_{z=0} dt + \int_0^{tblow} C_{C3H8} u_i\big|_{z=0} dt \right)} \qquad [7.30]$$

$$RECOVERY = \frac{\int_0^{tblow} C_{C3H6} u_i\big|_{z=0} dt - \int_0^{trinse} C_{C3H6} u_i\big|_{z=0} dt}{\int_0^{tfeed} C_{C3H6} u_i\big|_{z=0} dt} \qquad [7.31]$$

$$PRODUCTIVITY = \frac{\left(\int_0^{tblow} C_{C3H6} u|_{z=0} dt - \int_0^{trinse} C_{C3H6} u|_{z=0} dt \right) Q_o}{t_{total} w_{ads}} \quad [7.32]$$

where w_{ads} is the adsorbent weight loaded in the column, Q_o is the inlet flowrate, t_{feed}, t_{rinse} *and* t_{blow} are the times of the feed, rinse and counter-current blowdown steps, respectively.

The model described in this section was solved using gPROMS (PSA Enterprise, UK). The orthogonal collocation method on finite elements (OCFE) was used in all cases and the number of elements was 35 for zeolite 4A and 25 for CMS 4A. Two interior collocation points were used in each element of the adsorption bed. We have used numerical technique for PDE (Partial Diferential Equations) solution that was previously employed with gPROMS for PSA applications (Nilchan and Pantelides, 1998).

7.5 π-complexation adsorbents: Ag / SBA-15 = 0.5

The final application of these new π-complexation adsorbents is the propane and propylene separation by Pressure Swing Adsorption. As propylene is very strongly adsorbed pressures lower than atmospheric ones will be required and in this cases these units are termed Vacuum Pressure Swing Adsorption (VSA-PSA).

The use of these materials into a VSA-PSA unit requires a final shape into pellets / extrudates because powder adsorbents (like tested in Chapter 5) will produce very large pressure drop into the column that is not desired. It was reported in literature that even when the pore walls of SBA-15 are thicker than the MCM materials, the resistance to pressure is higher in the MCM materials. Even though, in the case of pure SBA-15, a compression of 52 MPa only produced a loss of area of 10% (Hartmann and Vinu, 2002). If the diffusion of both hydrocarbons remains high, the equilibration will

be very fast and main diffusion limitations will be produced by the macropores formed in the compacting procedure. Another alternative are new techniques of SBA-15 crystal growing over solid surfaces of an inert matrix, which may be developed in the near future. Unfortunately we do not have pellets of this material, nor even have enough amounts to fill a PSA column to make experiments and for this reason only simulations are presented in this study.

The LDF model was used to simplify the description of the diffusion process. A cycle with four steps was tested. The steps are:

1. Pressurization up to the final pressure of P_{high} = 250 kPa;
2. Feed at constant pressure where propane is recovered at the top of the column,
3. Rinse with pure propylene to improve product purity,
4. Counter-current blowdown at P_{low} = 10 kPa where propylene product is removed from the system and adsorbent is partially regenerated for a new cycle.

The temperature chosen for simulations was 343 K. A bed of 1 m x 0.0210m was used. Flow rates of feed and purge were 1.50 SLPM (at 101 kPa and 298.15 K) and 0.75 SLPM for the rinse step. Feed and pressurization is done with an equimolar stream of propylene and propane. Adsorbent properties (density and thermal parameters) were calculated as 80% of silica and 20% alumina (as binder).

In Table 7.2 we present some results obtained for propane-propylene separation by VSA-PSA. The parameters used for the simulations are reported in Table 7.1. To describe more in detail the behavior of the material, one of the simulations was chosen as example: run S1. In Figure 7.3, propylene concentration (a), propane concentration (b), propylene amount adsorbed (c), propane amount adsorbed (d) and temperature (e) at

the end of each step when cyclic steady state (CSS) was reached is plotted. In the entire cycle temperature has oscillations of around 20 K degrees. Diffusion of both hydrocarbons in this adsorbent is very fast and the length of mass transfer is limited by axial dispersion and by temperature effects.

Table 7.1. Parameters for VSA-PSA simulations using Ag/SBA-15 = 0.5 for propane – propylene separation at 343 K.

Column parameters		Adsorbent parameters (zeolite 4A)	
Column length, m	1.00	Rinse flowrate, SLPM	0.750
Column radius, m	0.0105	Pellet radius, m	8.10^{-4}
Column porosity	0.40	Pellet density, kg/m^3	1100
Bulk density, kg/m^3	700	Pellet porosity	0.31
Wall density, kg/m^3	8238	Pellet tortuosity	2.0
Wall specific heat, J/kg.K	500	Solid specific heat, J/kg.K	860
Wall heat film transfer coef., W/m^{2}K	45	Feed/Press. Flowrate, SLPM	1.50
Overall heat transfer coef., W/m^2.K	25		

Molar flowrate at the outlet of the column is shown in Figure 7.4. It should be noted that propane leaving the column in the feed and rinse step has a very small concentration of propylene (less than 2%) which means that it can be considered as fuel grade HD-5 propane (USEPA, 2003). This propane is available at higher pressure requiring much less effort for compression into LPG (liquefied petroleum gas) cylinders than using distillation (where it needs to be recompressed). On the other side, in the blowdown step, propylene with purity over 91% is obtained reaching only chemical grade propylene. Even though, to obtain these products, a low value of the blowdown

pressure (P_{low} = 5 kPa) was used. If higher values are employed (P_{low} =10 and 15 kPa) the recovery of propylene decreases considerably due to the steepness of the isotherm and also propane contamination with propylene is unacceptable for fuel grade propane (> 5% propylene). The effect of blowdown pressure in the performance parameters (purity and temperature) for the run S1 (see step times in Table 7.2) is shown in Figure 7.5.

Table 7.2. Propylene purity and recovery for different VSA-PSA cycle conditions with Ag/SBA-15 = 0.5 adsorbent.

Run	P_{low}, kPa	t_{pres}, s	t_{feed}, s	t_{rinse}, s	t_{blow}, s	Purity (%)	Recovery (%)
S1	0.05	50	60	40	140	90.9	97.8
S2	0.10	50	60	40	140	91.0	92.6
S3	0.15	50	60	40	140	91.2	74.7
S4	0.10	50	70	40	140	92.2	81.8
S5	0.10	50	60	50	140	94.2	85.1

If the objective is to obtain polymer grade propylene, an additional step (co-current depressurization to intermediate pressure) has to be included between the rinse step and the counter-current blowdown or increase the rinse step. Both procedures will diminish the propylene recovery lo lower values. Purity of 99.0% was obtained with the 5-step cycle configuration (step times like in run S1 with a depressurization to intermediate pressure of 50 kPa for 20 seconds) but recovery falls to 63%, although the outlet stream of this new step has almost the same composition of the feed and can be recycled to increase the overall recovery, although this scheme was not further studied.

Also, propane contamination with propylene is higher than 5% and thus requiring additional purification for propane fuel grade HD-5.

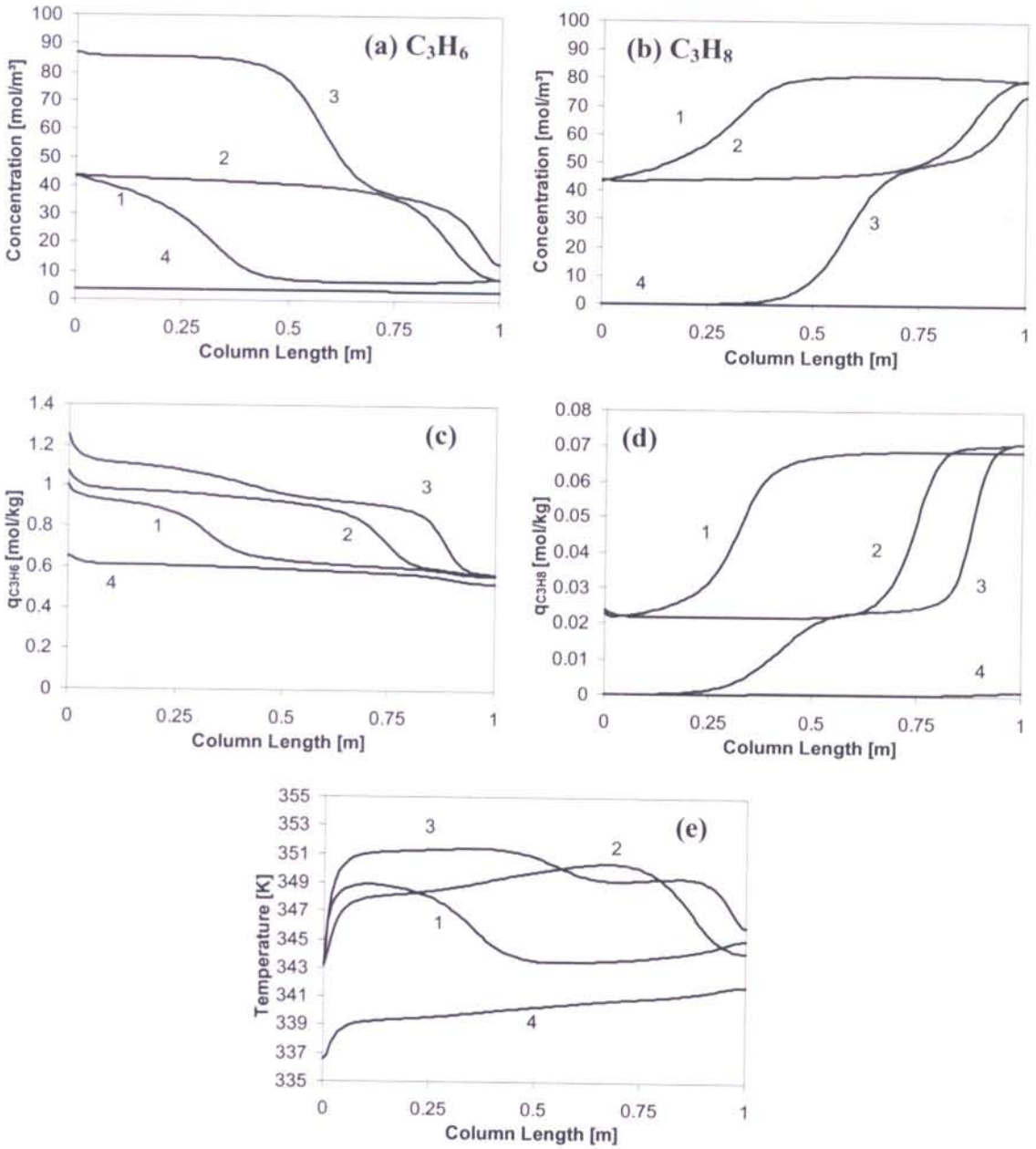

Figure 7.3. VSA-PSA simulation (run S1). (a) propylene concentration, (b) propane concentration in gas phase, (c) propylene adsorbed in the column, (d) propane adsorbed in the column and (e) temperature at the end of each step in cyclic steady state: 1.pressurization (50s); 2. feed (60s); 3. rinse (40s); 4. counter-current blowdown (140s).

As a conclusion we can mention that with a four-step cycle (comprising feed, pressurization, rinse and blowdown) recovery of 97% and propylene with chemical grade purity (91%) was obtained and also fuel grade HD-5 propane was produced at high pressure. If higher propylene purity is required, a five-step cycle has to be used (pressurization, feed, rinse, co-current depressurization to intermediate pressure and counter-current blowdown). Of course that in this case, higher purity can be obtained but with decrease in recovery and productivity (larger cycles).

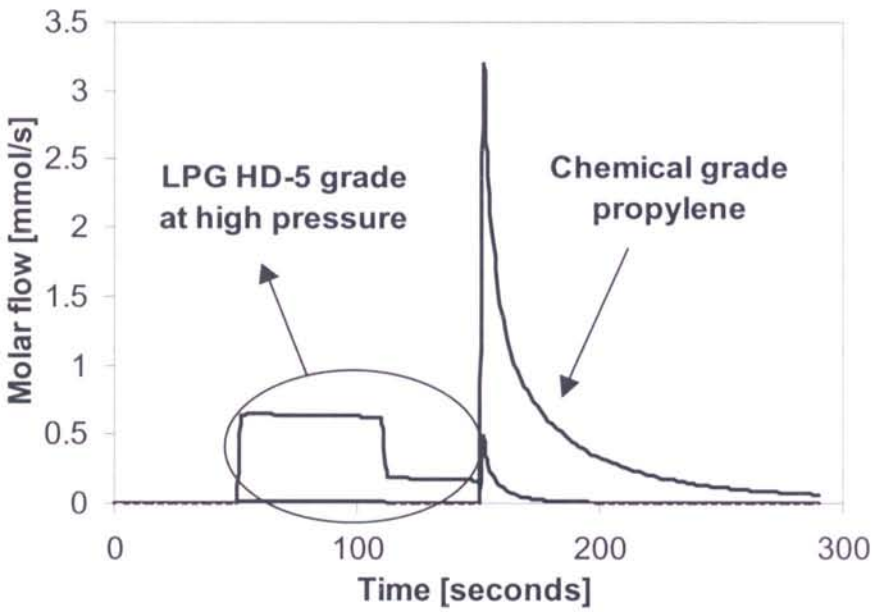

Figure 7.4. Simulated results of molar flowrate of propane and propylene from run S1. LPG HD-5 propane flowrate in the feed and rinse step is circled and chemical grade propylene is indicated from the blowdown step.

As mentioned before, the use of these "silver-loaded" materials is not yet applicable to industrial situations. For this reason the study was not continued for process optimization. Mainly the deactivation of the adsorbent due to the reduction of the Ag^{+} by hydrogen limits the life of the adsorbent. The other contaminants like H_2S or

C_2H_2 can be treated previously to remove them to acceptable conditions but removing the amount of hydrogen "dissolved" in the C_3 mixture will be a very difficult task.

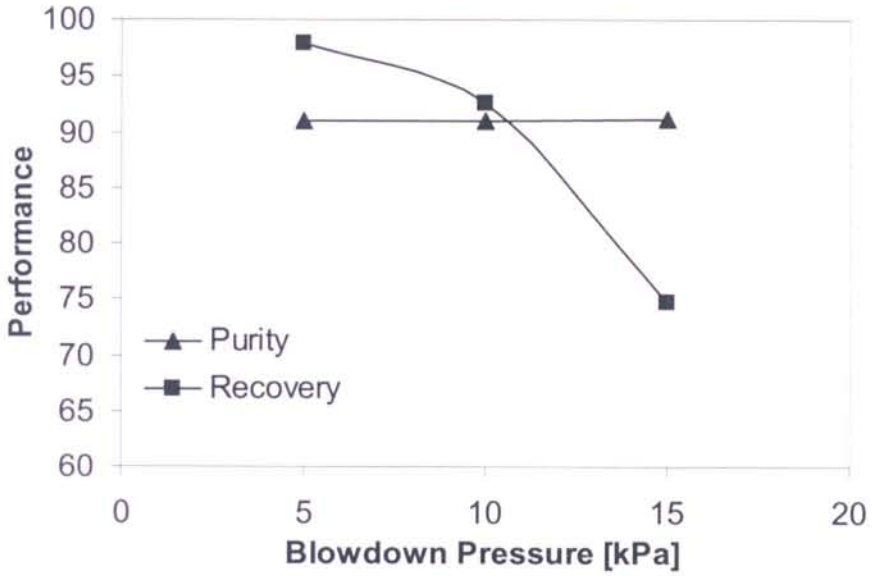

Figure 7.5. Simulated results showing the effect of blowdown pressure in performance parameters for the propane – propylene separation with Ag/SBA-15 = 0.5 (in cyclic steady state regime) with the following step times: 1.pressurization (50s); 2. feed (60s); 3. rinse (40s); 4. counter-current blowdown (140s)

7.6 Carbon Molecular Sieve 4A Takeda

In previous chapters we have presented adsorption equilibrium and kinetics of pure propane and propylene in this adsorbent at 343, 373 and 423 K. Adsorption equilibrium of the binary mixture was also presented in Chapter 3 at 373 K. The next step is to study the binary behavior of the hydrocarbon mixture in fixed bed to "calibrate" the transport parameters to be used in PSA simulations. Fixed bed adsorption equilibrium experiments were already used in literature to determine binary adsorption equilibrium data (Malek and Farooq, 1995; Gorbach et al., 2004), although when large thermal effects are present, the number of transport parameters makes the measurement more complicated.

In this work we have carried out a set of experiments covering the entire range of temperatures used for single component measurements: 343 – 423 K and also explore different pressures: 110, 180, 250 and 320 kPa. Measurements were performed using three feed mixtures with propylene molar fractions of 0.29, 0.55 and 0.80. These molar fractions correspond approximately to three different compositions that may be found in industrial streams (downstream of propane dehydrogenation reaction, refinery grade propylene and fluid catalytic cracking for olefin production, respectively). The parameters required for simulation of all the experiments are listed in Table 7.3.

Table 7.3. Fixed bed parameters and adsorbent properties used in binary fixed-bed experiments of propane – propylene adsorption in CMS4A (Takeda).

Bed Radius, m	0.0105
Bed length, m	0.83
Bed porosity	0.246
Bulk density, kg/m^3	678
Column wall density, kg/m^3	8238
Wall specific heat, J/kgK	500
Wall heat transfer coefficient, W/m^{2}K	40
Overall heat transfer coefficient, W/m^{2}K	20
Pellet radius (infinite cylinder), m	8.0×10^{-3}
Pellet density, kg/m^3	900
Pellet porosity	0.315
Tortuosity	2.0[a]
Solid specific heat, J/kgK	880

[a] Assumed value

Experiments started by passing a fixed flowrate of nitrogen in the column (considered inert in the entire range of temperature) at the corresponding pressure used for measurements. At time zero, the stream is switched to the binary mixture with almost the same flowrate to avoid variations due to change in gas velocity conditions.

The experiments performed at 343 and 423 K at the different propylene molar fractions are presented in two figures to show the data collected. Figure 7.6 contains the molar flowrate of propane and propylene at the exit of the column while Figure 7.7 has the temperature profiles measured in three different points of the column (0.17, 0.43 and 0.68 m) from feed inlet. Solid lines in both figures correspond to the prediction of the model described in the theoretical section. It can be seen that the model can describe well the full set of data based only on pure component adsorption equilibrium and kinetics previously measured (Grande et al., 2003b).

Note that for high propylene molar fractions the temperature variations due to adsorption is larger than 30 K in the experiment made at the lower temperatures (343 K). Also, in all the curves separate temperature peaks corresponding to the adsorption of propane and propylene can be separately observed. This allows us to confirm that the isosteric heats of adsorption determined from the multisite Langmuir can be correctly used in the energy balance to describe multicomponent adsorption equilibrium in fixed bed adsorption. This check is very important in the design of Vacuum Pressure Swing Adsorption (VSA-PSA) units.

Another operational variable that was studied in this work was the total pressure. In Figure 7.8 we can see the curves with 55-45 (propylene to propane ratio) at 110, 180, 250 and 320 kPa measured at 373 K. In this case also the model represents well the molar flowrate exiting the column as well as the temperature variations in the column. It can be seen also that as higher is the pressure the amount of gases adsorbed in the bed is

higher (takes more time to breakthrough of propane and propylene) and also the temperature variations are higher.

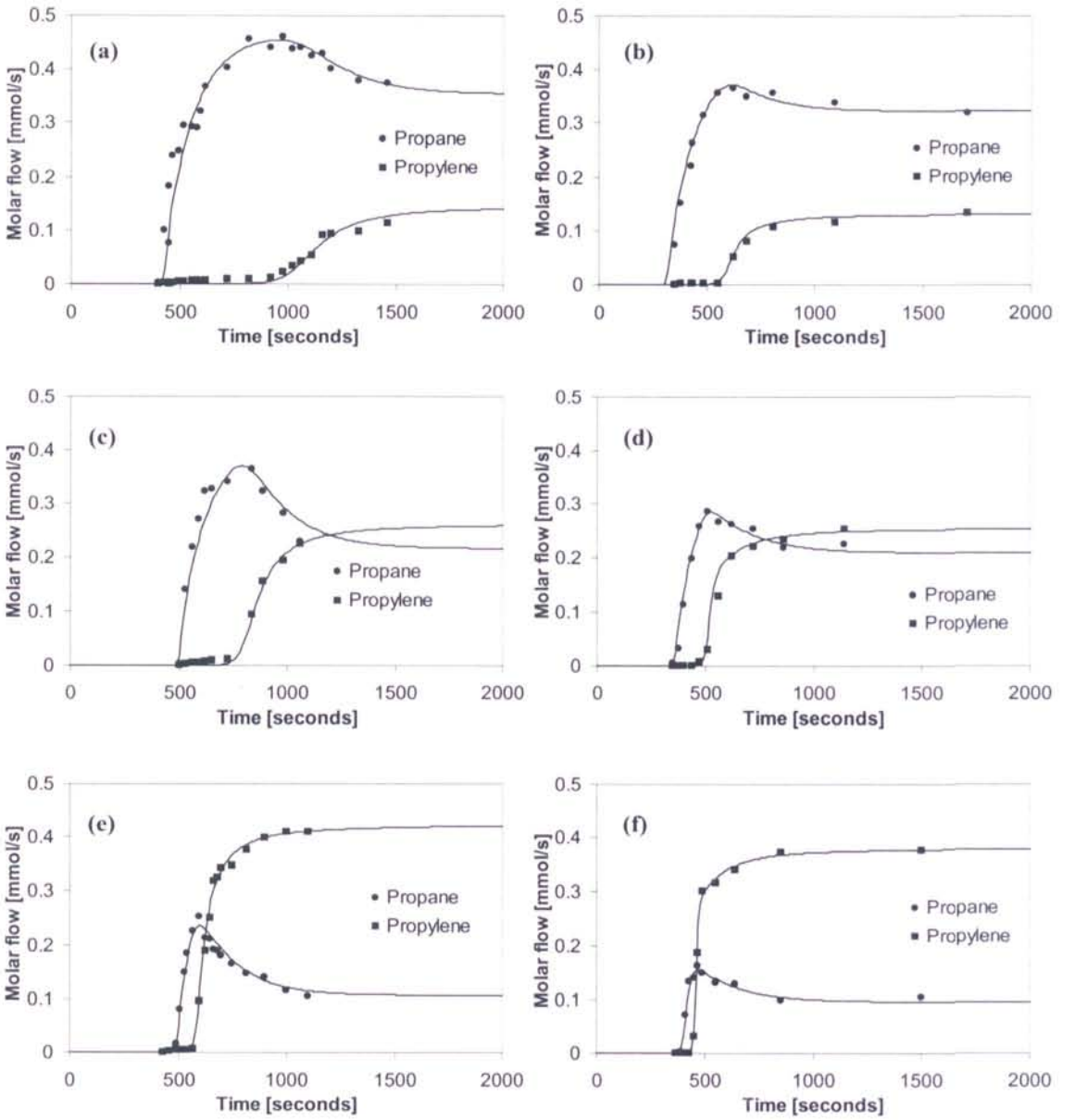

Figure 7.6. Binary propane – propylene breakthrough curves (expressed in molar flow of gases at the exit of the column) in CMS4A (Takeda) at 250 kPa. Curves (a) and (b) have a molar fraction of propylene of 0.29 (0.71 of propane); (c) and (d) have a molar fraction of propylene of 0.55 (0.45 for propane); (e) and (f) have 0.80 propylene and 0.20 propane. Figures (a), (c) and (e) were measured at 343 K while (b), (d) and (f) were at 423 K. Solid points are experimental data and lines are the prediction with the model.

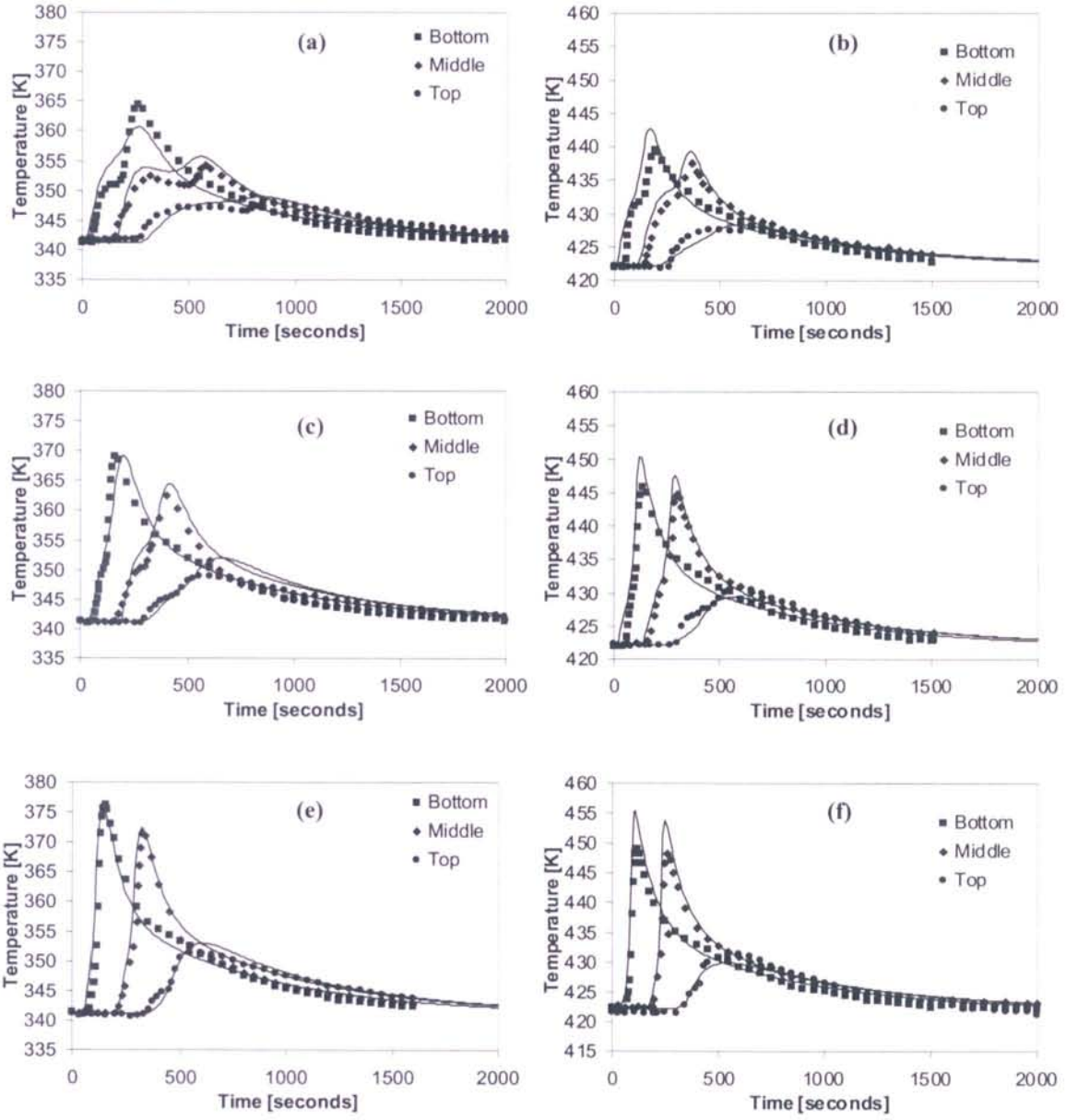

Figure 7.7. Temperature profiles corresponding to the binary propane – propylene breakthrough curves in CMS 4A (Takeda) at 250 kPa. Molar fractions of the curves are: (a) and (b) 0.29 C_3H_6 - 0.71 C_3H_8; (c) and (d) 0.55 C_3H_6 - 0.45 C_3H_8; (e) and (f) 0.80 C_3H_6 - 0.20 C_3H_8. Figures (a), (c) and (e) were measured at 343 K while (b), (d) and (f) were at 423 K. Temperatures were measured at 0.17m (Bottom), 0.43 m (Middle) and 0.68 m (Top) from feed inlet. Solid points are experimental data and lines are the prediction with the model.

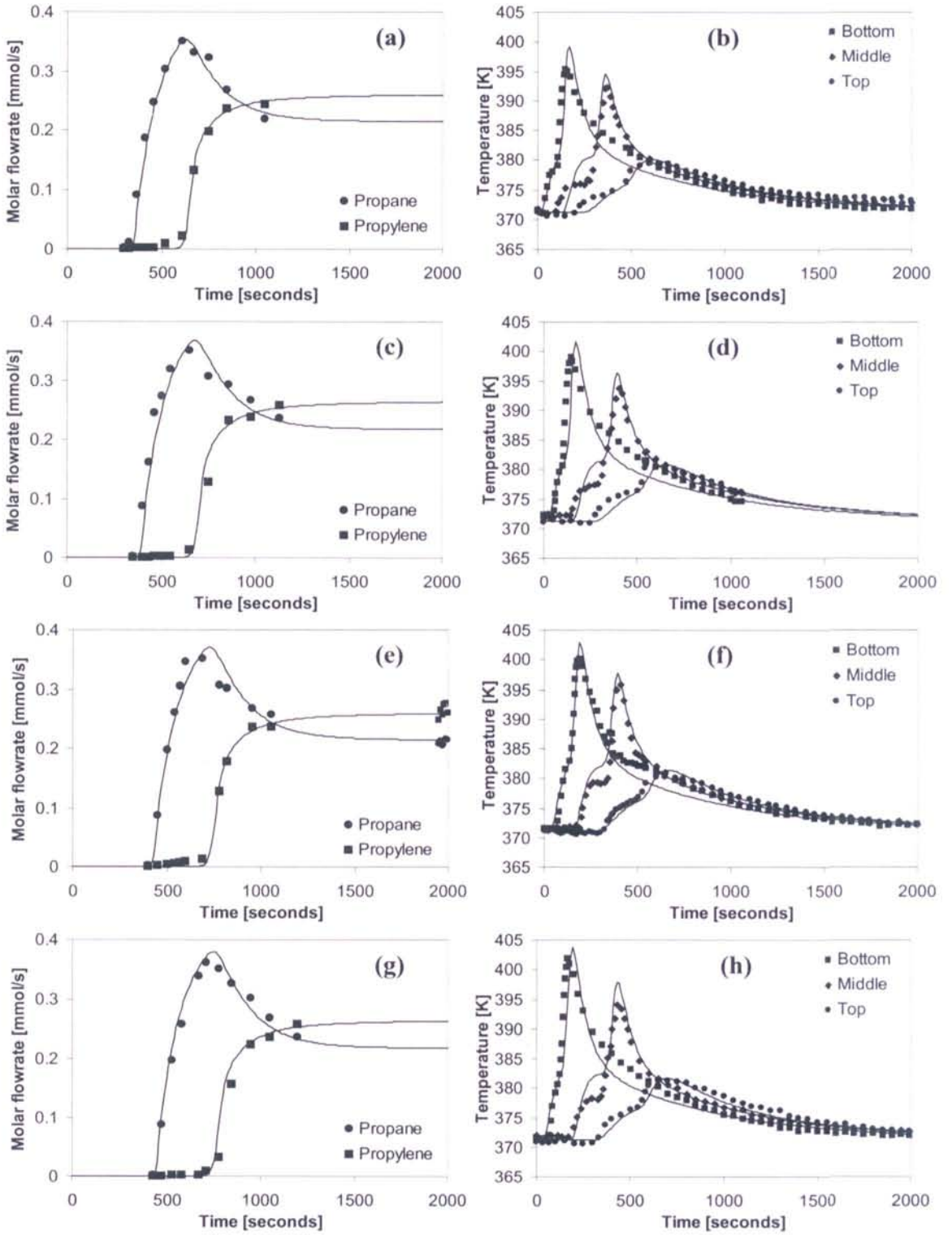

Figure 7.8. Molar flowrate and temperature profiles corresponding to propane – propylene breakthrough curves at 373 K in CMS 4A (Takeda) at 110 kPa (a and b); 180 kPa (c and d); 250 kPa (e and f) and 320 kPa (g and h). Molar fractions of the curves are 0.55 C_3H_6 - 0.45 C_3H_8. Temperatures were measured at 0.17m (Bottom), 0.43 m (Middle) and 0.68 m (Top) from feed inlet.

From the molar flowrate curves shown in Figure 7.6 it can be seen that for molar fractions of 80% propylene, the VSA-PSA separation of both gases with this adsorbent will be very difficult when compared to other adsorbents like zeolite 4A where purity over 99% can be obtained (Ramachandran et al., 1994; Da Silva, 1999). Also, large temperature excursions (increase of temperature in adsorbing and decrease of temperature when desorbing for adsorbent regeneration) are also detrimental to VSA-PSA performance (Yang, 1987).

Once verified that the model that uses pure component parameters (determined in separated experiments) can correctly describe the column behavior with the binary mixture, we can proceed to the PSA modeling and experiments. In this case we have used a feed pressure of 250 kPa composed by 52% of propylene and 48% of propane. The starting condition is the column filled with nitrogen (considered inert) at 373 K and 120 kPa. The adsorbent was activated under a flow of nitrogen at 523 K overnight. The experiments performed together with some simulations are shown in Table 7.4. In this table, when the run starts with an S followed by a number means that only simulation results are presented.

As this process involves five steps as described previously, we have initially fixed the operating variables (temperature, step pressures, flowrate and molar fractions) and concentrate in the effect of different step times in the overall performance of the unit trying to maximize purity and recovery of propylene. Initially, some of the parameters (intermediate and counter-current blowdown) were based on previous work with zeolite 4A (Da Silva, 1999). In this case, when the intermediate blowdown step is used, instead of a further enrichment of propylene in the column (step for pre-purification of the product), much of the propylene is lost. For this reason, this step was initially diminished and further omitted.

Table 7.4 – Performance parameters of 5-step PSA cycle for propylene purification using CMS4A at 373 K with 52/48 propylene/propane mixture*

Run	t_{pres}, s	t_{feed}, s	t_{rinse}, s	t_{depres}, s	t_{ccblow}, s	C_3H_6 purity (%)	C_3H_6 recovery (%)
1	100	100	75	40	220	80.8	22.5
2	100	100	75	40	300	80.3	26.1
S3	100	150	75	40	300	81.3	19.8
4	100	100	75	10	300	80.0	53.0
5	100	100	90	10	300	82.2	40.8
6	100	100	90	0	300	83.6	84.4
S7	100	75	75	0	300	78.8	95.3
S8	100	125	25	0	300	71.9	93.1
10	100	125	25	0	250	72.3	92.4
S11	100	125	50	0	300	78.1	94.8
12	100	100	75	0	300	80.8	95.7

* Conditions: Feed pressure: 250 kPa; Intermediate blowdown pressure: 50 kPa; Counter-current blowdown pressure: 10 kPa; Total feed flowrate: 0.7 SLPM; Rinse with pure propylene. Column and adsorbent properties are detailed in Table 3.

The effect of counter-current blowdown time (t_{ccblow}) is not very important in terms of purity (less than 0.5%) but has larger influence in the recovery (4% difference between runs 1 and 2). For this reason it was kept at 300s. For a better visualization of the effects of feed and rinse timings we show in Figure 7.9 the purity and recovery variations when t_{press} = 100s and t_{ccblow} = 300s.

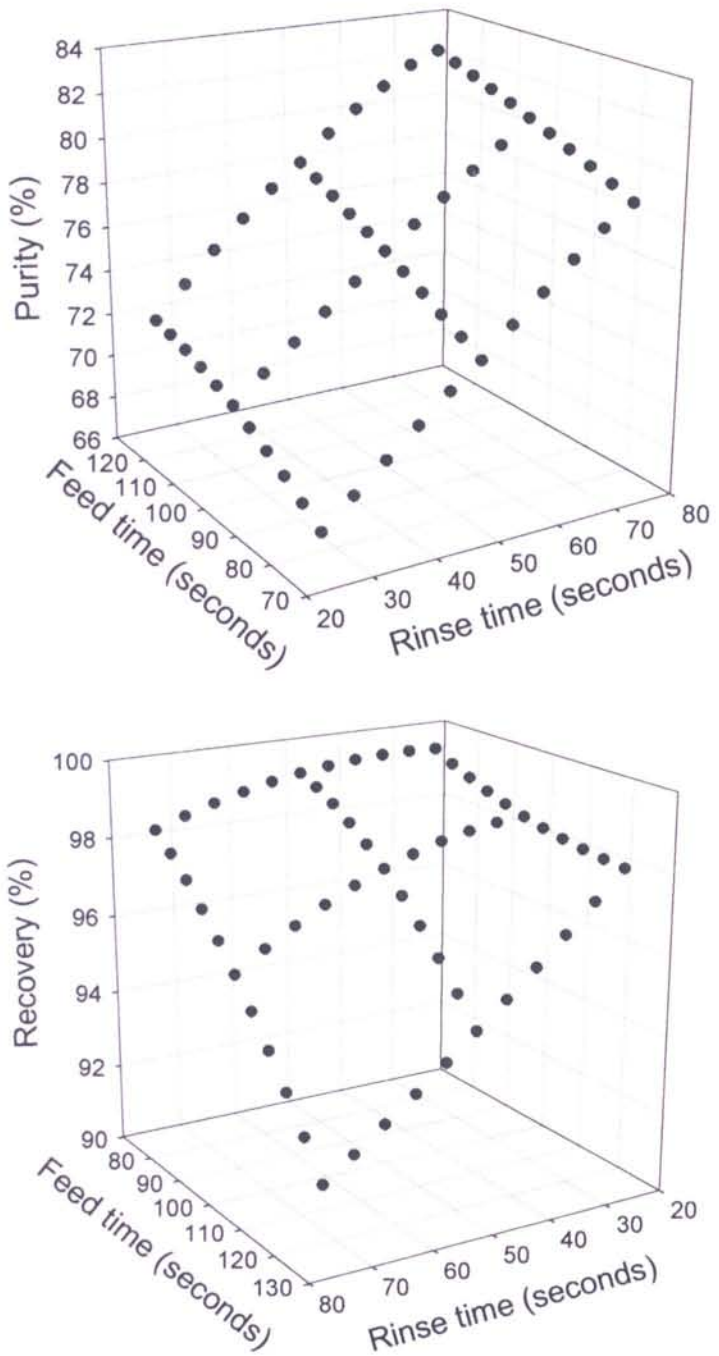

Figure 7.9. Simulated results for performance parameters of propane – propylene separation by VSA-PSA with different feed and rinse step times. t_{press} = 100s; t_{ccblow} = 300s.

From Table 7.4 we took run 12 as an example to show the experimental results obtained in the PSA unit. The molar flowrate of the first cycle and of the cyclic steady state (CSS) are shown in Figure 7.10. Temperature histories at the bottom, middle and

top of the column are also plotted in this figure. The solid lines correspond to the model described in the theoretical section. As can be seen, the prediction of the mathematical model was also very good. Cyclic steady state was reached after 20 cycles. As can be seen, the model fits the experiment very well confirming the validity of conclusions taken from simulations presented in Figure 7.9 and also for the simulations performed in Table 7.4.

The purity around 80% obtained in all the simulations is far away of the 99.5% required for polymer degree propylene. Also an important issue is the temperature excursion of around 20 K in one cycle. This variation has to be diminished for a better equipment performance. In the binary breakthrough experiments it was shown that when the mixture has a large amount of propylene against a small amount of propane, the separation of both gases is very difficult with a very small portion of time to perform a separation (see Figure 7.6f). In this work we did not made an optimization of the operating variables (temperature and step pressures) but according to the binary breakthrough experiments and with the VSA-PSA results obtained it is clear that this adsorbent is not very good to perform the propane – propylene separation. As explained in previous chapters, this adsorbent was composed by micropores with different sizes ranging from 4-6 Å. The adsorption – desorption of propane in the larger pores is faster, reason why the propane adsorbed in the pressurization and feed steps leaves the column in the blowdown step, contaminating the propylene product.

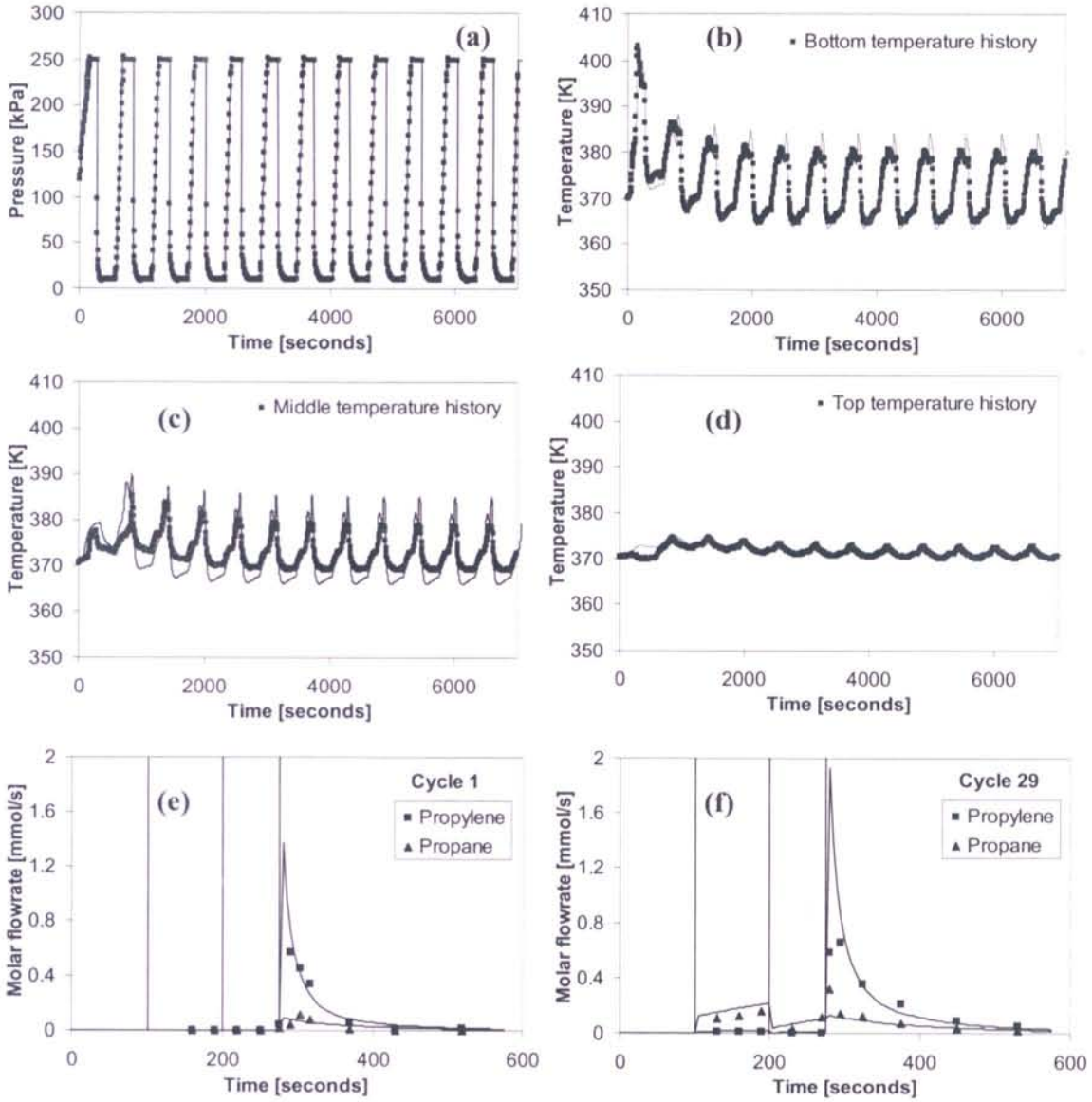

Figure 7.10. VSA-PSA experiment of propane – propylene separation at 373 K (see conditions in Table 7.4): (a) history of pressure at the end of the column, (b-d) temperature history measured in different points of the column (0.17m bottom; 0.43m middle; 0.68m top) and molar flowrates at the exit of the column for the first cycle (e) and in cycle 29 (f) when cyclic steady state was reached.

7.7 Zeolite 4A CECA

The previous adsorbents reported in this Chapter were employed for propane – propylene separation for the first time and for this reason it is not possible to compare their performance with previously published results. In the case of zeolite 4A some data are available, including much work done in this laboratory by Dr. Da Silva (Da Silva, 1999) and by Davesac (Davesac, PhD in preparation). They have already tested zeolite 4A (Rhone Poulênc, France) for this separation at temperatures between 423 – 473 K. Also in the existing patent for propane – propylene splitting by VSA-PSA it is mentioned that this temperature range is recommended to perform the separation with good recovery and purity (Ramachandran et al., 1994). Also from adsorption equilibrium and kinetic data, other authors have performed simulation of other VSA-PSA cycles using this adsorbent. A brief summary of the state of the art of propane – propylene separation by PSA using zeolite 4A is done in Table 7.5.

The main objective of this work is to improve the PSA performance previously obtained in this laboratory using zeolite 4A (CECA, France) as selective adsorbent without forgetting the final target of required purity of 99.5% for polymer grade propylene. To improve the VSA-PSA parameters (starting from the previously existent knowledge at the LSRE) we have studied the effect of step – times for a pre-established set of operating variables and the effect of feed pressure, temperature and the amount of nitrogen present in the cycle was also varied, as well as the diameter of the crystals in the extrudates.

BIBLIOTECA F.E. PORTO

Table 7.5. Summary of the state of the art for propane-propylene separation by PSA using zeolite 4A.

T, [K]	Cycle definitions		Purity	Recovery	Ref.
373	Four steps: pressurization, feed, rinse, blowdown. Step times: 400 s (for all). P_{High} = 1.0 bar; P_{Low} = 0.1 bar. Feed: 70 C_3H_6 / 30 C_3H_8.[b]		99.97	23.6	1
			99.1	10.5	
343	Five steps: pressure equalization (9s), counter-current pressurization with propane (7s), feed (34), bed equalization (9s), blowdown (41s). P_{High} = 1.7 bar; P_{Low} = 0.26-0.13 bar. Feed: 88 C_3H_6 / 12 C_3H_8.[a]		95.6	96.3	2
363			96.2	97.4	
383			96.2	98.2	
448			97.6	91.0	
373	Four steps: pressurization, feed, rinse, blowdown. All step times have equal duration. P_{High} = 1.0 bar; P_{Low} = 0.1 bar. Feed: 50 C_3H_6 / 50 C_3H_8.[b]	Step time			3
		100	99.94	7.95	
		400	99.01	12.16	
		600	99.98	27.29	
		800	99.97	23.59	
	Five steps: pressurization (60s), feed (120s), rinse (120s), depresurization to intermediate pressure (60s), blowdown (120s). P_{High} = 5.0 bar; P_{Low} = 0.1 bar. Feed: 25 C_3H_6 / 25 C_3H_8/ 50 N_2. Different total flowrates.[a]	P/F			4
423		0.78	91.2	20.0	
393		0.45	97.4	9.4	
423		0.28	98.6	17.1	
423		0.23	94.5	27.3	
423		0.13	87.9	46.5	

[a] Experimental values; [b] Simulated values

Refs: 1) Patent 6,406,521 (Cheng et al., 2002); Patent 5,365,011 (Ramachandran et al., 1994); Patent 6,423,881 (Yang et al., 2001); 4) Da Silva and Rodrigues, 2001.

7.7.1 Fixed bed experiments

Before starting with PSA experiments, the transport parameters calculated from correlations presented in literature have to be checked. The binary fixed bed runs are actually used as "model calibration" experiments, where the correct values of the mass and energy parameters are inserted in the program for future use in PSA simulations. For this reason, some fixed bed experiments were performed with the binary mixture of propane and propylene (diluted with nitrogen): one with a composition of 0.450 C_3H_6 / 0.035 C_3H_8 / 0.510 N_2 (corresponding to a propylene to propane ratio of 85/15) and another with a nearly equimolar C_3 composition: 0.250 C_3H_6 / 0.240 C_3H_8 / 0.510 N_2. Both experiments are reported in Figure 7.11. In both of them the solid lines correspond to the model described in the theoretical section of this chapter. The parameters used in the mathematical model are described in Table 7.6. In both experiments the temperature increase due to propylene adsorption is also shown. The heat transfer parameters (λ, h_f, h_w *and* U) used for the simulations were the same as the ones reported by Da Silva for a similar system (Da Silva, 1999).

These binary curves also show that the separation of propane and propylene is much better than in the case of CMS 4A, particularly for the mixture with higher propylene concentration. In both curves a stream containing only propane can be taken out of the column without any propylene. Note also that the temperature increase due to propane adsorption is negligible while the one for propylene adsorption is not as high as with the CMS 4A being only of 12K against the 30K observed in binary breakthrough curves in CMS4A .

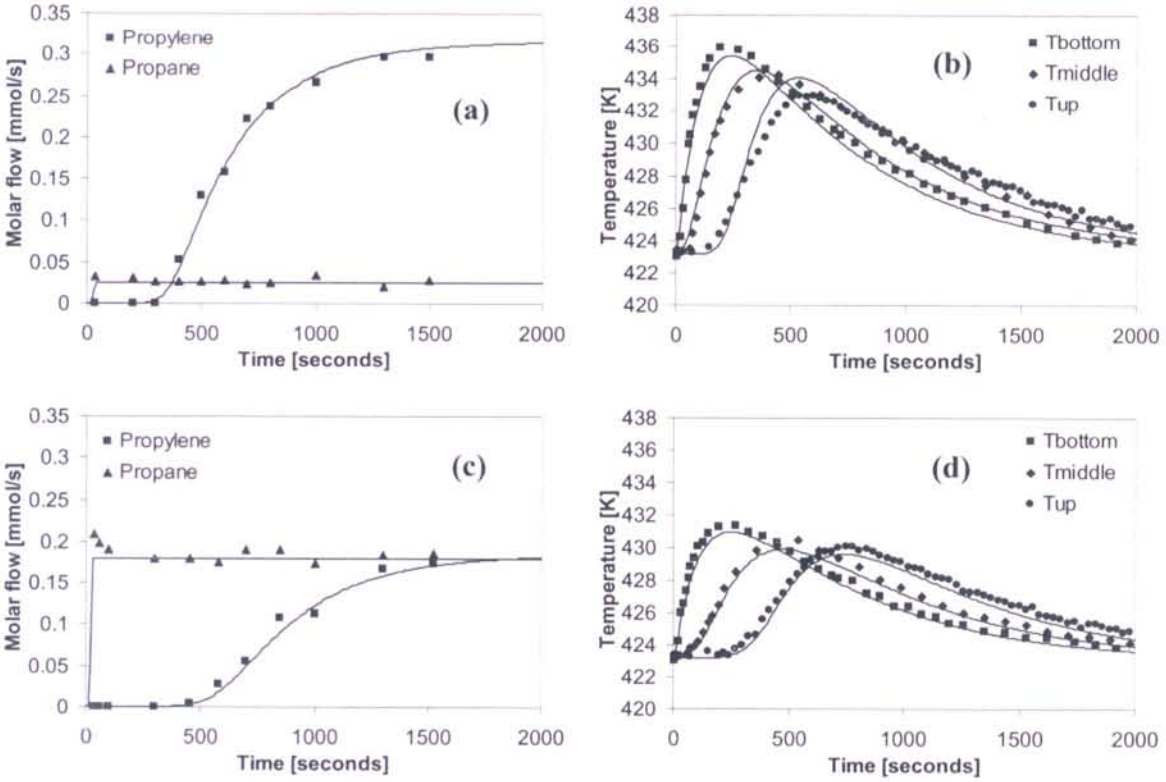

Figure 7.11. Propane – propylene breakthrough curves using zeolite 4A at 423 K for different hydrocarbon ratios: (a and b) composition of the mixture: 0.450 C_3H_6 / 0.035 C_3H_8 / 0.515 N_2 and (c, d) composition of the mixture: 0.250 C_3H_6 / 0.240 C_3H_8 / 0.510 N_2. Temperatures were measured at 0.18 (bottom), 0.43 (middle) and 0.68 (top) m from the feed inlet.

A more important feature shown in these curves is that the adsorption equilibrium and kinetics of pure components obtained from different and independent methods were validated, predicting very well the behavior of concentrated fixed bed experiments. Once the correct parameters of the fixed bed system were established all the conditions are satisfied to start with VSA-PSA simulation and experiments.

Table 7.6 – Experimental conditions of breakthrough curves of propane – propylene mixtures in zeolite 4A extrudates (CECA)

Column parameters		Adsorbent parameters (zeolite 4A)	
Column length, m	0.87	Crystal radius, m	1.9×10^{-6}
Column radius, m	0.0105	Pellet radius, m	8.10^{-4}
Column porosity	0.43	Pellet density, kg/m³	1210
Bulk density, kg/m³	758	Pellet porosity	0.34
Wall density, kg/m³	8238	Pellet tortuosity	2.0
Wall specific heat, J/kg.K	500	Solid specific heat, J/kg.K	920
Wall heat transfer coefficient, W/m²K	60		
Overall heat transfer coef., W/m².K	30		
Total Flowrate, SLPM	1.10		

7.7.2 Definition of operating variables

The operation of a five-step cycle to be used for C_3 separation in the laboratory unit (with column length and volume already specified) has the following operating and process variables: T_{feed}, T_{rinse}, Q_{pres}, Q_{feed}, Q_{rinse}, P_{high}, P_{inter}, P_{low}, t_{pres}, t_{feed}, t_{rinse}, t_{depres}, t_{blow} and feed composition. The optimization of a process with so many variables is very difficult, particularly when they are related by a system of partial differential equations. In the group of variables mentioned we can distinguish two general types: the operating variables and the process variables (cycle step times). In order to simplify the study of the process, it is desirable to reduce the number of operating conditions. The first assumption is to use the same temperature for the feed (and pressurization) and for the rinse streams. Other important variables are the flowrates. In this work the flowrates of all streams (pressurization, feed and rinse) will assume a fixed value and will not be

considered as a variable. Also, inlet stream compositions were fixed for all the steps assuming two different propylene to propane ratios: 85/15 and 54/46. The change in composition studied in this work is the nitrogen removal from the process, but keeping propylene to propane ratio constant. Still the system has 9 variables (inlet streams temperature, three step-pressures and five step times). In this work the effect of these variables will be studied. Initially, the step pressures used by Da Silva (P_{high} = 500 kPa; P_{inter} = 50 kPa; P_{low} = 10 kPa) were chosen to perform most of the experimental data collection. Initially, also a temperature should be defined to start investigating the effect of changing the cycle step - times of the unit (process variables determination). For this reason again the selectivity factor was used. After studying the effect of the step – times in the cycle performance, the operating variables (temperature and step pressures) will be addressed. Also another variable was introduced concerning the adsorbent: the adsorbent crystal size that may limit the separation in a kinetically driven PSA unit.

7.7.3 Temperature selection

In a previous section of this chapter the kinetic selectivity factor was defined and used for the selection of the appropriate adsorbents to test in the PSA unit. Other alternative use of this selectivity factor is to assess the effect of temperature in the selectivity of the zeolite 4A towards propylene. For higher kinetic selectivity we are expecting better performance of the PSA unit. As we have already fixed the feed pressure and composition (values previously used by Da Silva, 1999), the kinetic selectivity factor can be calculated: feed pressure at 250 kPa with an equimolar mixture of propane – propylene and with a blowdown pressure of 10 kPa. In the feed step, the partial pressures of both components are specified (250 kPa), but in the blowdown step, the step was considered as having no propane (all propane was considered as displaced

in the rinse step) so Δq_{C3H6} is calculated between the propylene partial pressure in the feed step and 10 kPa while Δq_{C3H8} is calculated between the propane partial pressure in feed and 0 kPa. To calculate the kinetic factor the infinite dilution diffusivity coefficients of pure gases (values determined by ZLC, diluted breakthrough curves and static-batch method) were employed. The kinetic selectivity factor for the system propylene – propane – zeolite 4A is plotted in Figure 7.12 as a function of temperature. It passes through a maximum around 463 K, which should be initially considered as the working temperature. Even though, as temperature is increased the amount adsorbed of both gases decreases and also does the productivity of the column. For this reason, the selectivity plot was decomposed in two straight lines with different slopes. As a trade-off between the best kinetic selectivity and productivity we have chosen the temperature corresponding to the interception point of these lines, which is around 433 K.

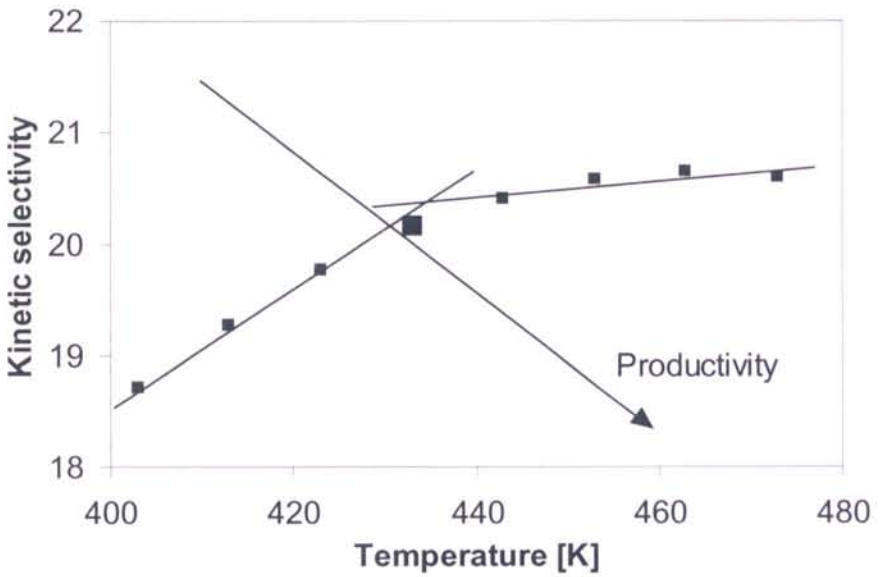

Figure 7.12 - Kinetic selectivity of zeolite 4A towards propylene at different temperatures.

7.7.4 VSA-PSA experiments with zeolite 4A: initial runs

Before studying the effects of the different variables, it is convenient to give an example of an experimental run obtained in a VSA-PSA experiment using zeolite 4A

(CECA, France). For this purpose an experiment was performed with 60 seconds of pressurization, 70 seconds for feed step, 130 seconds of rinse, 60 seconds of co-current depressurization and 220 seconds for counter-current blowdown step (run 1, Table 7.11). Operating variables were kept at: T = 433 K (for all inlet streams and surroundings of the column); P_{high} = 500 kPa (pressurization + feed); P_{inter} = 50 kPa (co-current depressurization); P_{low} = 10 kPa (counter-current blowdown); Pressurization and feed flowrate: 3.16 SLPM; Rinse flowrate: 2.70 SLPM; Molar fraction of pressurization and feed stream: 0.453 C_3H_6 / 0.074 C_3H_8 / 0.473 N_2; Molar fraction of rinse stream: 0.077 C_3H_6 / 0.000 C_3H_8 / 0.923 N_2. The molar fraction used in the feed step corresponds to a stream having a ratio of 85/15 propylene to propane. The relevant experimental information collected from the VSA-PSA unit (pressure and temperature) and GC (molar flowrate of gases exiting the column) can be summarized in Figure 7.13. The pressure at the exit of the column and the temperatures measured by the three thermocouples located at 0.18, 0.43 and 0.68 m from the feed inlet are reported for the first 15 cycles. In this figure we also show the molar flowrate analyzed by GC for the first step and for cycles 39 and 50 where no variation of molar flowrate was experimentally detected.

The solid lines in the figures represent the prediction of the model described in the theoretical section. The model is in good agreement with the experimental data indicating that the cyclic column behavior is well predicted. Some differences exist in the experimental and simulated molar flowrates in the co-current depressurization step that may be due to dead volumes of the equipment.

The experimental purity of this example is around 98.7%, even when simulated value is somewhat higher: 99.32%. Differences between experimental and simulated values may be due to dead volumes at the end of the VSA-PSA column and / or because

the propylene used for the experiments has 0.5% of propane in its composition and this may be critical, particularly in the rinse step.

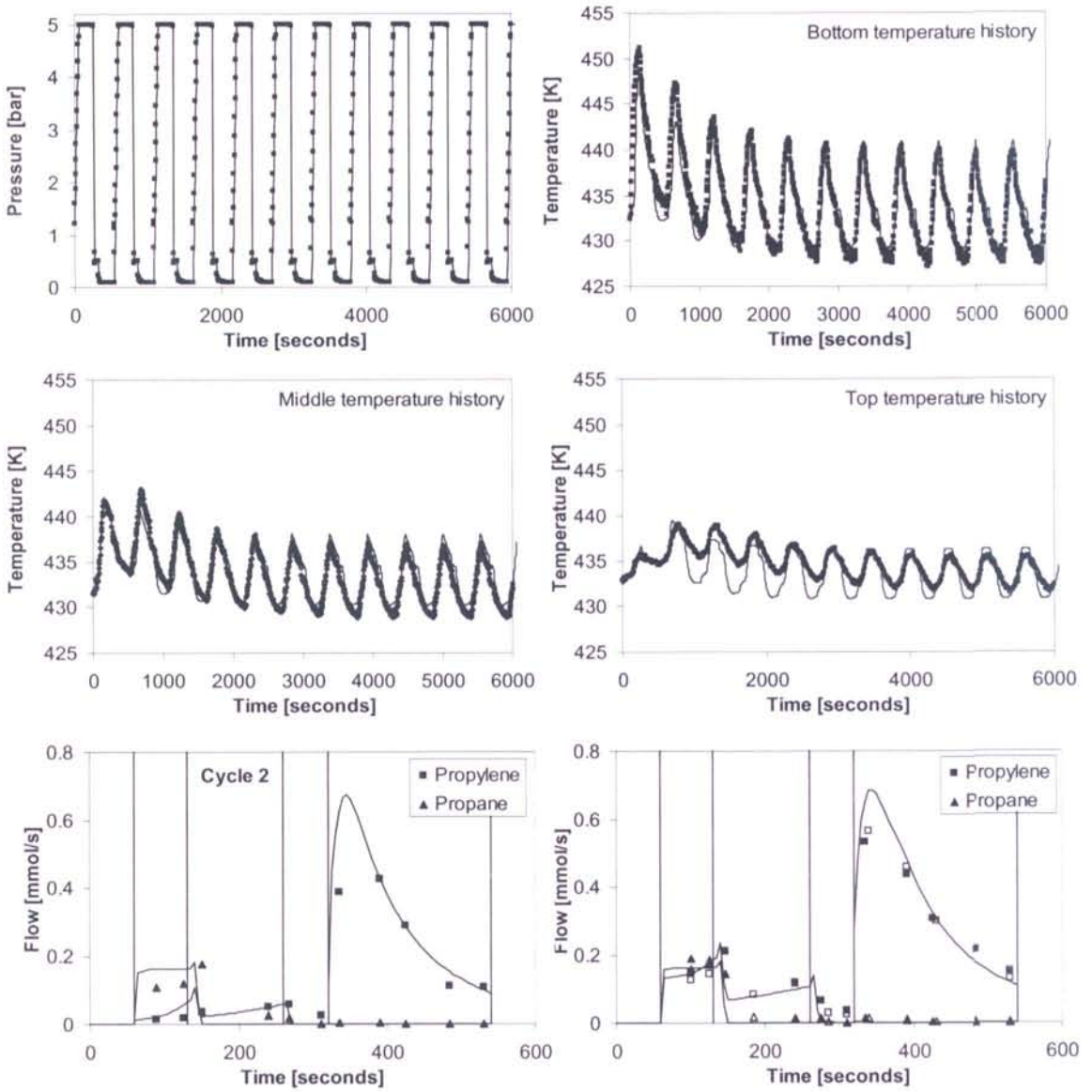

Figure 7.13. Experimental variables obtained at the VSA-PSA unit for propane – propylene separation using zeolite 4A at 433 K: histories of pressure at the outlet of the column and temperature in the bottom, middle and top thermocouples (0.18, 0.43 and 0.68 m from inlet) and molar flowrate of propane and propylene in the second cycle and in cycle 39-50. Other operating conditions are reported in Table 7.11, run 1.

The recovery of propylene in this experiment was 62.7%. This value is higher than corresponding values of zeolite 4A Rhone-Poulenc (Da Silva, 1999) confirming that the Rhone-Poulenc zeolite used in previous experiments had poorer performance for this separation. The main difference of these zeolites is due to differences in propane diffusivity (much smaller in the zeolite 4A CECA sample used in this work). Even when adsorption equilibrium reported on this adsorbent is higher than in the Rhone-Poulenc sample, the effect of lower propane diffusivity is more important than the higher adsorption capacity. One possible explanation for the difference in the propane kinetics can be due to the thermal treatment of the samples (activation protocol) that may dislocate the Na^+ ions from the structure producing small differences in the channel aperture as reported for smaller molecules (Ruthven, 2001).

Once those experimental results were well simulated by the model proposed, we can start with the improvement of the process studying the effect of the different variables by simulations. Just from the plot of the molar flow rate it is possible to identify that some of the step times can be improved to have at least higher recovery.

7.7.5 Cyclic Steady State (CSS) and multiplicity of steady states

Before studying the effect of the operating and process variables the cyclic steady state and its multiplicity were investigated. In Chapter 4 an extremely small value of propane diffusivity on zeolite 4A was measured. A small diffusivity coefficient can have detrimental implications at large times. In Figure 7.13, the temperature and pressure history were plotted for the first fifteen cycles and it can be seen that they reached the cyclic steady state. In the case of the molar flowrate, fifty cycles were performed and no detectable difference was observed after cycle 20. Even though, if we perform simulations for over 500 cycles and we see in detail the evolution of all the

variables, we can note that the product purity is continuously decreasing up to a steady state value that is only reached after 250 cycles. This continuous purity decrease is due to a very small increase of the adsorbed phase concentration of propane, which result in a slightly higher release of propane in the blowdown step, contaminating propylene. The evolution of product purity in run 1 (see Table 7.11) is shown in Figure 7.14. The experimental points collected in the first 50 cycles are also plotted in this picture. The difference between the simulated values and the experimental ones may be due to dead volumes in the installation or even to the fact that we are feeding propylene 99.4 % purity with around 0.5% impurity of propane in the rinse step.

The results shown in the blue line in Figure 7.14 were obtained starting from an initially clean bed and then passing an inert stream of nitrogen for 48 hours. To confirm the cyclic steady state and to check if multiplicity of steady states exists, the same experiment was repeated but starting from a column saturated with propane (125 kPa partial pressure) for three hours. Multiplicity of steady states in PSA applications was previously reported in the separation of propane – propylene mixtures (Rege et al., 2002) and can also exist in this system that has non-isothermal behavior and non-linear isotherms (Sundaram and Yang, 1998).

The experiment started with the column initially filled with propane (pressure and temperature histories and molar flowrates of gases) was also well described by the model. The evolution of the purity profile instead of starting from a very high value in the initial cycles and then decrease as shown before, in the case of the column previously saturated with propane, the purity started from lower values and improves with time until a constant value around 98.6%. The purity evolution with time (simulated and experimental values) of this experiment is also shown in Figure 7.14. The same cyclic steady state line was obtained (although in this case it starts from a

lower value of purity passing through a maximum slightly higher than 99.5% and decreasing to 99.32% where it stays constant) indicating no multiplicity of steady states in runs starting with different saturation conditions of the column.

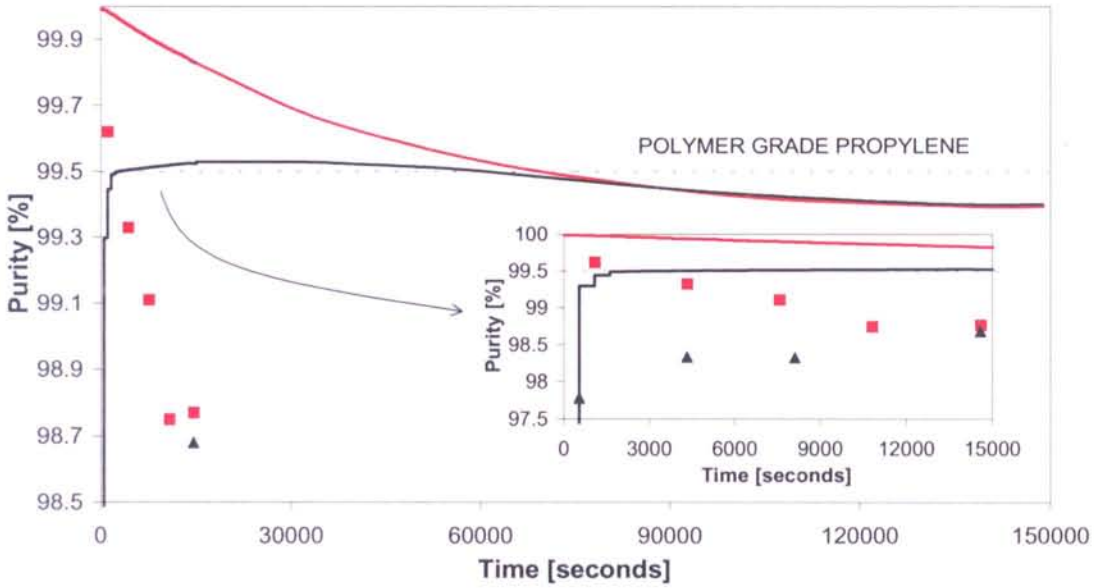

Figure 7.14. Purity evolution for the same experiment started with a clean bed passing a nitrogen flow before experiment started (red squares are experimental data and red line is simulation) and a column initially pre-saturated with propane (black triangles are experimental data and black line is simulation).

7.7.6 Improving the step times (process variables)

From the list of variables mentioned above, once all the operating variables are specified, the other variables to be studied are the step – times, that are the process variables, which determine the overall performance of the unit. Although the initial experiment was performed with propylene to propane ratio of 85 / 15, in the following section, except when explicitly mentioned, the propylene to propane ratio will be 54 / 46. Experimentally it was verified that with the column used and for a specific flowrate (Q_{pres} = 2.785 SLPM), the pressurization step cannot take less than 54 seconds, and this

value was used in almost all the experiments as fixed time for the pressurization step (note that also the flowrate of pressurization step was kept constant).

This cycle has no counter-current purge with light product after the counter-current blowdown step. Light product purification is normally used when the light gas is the purified product (Cavenati et al., 2004). Having no counter-current purge allows a straight route to calculate the upper limiting time of the feed step (before breakthrough of propylene). Assuming that the counter-current blowdown (last step of the cycle) is very long, the column will reach adsorption equilibrium at 10 kPa with almost pure propylene. Starting with a column filled with the adsorbent saturated (in equilibrium) with propylene at 10 kPa and with a pressurization step of 54 seconds, the maximum feed time can be determined.

The simulated behavior of the column (molar flowrate exiting the column, temperature and propylene concentration and amount adsorbed at different times) is shown in Figure 7.15. Propylene is exiting the column since time zero of the feed step, but major breakthrough happens after 160 seconds of feed step (dotted line in Figure 7.15a). This time is the maximum limiting time because the blowdown step will never be large enough to allow the column to reach equilibrium; therefore, more propylene will stay in the column and the feed time has to be shortened. In Figure 7.15 the temperature variation and propylene concentration in gas and adsorbed phases are also shown.

Once the maximum feed step is known, some comments on the experiment shown in Figure 7.13 will be made. In the molar flowrate plots, it can be seen that there is much propylene being lost in the feed step and in the rinse step, even in the second cycle where the column is only partially saturated. The propylene losses get worse for large number of cycles. This is an indication that too much propylene is entering to the

system. Also, the amount of propane leaving the column in the rinse step is only considerable only in the first moments.

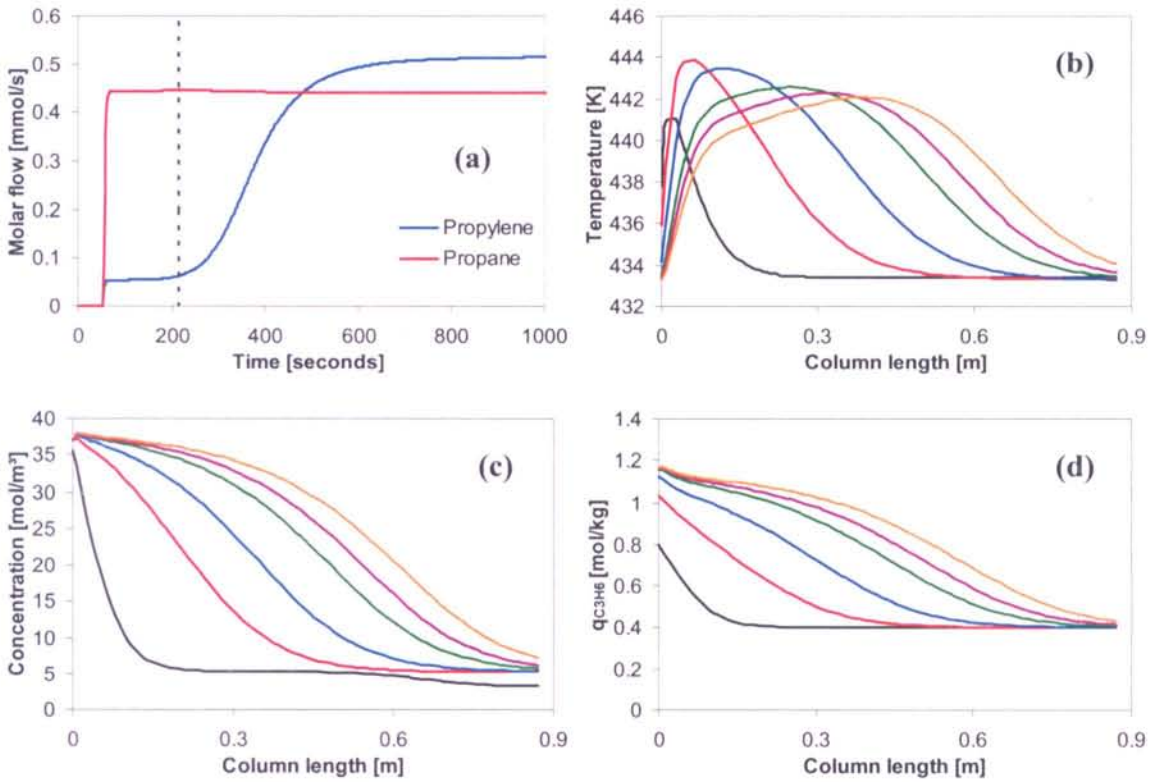

Figure 7.15. Behavior of the PSA column started with the bed saturated with propylene at 10 kPa: (a) molar flowrate of gases exiting the column; (b) temperature profiles; (c) propylene concentration; (d) amount of propylene adsorbed. Solid colored lines in (b, c, d) are: black (54 s), red (100 s), blue (150 s), green (200 s), cyan (225 s), orange (250 s).

A way to reduce propylene losses to improve recovery and also with positive effects on productivity is to reduce the rinse step time. This decrease in the rinse time with only minor effects in product purity can be explained in terms of the small value of the propane diffusivity: the amount of propane adsorbed in the pressurization and feed steps is small but also this amount will not be easily desorbed from the zeolite in the rinse step. For this reason, the rinse step has the only purpose of removing propane from the column and pellets (macropores) voidage. The lower boundary of the rinse step is

the residence time of the gas into the column. Although the purpose of this step is to exclude propane from the column voidage and also from the larger macropores of the adsorbent and since some propylene will adsorb in the zeolite, a reasonable limit of 25 seconds was assumed as lower boundary.

In Table 7.7 the result of different VSA-PSA experiments is summarized. All the operating variables were kept constant and only step times were changed. The mathematical model predicts well all the collected data. Due to reasons explained above (contamination of propane in the propylene bottle and dead volumes of the experimental set-up) a difference of around 0.5 was detected in all the experiments (purity around 98.4 – 98.8 %). For this reason the purity presented in Table 7.7 corresponds to the simulated value while the recovery and productivity values (calculated from the integral of the propylene molar flowrate) correspond to the experimental values.

For a constant value of all other step times, only the rinse time was changed from 25 to 75 seconds as can be seen in Table 7.7. In all the experiments when the rinse step is more than 25 seconds, the recovery drops to values around 80% instead of 85% and changes in purity are only of within 0.1%. Clearly the rinse time of 130 seconds is excessive for this zeolite sample and the decrease in the rinse time lead directly to the possibility of a larger feed time, increasing the productivity of the unit. Note that with a decrease in the rinse time, the recovery of product in all the experiments jumped from 63% to more than 80%.

The co-current depressurization step can be reduced only up to 30 seconds when purity begins to decrease. In this work this step-time was kept constant at 40 seconds, a little less than prior experiments, but still without negative effects on purity.

Blowdown step in this case is used to regenerate partially the adsorbent but also to extract the product. The molar flowrate of propane that contaminates the product is

mainly taken out of the column in the initial moments of the step. For this reason, shorter steps have lower purity, but a large step produce low productivity of the unit. In Table 7.7 we show experiments with 180 and 220 seconds to show the increasing of purity with larger step. Periods higher than 220 seconds did not improve purity considerably but decrease the productivity.

Table 7.7 – VSA-PSA performance for propane-propylene separation with zeolite 4A. Operating conditions were: T = 433 K; P_{high} = 500 kPa; P_{inter} = 50 kPa; P_{low} = 10 kPa; Pressurization, feed and rinse flowrate: 2.785 SLPM; y_{C3H6}=0.27, y_{C3H8}=0.23, y_{N2}=0.50.

Exp. N°	Pres, s	Feed, s	Rinse, s	Depres., s	Blow, s	Purity %, simulated	Recovery %, experimental	Productivity, mol/h.kg
4	60	60	25	40	220	99.27 (98.7±0.3)[#]	87.3	1.75
5	54	100	25	40	180	99.31 (98.6±0.2)[#]	85.6	2.64
7	54	100	25	40	220	99.35 (98.7±0.3)[#]	86.7	2.36
8	54	100	75	40	220	99.39 (98.8±0.4)[#]	81.6	2.28
9	54	100	75	40	180	99.27 (98.7±0.2)[#]	85.6	2.38
10	54	60	25	40	180	98.91 (98.4±0.3)[#]	86.4	1.97
12	54	60	75	40	180	99.12 (98.6±0.4)[#]	80.0	1.73
13	54	60	75	40	220	99.33 (99.0±0.3)[#]	81.3	1.58
16	54	60	15	25	180	98.48 (98.2±0.2)[#]	84.1	1.64
17	54	85	15	25	220	98.61 (98.3±0.3)[#]	85.7	2.38

[#] Experimental values

As an example of the improvement of the PSA performance we show in Figure 7.16 a PSA cycle (molar flowrate in the initial cycle and cycle 41 and temperature and

pressure history). As the total time of the cycle was diminished (see run #4 in Table 7.7), the productivity was also improved.

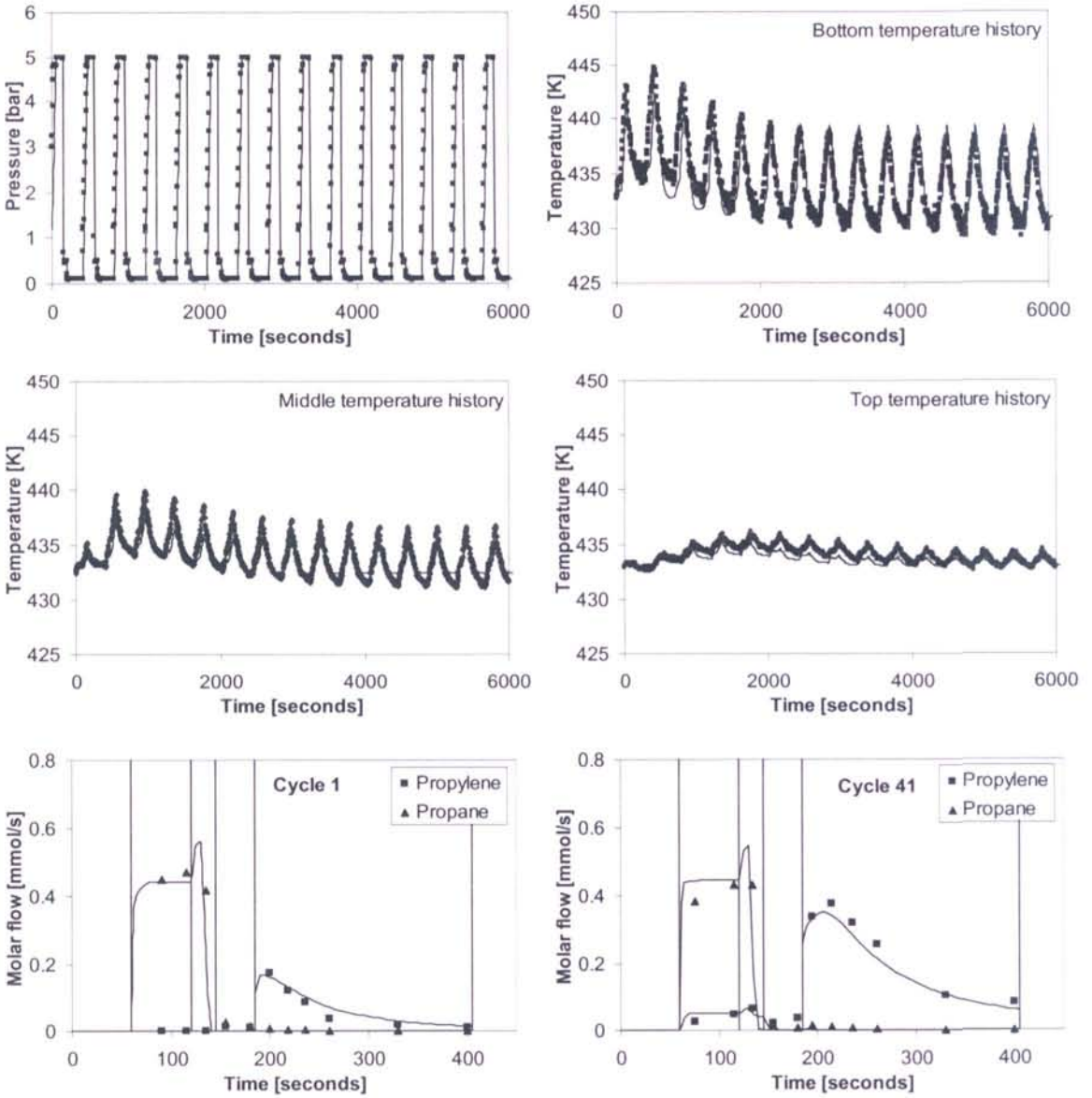

Figure 7.16. Experimental variables obtained in the VSA-PSA unit for propane – propylene separation using zeolite 4A at 433 K: histories of pressure at the outlet of the column and temperature in the bottom, middle and top thermocouples (0.18, 0.43 and 0.68 m from inlet) and molar flowrate of propane and propylene in the first cycle and in cycle 41. Other operating conditions are reported in Table 7.7, run 4.

7.7.7 Effect of crystal size

Another variable not even considered before is the adsorbent modification. The zeolite 4A we are using allows a selective adsorption of propylene, but the diffusivity of propylene is small (of course that propane diffusivity is much smaller) when compared to other industrial processes. For this reason initially this material was not further studied in previous works (Järvelin and Fair, 1993). To enhance the diffusivity of propylene two ways are possible:

1) partial exchange of the zeolite with calcium ions
2) reduction in the crystal size to increase the value of the D_c / r_c^2 ratio.

If the zeolite is partially exchanged with calcium ions the propylene diffusivity will increase but the propane diffusion will increase more and so the difference in adsorption kinetics and thus in the selectivity is lost. For this reason, a reduction in the crystal size will produce, as shown in Chapter 5, sharper concentration profiles and a more effective use of the bed, obtaining a higher productivity.

Unfortunately there are no extrudates or pellets with crystal sizes different from 3.5 – 3.9 μm. Zeolite crystals with 3.5 μm and a uniform size distribution are used as detergent builder (being the most extensive application of zeolites with 90% of the market of zeolite production with nearly a million tons per year) to exchange ions that cause water hardness (Ullman's Encyclopedia, 2003). For this reason most commercial extrudates or pellets available have this crystal diameter.

To study the effect of the crystal size in VSA-PSA behavior, we have chosen a particular experiment and compare the performance of the commercial extrudates with extrudates having smaller crystals sizes. Forty cycles were performed using the scheduling described in run 7 in Table 7.7 using the commercial sample zeolite 4A CECA. Experimental results of the VSA-PSA example experiment are shown in Figure

7.17 where temperature in three different points of the column (0.18, 0.43 and 0.68 m) and pressure history at the end of the column and molar flowrate of the initial cycle and in cycle 39 are reported. Solid lines are the fitting of the model used to simulate the process. Propylene was obtained with high purity in the blowdown step: 98.8% ± 0.3 experimental and 99.4% simulated with 86.6% recovery. Again as explained before, there is a difference of around 0.5% in the purity obtained in the blowdown step while the other variables are well fitted by the model.

We have simulated the same experiments with extrudates of zeolite 4A having the same properties but with zeolite crystal diameters of 1 μm, 2 μm, 3 μm and 5 μm. If we look at the simulated concentration profiles of propylene inside the column using the commercial pellets (3.8 μm) we can see that they are rather disperse because of its low diffusivity. The concentration profiles of propylene at the end of each step in the cyclic steady state (CSS) are shown in Figure 7.18a. For comparison, in Figure 7.18b we show the concentration profiles for the same experiment but using crystals of 1 μm diameter. In this case, the Length of Unused Bed (LUB) can be further diminished (by increasing the feed time) without increasing propylene losses. In this case, intuitively, we notice that the feed time can be increased (increasing productivity) without significant propylene losses. Using smaller crystals in a micropore diffusion controlled process, we have sharper concentration fronts thus enhancing the productivity of the unit.

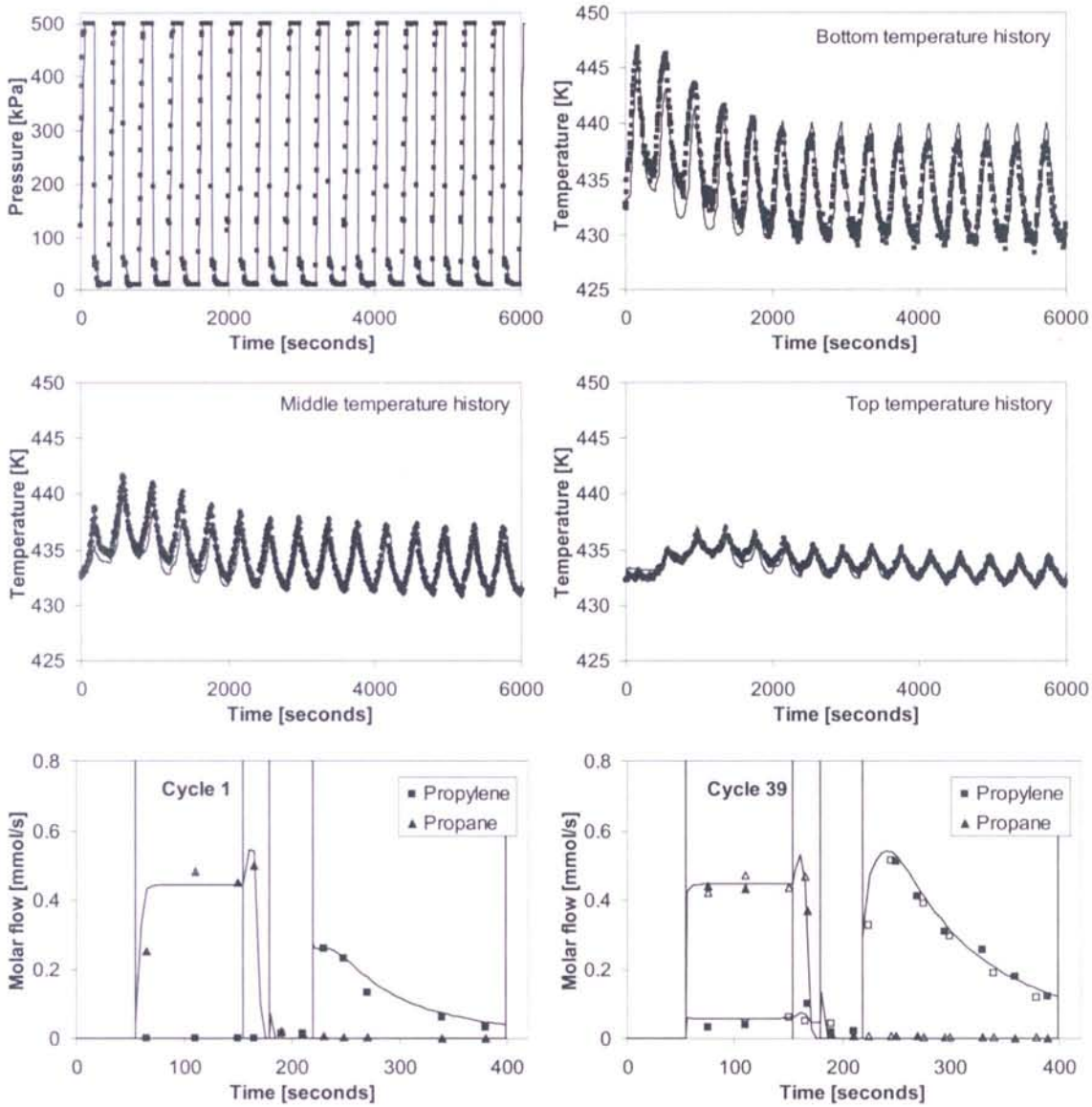

Figure 7.17. Experimental pressure at the outlet of the column, temperature in the bottom, middle and top thermocouples (0.18, 0.43 and 0.68 m from inlet) and molar flowrate of propane and propylene in the first cycle and in cycle 39 for VSA-PSA for propane-propylene separation using zeolite 4A (for experimental conditions see Table 7.7, run 7).

Even though using smaller crystals propylene purity is smaller. As the crystal size decreases, the time constant (crystal radius ^{2} / diffusivity) decreases, reason why breakthrough curves get sharper (as shown for propylene in Chapter 5). The sharpness of the pure component breakthrough curves is important for propylene but for propane as well. In a VSA-PSA cycle the binary mixture is introduced. In the case of smaller crystals, the amount of propylene adsorbed in the bed is higher than in the larger crystals. The concentration of propylene in the gas phase (directly related to the amount adsorbed) is shown in Figure 7.18 for two different crystal sizes showing that more propylene is adsorbed in the bed with smaller crystals. But also with smaller crystals, the propane adsorbed in the bed is higher as shown in Figure 7.19, especially at the end of the column where less propylene is there to displace propane. When the crystal size decreases the time constant is smaller and so more propane will diffuse into and also out of the crystals. For this reason during blowdown, higher amounts of propane are desorbed from the column contaminating the propylene and thus obtaining propylene with less purity when decreasing the crystal size. The difference between the amount of propane adsorbed in the bed at the end of the depressurization step and at the end of the blowdown step (see Figure 7.19) corresponds to the contamination of the product: in the case of crystals with 3.8 μm this difference is extremely small, while for the smaller crystals, larger differences are obtained.

Simulations of the same experiment with crystal diameters varying from 1-5 μm were done. The performance results shown in Figure 7.20 only mean that it will be very difficult to reach very high purity of propylene with small crystals while keeping high recovery and productivity. Results obtained here have higher productivity, recovery and purity than previously obtained before (Da Silva, 1999).

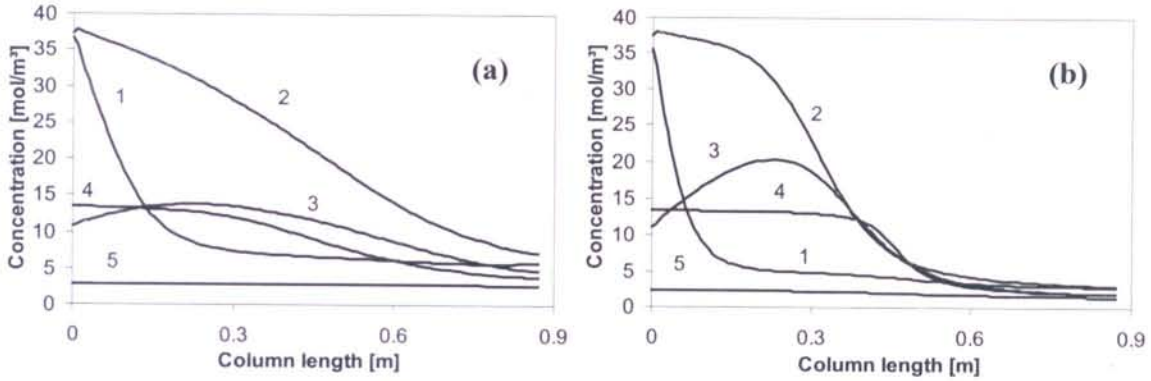

Figure 7.18. Simulated concentration profiles of propylene at the end of each step (1: pressurization; 2: feed; 3: rinse; 4: depressurization to intermediate pressure; 5: blowdown) for commercial sample with crystal diameter of 3.8 μm (a) and for 1.0 μm diameter (b).

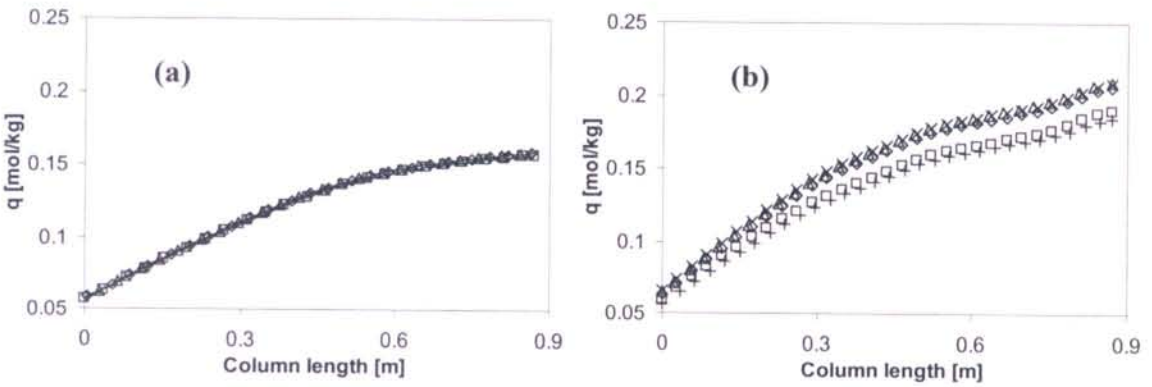

Figure 7.19. Simulated adsorbed phase concentration profiles of propane at the end of each step (□: pressurization; x: feed; Δ: rinse; ◊: depressurization to intermediate pressure; +: blowdown) for commercial sample with crystal diameter of 3.8 μm (a) and for 1.0 μm diameter (b).

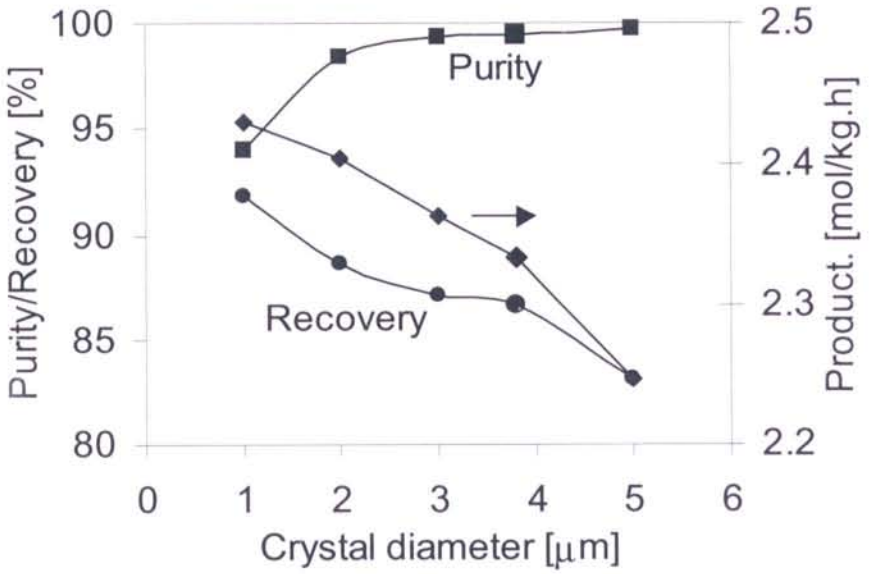

Figure 7.20. Effect of crystal size in purity (■), recovery (●) and productivity (◆) of VSA-PSA experiment.

Also, cyclic steady state (CSS) approach is different according to crystal size. Even when the temperature, pressure and the molar flowrate exiting each step seems to reach the cyclic steady state in the first 15 cycles, the purity of propylene extracted in the blowdown step is decreasing continuously and very slowly in the first 300 cycles. The propylene purity obtained in the example experiment with crystal diameters varying from 1-5 μm is shown in Figure 7.21. When commercial samples are used 300 cycles are needed for CSS while only 25 are required in the case of crystals with 1 μm. This small and continuous decrease is directly related to the very small value of propane diffusivity. As the time constant of the process is related to the value of D_c/r_c^2, diminishing the crystal size the cyclic steady will be achieved faster.

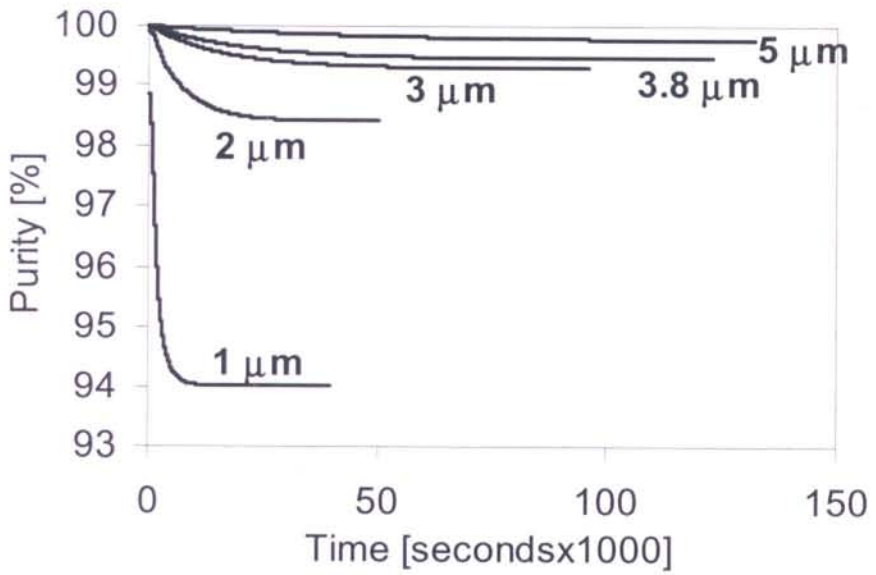

Figure 7.21. Cyclic steady state (CSS) approach with different zeolite 4A crystal sizes.

Although this experiment was performed using cycle times to obtain high purity and recovery in the commercial extrudates and conditions were not optimized for smaller crystals. In VSA-PSA application for polymer grade propylene production (target of >99.5% purity), crystals from 4-5 μm (higher than the ones in the commercial sample used in this work) should be used with acceptable values of recovery and productivity, while for chemical grade propylene (target of >96% purity) smaller crystals, having almost the same recovery but much higher productivity, can be used. As this example was far away from being optimized for smaller crystals (see Figure 7.18b), in the case of the 1 μm crystals, we performed a simulation using the same pressure and temperature conditions and same flowrates but changing step times (t_{press} = 55s; t_{feed} = 170s; t_{rinse}= 25s; t_{depres}= 30s; t_{blow} = 170s) obtaining purity of 96.5%, recovery of 87.2% and with a productivity of 3.5 mol C_3H_6/Kg.h, much higher than the one obtained with larger crystals.

7.7.8 Decrease in the nitrogen content

Another item studied here was the decrease of inert in the process. The fact of having an added inert in the process makes it undesirable for industrial applications because additional units are required for separation of the olefin from the inert and for recycling – recompressing the inert that is not always available in a petrochemical plant (carrying consequent additional costs to the overall process).

As we had 50% of nitrogen in the total flowrate the strategy used to diminish the nitrogen was to run two other experiments reducing the molar fraction of inert up to 14% in the feed and pressurization steps. If nitrogen is completely eliminated from these streams the peaks in the gas chromatograph saturates reason why only simulation values for a feed stream without nitrogen are presented. Also, nitrogen reduction in the rinse step is not so marked because of problems with peak saturation in the GC. The experiment without nitrogen was done for CMS 4A where the hydrocarbon flowrates were smaller.

In Table 7.8 it is shown the performance and conditions of the different experiments where the partial pressures of propane and propylene are kept almost constant but reducing the content of nitrogen continuously. In Figure 7.22 we show the molar flowrate of propane, propylene and nitrogen (nitrogen results corresponds only to simulated values because we were not detecting nitrogen in the VSA-PSA unit) of the three different experimental runs and the simulated one without nitrogen (S1). All the cycles shown were collected after reaching the thermal cyclic steady state.

The most important thing to mention is that only a difference in ± 3K in the temperature oscillation was verified. This increase is due to a lower flowrate of gas to remove heat generated by propylene adsorption. As it can be seen from Figure 7.22 the molar flowrate out of the column remains constant indicating that nitrogen was an inert

that in this case is not required to improve the system performance. Even though, using the same step times the recovery of product is higher when nitrogen content is decreased but the purity also decreases so new conditions (increase the rinse step-time) should be estabiished to improve purity without nitrogen.

Table 7.8. VSA – PSA experiments reducing the inert content in the feed and rinse streams for propane and propylene separation at 433 K using zeolite 4A *.

Exp. Nº	Flow, SLPM	y_{C3H6}, feed	y_{C3H8}, feed	y_{N2}, feed	P_{high}, kPa	Purity %, simulated	Recovery %, experimental	Productivity, mol/h.kg
5	2.785	0.27	0.23	0.50	500	99.31 (98.9±0.2)#	85.6	2.64
6	2.074	0.37	0.31	0.32	370	99.28 (98.7±0.3)#	86.6	2.61
14	1.700	0.45	0.41	0.14	250	99.25 (98.9±0.3)#	87.9	2.60
S1	1.700	0.55	0.45	0.00	250	99.09	89.5	3.41

* Step times: pressurization (54s), feed (100s), rinse (25s), depressurization (40s) and blowdown (180s) at a pressure of 10 kPa. # Experimental values.

When nitrogen content is reduced the recovery is increased slightly due to small reduction in the axial dispersion (lower flowrate of gas). Even when the nitrogen content was seriously decreased up to a molar fraction of 0.14, the amount of inert in the blowdown stream exiting the column together with the product remains near 5% that is very similar with the product contamination when using 50% inert in the feed stream. The simulated performance parameters as a function of the nitrogen molar flowrate in the pressurization and feed streams are shown in Figure 7.23.

As the nitrogen reduction did not show significant detrimental changes in the VSA-PSA performance for the study of other variables (temperature and feed pressure) the experiment with 14% of nitrogen will be used as the reference experiment at 433 K.

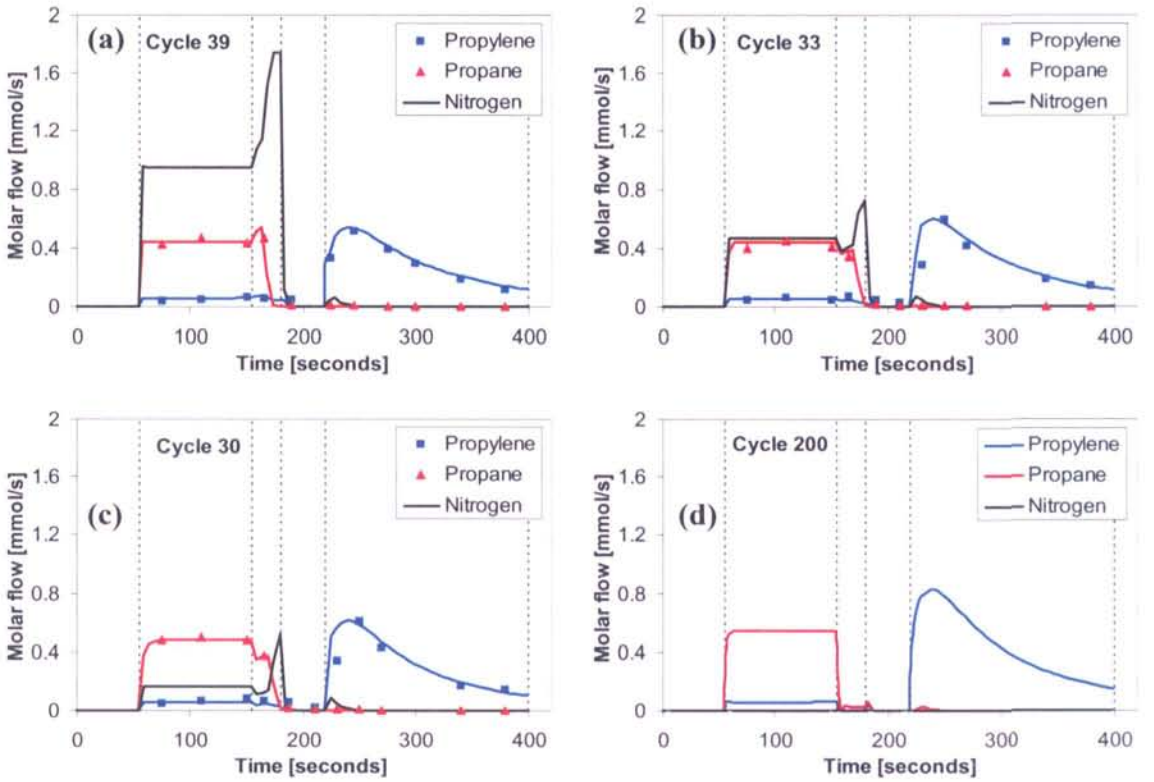

Figure 7.22. Molar flowrate (when thermal cyclic steady state was achieved) at the end of the VSA-PSA column for propane, propylene separation for different nitrogen molar fractions: (a) y_{N2} = 0.50; (b) y_{N2} = 0.32; (c) y_{N2} = 0.14; (d) y_{N2} = 0.00 (simulated results). Experimental conditions and performance parameters are reported in Table 7.8.

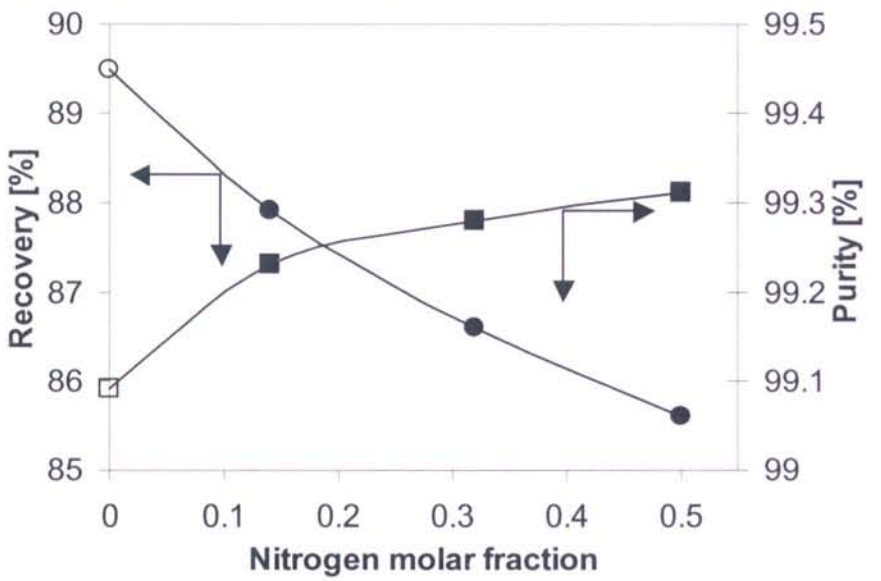

Figure 7.23. Performance parameters of VSA-PSA runs for different gas molar fraction of nitrogen in feed and pressurization steps. Experimental conditions are presented in Table 7.8.

7.7.9 Effects of temperature

In the experiments performed before, the set of operating values was constant and the effect of different step – times was studied. The crystal size of the zeolite 4A and the amount of nitrogen in the process can also be understood as process variables because even when they are not feed stream variables they are part of the process proposed in this thesis and its effect was also evaluated in previous sections. It is also interesting to know the effect that the operating variables have in the process. As the model was able to fit experiments in a wide range of conditions for a single set of operating variables, if we use other conditions and the model still works, there is a certain confidence to say that the simulations will be valid in a wider region.

The first operating variable to study is the temperature. All experiments presented above were performed at 433 K, chosen in a previous section as the trade-off condition between kinetic selectivity and productivity. In this case we will explore two other temperatures: 408 and 463 K. Simulations were also performed at 448 K, but no experiment was done. As mentioned before, the pressurization and feed streams will have only 14% of nitrogen. Experimental conditions at the different temperatures as well as the performance parameters (simulated purity and experimental recovery and productivity) are reported in Table 7.9.

In section 7.3 we have chosen the temperature of 433 K with the explanation that the productivity of the column decreases with temperature (less adsorption at higher temperatures). According to the performance parameters shown in Table 7.9 we can see that the recovery increases with temperature while purity of propylene decreases. The purity of product recovered in the blowdown step is lower because propane diffusivity increases with temperature. On the other side, if we decrease the temperature, the diffusivity of both gases is smaller and thus propylene purity is higher (less adsorption /

desorption of propane) but also the cycling of propylene adsorption / desorption is more difficult (smaller diffusivity coefficient) leading to smaller recovery. Also, the productivity of the bed increases continuously with temperature. In this case, the Δq_{C3H6} between the feed and blowdown steps together with the higher diffusivity of propylene leads to the increase of productivity with temperature, in contradiction with the kinetic selectivity calculations made in section 7.3 using adsorption equilibrium and infinite crystal diffusivity coefficients. The possible reason of this disagreement is the Darken dependence of the diffusivity coefficients required to fit the experimental data but not employed in the kinetic selectivity calculations.

The product purity obtained experimentally at 408 K was 99.0 ± 0.2%, even when this value is lower that the simulated value, is higher than in the experiments at 433 K where purity of 89.4 – 89.8% was obtained. Again the difference can be explained by dead volumes of the unit and the propane contamination in the propylene stream used particularly in the rinse step.

Table 7.9. Effect of temperature in propane – propylene separation by VSA – PSA using zeolite 4A extrudates (CECA)*.

Exp. Nº	T, K	Feed flow, SLPM	Purity %, simulated	Recovery %, experimental	Productivity, mol/h.kg
20	408	1.700	99.43 (99.0±0.2)#	84.3	2.57
14	433	1.700	99.25 (98.9±0.3)#	87.9	2.60
S3	448	1.700	99.18	88.3	2.66
21	463	1.700	99.06 (98.7±0.3)#	88.9	2.67

* Step times: pressurization (54s), feed (100s) at 250 kPa, rinse (25s), depressurization (40s) and blowdown (180s) at a pressure of 10 kPa; $y_{C3H6} = 0.45$; $y_{C3H8} = 0.41$; $y_{N2} = 0.14$. Rinse flowrate: 1.005 SLPM. # Experimental values

The plot of the experimental values obtained for the experiment at 408 K (run 20) where propylene was obtained with higher purity (99.43% propylene simulated against 99.0% obtained experimentally) is plotted in Figure 7.24. In this figure also the time variation of the amount adsorbed of propane in different positions of the column is shown until reaching cyclic steady state. Note that in these lines it is not possible to distinguish between adsorption and desorption of propane on a single cycle. This is similar to what is observed in Figure 7.19 where the amount of propane in all the steps is almost the same for a given cycle. In Figure 7.25 plots of some simulated variables in the cyclic steady state inside the column are shown (amount adsorbed, gas concentration, temperature).

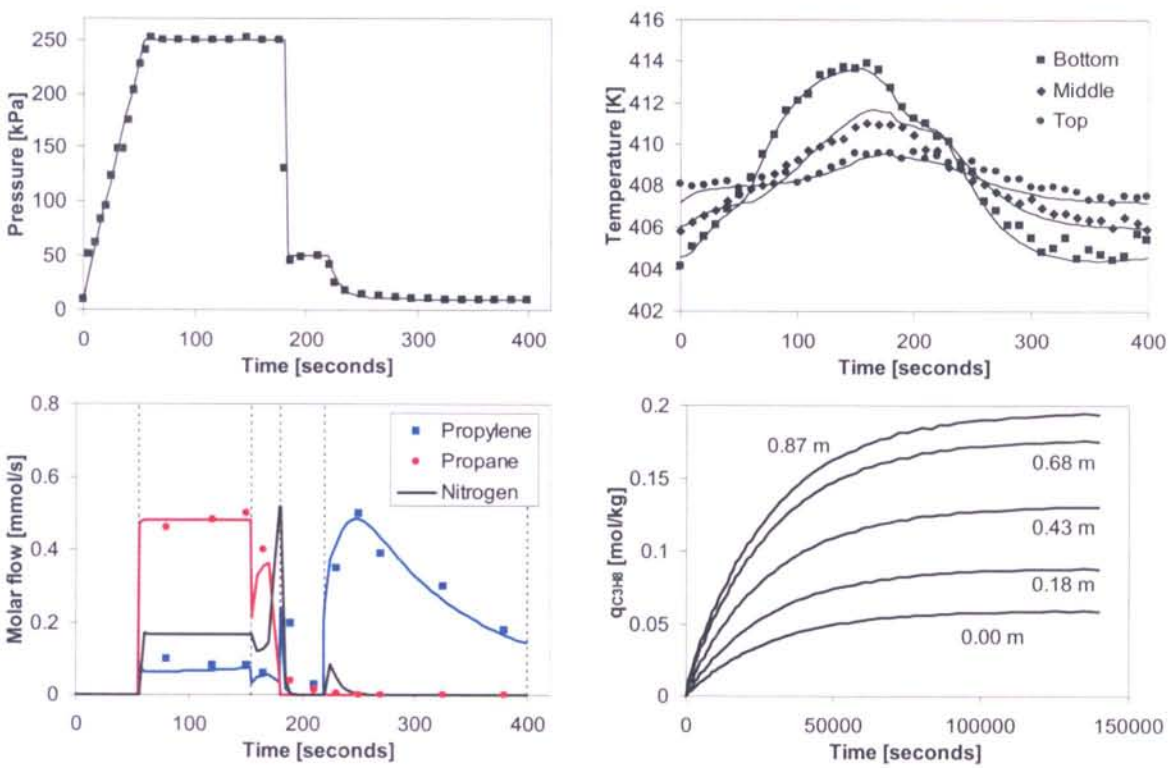

Figure 7.24. Experimental pressure at the outlet of the column, temperature in the bottom, middle and top thermocouples (0.18, 0.43 and 0.68 m from inlet) and molar flowrate of propane and propylene in cycle 35 for VSA-PSA for propane-propylene separation using zeolite 4A (for experimental conditions see Table 7.9, run 20). Adsorption of propane in different positions of the column are also shown.

As a brief summary of the results obtained when changing the temperature of the process, Figure 7.26 shows the performance parameters (recovery and purity) for the runs at 408, 433, 448 and 463 K. Empty symbols correspond to simulated run at 448 K

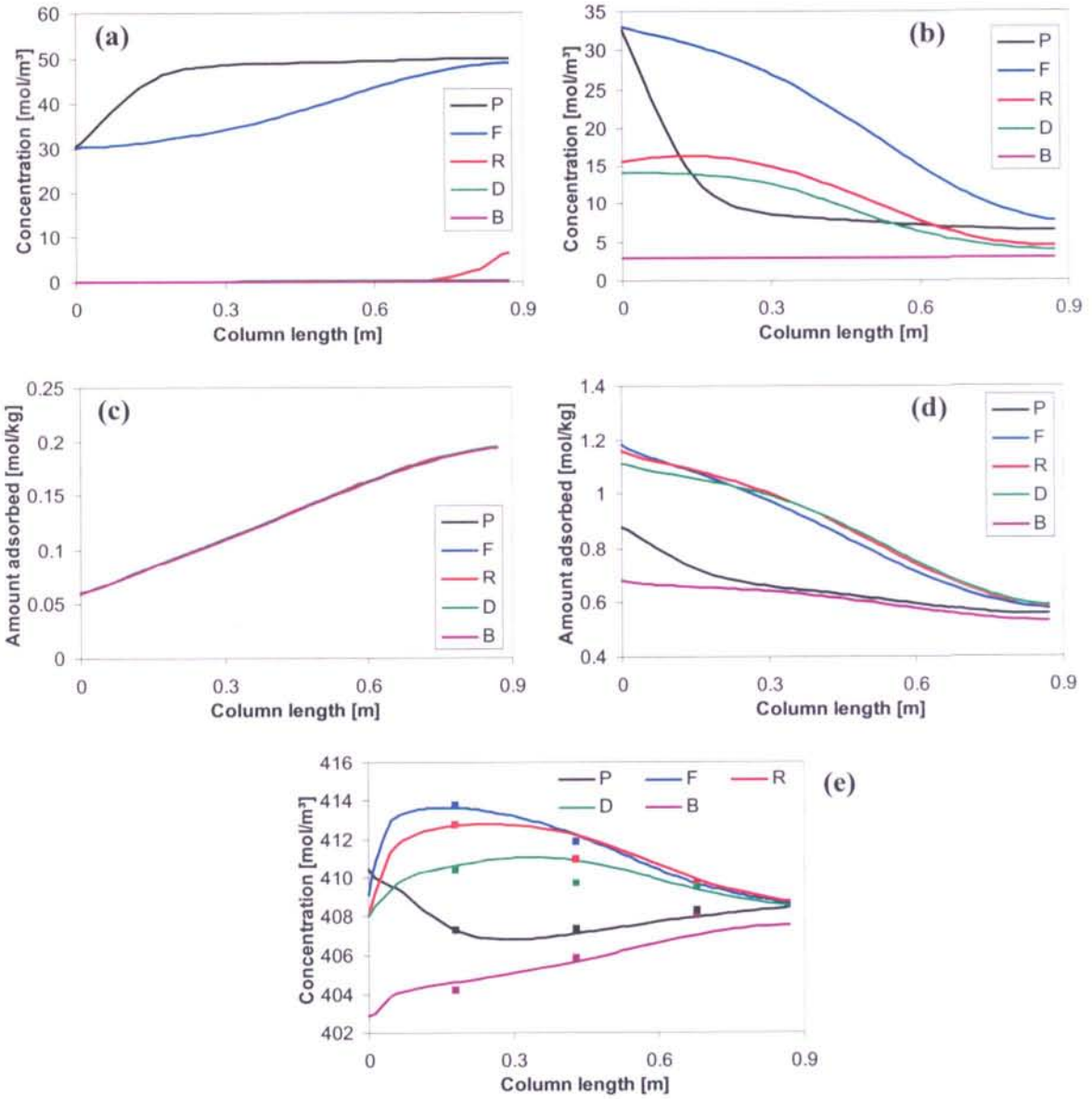

Figure 7.25. Simulated values of propane (a) and propylene (b) concentration, propane (c) and propylene (d) amount adsorbed in the column and solid temperature (e) at the end of each step (P: pressurization; F: feed; R:rinse; D:depressurization; B:blowdown) in cycle 35 for run 20 (for experimental conditions see Table 7.9).

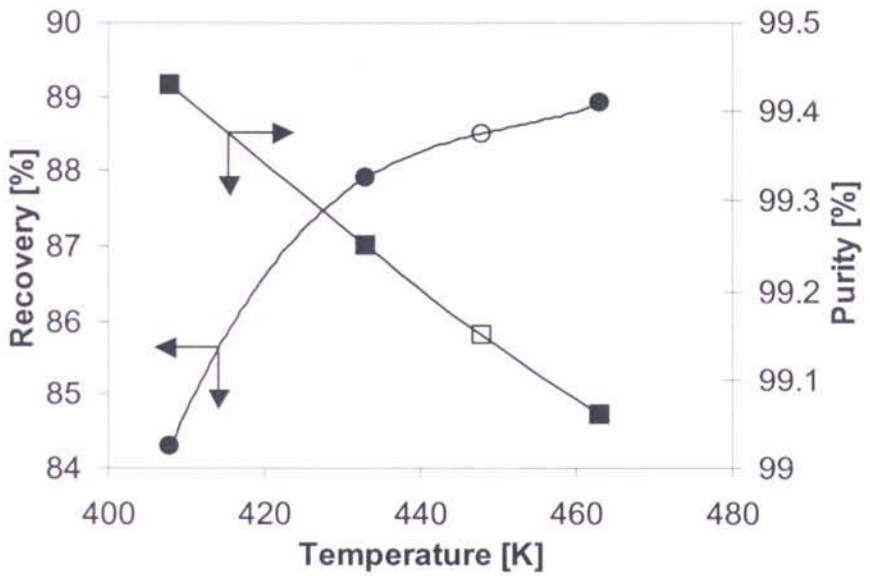

Figure 7.26. Temperature dependence of VSA-PSA performance parameters for propane and propylene separation using zeolite 4A (CECA). The empty point at 448 K represents simulated results for recovery. Points for purity correspond to simulated values. For experimental conditions see Table 7.9.

7.7.10 Effect of step pressures

As explained in previous sections, the step – pressures were chosen to compare this work with the results obtained by Da Silva at the LSRE (Da Silva, 1999). In this section we have chosen run 14 (see Table 7.9) as a reference. Note that temperature in run 14 is 408K where better results were obtained. The results obtained in this experiment (with feed pressure of 250 kPa) were compared with simulated results using higher feed pressures: 300 and 400 kPa. Unfortunately, if the feed pressure is further increased over 250 kPa, the FID detector of the gas chromatograph saturates in some of the steps of the VSA-PSA cycle and for this reason only simulations were carried out for comparison. Low pressure (blowdown) and intermediate pressure (depressurization) were kept constant at 10 kPa and 50 kPa, respectively. The feed pressures used for this parametric study were 250, 300 and 400 kPa.

When the pressure of the pressurization and feed step is changed, the times of these steps also have to be changed. Experimental studies were performed at 300 kPa and 400 kPa and the pressurization time corresponds to the real time that is necessary to pressurize the column. For the feed step, the time was initially selected to introduce approximately the same number of moles as in the cases with feed at 250 kPa using the ideal law of gases. Also at 400 kPa the feed step was increased to study this parameter. The complete set of operating variables for all the simulations is detailed in Table 7.10. Simulated performance parameters: purity, recovery and unit productivity, are detailed in this table.

Table 7.10. Simulated results for propane and propylene separation using VSA – PSA with different feed pressures and step times [*].

Exp. Nº	Pres, s	Feed, s	Rinse, s	P_{high}, kPa	Purity %, simulated	Recovery %, simulated	Productivity, mol/h.kg
20	54	100	25	250	99.43 (99.0±0.2)[#]	84.3[#]	2.57[#]
S4	65	80	25	300	99.33	86.6	2.49
S5	80	60	20	400	99.12	89.3	2.16
S6	80	80	20	400	99.17	88.4	2.47
S7	80	100	20	400	99.21	87.3	2.73
S8	80	120	20	400	99.24	85.8	2.93

[*] Temperature = 408 K; Step times: depressurization (40s) and blowdown (180s) at a pressure of 10 kPa; $y_{C3H6} = 0.45$; $y_{C3H8} = 0.41$; $y_{N2} = 0.14$. Feed flowrate: 1.700 SLPM; Rinse flowrate: 1.005 SLPM. [#] Experimental value.

The first thing to notice is that the purity of propylene obtained as product decreases when feed pressure is increased. The opposite trend holds for recovery. To help in understanding these results purity and recovery versus feed pressure are presented in Figure 7.27. The explanation of this trend is the following: when pressure is increased, the capacity of the column also increases (favorable isotherm), so the number of moles of propylene initially distributed in all the column now will be more concentrated near the entrance of the column. For this reason less propylene is lost in the feed and rinse steps, increasing the recovery. Also because propylene is not occupying the last portion of the column, more propane can be adsorbed and desorbed in the blowdown step, decreasing purity.

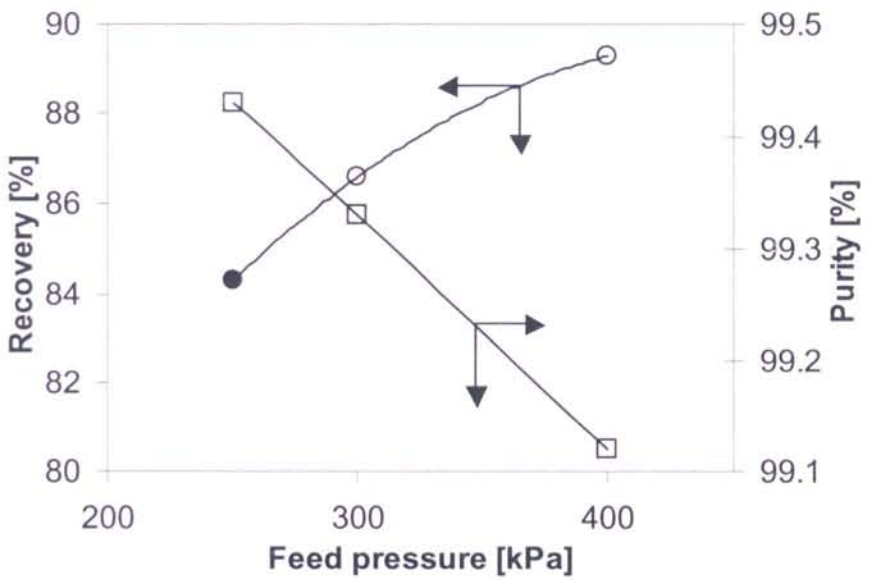

Figure 7.27. Effect of feed pressure in performance of a VSA-PSA unit for propane and propylene for similar number of moles treated using zeolite 4A at 408K. Operating conditions are specified in Table 7.10. Empty point corresponds to simulated values while solid point correspond to experimental value of run 20 (see Table 7.10)

An alternative to improve purity at higher pressures is to make a more effective use of the column. A possible option can be the increase of the feed step-time. Results

of simulations with the same conditions but increasing the feed step-time are presented for the case of feed pressure at 400 kPa in Figure 7.28 and also in Table 7.10. The number of moles of propane adsorbed in the last portion of the column decreases when more propylene is adsorbed and thus purity increases at the expense of decreasing recovery (more propylene is lost in feed and rinse steps).

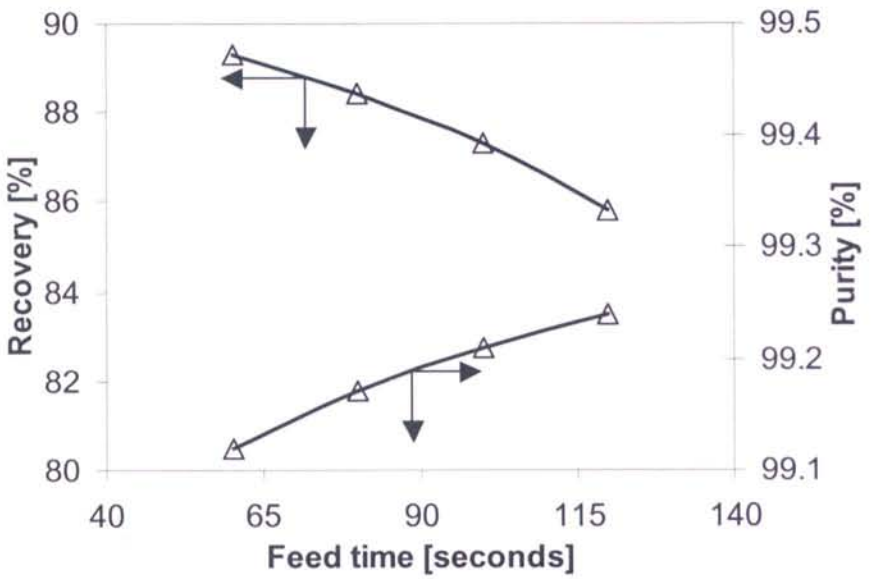

Figure 7.28. Effect of feed step-time in performance of a VSA-PSA unit using zeolite 4A for propane and propylene using feed stream at 400 kPa and 408K (simulated results). Operating conditions are specified in Table 7.10.

7.7.11 Mixtures with ratio 85% propylene – 15 % propane

Finally, a mixture having much more propylene than propane was studied. The mixture with 85/15 propylene to propane ratio may be obtained in the Fluid Catalytic Cracking (FCC) process optimized for propylene production. This characteristic composition is available only when economic constraints are favorable to this operation.

The set of experiments performed is shown in Table 7.11, together with the performance values obtained by simulation of the process. These experiments were performed also at 433K and using nitrogen to dilute the mixture almost to 50%.

All the experiments reported here were well predicted by the model; the relation between the experimental and simulated values of recovery and productivity are coincident. The experimental purity obtained ranged from 98.6 – 99.0%. These values were oscillating with ± 0.2% in the same experiment (all around 98.8%) and as no effective trend was observed in the experiments, the simulated value is being reported. As productivity is expressed in moles of propylene treated per hour per kilogram of zeolite, the values of productivity are higher than in the 54/46 mixtures because more moles of propylene per second are introduced to the column.

Table 7.11 VSA – PSA results for propane - propylene separation by VSA – PSA using zeolite 4A (mixture 85/15 propylene to propane ratio diluted to 50% with nitrogen)*.

Exp. Nº	Pres, s	Feed, s	Rinse, s	Depres., s	Blow, s	Purity %, simulated	Recovery %, experimental	Productivity, mol/h.kg
1	60	70	130	60	220	99.32 (99.0±0.2)#	62.7	2.69
3	60	60	25	40	220	99.18 (98.9±0.2)#	83.1	3.08
16	54	60	15	25	180	99.12 (98.6±0.3)#	92.2	4.10
17	54	85	15	25	220	99.23 (98.8±0.2)#	89.6	4.34
18	54	60	40	25	180	99.31 (98.5±0.4)#	90.2	3.90

* Temperature = 433 K; Feed at 500 kPa; Blowdown at 10 kPa; y_{C3H6} = 0.453; y_{C3H8} = 0.074; y_{N2} = 0.473. Feed flowrate: 3.160 SLPM; Rinse flowrate: 2.700 SLPM. # Experimental values.

In these experiments, the general trend is the same as previously observed for the 54/46 (propylene to propane ratio): if the rinse step is decreased to a minimum

value, the recovery also increases while purity is only slightly affected; when the blowdown time is reduced to 180s instead of 220s, the purity also decreases.

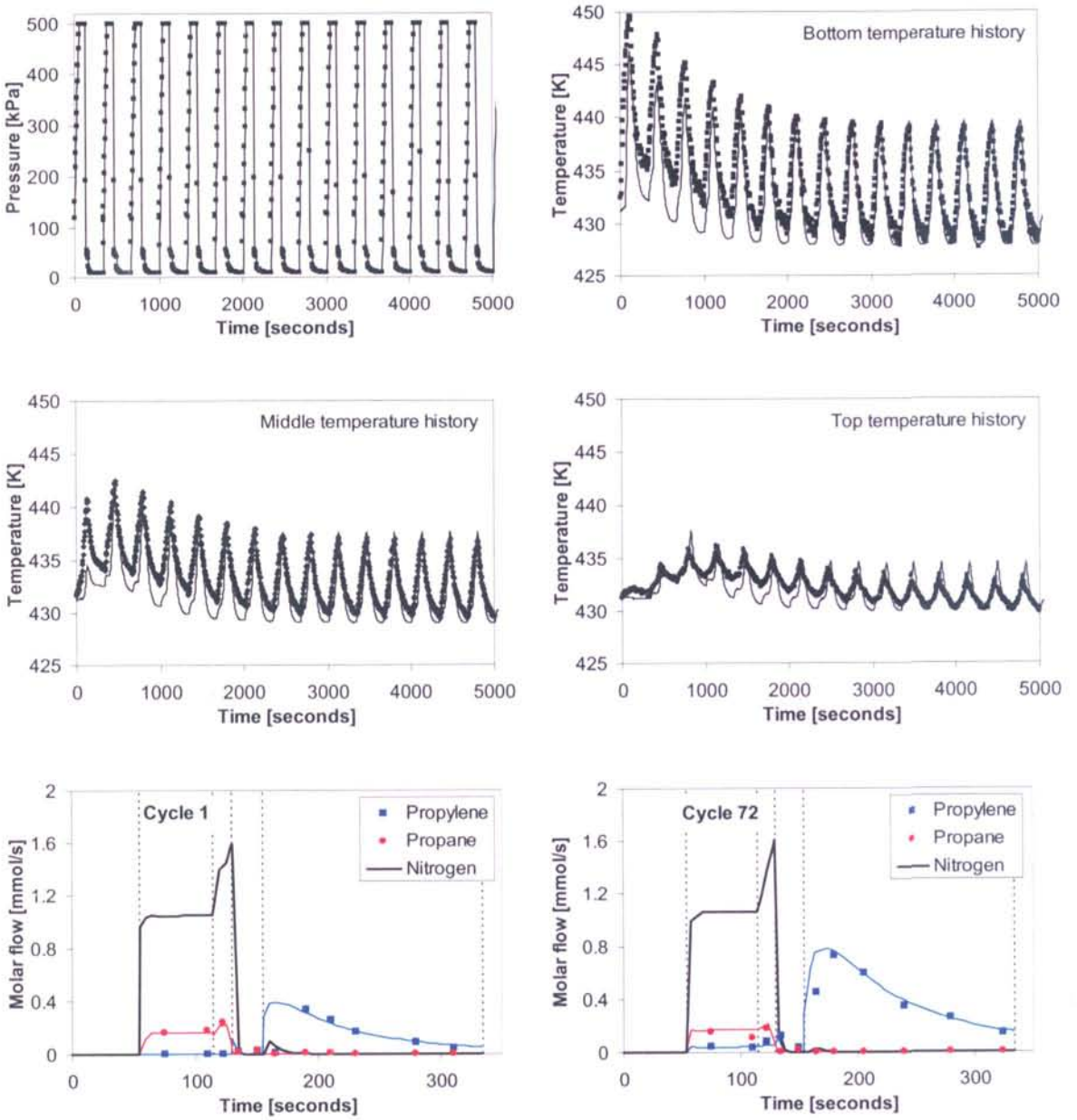

Figure 7.29. Experimental pressure at the outlet of the column, temperature in the bottom, middle and top thermocouples (0.18, 0.43 and 0.68 m from inlet) and molar flowrate of propane and propylene in the first cycle and in cycle 72 for VSA-PSA for propane-propylene separation using zeolite 4A (for experimental conditions see Table 7.11, run 16).

As an example of the experiments shown in Table 7.11 we report in Figure 7.29 the temperature and pressure profiles as well as the molar flowrates of propane and propylene leaving the column in cycles 1 and 72 obtained in run 16. In the flowrate plot also the nitrogen flow is reported. It can be seen that when compared with experiments performed with 54/46 propylene to propane ratio, the amount of nitrogen contaminating the propylene stream in the blowdown step is much less than before, even though a process without nitrogen is desired.

7.7.12 Degassing of the zeolite by heat treatment

The question about the degassing of the zeolite samples started in Chapter 2 where the first sample of zeolite 4A CECA was initially activated at 593K and a small adsorption of propylene (that is not reproducible) was obtained. If the sample is activated at 673K the amount of propylene is substantially higher (see Figure 2.21). With laboratory prepared crystal samples the situation was the same but as crystals were not heated at high temperature (calcination) like the zeolite crystals in the extrusion process, this difference could be explained. In addition, these examples showed that the problem of reproducibility was always present.

The problems with activation of zeolite 4A were mentioned for the first time for smaller molecules like nitrogen and methane where large differences of diffusivity coefficients (almost two orders of magnitude) were reported (Ruthven, 2001), but with almost the same activation energy. In this case we have observed this effect for propane when comparing our work with the one by Khodakov and Rees (1995) where almost the same activation energy was obtained with a difference of one order of magnitude in diffusivity coefficient. An increase of one order of magnitude in propane diffusion into

zeolite 4A may have very detrimental effects on product purity in kinetic propane – propylene separation by VSA-PSA.

We did not make different heat treatments to the zeolite but we have used the same activation protocol for all experiments, since adsorption equilibrium to VSA-PSA experiments. When modeling VSA-PSA behavior we have first used the model with a constant value of diffusivity for all range of concentrations and very high purity of propylene was obtained with around 45-50% of product recovery. These results were coincident with previous simulated ones mentioned in Table 7.5 (Cheng et al., 2002; Yang et al., 2001). When the first experiments of fixed bed were performed we have verified that the propylene diffusivity was much higher than the obtained by ZLC or diluted breakthrough experiments. For this reason the concentration dependence of the diffusivity coefficient with the Darken law was successfully implemented, not only for fixed bed experiments but also for VSA-PSA experiments. With that strategy 21 VSA-PSA experiments were successfully predicted, with the always reported difference between experimental and simulated values in product purity.

Once the set of experiments reported previously were performed the bed was stopped and atmospheric air was allowed to enter into the column. This may happen in industrial operation. Petrochemical industries stop once per year for maintenance (in Bahía Blanca, Argentina this is performed almost always the day 10 of December for a period of a week or 10 days). In this period the VSA-PSA unit will be without feeding. Two alternatives are possible: the unit remains closed if no maintenance is required or the unit is opened and the adsorbent after working with C_3 separation is contacted with air. Then a new degassing procedure is required with the same protocol used before. In the laboratory unit the column was in contact with air for 10 days, then closed and a new degassing procedure at 593K under flow of nitrogen.

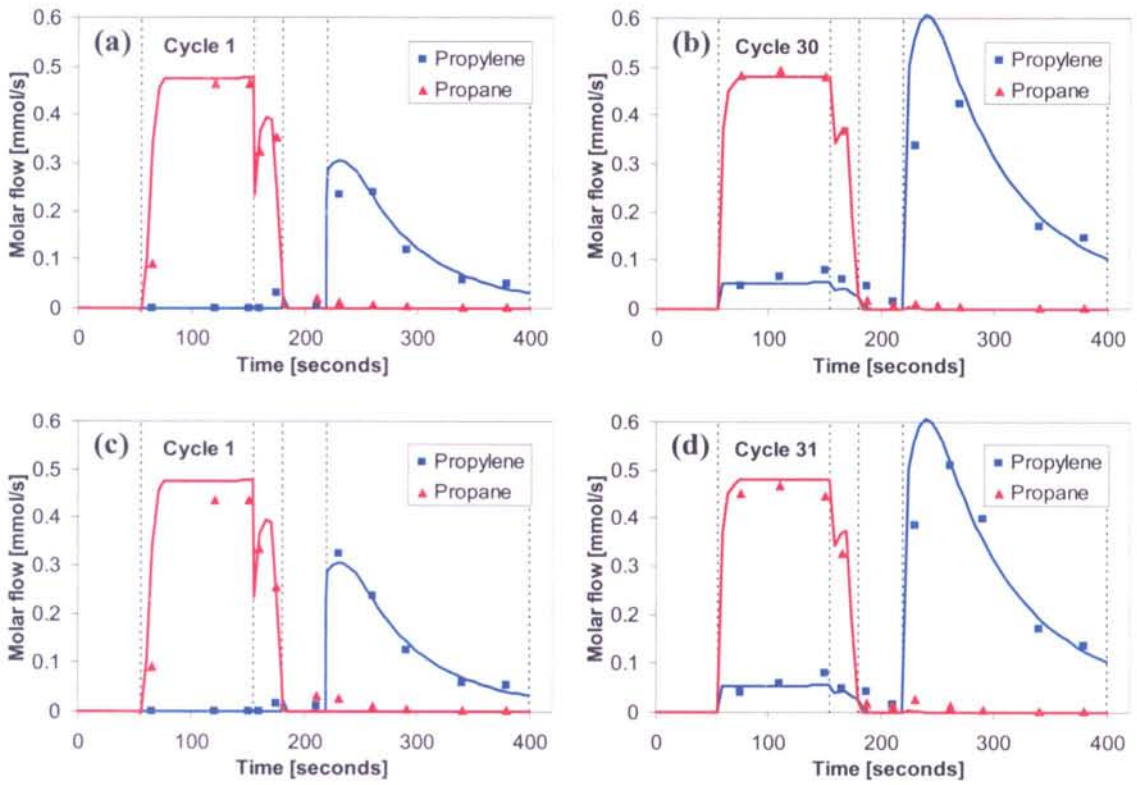

Figure 7.30. Molar flowrates of run 14 and same run after air contact and second heat treatment at high temperature: run 14 (*a and b*) and same run after second heat treatment (*c and d*) For experimental conditions see Table 7.8.

An experiment performed before (run 14, Table 7.8) was repeated after this second high temperature heat treatment. The pressure history and temperature profiles were nearly the same and do not require to be reported again. The main substantial difference was in the molar flowrate of propane in the column. A much higher contamination of the product was observed as shown in Figure 7.30 where the molar flowrates of the initial run 14 and the repeated run 14 after heat treatment are shown. After the new VSA-PSA experiment a flow of nitrogen was allowed to pass for 40 hours and experiment was repeated confirming that propane contamination of product is much higher (more than double of initial values). The propylene molar flow was comparable with run 7 (before the second heat treatment), so the possibility of zeolite coking was retrieved (also coking will not produce propane diffusivity enhancement).

Although no further study was performed on this item it is important to know that the activation protocol and /or contact of the zeolite with air is very important and both of them have to be avoided once the initial activation procedure has been performed performed.

7.8 Conclusions

The separation of propane – propylene streams was tested by VSA-PSA using two different commercial adsorbents (carbon molecular sieve 4A Takeda and zeolite 4A CECA) and simulations were performed for a laboratory-made sample Ag/SBA-15 = 0.5. A five-step cycle comprising pressurization, feed, rinse, depressurization to intermediate pressure and counter-current blowdown was employed. The modeling of the process was done using a model previously developed in this laboratory based in pure component data using the multisite-Langmuir model. Pure component diffusivity data previously determined were also used.

The sample Ag/SBA-15 = 0.5 has large equilibrium selectivity towards propylene due to π-complexation bonds with the olefin and was studied by simulations for propane – propylene separation by VSA-PSA. To obtain purity higher than 99% the recovery of propylene is 63% but polymer grade propylene could not be obtained in any of the conditions tested. If the purpose is to obtain chemical grade propylene, this adsorbent may be a good choice because for product purity of 91% the recovery can be higher than 90% with only a small contamination of the propane stream with propylene achieving propane HD-5 specification (fuel degree with less than 5% propylene).

Carbon Molecular Sieve 4A (Takeda) and zeolite 4A (CECA) were tested experimentally for propane – propylene separation in a VSA-PSA unit. Binary breakthrough curves of CMS 4A were measured using three different propylene molar

fractions: 0.29, 0.55 and 0.80 counterbalanced only with propane. No nitrogen was used in the feed stream. Also some VSA-PSA experiments were performed. Purity of propylene was never higher than 90%. To obtain high propylene recovery also the depressurization step was eliminated from the cycle. According to the results obtained in binary breakthrough experiments with 0.8 molar fraction of propylene it can be seen that the separation of both gases will be very difficult and for this reason no more detailed studies were performed.

Zeolite 4A (CECA) proved to be the best adsorbent for propane – propylene separation. Initially the VSA-PSA separation was studied with parameters and operating variables previously used by Da Silva at the LSRE (Da Silva, 1999). Even though, the results obtained with the sample of zeolite used in this work were better than with Rhone-Poulenc previously tested due to a smaller diffusivity coefficient of propane. Due to this lower diffusivity of propane in zeolite 4A the rinse step could be strongly minimized and also other step-times were improved to obtain high purity and also high recovery. Modeling of the VSA-PSA experiments were done also with multisite-Langmuir model and pure component diffusivities corrected with the Darken law to account for concentration dependence. Experimental data were successfully predicted with the model. Differences between simulated and experimental values of purity were around 0.8%. Experimentally, purity was around 98.8% in all experiments and no significant variations were observed when changing the step times, operating variables and feed composition. The differences between simulated values and experimental ones may be due to dead volumes in the installation and to the propylene feed with 0.5% of propane (99.4% purity specified by Air Liquide). The crystal size of the sample was also varied (study performed only by simulations) determining that with smaller crystals

the propane time constant (r_c^2 / D_c) decreases and more propane diffuses into and out of zeolite 4A desorbing more in the blowdown step and contaminating the product.

In the runs initially tested the feed was diluted to 50% with nitrogen. The content of inert was successively diminished experimentally up to 14% having only minor effects in recovery and purity.

Also the effect of some operating variables used were studied, namely temperature and feed pressure. Most of the runs were performed at 433 K according to a previous selection using a defined kinetic selectivity factor. According to experiments and simulations it was determined that higher purity propylene can be obtained at 408 K still with recovery higher than 80%. Further increase of the temperature results in a decrease of purity and an increase of recovery. Also at higher temperatures, higher productivities were obtained. When the pressure of the feed stream is increased the purity decreases and the recovery increases (for similar number of moles treated by the unit). Even though the purity can be improved by increasing the feed step (at the expense of decreasing the recovery) and also enhancing the process productivity.

A mixture having larger propylene to propane ratio (85 / 15) was also studied and the same trend observed for all the variables.

After two months of VSA-PSA operation, no coking was observed in the zeolite 4A sample. Although, as reported here, the heat treatment of the sample combined with the contact with atmospheric air is a very important operational variable and further studies are required to explain the behavior of zeolite 4A under these conditions.

Nomenclature

a'	area to volume ratio, m^{-1}
a_i	number of neighboring sites occupied by component *i*

Bi_i	Biot number of component i
C_i	bulk molar concentration of component i in the gas phase, mol/m^3
$\overline{c_i}$	averaged concentration in the macropores for component i, mol/m^3
$\widetilde{C}_p$	molar constant pressure specific heat of the gas mixture, J/mol.K
$\widetilde{C}_{ps}$	constant pressure specific heat of the adsorbent, J/kg.K
$\hat{C}_{pw}$	specific heat of the column wall, J/kg.K
C_T	total gas concentration, mol/m^3
$\widetilde{C}_v$	molar constant volumetric specific heat of the gas mixture, J/mol.K
$\widetilde{C}_{vi}$	molar constant volumetric specific heat of component i, J/mol.K
$D_{ax,i}$	axial dispersion coefficient of component i, m^2/s
$D_{p,i}$	pore diffusivity of component i, m^2/s
$D_{c,i}$	crystal diffusivity of component i, m^2/s
$D^{\infty}_{c,i}$	infinite dilution crystal diffusivity of component i, m^2/s
$D^{\infty}_{c,io}$	infinite dilution crystal diffusivity of component i at infinite temperature, m^2/s
d_p	pellet diameter, m
$K_{eq,i}$	adsorption constant of component i, 1/kPa
$K_{eq,i}^{o}$	adsorption constant at limit T $\rightarrow \infty$ for component i, 1/ kPa
h_f	film heat transfer coefficient between the gas and the solid phase, W/m^2.K
h_w	film heat transfer coefficient between the gas phase and the column wall, W/m^2.K
k_{fi}	film mass transfer resistance, m/s
k_g	gas thermal conductivity, W/m.K

$k_{g,ex}$ thermal conductivity of the gas surrounding the column, W/m.K

P total pressure, kPa

q_i adsorbed phase concentration of component *i*, mol/kg

q_i^* equilibrium adsorbed phase concentration of component *i*, mol/kg

$\langle \overline{q_i} \rangle$ extrudate averaged adsorbed phase concentration, mol/kg

$\overline{q_i}$ crystal averaged adsorbed phase concentration, mol/kg

$q_{max,i}$ saturation capacity of component *i*, mol/kg

R_g ideal gas constant, 8.314 kJ/mol.K

r_c crystal radius, m

t_{blow} blowdown step time, s

t_{rinse} rinse step time, s

t_{total} total cycle time, s

T_g temperature of the gas-phase, K

T_s solid (extrudate) temperature), K

T_w wall temperature, K

U global external heat transfer coefficient, W/m².K

u_i superficial velocity, m/s

x_i adsorbed phase molar fraction of component *i*

y_i molar fraction of component *i* in the gas phase

Greek Letters

α_w ratio of the internal surface area to the volume of the column wall, m^{-1}

α_{wl} ratio of the logarithmic mean surface area of the column shell to the volume of the column wall, m^{-1}

β_{eq} equilibrium selectivity factor

β_{sel} kinetic selectivity factor calculated by eq. 7.1

ρ_g	gas density, kg/m^3
ρ_p	adsorbent density, kg/m^3
λ	axial heat dispersion, W/m^2.K
$(-\Delta H_i)$	heat of adsorption of component *i*, J/mol
ε_c	column void fraction
ε_p	porosity of the pellet
τ_p	pore tortuosity
μ_g	gas viscosity, Pa.s

References

Bird, R.B.; Stewart, W.E.; Lightfoot, E.N. *Transport Phenomena* (2nd edition), Wiley International, Singapore, **2002**.

Cavenati, S.; Grande, C. A.; Rodrigues, A. E. Layered Pressure Swing Adsorption for Methane Recovery from $CH_4/CO_2/N_2$ Streams, *Adsorption,* **2004**, in press.

Cheng, L. S.; Wilson, S. T. *Vacuum Swing Adsorption Process for Separating Propylene from Propane*. U.S. Patent 6,296,688, **2001**.

Cho, S. H.; Han, S. S.; Kim, J. N.; Choudary, N. V.; Kumar, P.; Bhat, S. G. T. *Adsorbents, Method for the Preparation and Method for the Separation of Unsaturated Hydrocarbons for Gas Mixtures*. U.S. Patent, 6,315,816, **2001**.

Choudary, N. V.; Kumar, P.; Puranik, V. R.; Bhat, S. G. T. *Adsorbents, Method for the Manufacture Thereof And Process for the Separation of Unsaturated Hydrocarbons from Gas Mixture*. U.S. Patent Application US2003/0097933A1, **2003**.

Da Silva, F. A. *Cyclic Adsorption Processes: Application to Propane / Propylene Separation*. Ph.D. Dissertation, University of Porto, Portugal, **1999**.

BIBLIOTECA F.E. PORTO

Da Silva, F. A.; Rodrigues A. E. Adsorption equilibria and kinetics for propylene and propane over 13X and 4A zeolite pellets. *Ind. Eng. Chem. Res.*, **1999**, 38, 2434-2438.

Da Silva, F. A.; Rodrigues A. E. Propylene/Propane separation by VSA using commercial 13X zeolite pellets *AIChE J.*, **2001**, 47(2), 341-357.

Da Silva, F. A.; Rodrigues A. E. Vacuum swing adsorption for Propylene/Propane separation with 4A zeolite pellets. *Ind. Eng. Chem. Res.*, **2001**, 40(24), 5758-5774.

Davesac, R. R. *Separação Propano / Propileno e Reactores Adsorptivos com Modulação de Pressão*. Ph.D., University of Porto, Portugal (in preparation).

Do, D. D. *Adsorption Analysis: Equilibria and Kinetics*. Imperial College Press, London, **1998**.

Engelhard Corporation. *Purification Technologies Brochure*, **2001**.

Gorbach, A.; Stegmaier, M.; Eigenberger, G. Measurement and Modeling of Water Vapor Adsorption on Zeolite 4A – Equilibria and Kinetics. *Adsorption*, **2004**, 10, 29-46.

Grande, C. A.; Gigola, C.; Rodrigues, A. E. Propane-Propylene Binary Adsorption on Zeolite 4A. *Adsorption*, **2003a**, 9, 321-329.

Grande, C. A., Silva, V.M.T.M., Gigola, C., Rodrigues, A. E. Adsorption of Propane and Propylene Onto Carbon Molecular Sieve. *Carbon*, **2003b**, 41, 2533-2545.

Guerin de Montgareuil, P.; Domine, D. *Process for Separating a Binary Gaseous Mixture by Adsorption*. US Patent 3,155,468, **1964**.

Habgood, H. W. The Kinetics of Molecular Sieve Action. Sorption of Nitrogen-Methane Mixtures by Linde Molecular Sieve 4A. *Can. J.Chem.*, **1958**, 36, 1384-1397.

Incropera, F. P.; Witt, D. P. D. *Fundamentals of Heat and Mass Transfer*, 4ºdition, John Wiley & Sons, New York, **1996**.

Izumi, J. *Adsorption Technology Application to the Industries in Japan*. FOA-8 (Orhan Talu Chairman), May 23-28, Sedona, Arizona, USA, **2004**.

Järvelin, H.; Fair, J. R. Adsorptive Separation of Propane – Propylene Mixtures. *Ind. Eng. Chem. Res.*, **1993**, 32, 2201-2207.

Jee, J. G., Lee, J. S., Lee, C. H. Air Separation by a Small-Scale Two-Bed Medical O_2 Pressure Swing Adsorption. *Ind. Eng. Chem. Res.*, **2001**, 40, 3647-3658.

Khodakov, A. Y.; Rees, L. V. C. Effect of Propane on the Kinetics of Carbon Dioxide Adsorption in NaA Zeolites. *Gas Sep. Purif.*, **1995**, 9, 253-257.

Ko, D., Siriwardane, R., Biegler, L. T. Optimization of a Pressure-Swing Adsorption Process Using Zeolite 13X for CO_2 Sequestration. *Ind. Eng. Chem. Res.*, **2003**, 42, 339-348.

Kulvaranon, S.; Findley, M. E.; Liapis, A. I. Increased Separation by Variable Temperature Stepwise Desorption in Multicomponent Adsorption Processes. Ind. Eng. Chem. Res., **1990**, 29, 106-115.

Kuznicki, S. M.; Bell, V. A. *Olefin Separation Employing ETS Molecular Sieves*. U.S. Patent, 6,517,611, **2003**.

Liapis, A.; Findley, M.; Johnson, J.; Jetz, S.; Finebrock, Q. Rates and equilibria of adsorption and desorption of propane and propylene on 13X molecular sieves determined experimentally using a differential sorption bed system, *Sep Technol.* **1992**, 2, 141-154.

Liu, Y.; Delgado, J.; Ritter, J. A. Comparison of Difference Techniques for Simulation Pressure Swing Adsorption. *Adsorption*, **1998**, 4, 337-344.

Malek, A.; Farooq, S. Determination of Equilibrium Isotherms Using Dynamic Column Breakthrough and Constant Flow Equilibrium Desorption. *J. Chem. Eng. Data*, **1995**, 40, 25-32.

Mersmann, A.; Fill, B.; Hartmann, R.; Maurer, S. The Potential of Energy Saving by Gas Phase Adsorption Processes. *Chem. Eng. Technol.*, **2000**, 23, 937-944.

Na, B. K.; Lee, H.; Koo, K. K.; Song, H. K. Effect of Rinse and Recycle Methods on the Pressure Swing Adsorption Process To Recover CO_2 from Power Plant Flue Gas Using Activated Carbon. *Ind. Eng. Chem. Res.* **2002**, 41, 5498-5503.

Newalkar, B. L., Choudary, N. V., Kumar, P., Komarneni, S. Bhat, T. S. G. Exploring the Potential of Mesoporous Silica, SBA-15, as an Adsorbent for Light Hydrocarbon Separation. *Chem. Mater*, **2002**, 14, 304-309.

Nilchan, S.; Pantelides, C. C. On the Optimisation of Periodic Adsorption Processes. *Adsorption*, **1998**, 4, 113-147.

Nitta, T.; Shigetomi, T.; Kuro-Oka, M.; Katayama, T. An adsorption isotherm of multi-site occupancy model for homogeneous surface. *J. Chem. Eng. Japan*, **1984**, 17, 39-45.

Olson, D.H. *Light Hydrocarbon Separation Using 8-Member Ring Zeolites*. U.S. Patent 6,488,741, **2002**.

Ramachandran, R., Dao, L.H. and Brooks, B. *Method of Producing Unsaturated Hydrocarbons and Separating the Same from Saturated Hydrocarbons*, U.S. Patent 5,365,011, **1994**.

Rege, S. U.; Padin, J.; Yang, R. T. Olefin/Paraffin Separations by Adsorption - Pi-Complexation vs. Kinetic Separation. *AIChE J.*, **1998**, 44, 799-809.

Rege, S. U.; Yang, R.T. A Simple Parameter for Selecting an Adsorbent for Gas Separation by Pressure Swing Adsorption. *Sep. Sci. Technol.*, **2001**, 36, 3355-3365.

Reyes, S.; Krishnan, V. V.; De Martin, G. J.; Sinfelt, J. H.; Strohmaier, K. G.; Santiesteban, J. G. *Separation of Propylene from Hydrocarbon Mixtures*. International Patent, WO 03/080548 A1, **2003**.

Rota, R.; Wankat, P. C. Intensification of Pressure Swing Adsorption Processes, *AIChE J.*, **1990**, 36(9), 1299-1312.

Ruthven, D. M. *Principles of adsorption and adsorption processes*. Wiley, New York, **1984**.

Ruthven, D. M. Short Communication: Diffusion of Simple Molecules in 4A Zeolite. *Adsorption*, **2001**, 7, 301-304.

Ruthven, D. M.; Raghavan, N. S.; Hassan, M. M. Adsorption and Diffusion of Nitrogen and Oxygen in a Carbon Molecular Sieve. *Chem. Eng. Sci.*, **1986**, 41, 1325-1332.

Ruthven, D. M., Farooq, S., Knaebel, K. S. Pressure Swing Adsorption, VCH Publishers, New York, **1994**.

Schröter H. J.; Jüntgen H. *Gas Separation by Pressure Swing Adsorption Using Carbon Molecular Sieves.* In: Adsorption: Science and Technology, NATO ASI Series (Rodrigues, LeVan and Tondeur editors), Netherlands: Kluwer Academic Publishers; **1988**.

Sircar, S. Pressure Swing Adsorption. *Ind. Eng. Chem. Res.*, **2002**, 41, 1389-1392.

Silva, J. A. C. *Separation of n/iso – Paraffins by Adsorption Process.* Ph.D. Dissertation, University of Porto, Portugal, **1998**.

Skarstrom, C. W. *Method and Apparatus for Fractionating Gaseous Mixtures by Adsorption*. U.S. Patent 2,944,627, **1960**.

Sundaram, N.; Yang, R. T. On the Pseudomultiplicity of Pressure Swing Adsorption Periodic States. *Ind. Eng. Chem. Res.*, **1998**, 37, 154-158.

Theague, K. G.; Edgar, T. F. Predictive Dynamic Model of a Small Pressure Swing Adsorption Air Separation Unit. *Ind. Eng. Chem. Res.*, **1999**, 38, 3761-3775.

Ullmann's Encyclopedia of Industrial Chemistry; 7ª Edition, Wiley-VCH, Verlag GmbH & Co..KGaA, **2003**.

Wakao, N.; Funazkri, T. Effect of Fluid Dispersion Coefficients on Particle-te-Fluid Mass Transfer Coefficients in Packed Beds. *Chem. Eng. Sci.*, **1978**, 33, 1375-1384.

Wasch, A. P. D.; Froment, G. F. Heat Transfer in Packed Beds. *Chem. Eng. Sci.*, **1972**, 27, 567-576

Yang, R. T. *Gas Separation by Adsorption Processes.* Butterworths, Boston, **1987**.

Yang, R. T. *Adsorbents. Fundamentals and Applications,* J. Wiley, New Jersey, USA, **2003**.

Yang, R. T.; Padin, J.; Rege, S. U. *Selective Adsorption of Alkenes Using Supported Metal Compounds*. U.S. Patent 6,423,881, **2001**.

Zhu, W.; Kapteijn, F.; Moulijn, J. A.; den Exter, M. C.; Jansen, J. C. Shape Selectivity in Adsorption of the All- Silica DD3R. *Langmuir*, **2000**, 16, 3322-3329.

8. Conclusions and Recommendation for Future Work

8.1 Conclusions of Ph.D. work

In this work, the separation of propane-propylene mixtures was studied by Vacuum Pressure Swing Adsorption, VSA-PSA. Although research work was done at the LSRE prior to the starting point of this thesis (Da Silva, 1999), the fundamental reason why this VSA-PSA process was still under research was the lack of a selective adsorbent to achieve the separation in order to obtain polymer grade propylene (purity higher than 99.5%). For this reason, large attention was given to the experimental measurement of adsorption equilibrium and kinetics of both hydrocarbons in several adsorbents. This work was done firstly in three commercial samples: wide pore and narrow pore silica gel (Grace Davison, Spain) and zeolite 5A (Grace Davison, Spain). Adsorption equilibrium on these samples was already reported in literature (Lewis et al., 1950; Ruthven and Derrah, 1972), but the initial idea (suggested by Dr. Da Silva in his PhD dissertation) was to spread some transition metal in a matrix to enhance propylene adsorption (Yang and Kikkinides, 1995) and these samples would be the starting matrices. At that time, two new adsorbents came into scene in the framework of project CYTED V.8: zeolite 4A (CECA) and Carbon Molecular Sieve 4A (Takeda), CMS4A. In these adsorbents, the separation of the gases was supposed to be controlled by the micropore diameter having a kinetic separation by VSA-PSA. The measurement of adsorption equilibrium and kinetics on these adsorbents was not straightforward, because of problems with the activation of the samples and non-reproducibility of the data obtained. Another point that was critical was the gas-adsorbent contact time required to establish an equilibrium point. Once the conditions to obtain reproducible results were found, adsorption equilibrium and kinetic data of pure components and

binary mixtures were measured (Grande et al., 2003a; Grande et al., 2003b; Grande and Rodrigues, 2004a; Grande and Rodrigues, 2004b) confirming a much higher kinetic selectivity of these adsorbents when compared with silica gel and zeolite 5A(Grande and Rodrigues, 2001; Grande et al., 2002). In both adsorbents, the complete exclusion of propane previously reported was not observed (Rege et al., 1998; Da Silva, 1999; Patiño-Iglesias et al., 2004). Propane penetrates the structure of zeolite 4A crystals very slowly taking three days to reach a single adsorption equilibrium point at 423 K. The values of equilibrium reported are much higher than previously reported (Da Silva, 1999; Patiño-Iglesias et al., 2004). Activation energy of propane diffusion in 4A crystals is in agreement with the value reported by Khodakov and Rees (1995) although the crystal diffusivity is around one order of magnitude smaller.

The adsorption equilibrium of pure propane and propylene and their binary mixtures on zeolite 4A (423 and 473 K) and carbon molecular sieve 4A (373 K) was measured in a manometric-chromatographic unit built during this work. The unit is also able to measure adsorption equilibrium and kinetics of pure components extending the laboratory capabilities up to 500 kPa against the previous microbalance unit which maximum pressure was 100 kPa.

None of the commercial adsorbents tested have high equilibrium selectivity against propylene. For this reason, new adsorbents were prepared in laboratory by Elena I. Basaldella's group (CINDECA, La Plata, Argentina). These adsorbents were prepared by dispersion of silver nitrate in a mesoporous ordered silica matrix of SBA-15 (Zhao et al., 1998). Two different loadings of silver were employed with the ratios $Ag/SiO_2 = 0.5$ and $Ag/SiO_2 = 1.0$. Adsorption equilibrium and kinetics of pure propane and propylene in these two samples as well as in the SBA-15 matrix were measured (Grande et al., 2004a). The adsorbent Ag/SBA-15 = 0.5 (having the ratio $Ag/SiO_2 = 0.5$) was the best

adsorbent presenting equilibrium selectivity over 10 at 100 kPa and 343 K. Results on this kind of adsorbents were recently published with similar results but with slightly lower selectivity for propylene because of higher adsorption of propane (Choudary et al., 2003). Due to the small amount of material and since it is in powder form, no other experimental studies were performed with those adsorbents, although with the Ag/SBA-15 = 0.5 sample, VSA-PSA simulations were performed. Also, in industrial propane – propylene streams there is around 0.2 – 0.8% of hydrogen which will reduce the Ag^{+} dispersed in the adsorbent to Ag^{0} requiring periodically adsorbent regeneration.

As mentioned before, only VSA-PSA simulation studies at 343 K were performed with the sample Ag/SBA-15 = 0.5 that has large equilibrium selectivity towards propylene due to π-complexation bonds with the olefin. As propane and propylene desorption is very fast, the co-current depressurization step was eliminated from the cycle to avoid propylene losses. To obtain purity higher than 99%, the recovery of propylene is 63% but polymer grade propylene could not be obtained in any of the conditions tested (Grande et al., 2004b). If the purpose is to obtain chemical grade propylene, this adsorbent may be a good choice because for product purity of 91% the recovery can be higher than 90% with only small contamination of the propane stream with propylene achieving propane HD-5 specification (fuel degree with less than 5% propylene).

Experimental data were measured in the VSA-PSA unit already existing at the LSRE (Da Silva, 1999) using Carbon Molecular Sieve 4A (Takeda) and zeolite 4A (CECA). A VSA-PSA cycle comprising five-steps (pressurization, feed, rinse, depressurization to intermediate pressure and counter-current blowdown) was employed. The modeling of the process was done using a model previously developed in this laboratory (Da Silva, 1999) using the multisite-Langmuir model for description

of multicomponent adsorption equilibrium and pure component diffusivity data determined during this work. The mathematical model was solved in gPROMS (PSE Enterprise, UK) using the orthogonal collocation method.

Prior to VSA-PSA experiments binary breakthrough curves of CMS4A were measured using three different propylene molar fractions: 0.29, 0.55 and 0.80 counterbalanced only with propane. No nitrogen was used in the feed stream. In the experiments having a molar fraction of propylene of 0.8 it can be seen that the separation of both gases will be very difficult for high propylene concentrations. The VSA-PSA experiments performed at 373 K showed that purity of propylene was never higher than 90%, but with recoveries that can be up to 92%. Experimental data were successfully predicted with the model. To obtain high propylene recovery also the co-current depressurization step was eliminated from the cycle.

Initially the VSA-PSA separation was studied with parameters and operating variables previously used by Da Silva at the LSRE (Da Silva, 1999). Even though, the results obtained with the sample of zeolite used in this work were better than with Rhone-Poulenc previously tested due to a smaller diffusivity of propane. This lower diffusivity of propane in zeolite 4A alows a strong minimization on the rinse step and also other step-times were improved to obtain high purity and also high recovery. Modeling of the VSA-PSA experiments were done also with multisite-Langmuir model and pure component diffusivities corrected with the Darken law to account for concentration dependence. Experimental data were successfully predicted with the model. Differences between simulated and experimental values of purity were around 0.5%. Experimentally, purity was around 98.8% in all experiments and no significant variations were observed when changing the operating variables studied in this work. The differences between simulated values and experimental ones may be due to dead

volumes in the installation and to the propylene feed with 0.5% of propane (99.4% purity specified by Air Liquide).

In the runs initially tested the feed was diluted to 50% with nitrogen. The content of inert was successively diminished experimentally up to 14% having only slight effects in recovery and purity. Also, a mixture having larger propylene to propane ratio (85 / 15 diluted to 50% with nitrogen) was studied.

The effect of some operating variables used were studied: step times, temperature, inert content and feed pressure (parameter studied only by simulations). Most of the experimental runs were performed at 433 K according to a previous selection based on the definition of a kinetic selectivity factor. According to experiments and simulations it was determined that higher purity propylene can be obtained at 408 K still with recovery higher than 80%. Increasing the temperature results in a decrease of purity and an increase in recovery and unit productivity. When the pressure of the feed stream is increased the purity decreases and the recovery increases (for similar number of moles treated by the unit). Even though the purity was improved by increasing the time of the feed step (with the expense of decreasing the recovery) and also enhancing the process productivity. The best experimental result was obtained at 408 K (run 20, Table 7.10) with a simulated purity of propylene of 99.43 % (as explained before, purity was always lower than simulated results; in this case around 99.0%) and a recovery of 84.3% with a unit productivity of 2.57 mol/h.kg.

The crystal size of the sample was also varied (study performed only by simulations) determining that with smaller crystals the propane time constant (r_c^2 / D_c) decreases and more propane diffuses into and out of zeolite 4A desorbing more in the blowdown step and contaminating the product. Prior to VSA-PSA studies, adsorption equilibrium and kinetics of pure propane and propylene on four samples of zeolite 4A

prepared in the laboratory of Elena I. Basaldella's group (CINDECA, La Plata, Argentina) was studied (Grande et al., 2004c). By simulations, with 4A zeolite crystals having a diameter of 5μm polymer grade propylene can be obtained (99.61%) with recovery of 83.1% and productivity of 2.25 mol/h.kg.

Finally, studies on an extruded honeycomb monolith containing zeolite 4A were performed. The monoliths of 900 square cells having crystals with a dimaeter of 1.4 μm were kindly supplied by Prof. Dr.-Ing. H.-G. Fritz from the University of Stuttgart. Adsorption equilibrium and kinetic studies of pure propane and propylene were performed in this material. Adsorption equilibrium of both gases were coincident with experimental data obtained in the commercial adsorbent (CECA). Crystal diffusivity of propane and propylene measured by batch adsorption were smaller than in the commercial sample and laboratory prepared ones. The lower values of both hydrocarbon diffusivity coefficients were confirmed by breakthrough curves. A mathematical model for pure component adsorption from a mixture adsorbate – inert gas in a monolith was developed. Its simplification applied only for dilute systems was solved in gPROMS. Also further simplifications (lumped parameter model) were solved for non-isothermal behavior when adsorption of mixtures with a higher propylene molar fraction (0.05 and 0.10) were used.

From all the results presented in this thesis it is clear that further studies are required to scale-up this process to separate industrial propane – propylene streams. Even though, for the case of using VSA-PSA processes, these studies should point zeolite 4A as the best adsorbent.

8.2 Recommendations for future work

As pointed out before adsorbents based on complexation with transition metals to enhance propylene adsorption will have to face problems with the contaminants in the industrial streams, namely hydrogen, acetylene and H_2S. For this reason if one large surface area material is impregnated with one of these metals, apart from the propane and propylene adsorption, the effect of hydrogen and at least acetylene (impurity of the industrial stream) have to be studied together.

Other materials (ALPO-14 and 8-member ring zeolites) to perform kinetic separation of propane and propylene were reported in the last years (Cheng et al., 2001; Olson, 2002). Up to now, the zeolite 4A used as detergent builder is much more cheaper than these adsorbents and, as shown in this thesis, presented very good results. Other materials already produced industrially for the difficult separation of CH_4-N_2 are the Engelhard titanosilicates, ETS (Engelhard, 2001). The size of the micropores of these materials can be tunned with thermal treatment and a patent for propane – propylene separation already exists (Kuznicki and Bell, 2003). If the idea is to study new materials to perform this separation, an innovative material will be one that adsorbs more propane than propylene with faster adsorption kinetics.

In order to continue the work on zeolite 4A two basic studies not performed here have to be done: effects of contaminants (acetylene and H_2S) and changes of the zeolite structure according to different thermal treatments. The study on the activation of the zeolite at different temperatures and possible modifications of the zeolite structure with displacements of the Na^+ ions or the structural water may allow us to have a tunnable material, similar to the ETS adsorbents.

In a more general way, the separation of olefins from paraffins to be performed by VSA-PSA has to be considered in a more general way and try to introduce this

separation not as a particular separation ethane – ethylene or propane – propylene but a more general one of olefins – paraffins. At this point, the operating variables can be more adjusted by the process and not previously imposed by the separation train already existing in the plant.

Finally it can be suggested that other cyclic processes, such as Simulated Moving Bed (SMB) technology, are worth trying for propane – propylene separation, not necessarily with the same type of adsorbents (Rao et al., 2004).

References

Cheng, L. S.; Wilson, S. T. *Vacuum Swing Adsorption Process for Separating Propylene from Propane*. U.S. Patent 6,296,688, **2001**.

Choudary, N. V.; Kumar, P.; Puranik, V. R.; Bhat, S. G. T. *Adsorbents, method for the manufacture thereof and process for the separation of unsaturated hydrocarbons from gas mixture*, U.S. Patent Application US2003/0097933A1, **2003**.

Da Silva, F. A. *Cyclic Adsorption Processes: Application to Propane / Propylene Separation*. Ph.D. Dissertation, University of Porto, Portugal, **1999**.

Engelhard Corporation. Purification Technologies Brochure, **2001**.

Grande, C. A.; Rodrigues, A. E. Adsorption Equilibria and Kinetics of Propane and Propylene in Silica Gel. *Ind. Eng. Chem. Res.*, **2001**, 40, 1686-1693.

Grande, C. A.; Rodrigues, A. E. Adsorption Kinetics of Propane and Propylene in Zeolite 4A, *Trans. Inst. Chem. Eng. A, Chem. Eng. Res. Dev.*, **2004**, in press.

Grande, C. A.; Rodrigues, A. E. Adsorption of Binary Mixtures of Propane – Propylene in Carbon Molecular Sieve 4A, *Ind. Eng. Chem. Res.*, **2004b**, accepted for publication.

Grande, C. A.; Gigola, C. E.; Rodrigues, A. E. Adsorption of Propane and Propylene in Pellets and Crystals of Zeolite 5A, *Ind. Eng. Chem. Res.*, **2002**, 41, 85-92.

Grande, C. A.; Gigola, C.; Rodrigues, A. E. Propane-Propylene Binary Adsorption on Zeolite 4A. *Adsorption,* **2003a**, 9, 321-329.

Grande, C. A., Silva, V.M.T.M., Gigola, C., Rodrigues, A. E. Adsorption of Propane and Propylene Onto Carbon Molecular Sieve. *Carbon*, **2003b**, 41, 2533-2545.

Grande, C. A.; Araujo, J. D. P.; Cavenati, S.; Firpo, N.; Basaldella, E. and Rodrigues, A. E. New PI-Complexation Adsorbents for Propane / Propylene Separation, *Langmuir*, **2004a,** 20, 5291-5297.

Grande, C. A.; Firpo, N.; Basaldella, E. and Rodrigues, A. E. Propane/Propylene Separation by SBA-15 and π-Complexated Ag-SBA-15, *Adsorption*, **2004b**, accepted for publication.

Grande, C. A.; Basaldella, E. I. And Rodrigues, E. I. Crystal Size Effect in Vacuum Pressure Swing Adsorption for Propane / Propylene Adsorption, *Ind. Eng. Chem. Res.*, **2004c**, 43, 7557-7565.

Kuznicki, S. M.; Bell, V. A. *Olefin Separation Employing ETS Molecular Sieves*. U.S. Patent, 6,517,611, **2003**.

Lewis, W. K.; Gilliland, E.; Chertow, B.; Cadogan, W. Pure Gas Isotherms. *Ind. Eng. Chem.*, **1950a**, 42, 1326-1332.

Olson, D.H. *Light Hydrocarbon Separation Using 8-Member Ring Zeolites*. U.S. Patent 6,488,741, **2002**.

Patiño-Iglesias, M. E.; Aguilar-Armenta, G.; Jimenez-Lopez, A.; Rodrigues-Castellón, E. Kinetics of the Total and Reversible Adsorption of Propylene and Propane on Zeolite 4A (CECA) at Different Temperatures. *Col. Surf. Sci. A.*, **2004**, 237, 73-77.

Rao, D. P.; Sivakumar, S. V.; Mandal, S.; Kota, S.; Ramaprasad, B. S. G. Novel Simulated Moving-Bed Adsorber for the Fractionation of Gas Mixtures. *J. Chromatogr. A*, **2004**, in press.

Rege, S. U.; Padin, J.; Yang, R. T. Olefin/Paraffin Separations by Adsorption - Pi-Complexation vs. Kinetic Separation. *AIChE J.*, **1998**, 44, 799-809.

Ruthven, D. M.; Derrah, R. I. Sorption in Davison 5A Molecular Sieves. *Can. J. Chem. Eng.*, **1972**, 50, 743-747.

Yang, R. T.; Kikkinides, E. S. New Sorbents for olefin / paraffin separations by Adsorption via π-Complexation. *AIChE J.*, **1995**, 41, 509-517.

Zhao, D.; Feng, J.; Huo, Q.; Melosh, N.; Fredrickson, G. H.; Chmelka, B. F.; Stucky, G. D. Triblock Copolymer Syntheses of Mesoporous Silica with Periodic 50 to 300 Angstrom Pores. *Science*, **1998**, 279, 548.

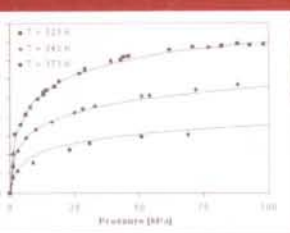

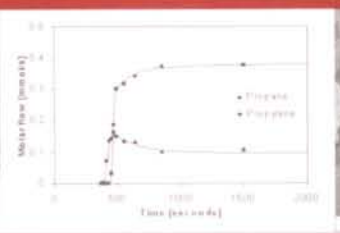

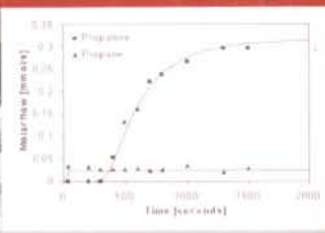

FACULDADE DE ENGENHARIA
UNIVERSIDADE DO PORTO
BIBLIOTECA
0000078375